LEONARD, R.A. 1985. *Induction motor fault recognition*. Robert Gordon's Institute of Technology, MPhil thesis. Hosted on OpenAIR [online]. Available from: https://doi.org/10.48526/rgu-wt-1993280

Induction motor fault recognition.

LEONARD, R.A.

1985

The author of this thesis retains the right to be identified as such on any occasion in which content from this thesis is referenced or re-used. The licence under which this thesis is distributed applies to the text and any original images only – re-use of any third-party content must still be cleared with the original copyright holder.

OpenAIR @RGU

This document was downloaded from https://openair.rgu.ac.uk

CC BY NC

INDUCTION MOTOR FAULT RECOGNITION

By

Raymond Alexander Leonard, BSc with

First Class Honours in Electronic & Electrical Engineering

A thesis submitted in partial fulfilment of the requirements of the Council for National Academic Awards for the Degree of Master of Philosophy (M. Phil)

Sponsoring Establishment
School of Electronic and Electrical Engineering
Robert Gordon's Institute of Technology
Schoolhill
Aberdeen
AB9 1FR

Collaborating Establishment
Britoil PLC
St Machar House
Aberdeen

July 1985.

DECLARATION

I hereby declare that this thesis is a record of work undertaken by myself, that it has not been the subject of any previous application for a degree, and that all sources of information have been duly acknowledged.

During this research the following conferences were attended:

1. International Conference on Electrical Machines
   - Design and Applications,
   IEE, Savoy Place, London.
   13 - 15 July 1982.

2. Seminar on Signal Processing,
   AEE, Harwell.
   1981.

Raymond A Leonard

July 1985

INDEX

		PAGE
ACKNOWLEDGEMENTS		
ABSTRACT		
CHAPTER ONE - INTRODUCTION		
1.1	The SCIM and its Operating Environment	1
1.2	Maintenance Strategies	2
1.3	Failures in SCIMs	3
1.4	Monitoring Techniques	4
1.5	Philosophies of Fault Detection	5
1.6	Conclusions	6
CHAPTER TWO - TEST RIG AND INSTRUMENTATION		
2.1	Introduction	8
2.2	The Test Rig	8
2.3	Monitored Signals and their Transducers	10
2.4	The Use of Search Coils	11
2.5	Additional Instrumentation	13
CHAPTER THREE - MACHINE FUNDAMENTALS		
3.1	Introduction	19
3.2	Derivation of Airgap Flux Density	20
3.3	Derivation of the Airgap Radial Force	24
3.4	Summary of Derived Frequencies	26
CHAPTER FOUR - THE EFFECTS OF UNBALANCED SUPPLY		
4.1	Introduction	27
4.2	Definition of the Magnitude of Unbalanced Supply	28
4.3	Airgap Forcing Functions	29
4.4	SCIM Vibration due to the Airgap Forcing Functions	32
4.5	Experimental Investigation	32
4.6	Using the Vibration Signal to Detect Unbalanced Supply	34
4.7	Conclusions	35
CHAPTER FIVE - THE EFFECTS OF ROTOR FAULTS		
5.1	Discussion	50
5.2	Sideband Components	52
5.3	Experimental Rotors	55
5.4	Cepstrum	56
5.5	Experimental Results	56
5.6	Conclusions	58
CHAPTER SIX - ECCENTRICITY & INTERTURN FAULTS		
6.1	Introduction	77
6.2	Rotor-Stator Static Eccentricity	77
6.3	Interturn Winding Faults	79
6.4	Conclusions	81

PAGE

CHAPTER SEVEN - STRUCTURAL RESPONSE OF THE MACHINE

7.1 Introduction 90
7.2 The Formulation of the Finite Element Model 91
7.3 Model Dimensions & Elements 93
7.4 The Data Required for 'PAFEC 75' 93
7.5 Results using "PAFEC 75' 93
7.6 More Complicated Model 94
7.7 Experimental 94
7.8 Comparison of Experimental & Theoretical Results 95
7.9 Conclusions 96

CHAPTER EIGHT - CONCLUSIONS & FUTURE WORK

8.1 Discussion 117
8.2 Future Work 118

REFERENCES 119

APPENDIX I - SURVEY QUESTIONNAIRE

APPENDIX II - UNBALANCED SUPPLY BY SYMMETRICAL COMPONENTS

APPENDIX III - DERIVATION OF TORQUE & SPEED FOR ROTOR WITH BROKEN BAR

PUBLICATIONS

ACKNOWLEDGEMENTS

I would like to take this opportunity to thank W.T. Thomson for his encouragement and his supervision of this project, A.J. Low and D. Sutherland for their work in the construction of the test rigs and A.J. Milne for the use of his computer storage and signal processing software.

The funding of this project by a SERC Marine Technology Grant is also acknowledged.

ABSTRACT

INDUCTION MOTOR FAULT RECOGNITION

by

RAYMOND A. LEONARD

The work presented in this thesis is based on theoretical and experimental investigations into the changes in measurable squirrel cage induction machine parameters such as vibration, line current and leakage flux which alter during machine faults.

Initially a survey was conducted to determine which machine failures were of concern to industrial operators.

Faults analysed in this thesis include rotor bar faults, unbalanced supply, eccentricity and interturn winding faults. Experimental results are given for each fault type.

Work was also done in predicting the natural frequencies of the experimental stator using a standard finite element package. The results from this analysis were compared with experimental results and shown to be realistic.

The main conclusion drawn from this thesis is that there are several differences in the parameters observed during normal and fault operation, the prediction of a fault being dependent on changes of certain components of the various signal spectra. The changes in these various components can be supported theoretically.

CHAPTER ONE

INTRODUCTION

1.1 THE SCIM AND ITS OPERATING ENVIRONMENT

The three-phase squirrel-cage induction motor (SCIM) is the workhorse of modern industry driving major pumps, compressors and fans in powers up to many megawatts. These motors are of particular importance in the production and refinement of oil and gas. Another important application is as gas circulator drives in the nuclear industry (1).

The operating environment plays a major role in the reliability and availability of SCIMs, for example on North Sea oil and gas installations the majority of machines are started direct on line (dol) because there is a lack of space for sophisticated starters. The voltage supplies can be as high as 13.8 kV, are not particularly stable and large transients can be expected when equipment is connected or disconnected (2). Vibration levels can be expected to be high due to the interaction of the structure with the wind and sea (3). There is also an increased risk of sea water contamination. These environmental factors contribute to a reduction in the reliability and useful working life of SCIMs and several premature failures have already been reported. To maximise safety and production an intelligent maintenance strategy is required.

1.2 MAINTENANCE STRATEGIES

There are three maintenance philosophies which can be applied to rotating machinery in general. The first of these is "RUN-TO-BREAK MAINTENANCE" where machines are run until they fail before repair or replacement is undertaken. The consequential damage from such breakdowns can greatly increase both loss of production and repair costs. The second philosophy is "TIME-BASED PREVENTIVE MAINTENANCE" where maintenance work is carried out at fixed time intervals whether or not the machine requires maintenance. These time intervals are often determined statistically. It has been shown that if machines are run for another time period without maintenance the number of machines failing will be less, or no higher, than in the first time period and less if maintenance has been performed between intervals (4). The third philosophy is "ON-CONDITION MAINTENANCE" where analysis of machine parameters is performed systematically and intelligently. This analysis is termed "CONDITION MONITORING" and allows determination of present machine "health" and information for trend analysis on which "PREDICTIVE MAINTENANCE" can be based.

The most effective of the above strategies in terms of reduced failures and increased profits has been shown to be on-condition maintenance (5). The operation of an on-condition maintenance strategy is dependent on effective condition monitoring which in turn relies on a knowledge of possible machine faults and their effects and the use of suitable instrumentation and signal processing techniques.

1.3 FAILURES IN SCIMs

At the start of this project a survey was conducted into failures in SCIMs in the offshore/onshore petrochemical industry. Appendix I contains a copy of the questionnaire. The survey gave details of the history of eighty two SCIMs. The supplies varied from 2.3 kV to 13.8 kV and 98% of the machines were started dol. Of the sample thirty had no reported failures while the remaining fifty two experienced a total of ninety four failures which were due to the following causes:

BEARING FAULTS	44.68%
WINDING FAULTS	44.68%
BROKEN ROTOR BAR FAULTS	4.25%
MISCELLANEOUS FAULTS	6.39%

It should be noted that although bearing faults are a major cause of failure their failure may be a secondary effect of a primary cause such as broken rotor bars, rotor-stator eccentricity or bearing currents. Stator winding failure can be due to excessive end-winding vibration which over stresses the insulation, contamination of insulation by oil or sea water or overcurrent due to unbalanced supply or machine overload or switching transients (6). Rotor bar failures are generally caused by the heavy accelerating and decelerating forces which act on the rotor bars and endrings (7). The rotor bars fracture and can eventually lift from their slots causing mechanical damage to rotor and stator. Additional informal

discussions with other operators and manufacturers of SCIMs has indicated that the problem of rotor faults in general is more significant than the survey results would suggest. The miscellaneous faults are due to such factors as contamination of bearing lubricant and foreign matter in the airgap.

1.4 MONITORING TECHNIQUES

The survey also provided information on present monitoring techniques applied to SCIMs. These are shown in Table 1.1. It is clearly seen that all the operators have some form of vibration monitoring. The majority of vibration monitoring involves the measurement of overall vibration levels with spectral analysis performed only if the levels become excessive. There is always an uncertainty as to what should constitute an excessive vibration level.

Another monitoring technique which is widely used is temperature sensing. This form of monitoring is applied to stator windings and core as well as to the bearings. If the stator windings or core get excessively hot this is an indication of either overcurrent due to insulation failure or machine overload or unbalanced supply or due to inadequate ventilation. If the bearings or their lubrication system are faulty there is increased friction and hence a rise in temperature.

Shaft speed monitoring is used for the detection of rotor faults such as broken bars and endrings. Shaft voltages are

occasionally monitored. A shaft voltage is the voltage which develops between the shaft and ground due to magnetic asymmetries in the motor. These asymmetries may be inherent in the machine's design or due to faults. Shaft voltages can lead to bearing currents which can severely reduce the life of a bearing (8). Stray flux is monitored by a small number of operators. The stray flux signal can be used to detect such faults as inter-turn winding short circuits on unenergised coils (9) and unbalanced supply conditions. (10).

Insulation tests are regularly employed by all operators. These tests are usually conducted while the machine is undergoing a regular off-line maintenance check.

From the survey results and further discussions with industrial operators there is a definite need for further instrumentation for fault detection and prediction.

1.5 PHILOSOPHIES OF FAULT DETECTION

Most fault detection systems are based on individual machine signals and are not 100% reliable. As a consequence operators are not always entirely convinced as to the existence of a fault. A more attractive approach with regard to the operator is to monitor several signals. If all the signals change then the operator will be more easily convinced that a fault is developing. There will also be less dependence on individual instrumentation circuits which will enhance the overall reliability of fault detection/protection.

To implement such a system work is required in increasing the fundamental knowledge of how a SCIM reacts under fault conditions and how signals such as vibration, line current, axial flux and endwinding leakage flux change with these faults.

1.6 CONCLUSIONS

The SCIM has to operate in hostile environments and as a result there is an increased rate of failure. Machine failure and unpredictable production stoppage leads to high loss of profit. It is therefore important to monitor the "health" of these machines, that is to CONDITION MONITOR them. To effectively condition monitor SCIMs it is necessary to investigate the fundamental effects of machine faults on various machine parameters such as vibration, line current, axial flux and endwinding leakage flux. It is this that is of interest to the author. The basic information obtained from such investigations can then be used in dedicated instrumentation systems.

MONITORING TECHNIQUE	USAGE
Subjective look, feel & listen	100 %
Vibration monitoring	100 %
Vibration spectral analysis	73 %
Stator winding temperature	91 %
Stator core temperature	9 %
Bearing temperature	91 %
Insulation tests	100 %
Ultrasonic discharge detector	9 %
Shaft voltage	27 %
Oil sample analysis	27 %
Wear debris monitoring	18 %
Stray flux monitoring	9 %
Rotor bar monitoring	27 %

Table 1.1 Usage of monitoring techniques

CHAPTER TWO

TEST RIG AND INSTRUMENTATION

2.1 INTRODUCTION

At the start of this project it was obviously impractical to intentionally produce faults on large SCIMs in an industrial environment. A laboratory test-rig was therefore designed and constructed to enable controlled repeatable fault simulation. Since machine theory applies equally to all sizes of machines faults produced on a small machine will have the same effect as faults produced on a large machine. The faults to be studied were:

(a) Unbalanced Supply

(b) Rotor Winding Faults

(c) Interturn Winding Faults

(d) Static Rotor-Stator Eccentricity

These faults were to be studied by the examination of the various signals which emanate from the machine.

2.2 THE TEST RIG

The test SCIM was based on a standard production stator, Type D160M, manufactured by Brook Crompton Parkinson Motors Ltd. The stator had an annealed steel laminated core having thirty

six slots and an alluminium frame. This type of stator is rated for use at 11 kW.

The stator frame was modified to give mounting points for an accelerometer. There were a total of twenty three mounting points around the circumference of the machine. It was impractical to have accelerometer mounting points on the underside of the stator. It was necessary to have these twenty three mounting points to establish if the vibration signal varied around the stator frame under normal and abnormal operation. Figure 2.1 shows the location of the accelerometer mounting studs.

The stator winding was double layered with thirty six coils of fifteen turns per coil. The ends of each coil were brought out to a connection matrix so that windings could be connected to simulate windings faults and to give varying pole numbers.

Various rotors were available for investigations into rotor faults, these rotors will be detailed in Chapter Five - The Effects of Rotor Faults. The rotor bearings were mounted in pedestals and the stator could be moved with respect to the rotor enabling the introduction of static rotor-stator eccentricity.

The shaft of the test SCIM was connected via a flexible shaft coupling to a separately excited d.e. generator which acted as a loading dynamometer. A resistive loading bank was constructed outwith the laboratory so that the generated

energy could be dissipated safely. The supply to the SCIM was via a three-phase, 415 volt, 50 Hz automatic starter.

2.3 MONITORED SIGNALS AND THEIR TRANSDUCERS

There were four basic signals of interest in the project, these were stator core vibration, line current, axial flux and endwinding leakage flux.

2.3.1 VIBRATION SIGNAL

The vibration transducer used was a B & K type 4370 piezo-electric accelerometer (with virtually undirectional response). The accelerometer was connected to a B & K type 2635 precision charge amplifier to give a calibrated output. Vibration measurements were made on the acceleration ranges of the charge amplifier. If velocity or displacement ranges were used the higher frequency components were much reduced by the necessary signals integrations. These higher frequencies were of interest in the project so it was decided to use the acceleration ranges.

2.3.2 LINE CURRENT SIGNAL

The line current to the SCIM contains frequency components which also appear in the airgap flux. Therefore by monitoring the line current an indication of changes in airgap flux can be obtained. To avoid the

problems of distortion by magnetic saturation of the current waveform and insulation from supply voltage an air-cored toroidal coil was used. This coil is shown in Figure 2.2.

2.3.3 AXIAL FLUX SIGNAL

The axial flux is the flux which passes through the SCIM shaft. The axial flux contains frequency components which reflect changes in the airgap flux. The axial flux was detected by means of a 100 turn coil wound around the shaft.

2.3.4 ENDWINDING LEAKAGE FLUX

The endwinding leakage flux is the flux which emanates radially from the motor near the stator endwindings. This flux also contains the frequency components which appear in the airgap flux. The endwinding leakage flux was detected by a 300 turn coil mounted near the stator endwindings.

2.4 THE USE OF SEARCH COILS

Since several of the transducers used were search coils a description of their use is necessary.

The relationship between the induced search coil voltage and the linking flux is given by Faraday's Law.

i.e. $$e = -\frac{N d\phi}{dt}$$

where e = induced voltage

N = Number of turns

$\frac{d\phi}{dt}$ = rate of change of flux

To produce a signal which is representative of the flux would require implementation of the following equation:

$$\phi = -\frac{1}{N}\int e\,dt$$

Now if e were to contain several frequencies

say $e = K_1 \sin w_1 t + K_2 \sin w_2 t + \cdots K_n \sin w_n t$

Then the flux signal could be written as:

$$\phi = \frac{1}{N}\left(\frac{K_1}{w_1}\cos w_1 t + \frac{K_2}{w_2}\cos w_2 t + \cdots \frac{Kn}{w_n}\cos w_n t\right)$$

If the integration was performed electronically the resulting magnitudes of the frequency components would be dependent on the frequency of the component. A high frequency component would therefore have to be divided by its own frequency thereby reducing its magnitude and perhaps obscure it in background noise.

It was decided to omit the integrating stage as it would obscure some of the higher frequency components which would be of interest. All values given in this thesis for axial flux and endwinding leakage flux are not for flux (Ø) but for the induced voltage (e).

2.5 ADDITIONAL INSTRUMENTATION

The signals from the various transducers were analysed in a B & K 2033 High Resolution Signal Analyser. The B & K 2033 performs a Fast Fourier Transform (FFT) on incoming signals.

The B & K, Type 2635, Charge Amplifier used with the piezzo-electric accelerometer for input to the B & K 2033 High Resolution Signal Analyser was set to give an output of 100 mV/ms^{-2}. Table 2.1 gives conversions for vibration, voltage and decibel rms values.

For overall vibration level measurements a B & K vibration meter was used.

The B & K 2033 High Resolution Signal Analyser existed as a peripheral to a PDP 11/03 computer which could perform additional signal processing, storage of data and give hard copy print outs of the spectra. The software for this system was developed by A.J. Milne (11).

A block diagram of the test-rig and instrumentation set is shown in Figure 2.3 and the actual set is shown in Figure 2.4

dB	Volts	ms^{-2}
130	3.16	31.6
120	1.00	10.0
110	0.316	3.16
100	0.100	1.00
90	31.6 m	0.316
80	10.0 m	0.100
70	3.16 m	31.6 m
60	1.00 m	10.0 m
50	0.316 m	3.16 m
40	0.100 m	1.00 m
30	0.0316 m	0.316 m

Table 2.1 Conversions - Vibration, Voltage & dBs

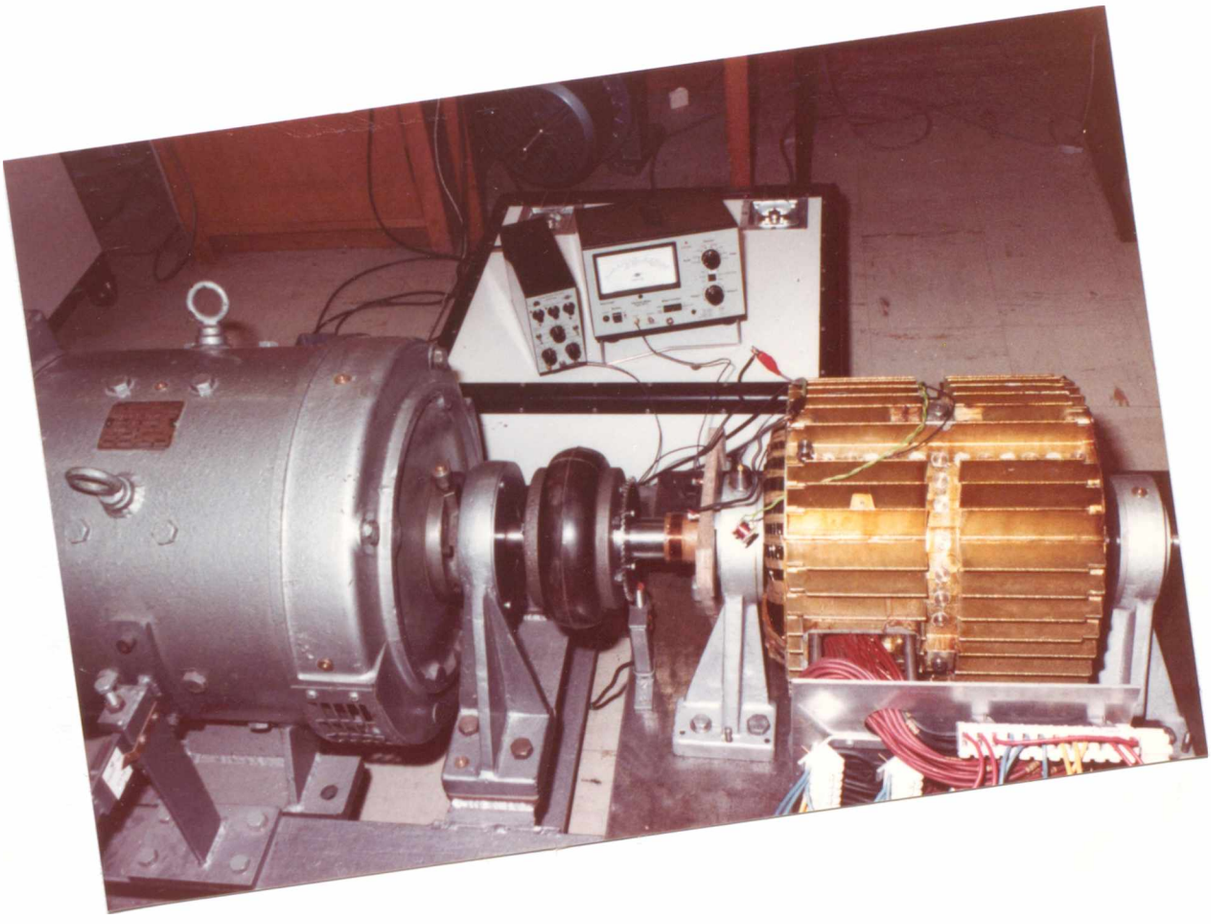

Figure 2.1 Accelerometer Mounting Studs

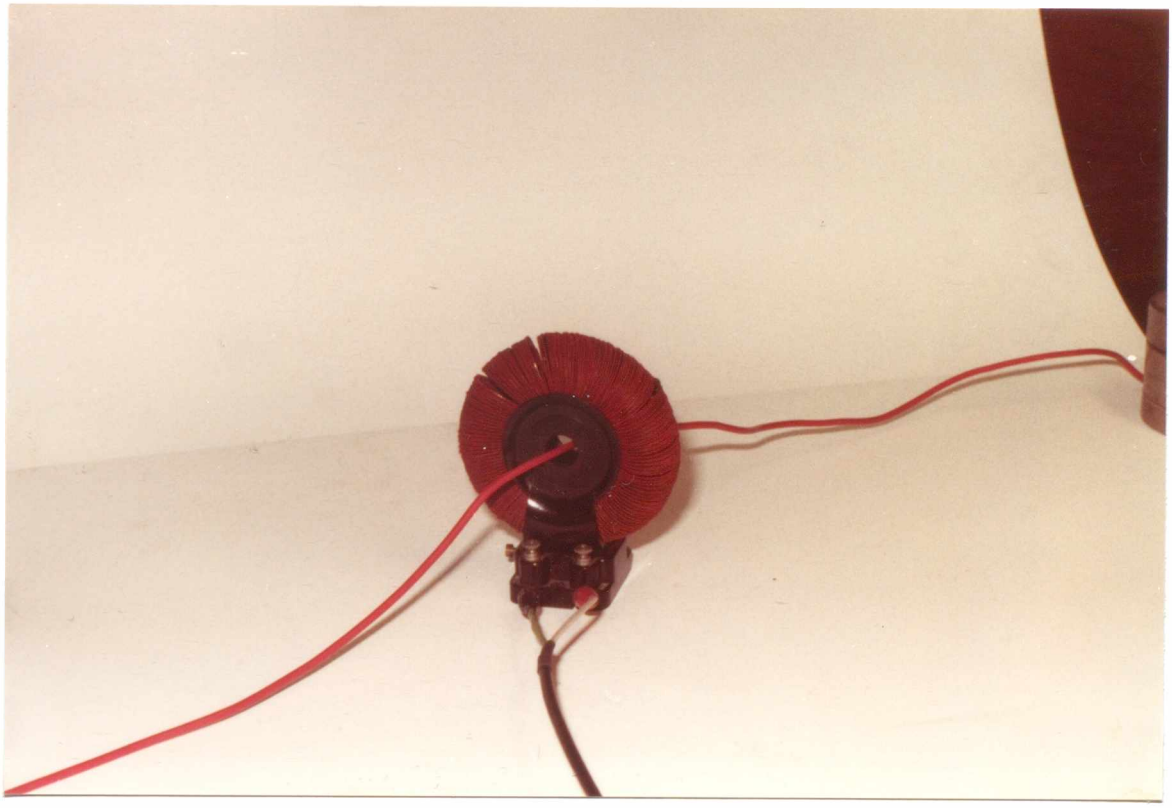

Figure 2.2 Toroidal Air Cored Coil for detecting Line Current

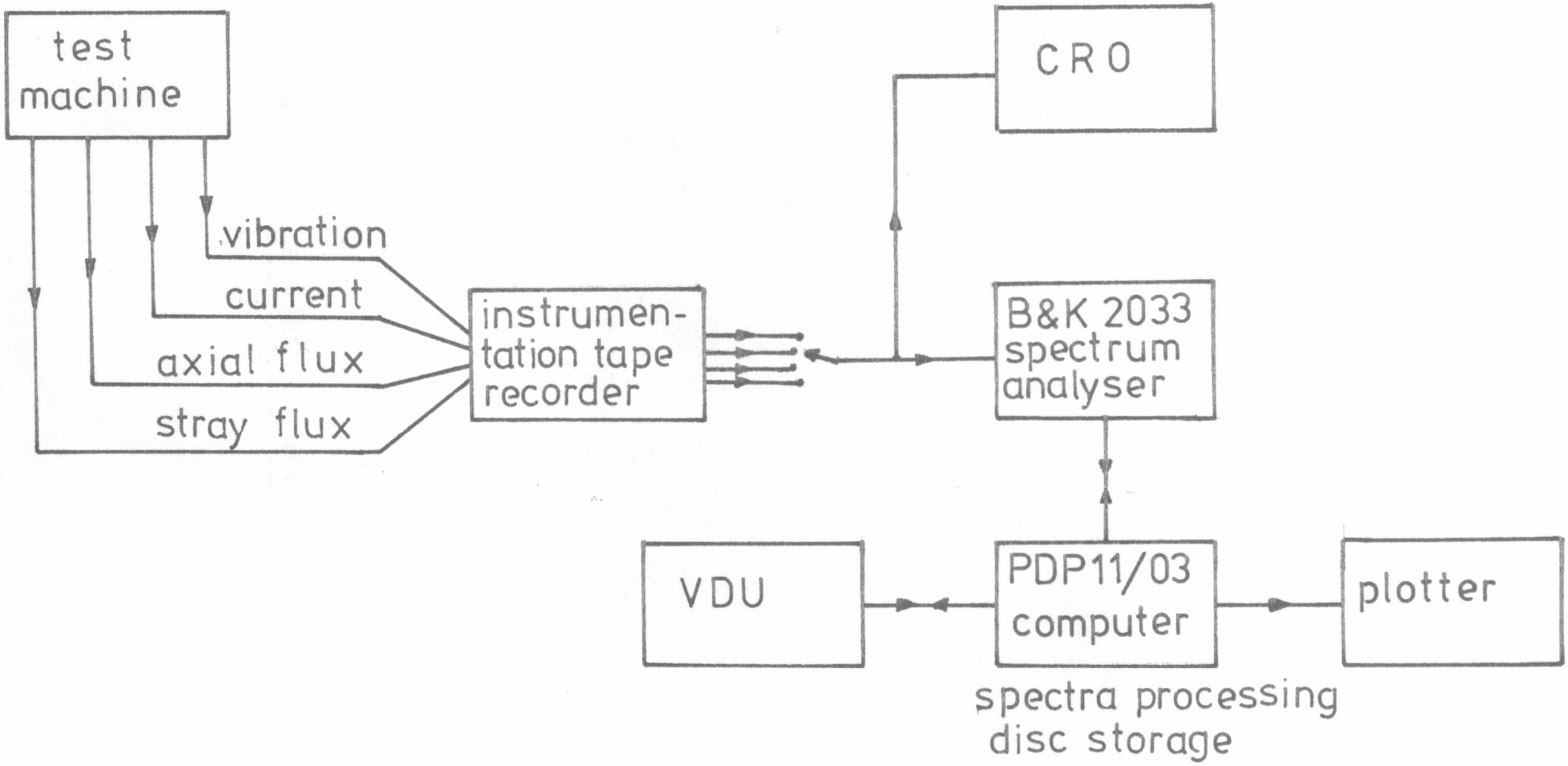

Figure 2.3 Block Diagram of Experimental Set Up

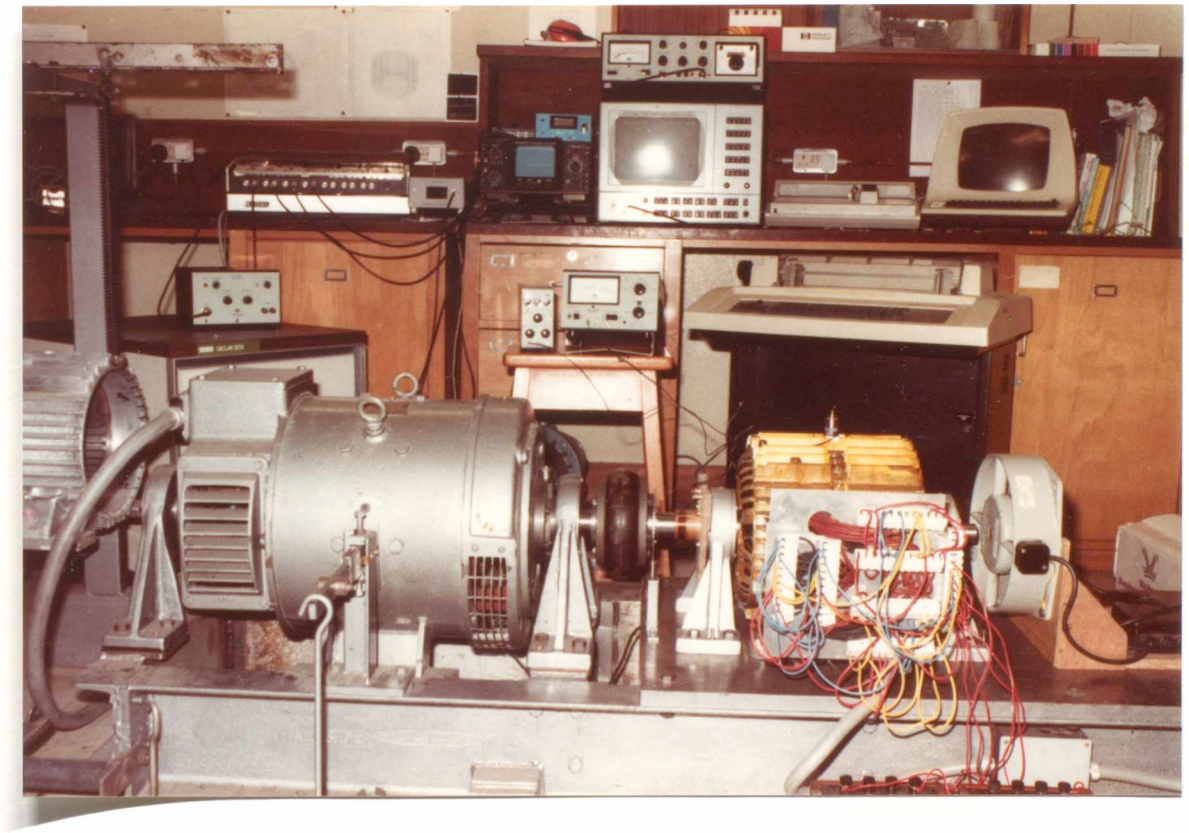

Figure 2.4 Actual Test Rig and Instrumentation

CHAPTER THREE

MACHINE FUNDAMENTALS

3.1 INTRODUCTION

The frequency components of the airgap electromagnetic field are dependent on the airgap permeance and the magnetomotive force (mmf) produced by the winding. The permeance is dependent on the numbers of stator and rotor slots while the mmf is dependent on the number of phases and distribution of the stator winding in conjunction with the power supply harmonics.

The frequency components in the airgap field will be "reflected" into the stator current and will also appear in the axial flux and end winding leakage flux signals.

The radial airgap forces which cause electromagnetic vibration are proportional to the square of the airgap flux density (12). The magnitude and mode of the resulting vibration is dependent on the number of poles and frequency of the electromagnetic force waves and the structural response of the stator.

The following sections of this chapter will derive the various frequency components of the airgap flux density and vibration.

3.2 DERIVATION OF AIRGAP FLUX DENSITY

The permeance of an airgap with a slotted stator and a smooth rotor can be written as:

$$\lambda_S = \sum_{m=0}^{\infty} a_m \cos (m \ Sx)$$

where a_m = coefficient

S = number of stator slots

x = radian distance around airgap

m = 0, 1, 2, 3 - - -

The permeance of an airgap with a slotted rotor and a smooth stator can be written as:

$$\lambda_r = \sum_{n=0}^{\infty} b_n \cos \ (nR \ (x - W_r t) \ )$$

where b_n = coefficient

R = number of rotor slots

W_r = radian speed of shaft

t = time

n = 0, 1, 2, 3 - - -

The total permeance of an airgap with a slotted stator and a slotted rotor can be written as (12):

$$\lambda = k \lambda_s \lambda_r$$

where k = constant

Therefore:

$$\lambda = k \sum_{m=0}^{\infty} \sum_{n=0}^{\infty} a_m b_n \cos (m Sx) \cos (nR (x - W_r t))$$

Using the trigonometric identity

$$\cos A \cos B = \frac{1}{2} (\cos (A + B) + \cos (A - B))$$

the airgap permeance can be expressed as

$$\lambda = \sum_{m=0}^{\infty} \sum_{n=0}^{\infty} C_{(m,n)} \cos ((nR \pm mS) x - nR w_r t)$$

This equation defines the frequency and the pole numbers of the permeance waves as follows:

nRw_r are the radian frequencies

and $(nR \pm mS)$ are the pole numbers.

The magneto-motive force (mmf) for a symmetrical integral slot three-phase winding can be written as:

$$M = \sum_{u=1}^{\infty} \sum_{v=1}^{\infty} A_{(u\ v)} \sin (uw_s t + v\ Px)$$

where $A\ (u_1 v)$ = peak magnitude of components

W_s = supply radian frequency ($=2\pi fs$)

P = number of pole pairs

u = 1, 2, 3 - - , the mmf time harmonics due to supply current time harmonics

v = $6c \pm 1$, the mmf space harmonics

c = 0, 1, 2, 3 - - - -

It should be noted that u also takes account of even supply harmonics. Even though it is usually stated that the supply only has odd harmonics, in some cases such as inverter driven machines even supply harmonics may also be present.

The pole numbers of the flux density are given by the expression ($\mp$ vP $\pm$ (nR $\pm$ mS)) while the radian frequency components are given by $(u \pm \frac{nR}{P}(1-s))\ W_s$.

However the hertzian frequencies are more usually considered.

The expression for hertzian frequencies is given by

$$\sum_{u=1}^{\infty}\sum_{n=0}^{\infty} (u \pm \frac{nR}{P}(1-s))\ fs,$$

where $fs = \frac{Ws}{2\pi}$

The airgap flux density can be written as the product of the mmf and permeance, which gives:

$$B = M \lambda$$

$$= \sum_{u=1}^{\infty}\sum_{v=1}^{\infty}\sum_{m=0}^{\infty}\sum_{n=0}^{\infty} A_{(u,v)} C_{(m,n)} \sin (uw_s t \mp v\,Px) \cos ((nR \pm mS)\,x - n\,Rw_r t)$$

Using the trigonometric identity

$$\text{Sin A cos B} = \frac{1}{2}(\sin (A + B) + \sin (A - B))$$

the flux density can be written as:

$$B = \sum_{u=1}^{\infty}\sum_{v=1}^{\infty}\sum_{m=0}^{\infty}\sum_{n=0}^{\infty} D_{(u,v,m,n)} \sin\left((\mp vP \pm (nR \pm mS))\, x + (uw_s \pm nRw_r)\, t\right)$$

but $W_r = (1-s)\, W_s/P$

where s = slip

Therefore

$$B = \sum_{u=1}^{\infty}\sum_{v=1}^{\infty}\sum_{m=0}^{\infty}\sum_{n=0}^{\infty} D_{(u,v,m,n)} \sin\left((\mp v\, P \pm (nR \pm mS))x + (u \pm \frac{nR}{P}(1-s))\, W_s t\right)$$

3.3 DERIVATION OF THE AIRGAP RADIAL FORCE

The radial electromagnetic forces which cause stator vibration are proportional to the square of the flux density and are written:

$$F = B^2/2\mu$$

where μ = airgap permeability.

Using the equation derived above for B the force, F, can now be written as:

$$F = \frac{1}{2\mu}\left[\sum_{u=1}^{\infty}\sum_{v=1}^{\infty}\sum_{m=0}^{\infty}\sum_{n=0}^{\infty} D_{(u,v,m,n)} \sin\left((\mp vP \pm (nR + mS))x + (u \pm \frac{nR}{P}(1-s))\, w_s t\right)\right]^2$$

This equation can now be written as

$$F = \frac{1}{2\mu} \sum_{u=1}^{\infty}\sum_{v=1}^{\infty}\sum_{m=0}^{\infty}\sum_{n=0}^{\infty} D_{(u,v,m,n)} \sin\left((\mp vP \pm (nR \pm mS))x + (u \pm \frac{nR}{P}(1-s))\omega_s t\right)$$

$$\times \sum_{y=1}^{\infty}\sum_{z=1}^{\infty}\sum_{a=0}^{\infty}\sum_{b=0}^{\infty} D_{(y,z,a,b)} \sin\left((\mp zP \pm (bR \pm aS))x + (y \pm \frac{bR}{P}(1-s))\omega_s t\right)$$

$$= \frac{1}{2\mu} \sum_{u=1}^{\infty}\sum_{v=1}^{\infty}\sum_{m=0}^{\infty}\sum_{n=0}^{\infty}\sum_{y=1}^{\infty}\sum_{z=1}^{\infty}\sum_{a=0}^{\infty}\sum_{b=0}^{\infty} E_{(u,v,m,n,y,z,a,b)}$$

$$\times \sin\left((\mp vP \pm (nR \pm mS))x + (u \pm \frac{nR}{P}(1-s)\omega_s t\right)$$

$$\times \sin\left((\mp zP \pm (bR \pm aS))x + (y \pm \frac{bR}{P}(1-s)\omega_s t\right)$$

Using the trigonometric identity

$$\sin A \sin B = 1/2\ (\ \mathrm{Cos}\ (A - B) - \mathrm{Cos}\ (A + B)\ )$$

the preceding equation can be written as:

$$F = \frac{1}{4\mu} \sum_{u=1}^{\infty}\sum_{v=1}^{\infty}\sum_{m=0}^{\infty}\sum_{n=0}^{\infty}\sum_{y=1}^{\infty}\sum_{z=1}^{\infty}\sum_{a=0}^{\infty}\sum_{b=0}^{\infty} E_{(u,v,m,n,y,z,a,b)}$$

$$\times \Big[\cos\{((\mp vP \pm (nR \pm mS)) - (\mp zP \pm (bR \pm aS)))x$$

$$+ (u - y + (\pm n \mp b)\frac{R}{P}(1-s))\omega_s t\}$$

$$- \cos\{((\mp vP \pm (nR \pm mS)) + (\mp zP \pm (bR \pm aS)))x$$

$$+ (u + y + (\pm n \pm b)\frac{R}{P}(1-s))\omega_s t\}\Big]$$

The hertzian frequencies of the airgap forces and hence the stator vibrations are given by:

$$\sum_{u=1}^{\infty}\sum_{n=0}^{\infty}\sum_{y=1}^{\infty}\sum_{b=0}^{\infty} (u \pm y + (\pm n \pm b)\frac{R}{P}(1-s))f_s$$

and the pole numbers given by

$$\sum_{v=1}^{\infty}\sum_{m=0}^{\infty}\sum_{n=0}^{\infty}\sum_{z=1}^{\infty}\sum_{a=0}^{\infty}\sum_{b=0}^{\infty}\left(\mp vP \pm (nR \pm mS)\right) \pm \left(\mp zP \pm (bR \mp aS)\right)$$

3.4 SUMMARY OF DERIVED FREQUENCIES

The equation derived for the frequency of the airgap flux density is given by:

$$\sum_{u=1}^{\infty}\sum_{n=0}^{\infty}\left(u \pm \frac{nR}{P}(1-s)\right) f_s$$

The frequencies described by this equation would also be expected in the current, axial flux and end winding leakage flux signals.

The equation derived for the frequencies of the stator core vibration is given by

$$\sum_{u=1}^{\infty}\sum_{n=0}^{\infty}\sum_{y=1}^{\infty}\sum_{b=0}^{\infty}\left(u \pm y + (\pm n \pm b)\frac{R}{P}(1-s)\right) f_s$$

CHAPTER FOUR

THE EFFECTS OF UNBALANCED SUPPLY

4.1 INTRODUCTION

Unbalanced supply is the condition when a three-phase supply is no longer symmetrical. Unbalanced supply of a SCIM leads to excess current, overheating of windings, insulation failure and eventual machine failure. Detection of unbalanced supply at an early stage will prevent winding failure and a costly repair as well as preventing the loss of valuable production. An extreme case of unbalanced supply is 'single-phasing', i.e. complete loss of one supply phase. Single-phasing of a SCIM can be caused by single-phased controls of power supplies, or open circuited winding or lead wire, or improper connection (13). Unbalanced supply can also be caused by generator faults, system faults and by excessive load on one supply line.

The effects of unbalanced supply on SCIMs have in the main been investigated from the electrical viewpoint to determine positive, negative and zero sequence currents and voltages and the resulting thermal effects (14 ,15 ,16). The information gained from such investigations has led to some of the present protection methods which include the sensing of overload current, the sensing of voltage or current asymmetry and the sensing of stator winding temperature. One of the more recent developments involves the use of the axial flux signal (9 ,10). Although these detection methods have been in use for many

years failures due to unbalanced supply still occur. Vincent (17) reports, in a survey of 380 machines, that 12% of failures were due to single-phasing.

None of the previous investigations has considered the effect of unbalanced supply on SCIM vibration. It is the main purpose of this chapter to examine the effects of unbalanced supply on SCIM vibration and to propose how vibration monitoring may be used in a protection strategy. The work in this chapter relating to the effects of unbalanced supply on vibration, is to the author's knowledge, the first investigation of its kind.

4.2 DEFINITION OF THE MAGNITUDE OF UNBALANCED SUPPLY

The British Standard definition of unbalanced supply is given as the ratio of the negative sequence or zero sequence voltage to the positive sequence voltage.

$$\text{i.e. unbalance} = V_o/V_+ \text{ or } V_-/V_+$$

In the investigation considered in this chapter it can be shown (Appendix II) that

$$V_o/V_+ = V_-/V_+$$

British Standards (18) and International Electrotechnical Commission state that SCIMs should withstand a 2% unbalance in supply. Unbalance greater than 2% will overheat the windings which will lead to their premature failure.

Figure 4.1 shows the relationship between reduction of a phase voltage and unbalanced supply.

4.3 AIRGAP FORCING FUNCTIONS

As an aid to understanding the effect of unbalanced supply on vibration the airgap forcing functions for normal three-phase and for single-phase operation will now be derived.

THREE PHASE OPERATION

Consider the delta connected winding of Figure 4.2 (a). If the system is totally symmetrical the phase currents can be written as:

$$\left.\begin{aligned} I_a &= I_m \sin(wt) \\ I_b &= I_m \sin(wt + \pi/3) \\ I_c &= I_m \sin(wt - \pi/3) \end{aligned}\right\} \quad 4.1$$

where I_m = peak current

w = supply radian frequency

t = time, secs

and I_a, I_b and I_c are phase currents.

Taking the mechanical displacement of the windings into account the mmf produced by each phase can be written as:

$$\left.\begin{aligned} M_a &= M_m \sin(wt)\cos(\pi x/\tau) \\ M_b &= M_m \sin(wt + \pi/3)\cos(\pi x/\tau - \pi/3) \\ M_c &= M_m \sin(wt - \pi/3)\cos(\pi x/\tau + \pi/3) \end{aligned}\right\} \quad 4.2$$

where $M_m = I_m N$, N = number of effective turns

τ = spacing between pole centres, rads.

and X = position between poles, rads.

Now the effective mmf can be written as:

$$M = M_a + M_b + M_c \quad 4.3$$

$$M = \frac{3}{2} IN \sin(wt - \pi x/\tau) \quad 4.4$$

The flux density is the product of the mmf and airgap permeance and can be written as:

$$B = M\lambda \quad 4.5$$

Assuming a constant permeance (λ) :

$$B = \frac{3}{2} IN \sin(wt - \pi x/\tau) \quad 4.6$$

The airgap force can now be written:

$$F = B^2 / 2\mu \quad 4.7$$

and substituting for B gives:

$$F = \frac{9(IN)^2}{16\mu^2} (1 - \cos(2wt - 2\pi x/\tau)) \quad 4.8$$

SINGLE PHASE OPERATION

For single-phase operation the circuit is as Figure 4.2(b) and the currents can be written as:

$$\left.\begin{aligned} I_a &= I_m \sin(w t) \\ I_b &= \frac{-I_m}{2} \sin(w t) \\ I_c &= \frac{-I_m}{2} \sin(w t) \end{aligned}\right\} \quad 4.9$$

The mmfs produced by each phase can be written as:

$$\left.\begin{aligned} M_a &= M_m \sin(w t) \cos(\pi x/\tau) \\ M_b &= \frac{-M_m}{2} \sin(w t) \cos(\pi x/\tau - \pi/3) \\ M_c &= \frac{-M_m}{2} \sin(w t) \cos(\pi x/\tau + \pi/3) \end{aligned}\right\} \quad 4.10$$

The effective mmf can now be written as:

$$M = \frac{3}{2} IN \sin(w t) \cos(\pi x/\tau) \quad) \quad 4.11$$

which leads to the airgap force:

$$F = \frac{9 (IN)^2}{32 \mu} (1 + \cos(2\pi x/\tau))(1 - \cos(2w t)) \quad 4.12$$

Equations 4.8 and 4.12 are functions of time and position. These equations are shown graphically in Figure 4.3 for various time intervals. The force wave for three-phase operation is a travelling wave and is a standing wave for single-phasing. Any other unbalanced supply condition will give a combination of travelling and standing waves. The resulting vibration will be at exactly twice supply frequency. The same relationship holds for a star connected winding.

4.4 SCIM VIBRATION DUE TO AIRGAP FORCING FUNCTIONS

A force wave travelling uniformly around the airgap will excite all parts of the stator bore equally therefore the level of twice supply frequency vibration circumferentially around the stator's outer surface should be uniform except near the regions where the machine is fixed to its foundation. In these regions the vibration will be reduced. A standing wave however does not excite all parts of the stator bore equally. This allows the stator to vibrate in a definite pattern. The vibration will again be restricted at stator fixing points. The vibration pattern and levels cannot be calculated, due to the complex nature of the structural response of the stator, but can be observed experimentally.

4.5 EXPERIMENTAL INVESTIGATION

The experimental test rig was as described in Chapter 2. Reductions of up to 10% in any one phase voltage were possible at full load without excessive stator winding heating effects. These reductions were achieved by inserting resistance into the supply lines. A 100% reduction, i.e. single-phasing, was possible on no load operation. The twice supply frequency vibration component, 100 Hz, was monitored circumferentially around the stator.

To establish that the twice supply frequency vibration was unaffected by load, tests were conducted at no load and full load operating conditions with a nominally balanced supply.

Figure 4.4 shows the results of these tests. It is clear that there are no significant differences between the two extreme operating conditions. This is because the SCIM operates with approximately constant fundamental airgap flux at all load conditions.

Tests were performed for reductions of 2.5%, 5.0% and 10% in each phase voltage in turn. These reductions represent unbalance in supply of 0.84%, 1.69% and 3.45% respectively. The results of these tests are shown in Figures 4.5, 4.6 and 4.7.

Figure 4.8 shows the effect of single-phasing each phase in turn on no load. These results show that the 100 Hz vibration component is extremely sensitive to changes in supply unbalance.

Single-phasing/ vibration tests were also conducted with the test machine connected with a six pole winding but still operating with the same total flux as per the four pole winding. The results of these tests are shown in Figure 4.9. There is, again, a significant change in the 100 Hz vibration component.

The 100 Hz vibration component is only one of many vibration components of a SCIM. If there is an increase in the 100 Hz component then there will also be an increase in the overall vibration level and a case could be made for monitoring the overall level as an indication of unbalanced supply. This would not be satisfactory as other factors such as load changes

and broken rotor bars can affect the overall vibration level and in any case the change in overall level due to unbalanced supply would be comparatively small. Figure 4.10 compares the overall vibration level with the 100 Hz level for increasing supply unbalance.

The (2-s)f component of axial flux also increases with unbalanced supply (10). Figure 4.11 shows that the 100 Hz component of vibration is more sensitive than the (2-s)f component of axial flux to small changes in supply unbalance.

4.6 USING THE VIBRATION SIGNAL TO DETECT UNBALANCED SUPPLY

It has been shown that the 100 Hz vibration component is extremely sensitive to supply unbalance. It can therefore be used in the detection of this condition. Care must be taken to choose an appropriate position on the stator for placement of the transducer. This will depend on the machine structure and its mountings. For the type of mounting used in these experiments the optimum positions are at approximately 100° from the top centre of the structure. The use of twice supply frequency vibration monitoring in detecting unbalanced supply has several advantages. These are:

(1) Vibration monitoring of electrical machines for mechanical faults is widely used in industry and the detection circuits could be paralleled up with existing monitoring circuits.

(2) The twice supply frequency vibration appears on all SCIMs and all other a.c. machines regardless of numbers of pole pairs or shaft speed whereas the principal component of axial flux which can be monitored for unbalanced supply is dependent on both of these variables (9, 10).

(3) There are none of the insulation problems of attaching instrumentation to the supply that are associated with electrical protection methods.

(4) Protection would be non-invasive requiring transducers on the outer surface of the stator core or frame and therefore relatively inexpensive.

The electronic circuitry required for detecting excessive 100 Hz vibration is straightforward and could be based on the block diagram of Figure 4.12 with typical wave forms as shown in Figure 4.13.

4.7 CONCLUSIONS

It has been shown in this chapter that the twice supply frequency airgap electromagnetic force wave is affected by unbalanced supply. Unbalanced supply therefore affects the twice supply frequency vibration. The experimental results show that the magnitude of the 100 Hz vibration component is a function of supply unbalance and transducer position. Optimum positions for detecting unbalanced supply via the vibration signal exist, for the type of stator mounting used in the

experiments, at approximately 100° from the top centre of the stator. Simple analogue electronic circuitry has been proposed which will detect excessive 100 Hz vibration and give an alarm.

It is expected that other types of machine mounting, e.g. vertical and flange (cantilever), will exhibit different twice supply frequency vibration patterns when supplied from an unbalanced three-phase voltage source. This is because of the position of fixed nodes determined by the mounting arrangement. Further work is required to determine the effect of unbalanced supply on the twice supply frequency vibration for these other types of machine mountings.

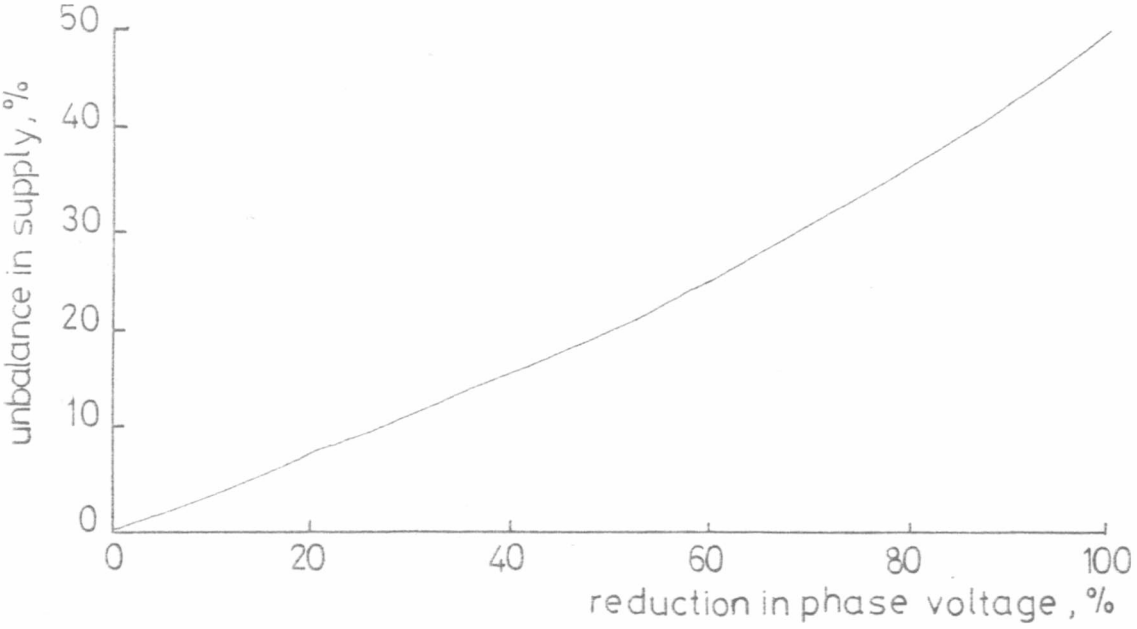

Figure 4.1 Unbalance in supply Vs. reduced phase voltage

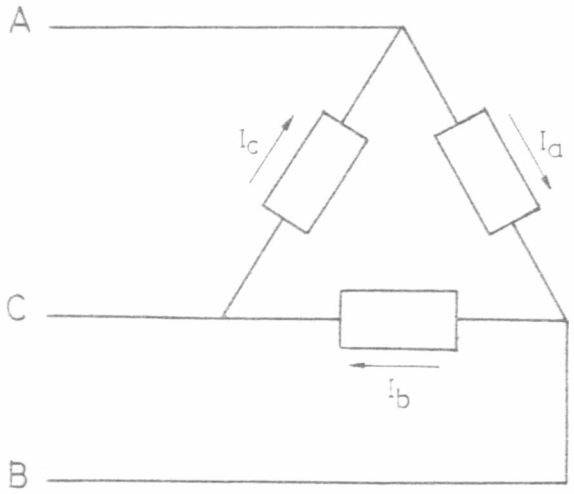

[a]

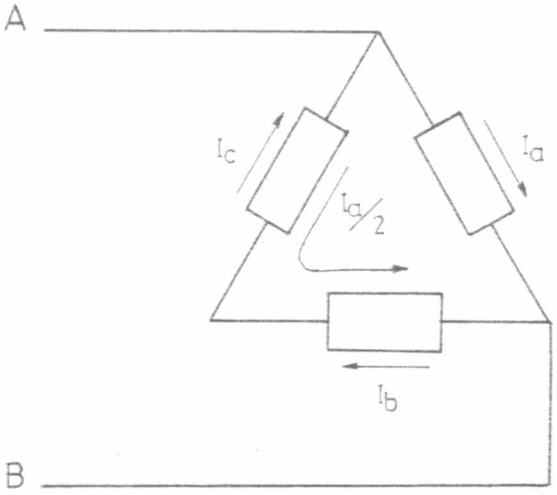

[b]

Figure 4.2 Modes of operation

[a] balanced three-phase

[b] single-phasing

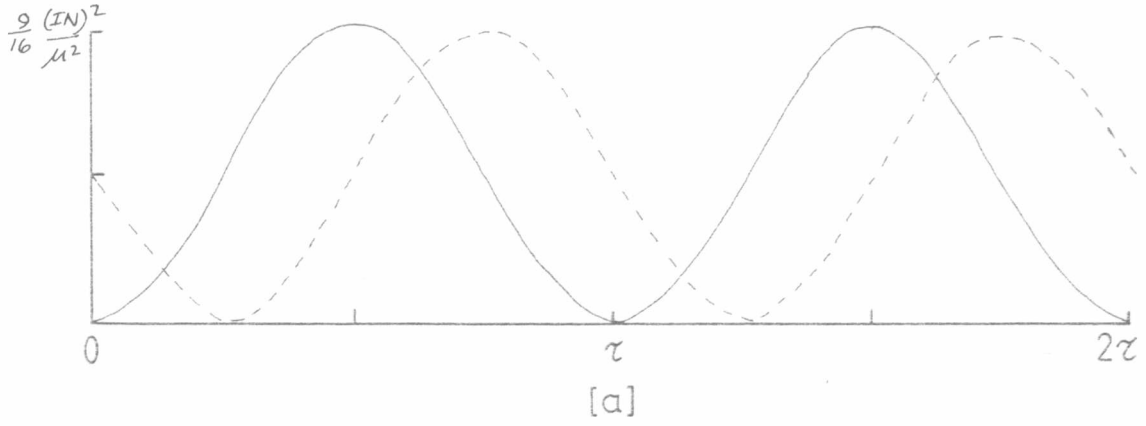

[a]

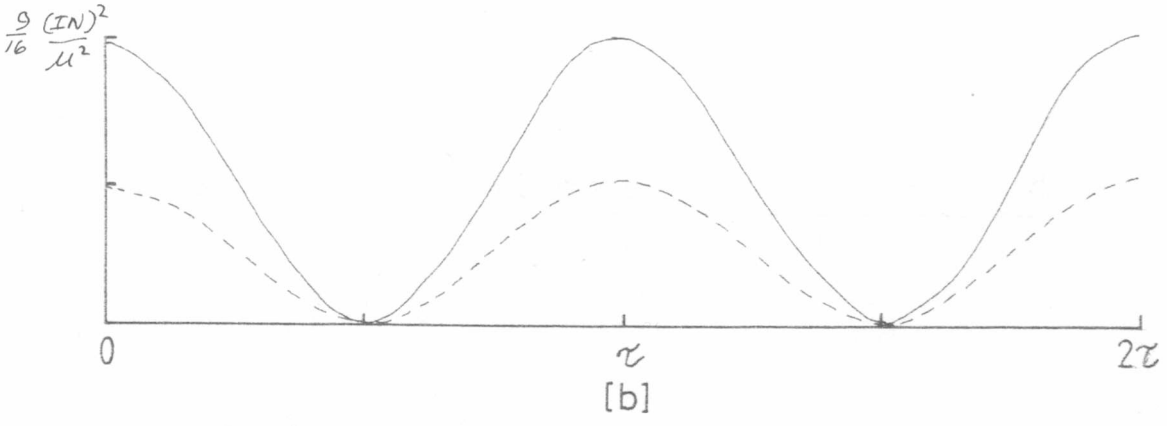

[b]

Figure 4.3 Fundamental airgap forces
[a] balanced three-phase
[b] single-phasing

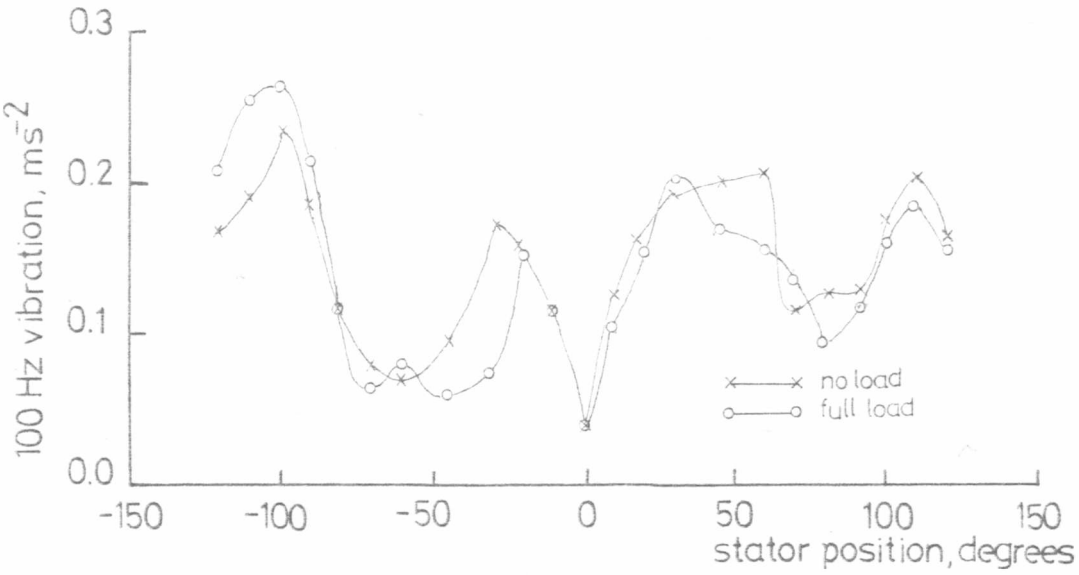

Figure 4.4 Comparison of 100 Hz Vibration - full load + no load

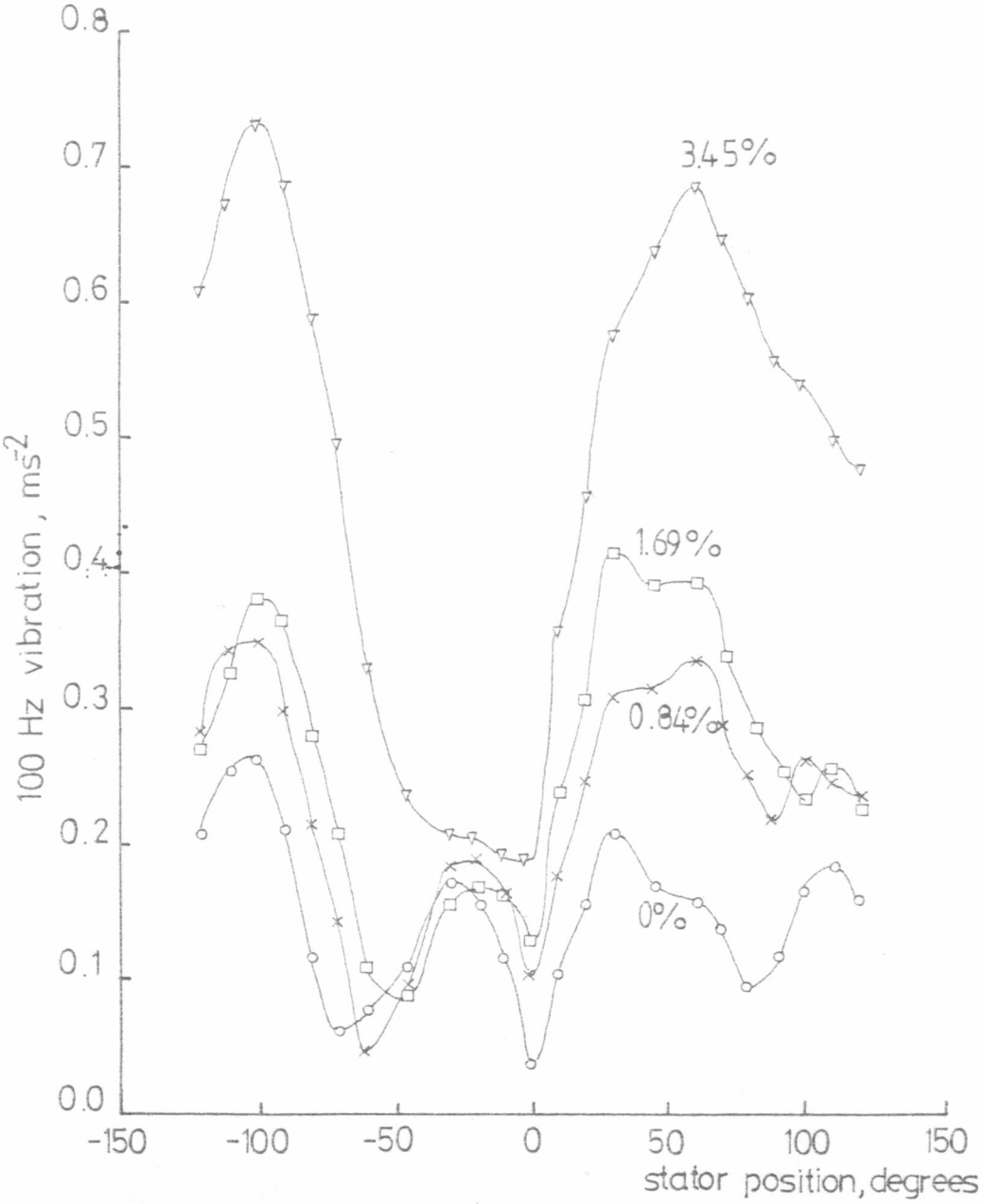

Figure 4.5 Vibration with unbalanced supply – Phase1 Full load

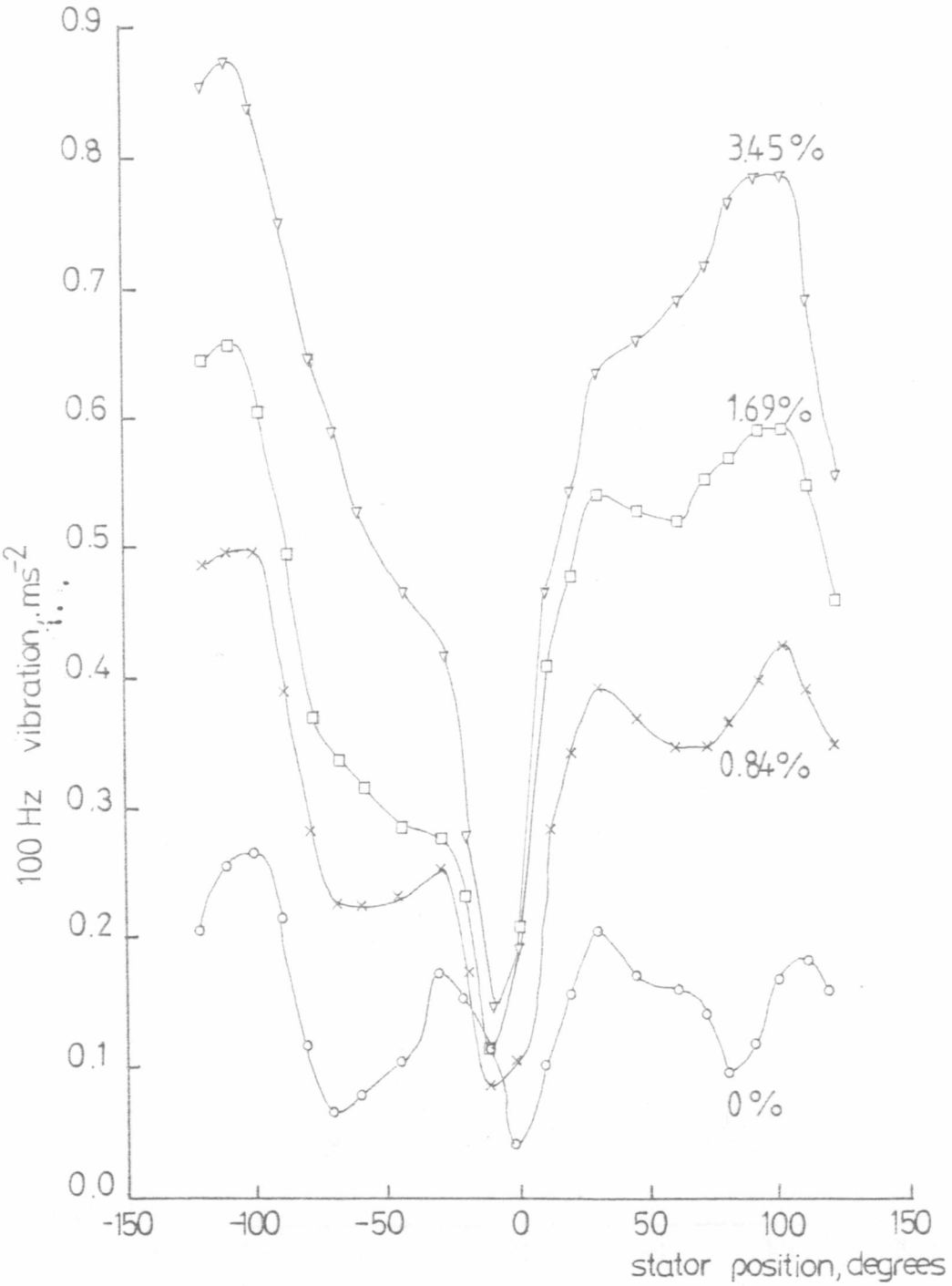

Figure4.6 Vibration with unbalanced supply – Phase 2 Full load

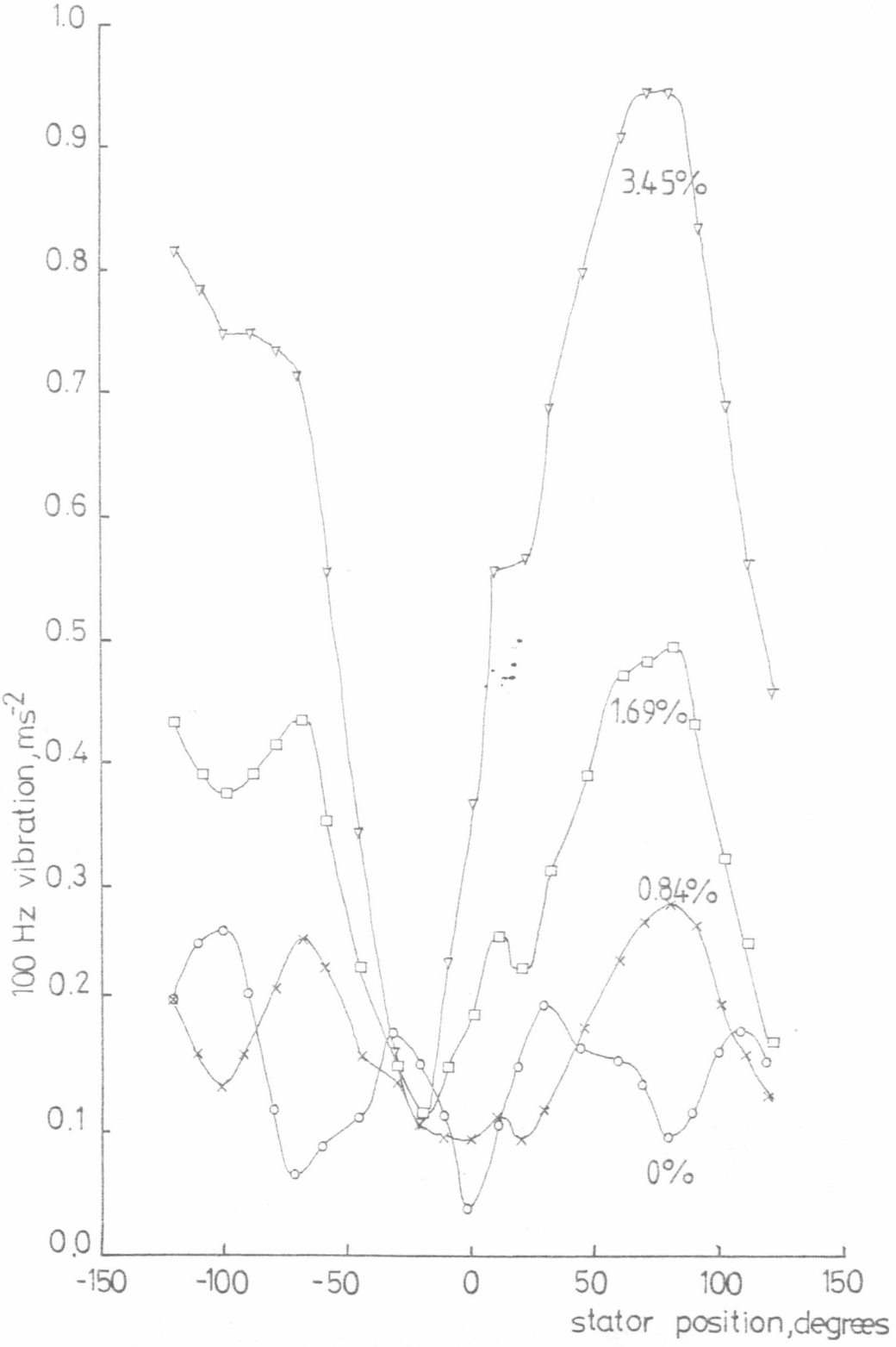

Figure 4.7 Vibration with unbalanced supply – Phase 3 Full load

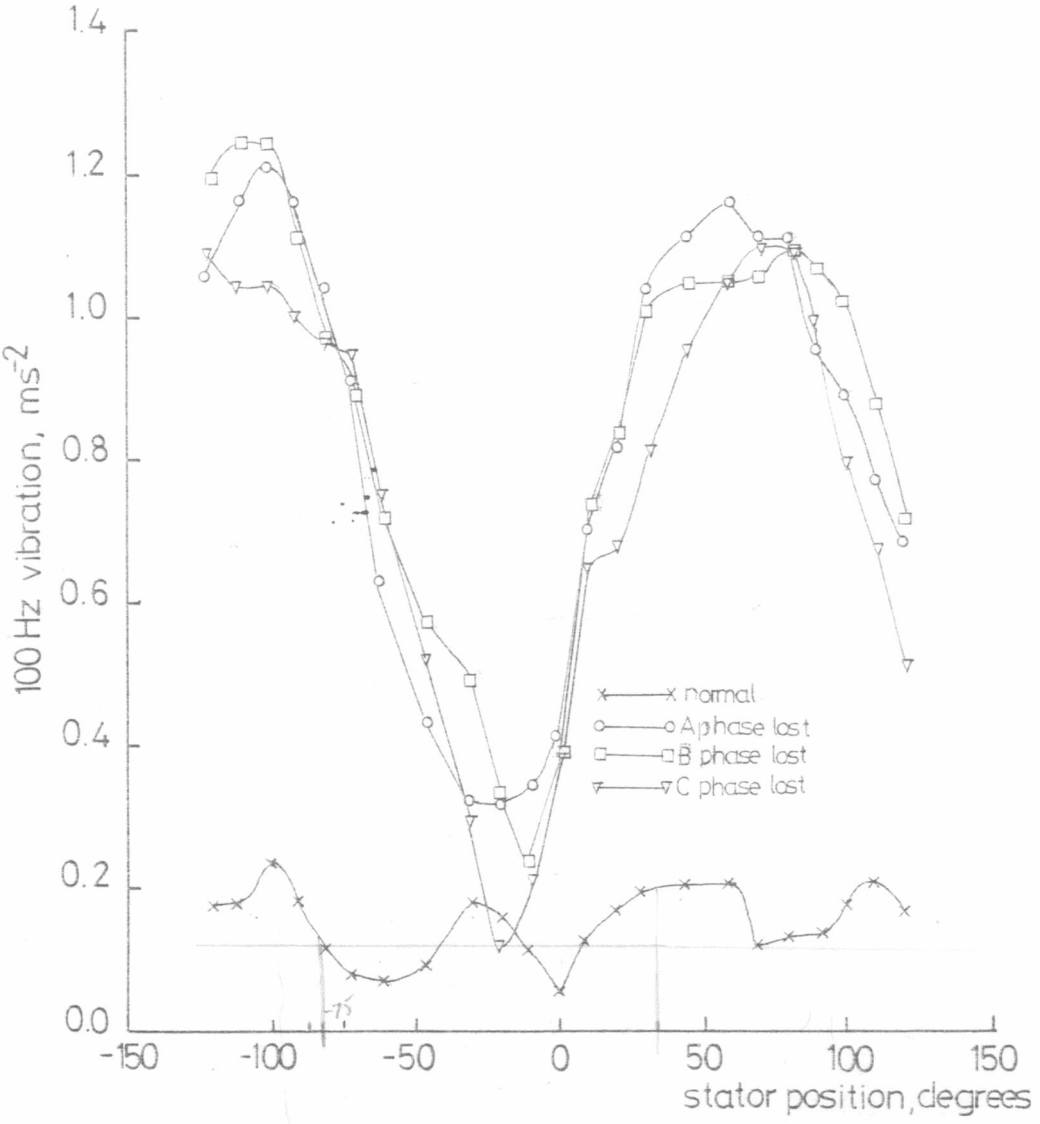

Figure 4.8 Vibration/Single-Phasing No Load

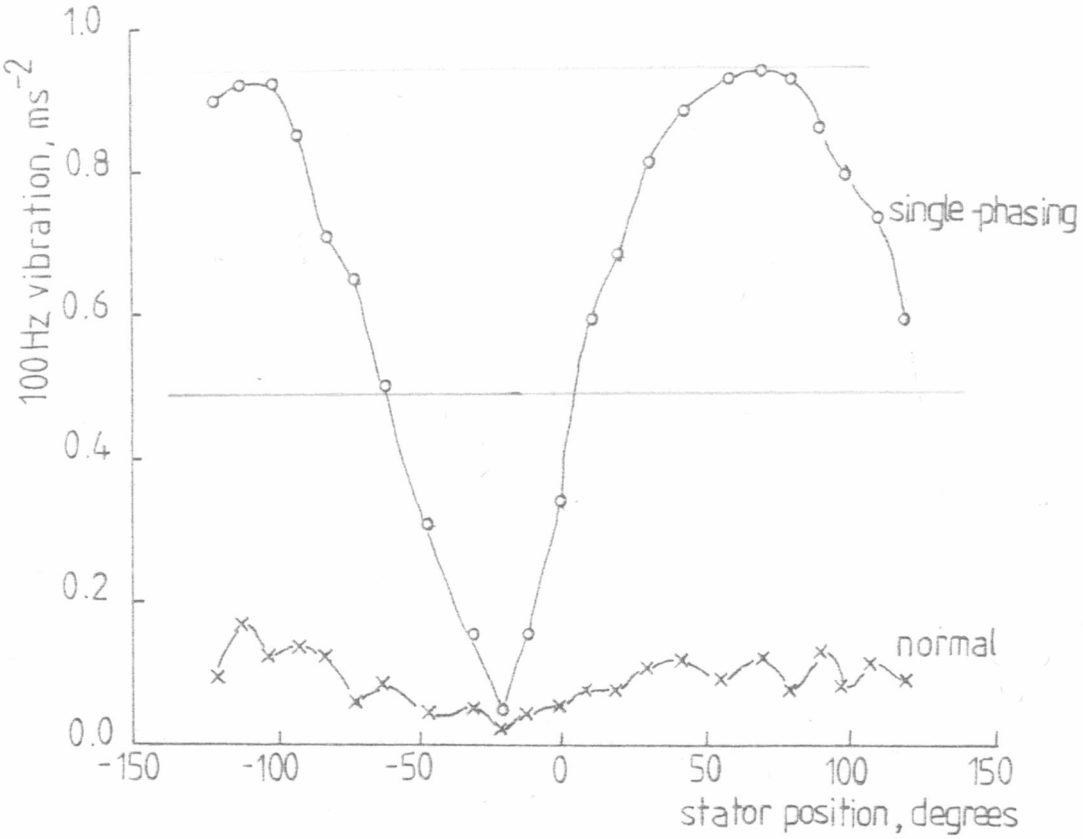

Figure 4.9 Single-phasing — Six Pole Winding

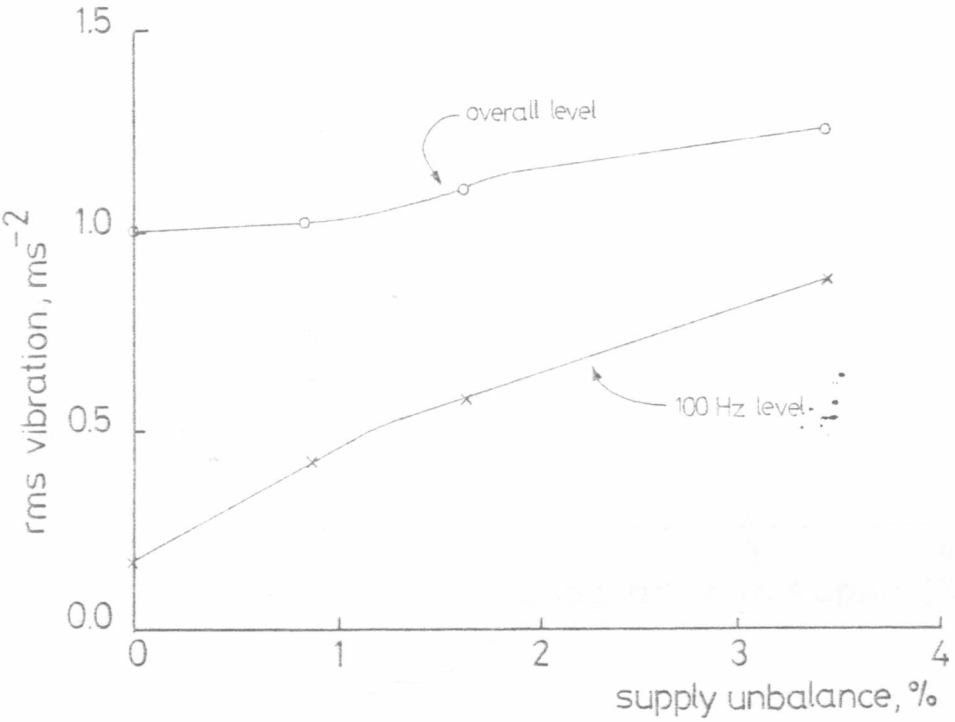

Figure 4.10 Comparison of Overall and 100 Hz Vibration Levels with Supply Unbalance

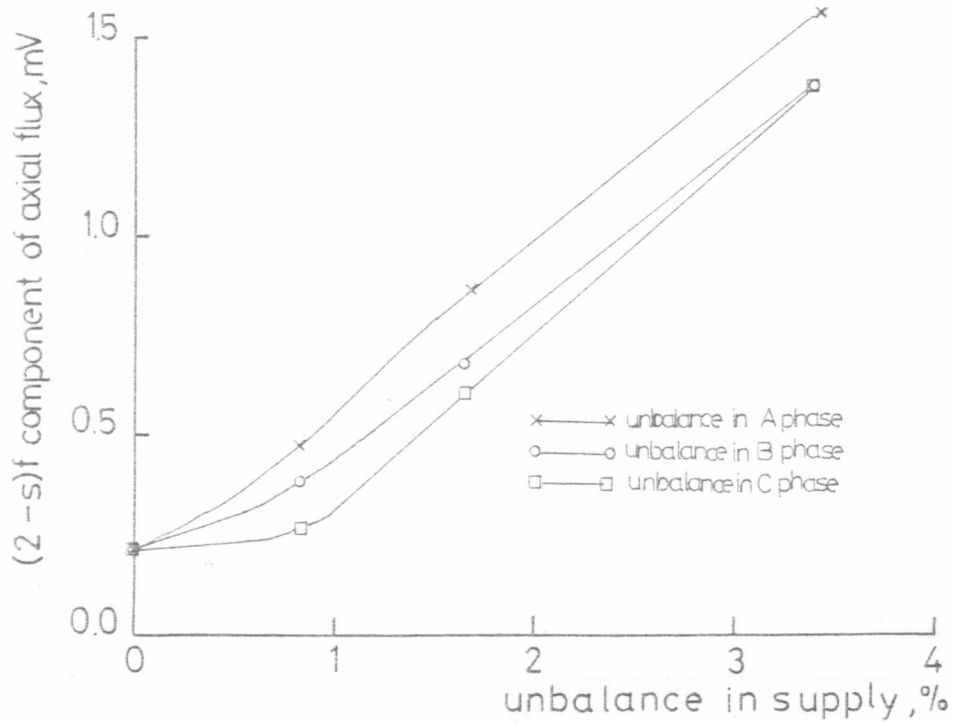

Figure 4.11 (2 - s)f axial flux Vs. supply unbalance

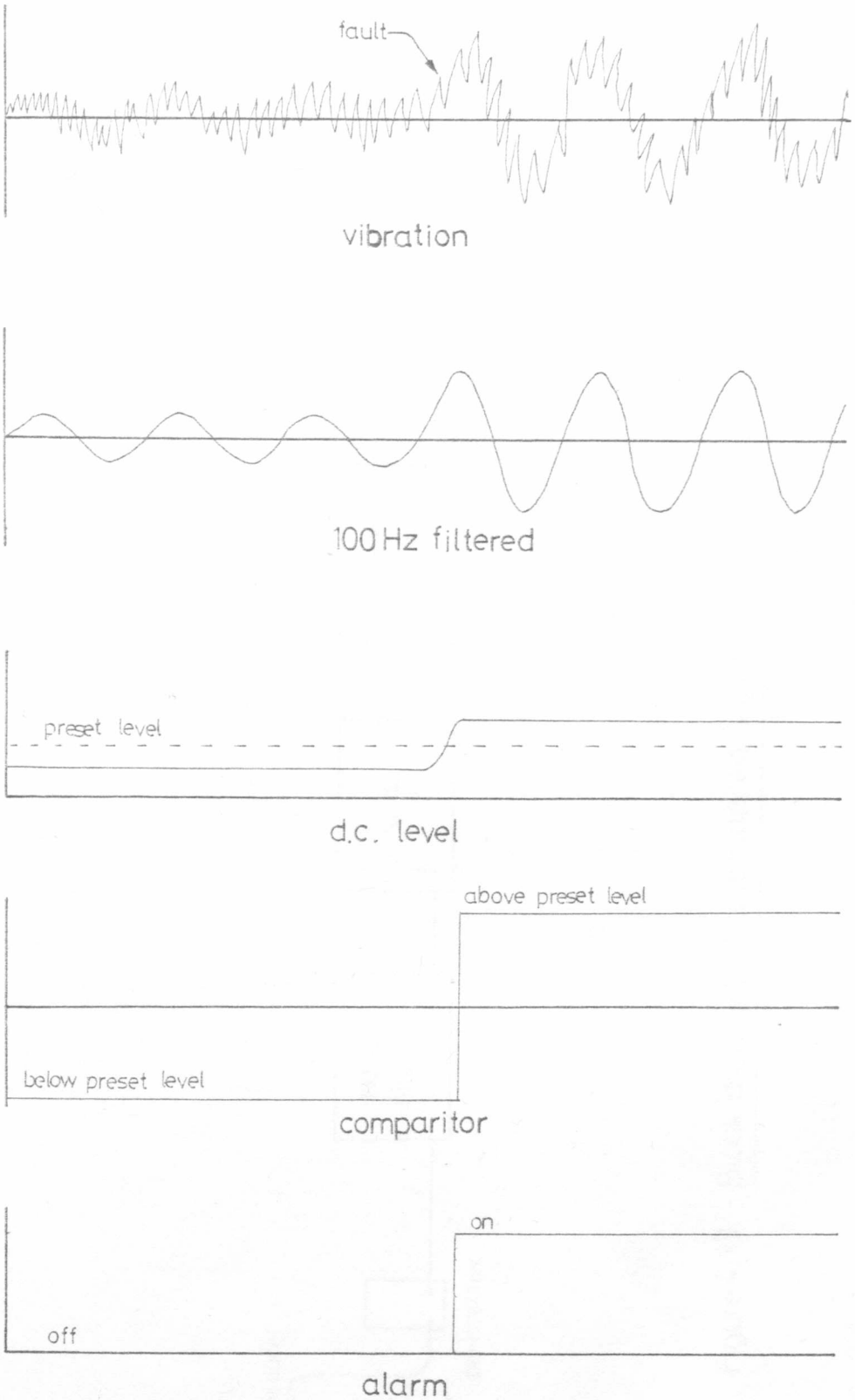

Figure 4.12 Typical detection circuit waveforms

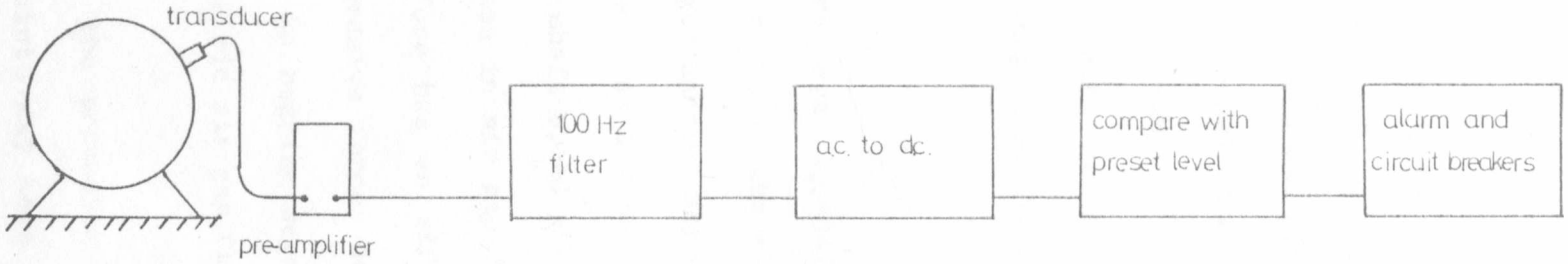

Figure 4.13 Block diagram of unbalanced supply detection circuit

CHAPTER FIVE

THE EFFECTS OF ROTOR FAULTS

5.1 DISCUSSION

SCIMs which are frequently started and stopped are particularly prone to broken rotor bars. The break usually occurs at a bar's connection to the end ring. These failures are due to the combination of thermal stresses and accelerating/decelerating forces (7). In some circumstances a broken bar may lift from its slot causing extensive damage to both rotor and stator. Under exceptional conditions it may be the end ring which breaks.

Broken rotor bars cause a local increase in the air gap flux and increased currents in the adjacent bars. Since the broken rotor bar no longer carries any current it cannot contribute to the total torque. As a consequence the torque will be non-constant and the shaft speed will fluctuate (see APPENDIX III). The local increase in air gap flux causes unbalanced magnetic pull and therefore has an effect on vibration and acoustic noise. The excessive forces due to unbalanced magnetic pull will contribute to bearing wear as will the bearing currents due to the asymmetric air gap flux.

Occasionally in the production of a squirrel-cage rotor the bars and/or joints may have non-uniform resistance. The effects of high resistance joints are similar to those of

broken rotor bars and an effort must be made to distinguish between the two conditions.

Hans Gorges (19) was the first to investigate the effects of unbalanced rotor windings showing how an unbalanced wound rotor winding could be used to make an induction machine run at approximately half normal speed. Jones (14) has analysed this effect using symmetrical components to show how a field (current) component exists at (2s - 1) f Hz. This type of analysis was later used by Vas (20) but it could not be fully extended to the case of the squirrel-cage rotor. Ito et al (21) used finite element analysis of the airgap field to determine rotor bar currents, unbalanced magnetic pull and the pulsating torques. Williamson and Smith (22) have produced an excellent theory based on rotor mesh currents. Their experimental machine, however, was somewhat unusual in that the rotor bars were actually in the stator while the three-phase winding was in the rotor.

Various methods have been used in the attempt to detect rotor faults. The modulation of the fundamental current by the (2s - 1)f component gives ammeter pulsations at twice slip frequency (2sf). These pulsations can therefore be regarded as an indication of rotor faults but an experienced operator is required to distinguish between the pulsation and fluctuations due to random load changes. Gaydon (23) has developed instrumentation to detect changes in shaft speed but stated that "inherent rotor asymmetries can give period fluctuations of the same magnitude as when one bar was open circuited".

Hargis et al (24) have shown how spectral analysis of the current and vibration waveforms can indicate rotor faults. No attempt has been made to explain the spectral changes in the vibration signal and the results presented for this are by no means extensive as the comparison of 'good' and 'bad' rotors is only between similar machines. Pozanski (25) has shown how the acoustic noise is changed by rotor faults. This technique is not a viable proposition in the typical noisy industrial environment.

The work detailed in this chapter will show for the first time how sidebands appear around the slot harmonics of current, vibration, axial flux and end winding leakage flux. An experimental investigation will then be presented showing how the sideband content in these signals varies for different numbers of broken rotor bars and high resistance joints.

5.2 SIDEBAND COMPONENTS

Applying machine theory to rotor asymmetrics gives the standard result of an additional air gap flux component at a frequency of $(2s - 1)f$ Hz (14). If the third time harmonic (3f) of the fundamental supply voltage is considered as another source (due to saturation effects) then, by argument a component of flux will exist in the airgap field at $(2s_3 - 1)f_3$ Hz.

But $S_3 = (3W_s - W_r)/ (3W_s)$

where W_s = synchronous speed

& W_r = actual shaft speed

Therefore $S_3 = (3 - \frac{W_r}{W_s}) /3$

$$= (2 + (1 - \frac{W_r}{W_s})) /3$$

$$= (2 + S) /3$$

Also $f_3 = 3f$

Therefore $(2s_3 - 1)f_3 = (\frac{2}{3} (2 + s) -1) 3f$

$$= \underline{(2s + 1) f} \qquad \text{——————} \quad 5.1$$

So when there are rotor asymmetrics the fundamental air gap flux has sideband components at $\pm 2sf$. The magnitude of the sideband components is dependent on slip. The typical variation in magnitude of the $(2s - 1)f$ component with slip is shown in Figure 5.1.

It is assumed for simplicity that the sidebands have equal magnitudes.

These sideband components can be considered as amplitude modulation so that the fundamental flux can be written as:

$$B = B_m (1 + a \sin (4\pi s\, ft + \phi)) \sin 2\pi ft \qquad \text{——————} 5.2$$

The interaction between the fundamental field (B) and the rotor slots will induce side bands around the slot harmonic components in the air gap field. That is the expected frequency components of the air gap field can be written as:

$$f_B = \sum_{u=1}^{\infty} \sum_{n=0}^{\infty} \left(u \pm \frac{nR}{P} (1 - s)\right) fs$$

$$+ \sum_{u=1}^{\infty} \sum_{n=0}^{\infty} \left(u + \frac{nR}{P} (1 - s)\right) (fs \pm 2sf) \qquad —5.3$$

These frequencies will be expected in the current signal and the leakage flux signals.

The squaring of the flux expression (see Chapter 3) to give the air gap force, and hence the stator vibration frequencies, will give multiple side bands around slot harmonic vibration frequencies.

5.3 EXPERIMENTAL ROTORS

Several rotors were available for rotor fault tests. Initially the test machine contained a nominally 'perfect' 28 slot aluminium die cast rotor.

A nominally identical 28 slot rotor had its connection between a rotor bar and the end ring removed, see Figure 5.2.

A further 28 slot rotor was modified by removing a large portion of the rotor end ring. The material connecting a rotor bar to the end ring was removed and a new end ring was cast and bolted onto the remainder of the existing end ring. This rotor is shown in Figure 5.3.

A 51 slot rotor was constructed specially for the test programme. This rotor had circular copper bars which were soldered into copper end rings. Several connections at each end of the rotor were so manufactured that the rotor/ end ring electrical connections could be made or broken by either inserting and bolting a copper tag or an insulating tag. This rotor is shown in Figure 5.4. When this rotor was used experimentally it was found that when all rotor connections were made that the motor still exhibited signs of rotor unbalance. A model of the end ring and the two types of connection was built to measure the joint resistances. Results of these tests showed that the normally soldered joints had a resistance in the region of 5 - 6 $\mu\Omega$ while the bolted connections were in the order of 21 - 22 $\mu\Omega$. This means

This means that the rotor was in fact always operating with an electrical unbalance.

5.4 CEPSTRUM

The monitored signals were Fast Fourier Transformered (FFTd) by the B & K Spectrum Analyser and displayed on its screen. The PDP11 computer read the Spectrum analyser screened and performed an FFT on the information, assuming the information to be a time varying signal, and wrote the results back to the Spectrum analyser screen. Any periodicity in the original FFT is displayed by a peak in the second FFT. The FFT of an FFT is termed CEPSTRUM (11).

5.5 EXPERIMENTAL RESULTS

5.5.1 28 SLOT ROTORS

Figures 5.5 to 5.18 compare the various spectra for the normal 28 slot rotor and the 28 slot rotor with the new end ring (i.e. one broken rotor bar). Comparing Figures 5.7 & 5.8 (current spectra) the $\pm$2sf sidebands about the supply frequency are clearly visible when there is a broken rotor bar. Figures 5.9 & 5.10 show a principle slot harmonic in the current waveform and again the $\pm$2sf sidebands are present when there is a broken bar present.

Figures 5.11 to 5.18 show spectra for the end winding leakage flux and axial flux signals with the normal rotor and with the broken rotor bar. Again the $\pm$ 2sf sidebands are present around the fundamental supply frequency and the slot harmonic components when there is a broken rotor bar.

Interestingly there is only one pair of sidebands around the slot harmonics in the current, axial flux and end winding leakage flux signals. This was as expected due to equation 5.3.

Figures 5.5 & 5.6 compare the vibration spectra for the normal rotor and for the case of the broken bar. However, there are several sideband pairs around the slot harmonic for the broken rotor bar. Again this is expected.

Figures 5.19 & 5.22 show cepstra of the vibration and the leakage flux signals. The increase in the sideband components in the vibration and leakage flux signals due to the broken bar is highlighted in the cepstra by a dramatic increase in the component at 0.5 secs.

NOTE: The component in the cepstrum which highlights the increased sideband content of the signals is dependent on the value of slip and therefore will not always occur at 0.5 secs. To calculate where the component will occur refer to A.J. Milne's report (11).

5.5.2 51 SLOT ROTOR

As stated in Section 5.3 the 51 slot rotor exhibited signs of rotor unbalance even when all bolted connections were made. This was because of the higher resistance of the bolted joint as compared with the soldered joints (22 $\mu\Omega$ as compared to 6 $\mu\Omega$). It was therefore decided to progressively solder the bolted connections to the end rings. Figures 5.23 to 5.29 show the effects of this experiment on the vibration signal. By the time all the joints had been soldered the sideband contents were much reduced.

Comparison of Figures 5.27 & 5.28 clearly shows the increased sideband content between no high resistance joints and one broken bar. However the difference between sideband components between one and two broken bars is not so pronounced, reference Figure 5.28 & 5.29.

5.6 CONCLUSIONS

It has been demonstrated in this chapter that additional components can be expected in all the signals when the rotor has broken bars or high resistance joints. These additional components appear as sidebands at $\pm$ 2sf around the fundamental supply frequency and the slot harmonics of the current, axial flux and end winding leakage flux signals. In the vibration signal several sideband pairs can be expected around the slot harmonic components. All these components were shown to exist under experimental conditions.

The experimental work done using the 51 slot rotor suggested that it is not possible to distinguish between several high resistance joints and broken rotor bars.

The use of cepstrum has been shown to indicate the presence of sidebands and hence rotor circuit unbalance. Only one component in the cepstrum is required to indicate broken rotor bars. However the cepstrum must be performed on part of the signal where it is known that sidebands would exist under broken rotor bar conditions. The most effective part of the vibration signal for such analysis is around the slot harmonics.

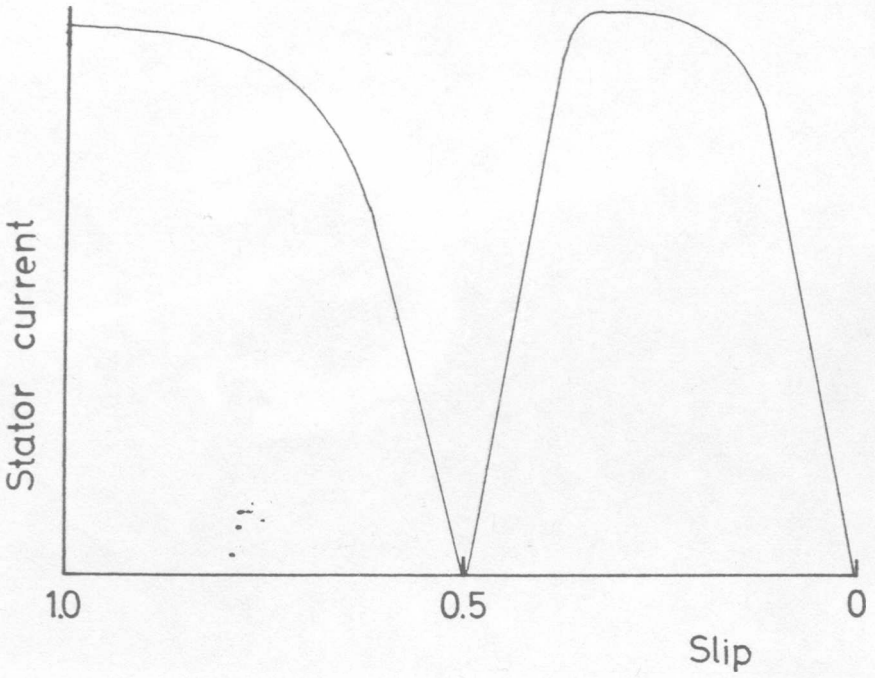

Figure 5.1 Variation of magnitude of (2s-1)f component of stator current

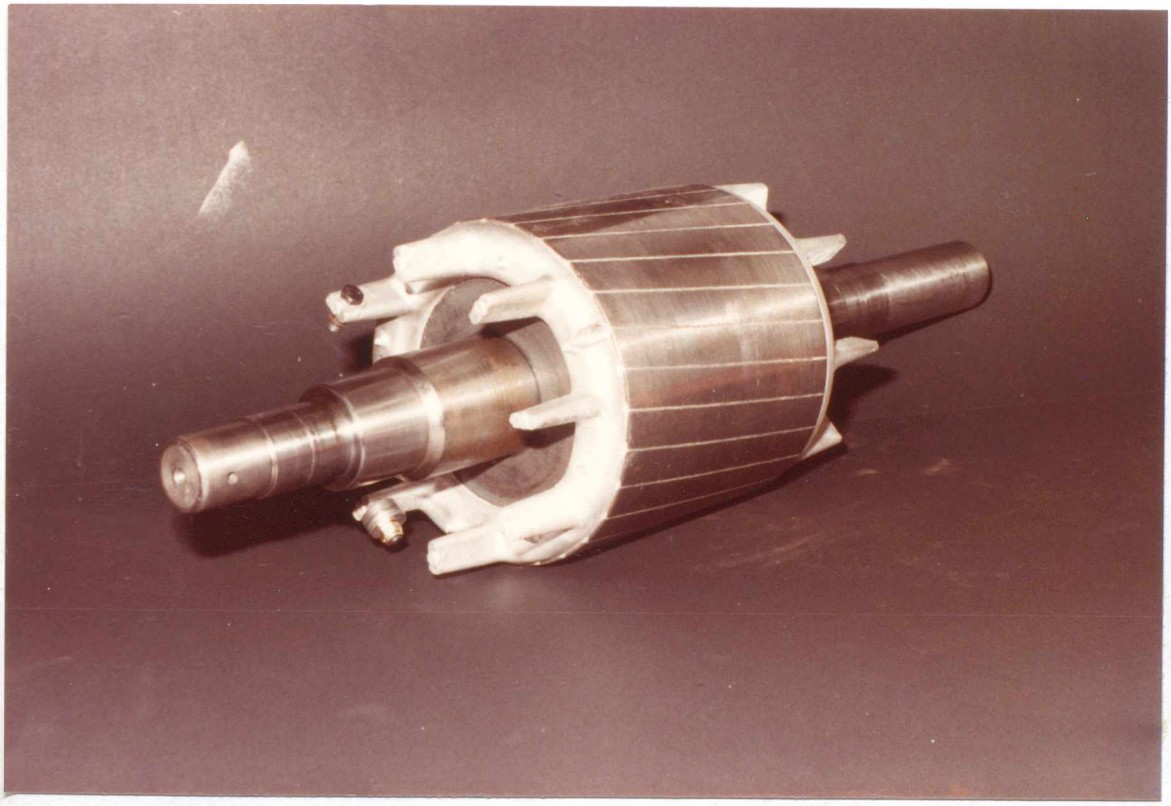

Figure 5.2 28 Slot Rotor – 1 Bar disconnected

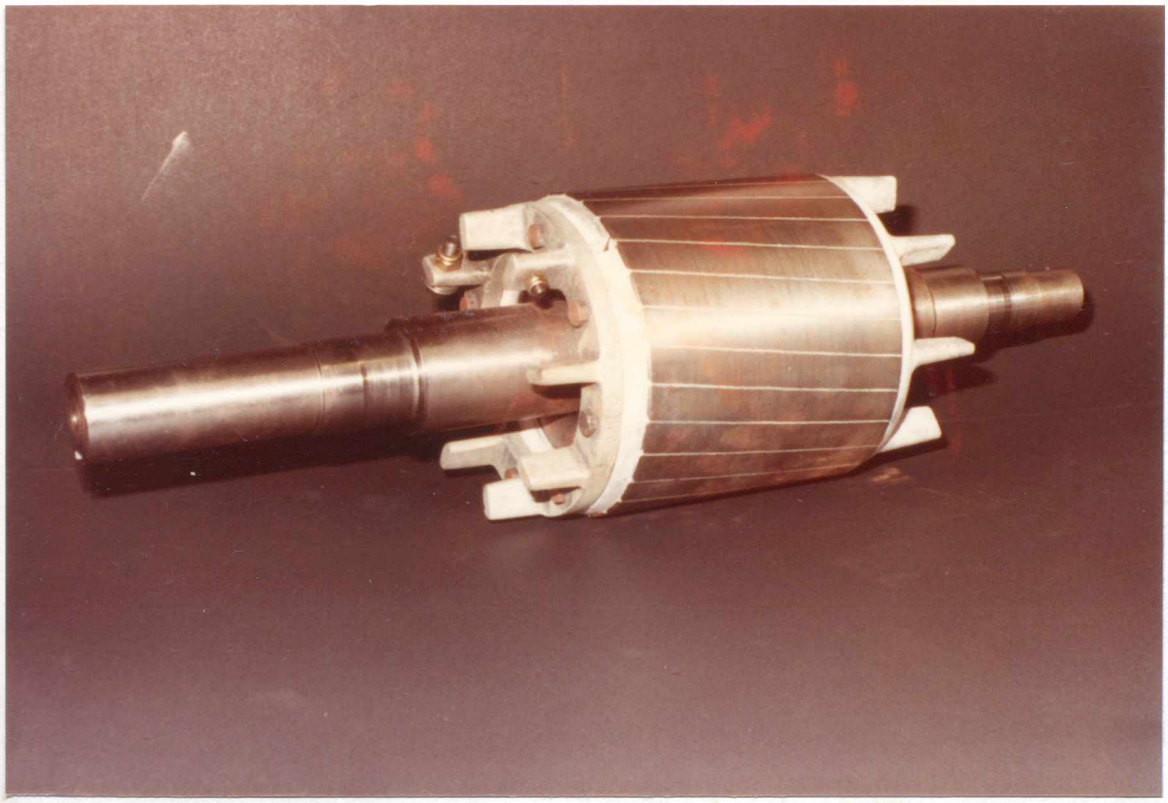

Figure 5.3 28 Slot Rotor – New End-ring

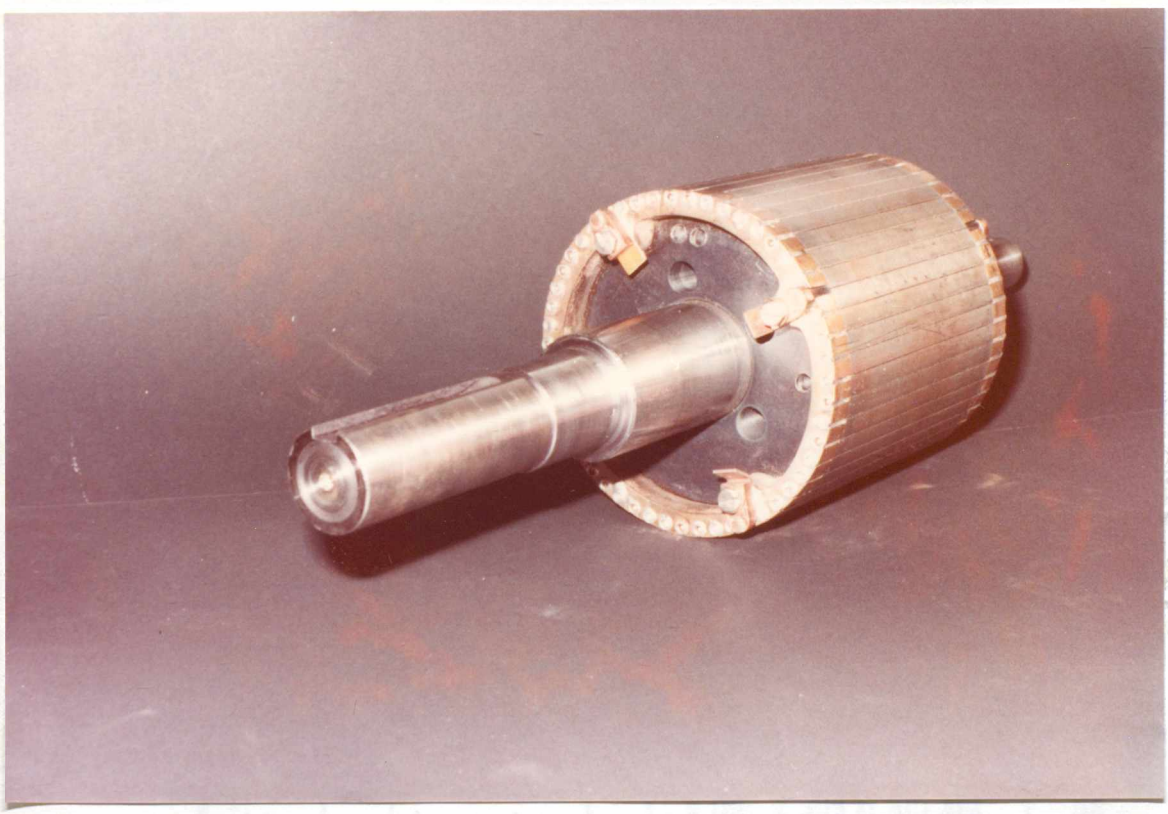

Figure 5.4 51 Slot Rotor

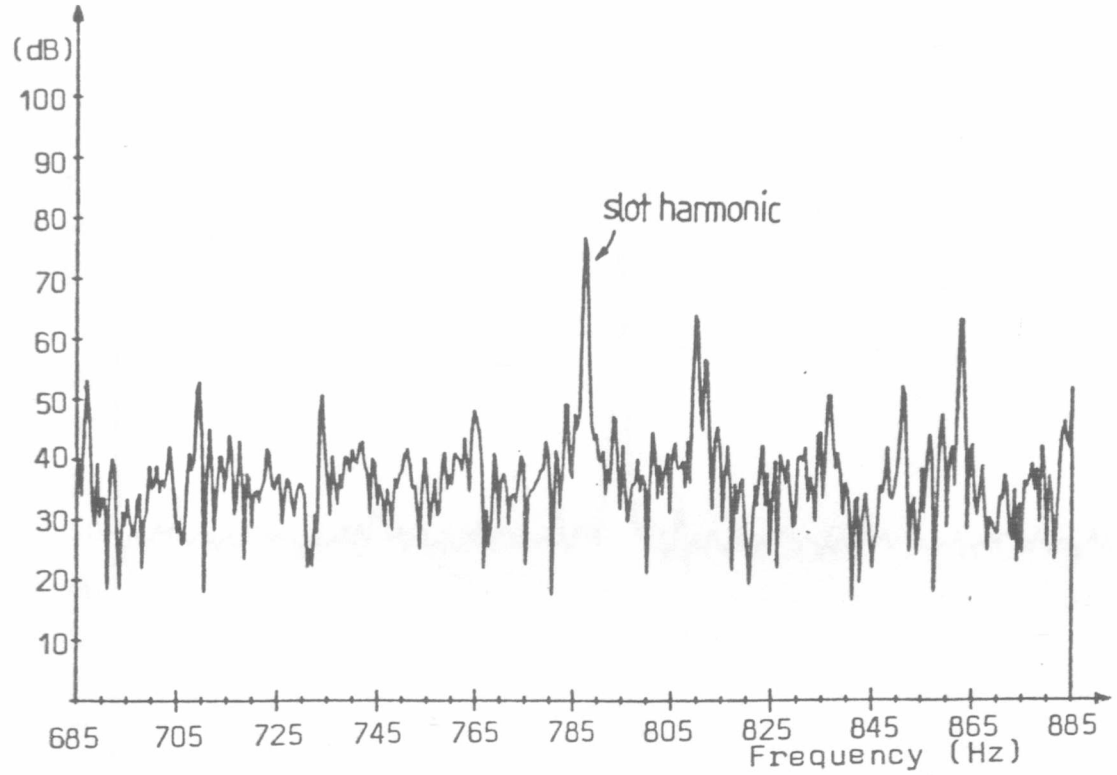

Figure 5.5 Zoom Spectrum Vibration - Normal Rotor

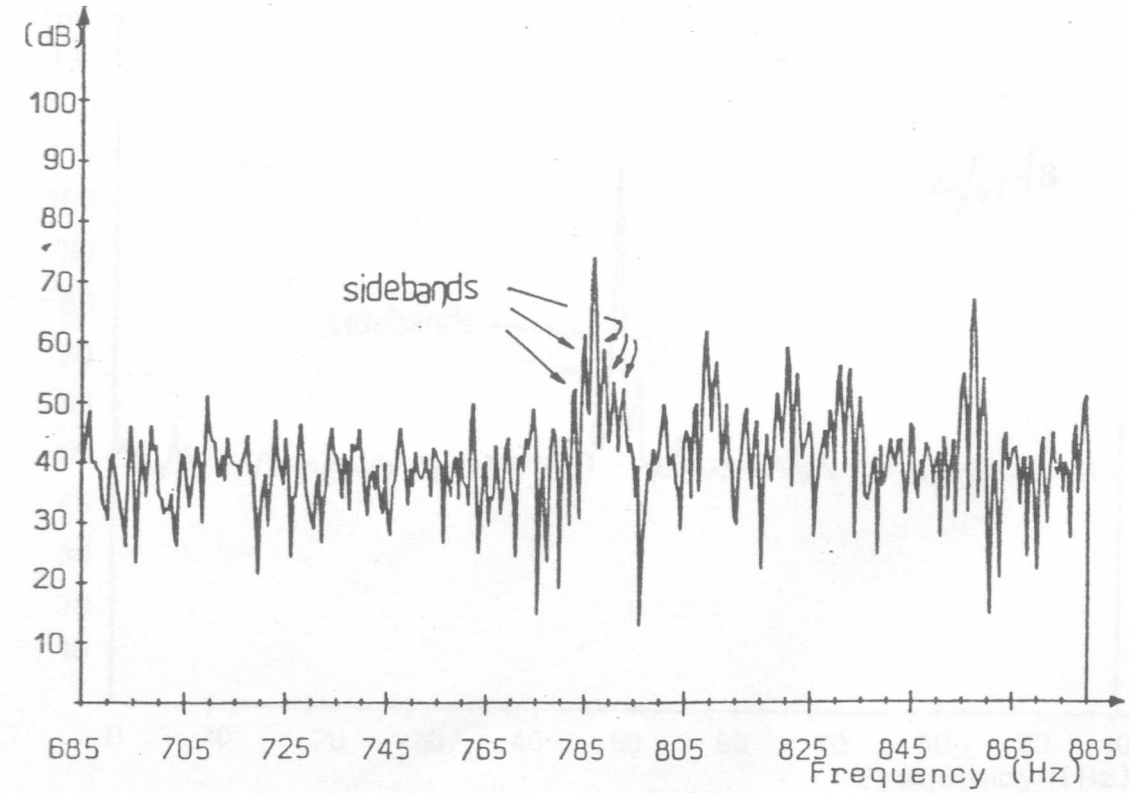

Figure 5.6 Zoom Spectrum Vibration - One Broken Bar

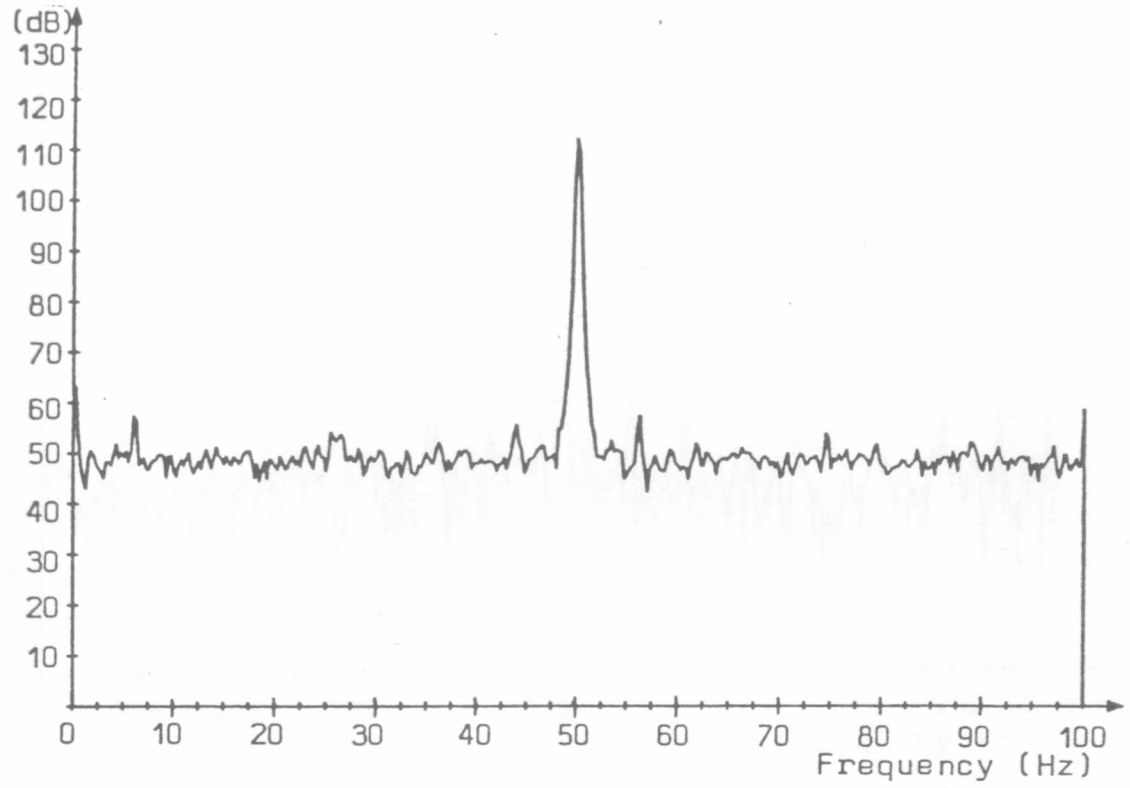

Figure 5.7 Current Spectrum - Normal Rotor

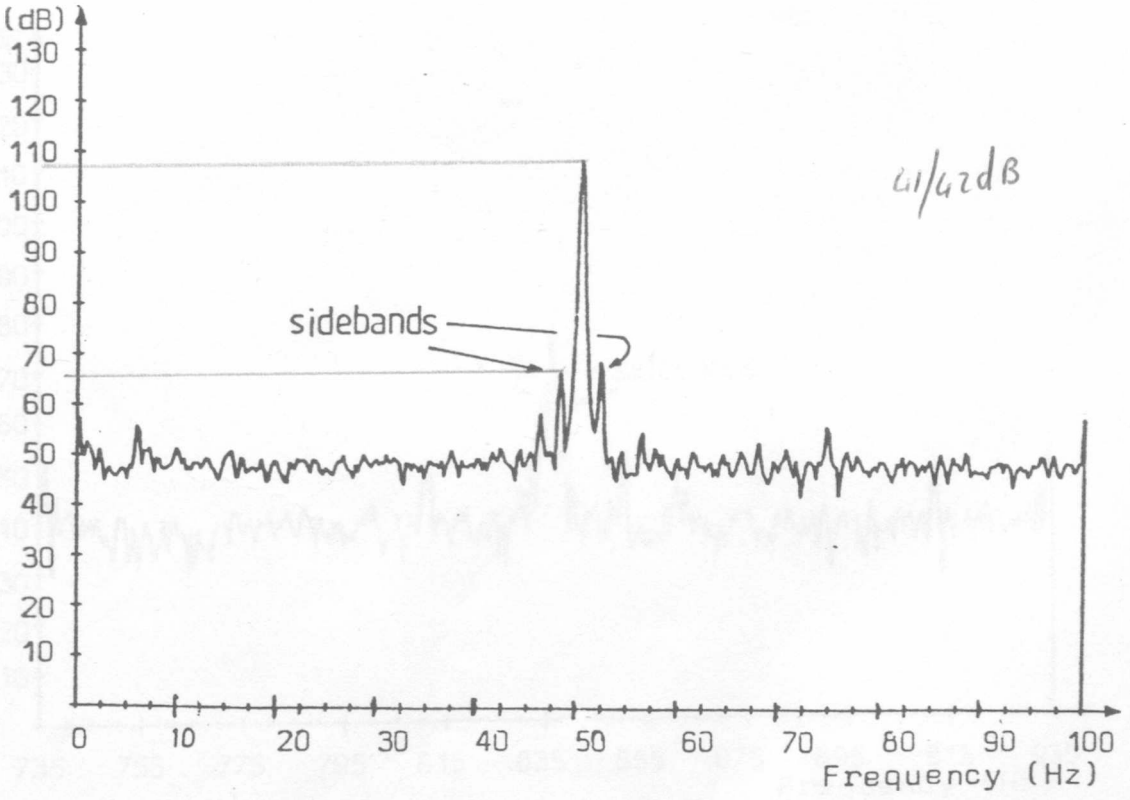

Figure 5.8 Current Spectrum – One Broken Bar

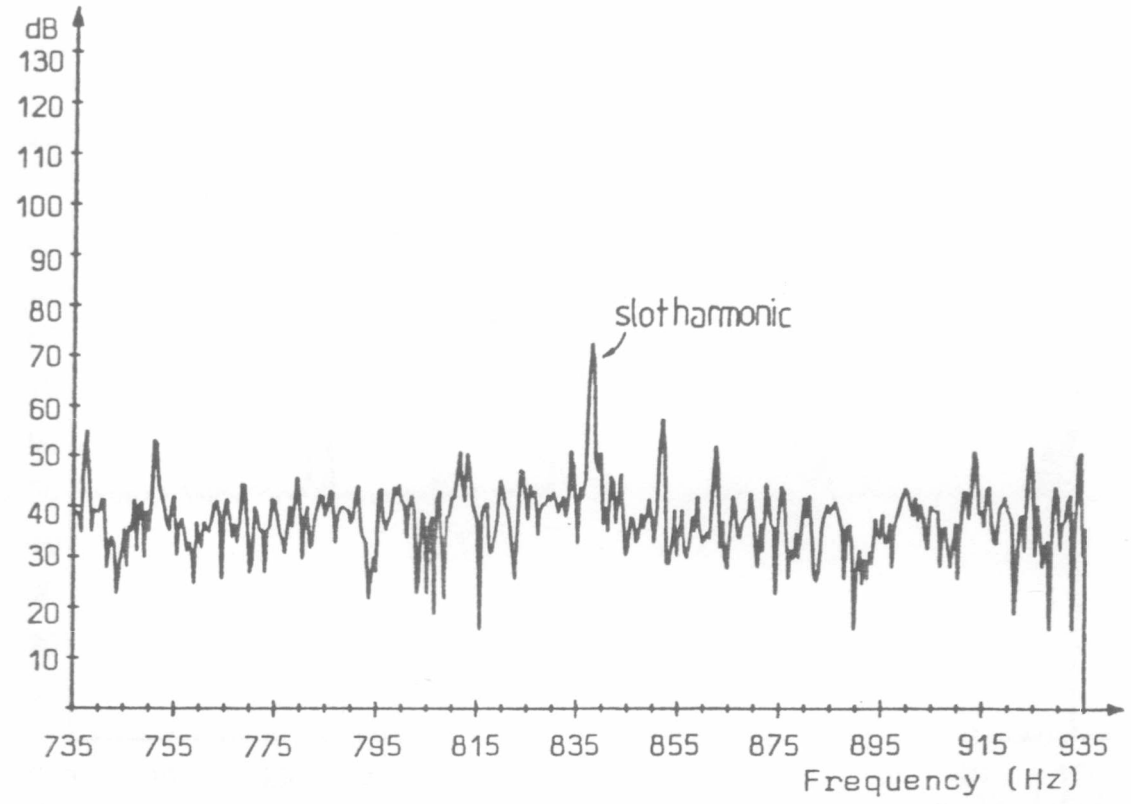

Figure 5.9 Current Zoom Spectrum – Normal Rotor

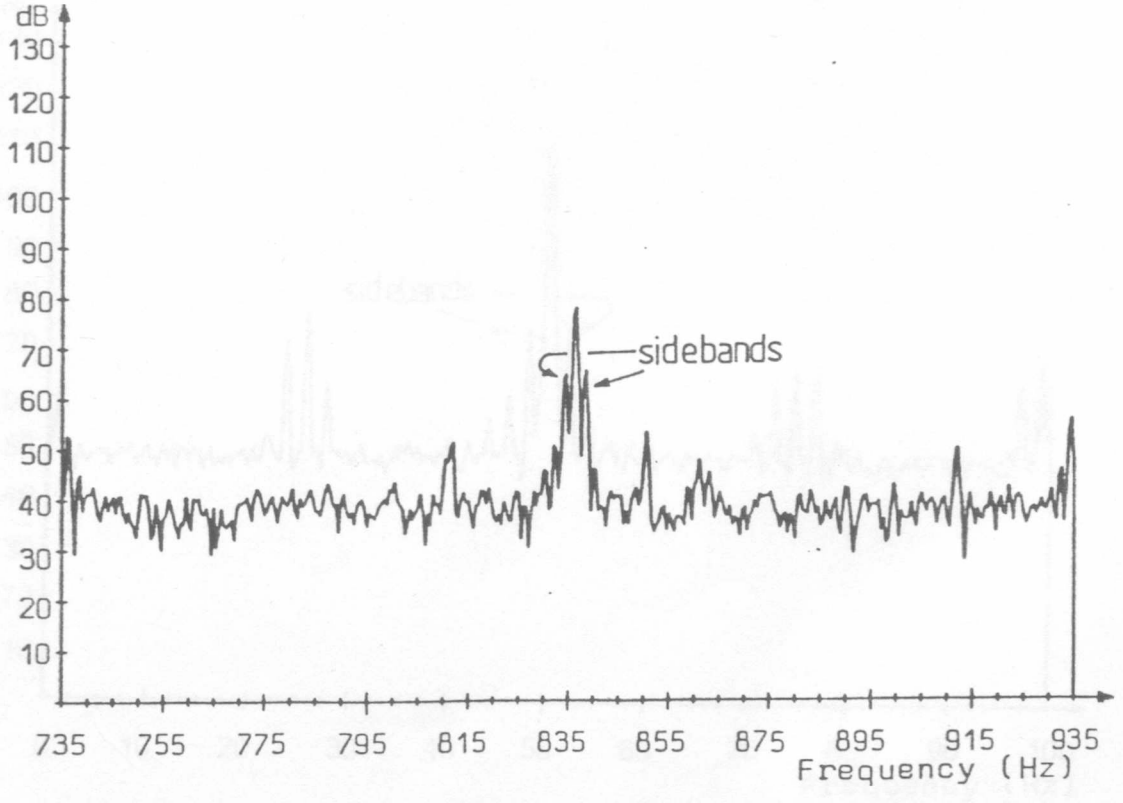

Figure 5.10 Current Zoom Spectrum – One Broken Bar

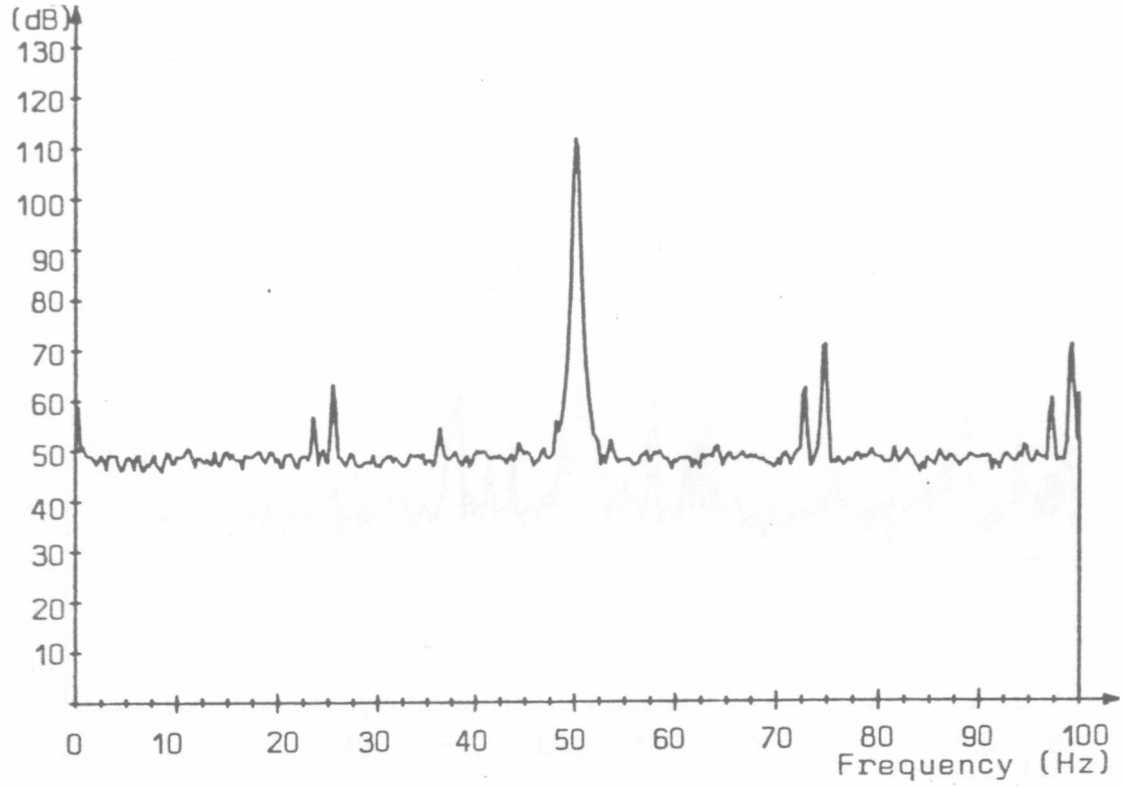

Figure 5.11 Endwinding Leakage Flux - Normal Rotor

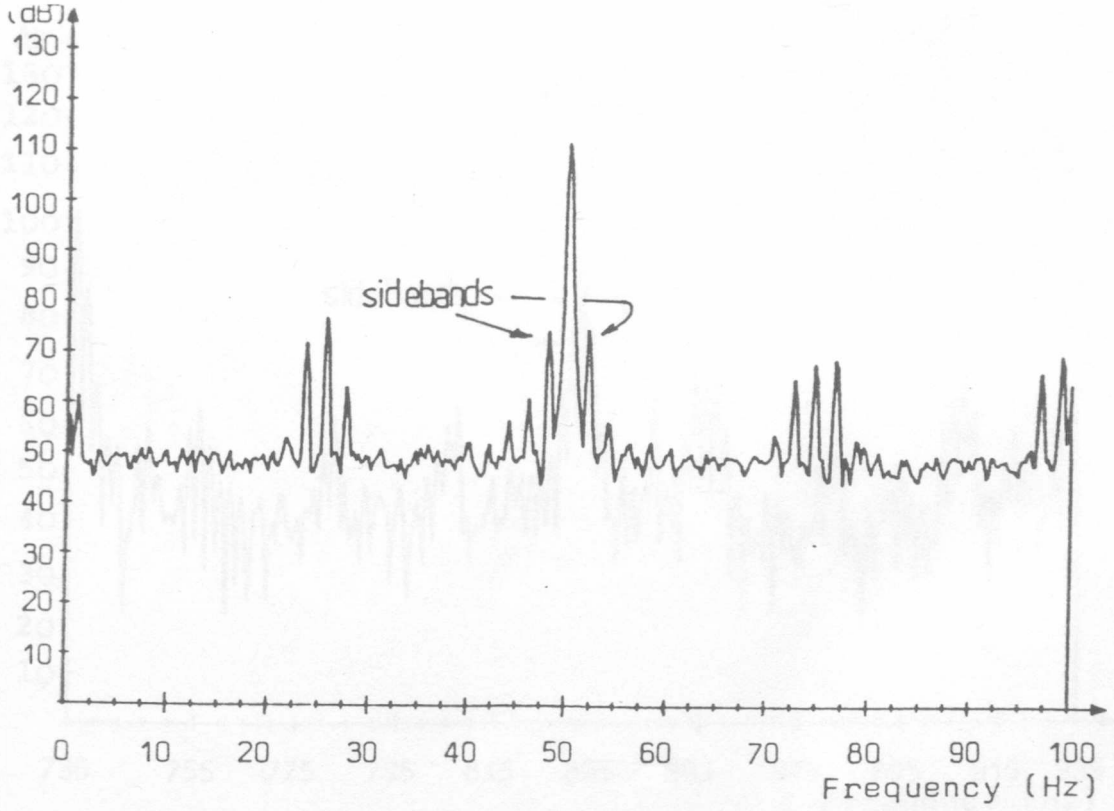

Figure 5.12 Endwinding Leakage Flux — One Broken Bar

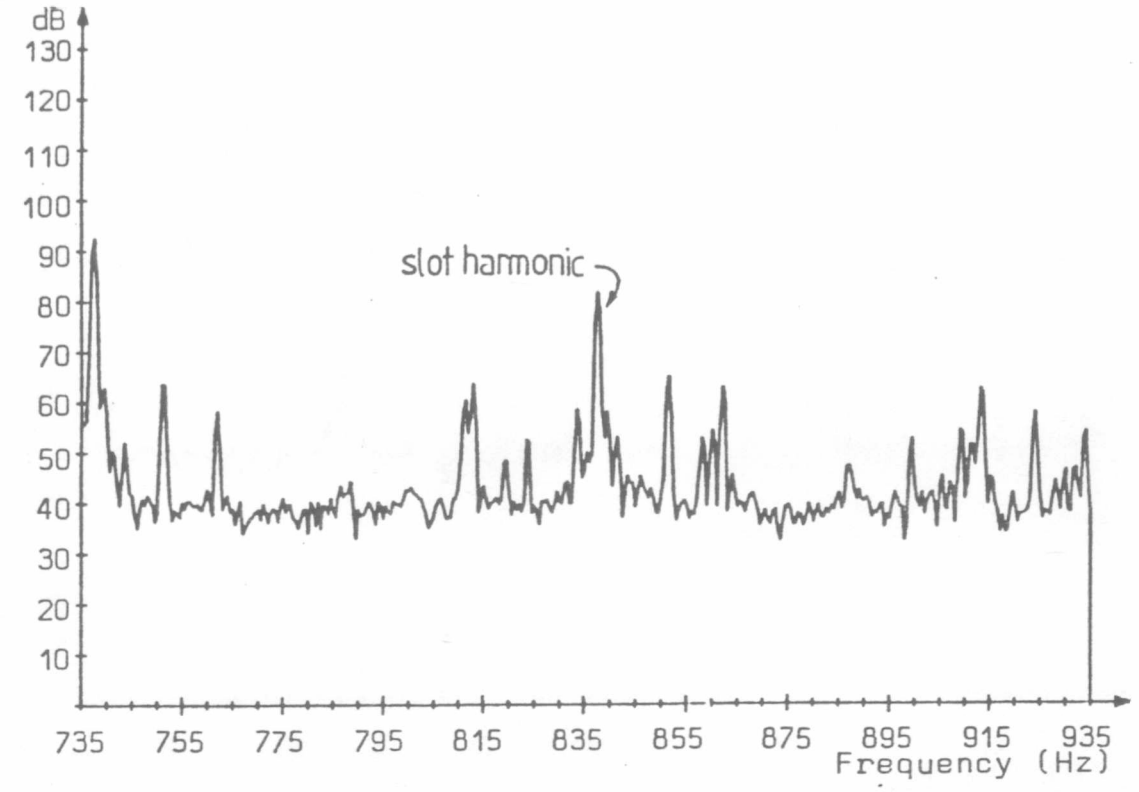

Figure 5.13 Zoom Endwinding Leakage Flux – Normal Rotor

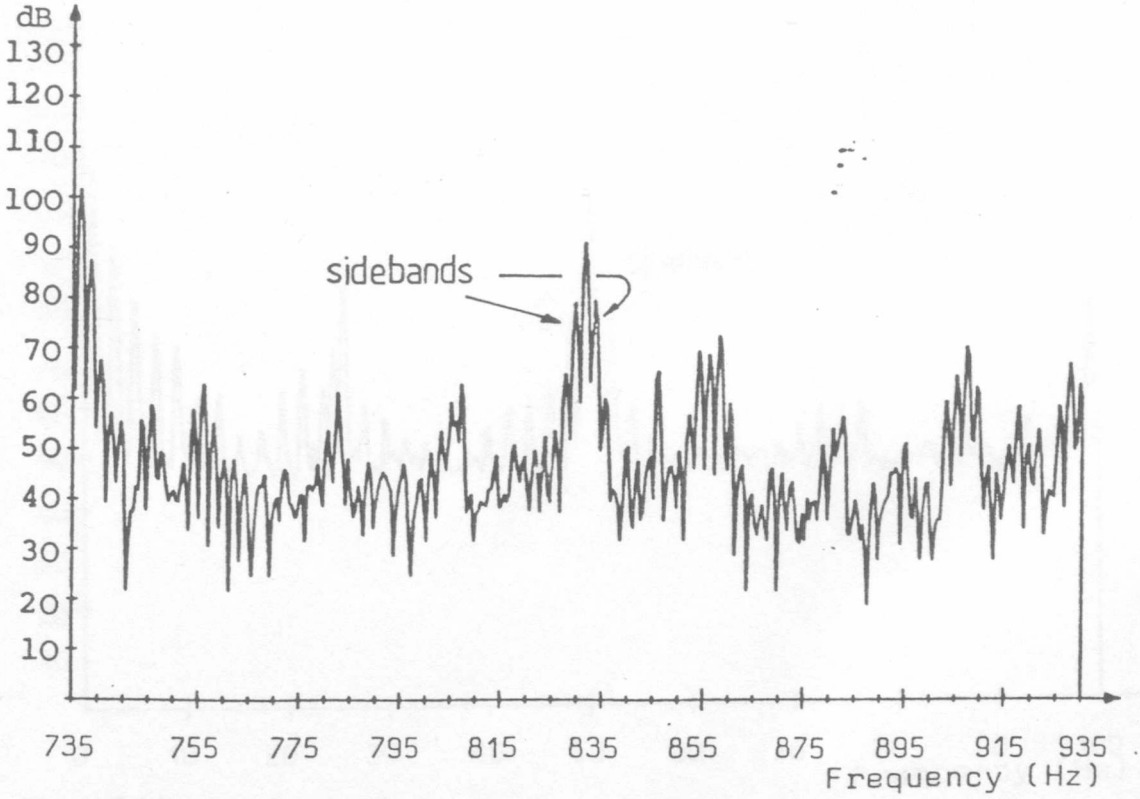

Figure 5.14 Zoom Endwinding Leakage Flux – One Broken Bar

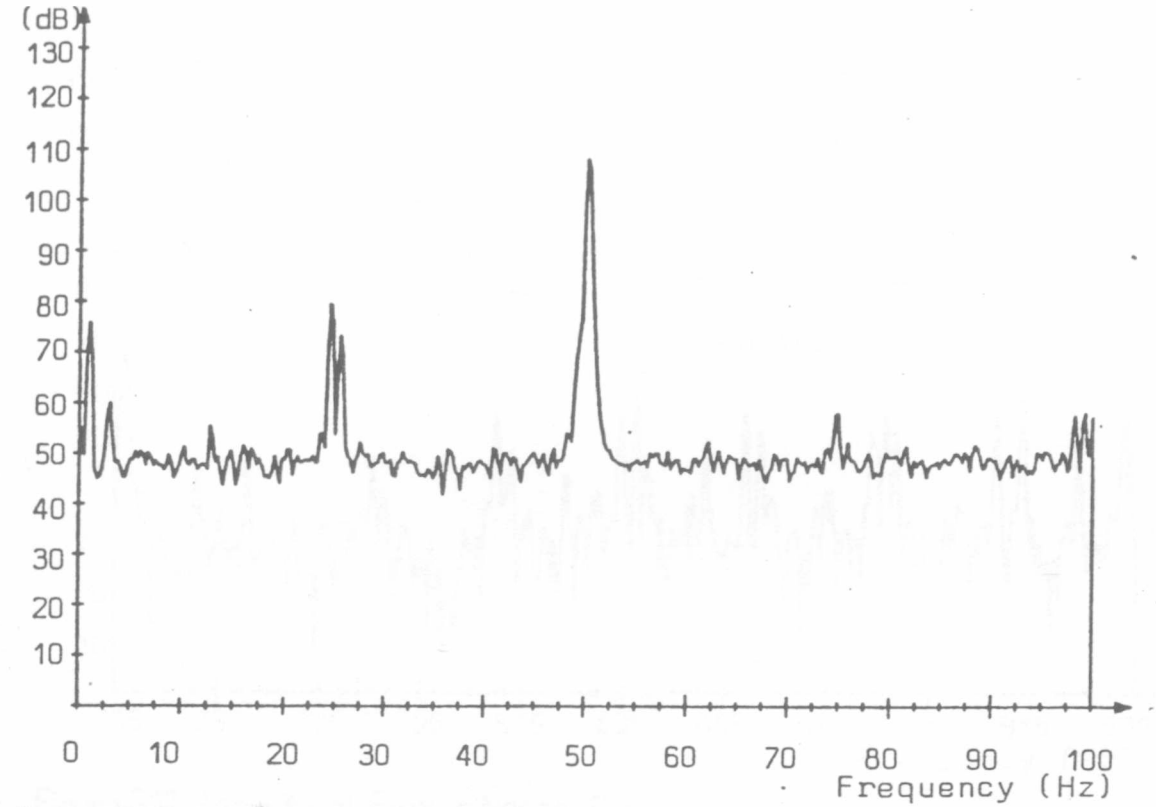

Figure 5.15 Axial Flux - Normal Rotor

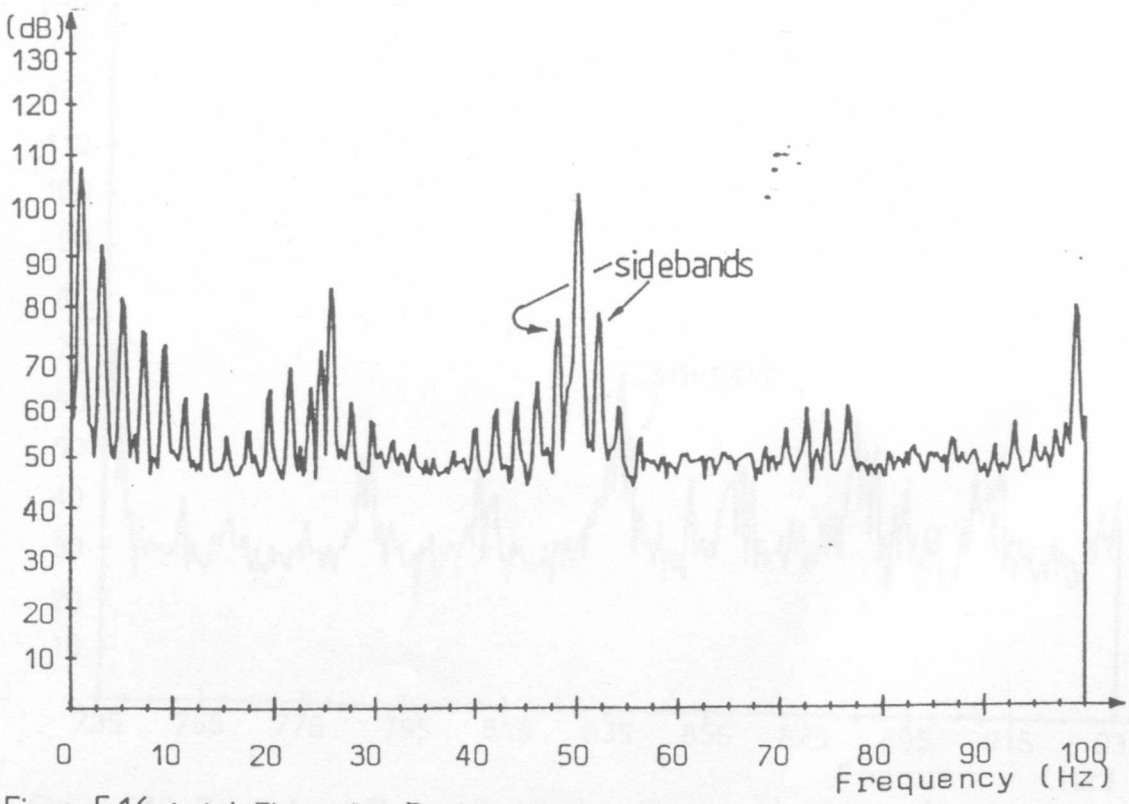

Figure 5.16 Axial Flux - One Broken Bar

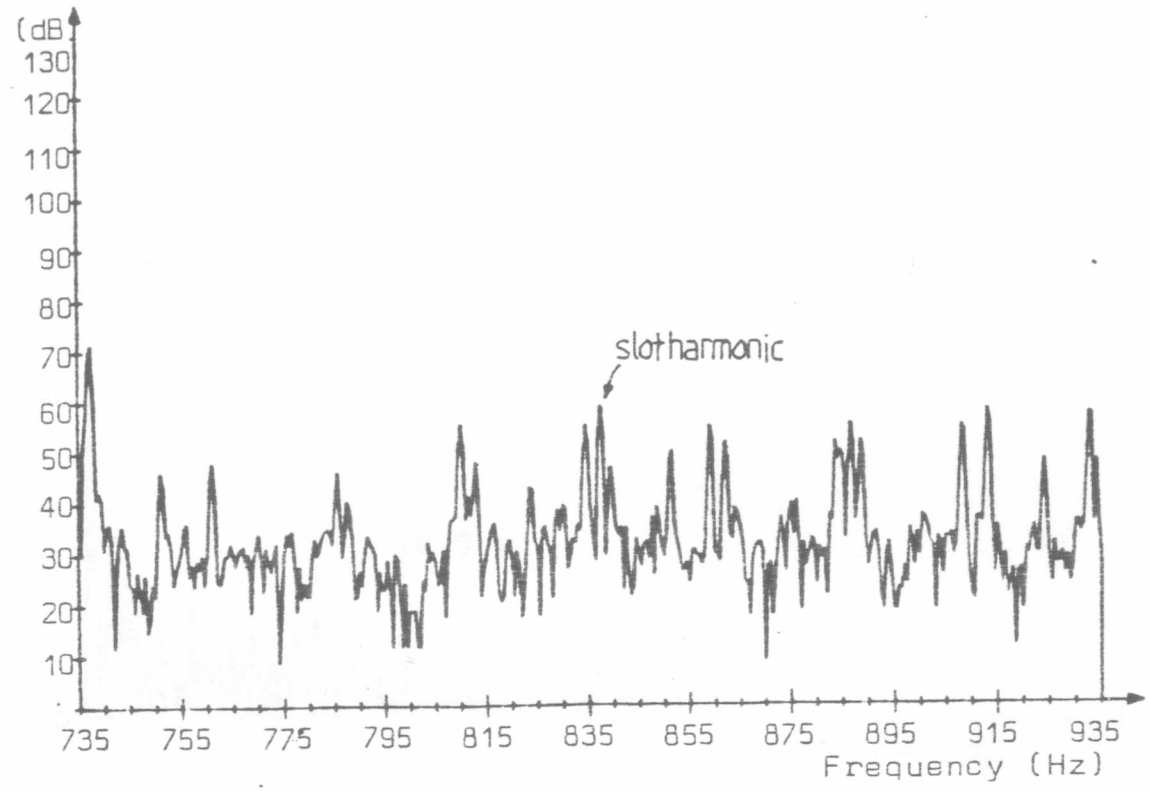

Figure 5.17 Zoom Axial Flux - Normal Rotor

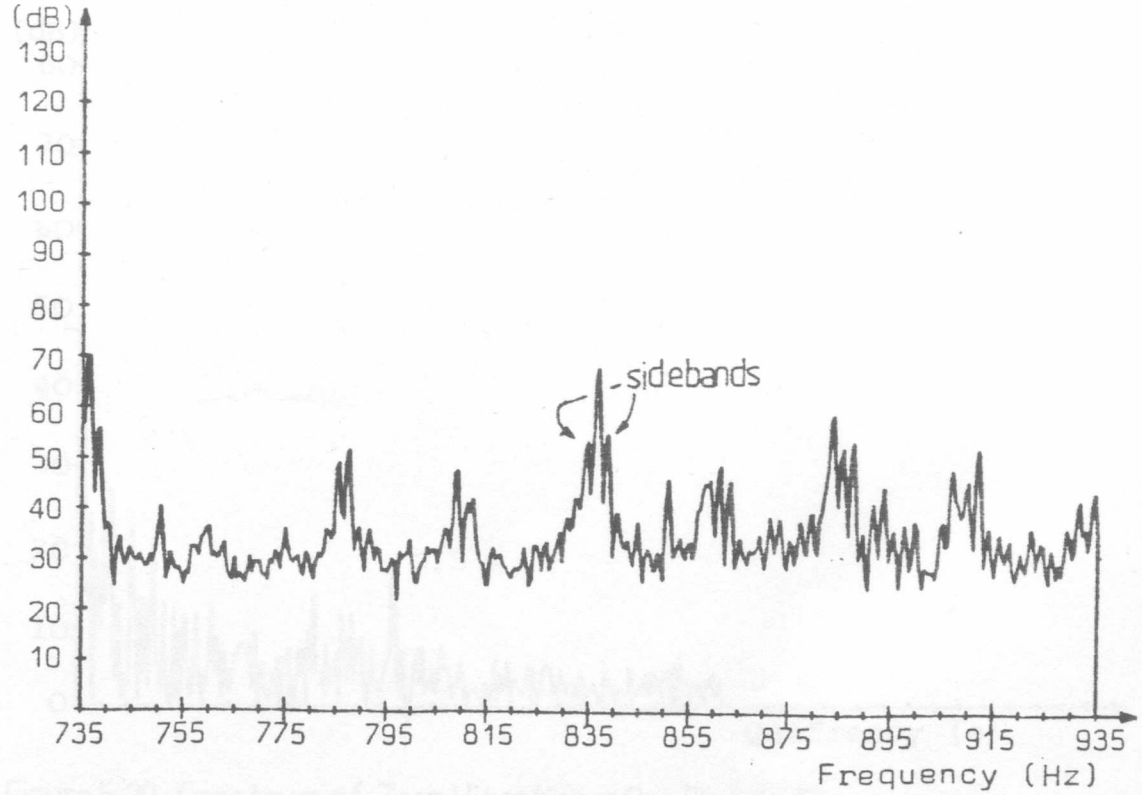

Figure 5.18 Zoom Axial Flux - One Broken Bar

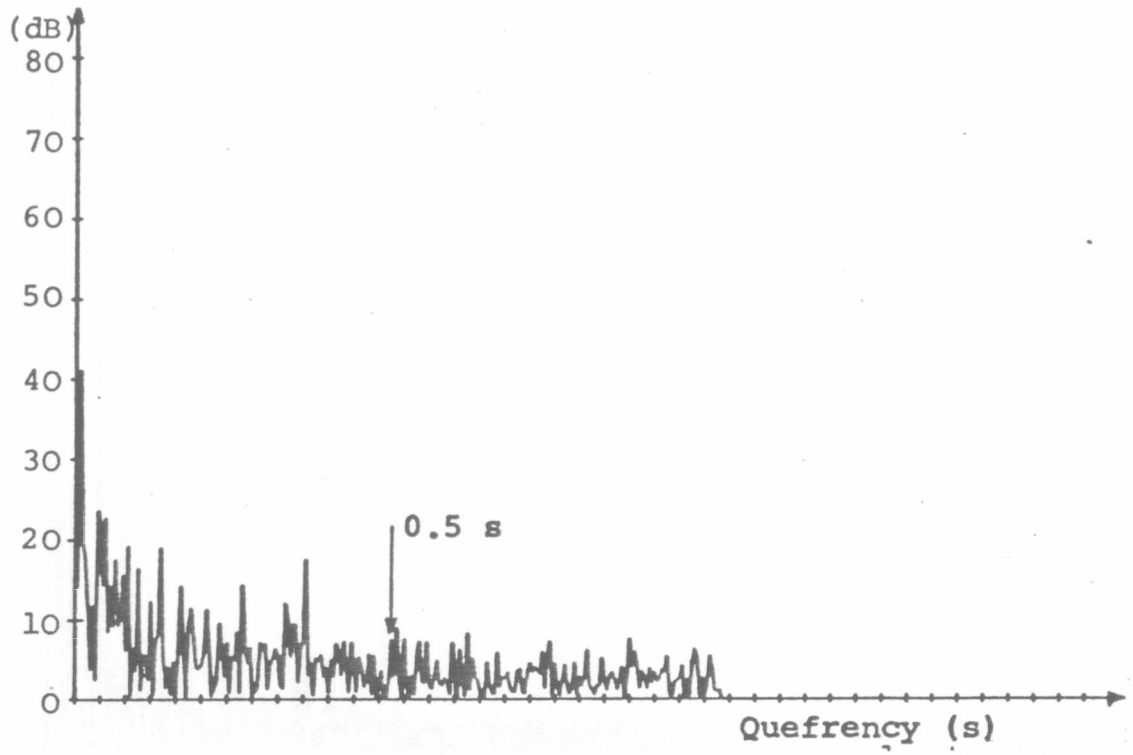

Figure 5.19 Cepstrum of Zoom Vibration - Normal Rotor

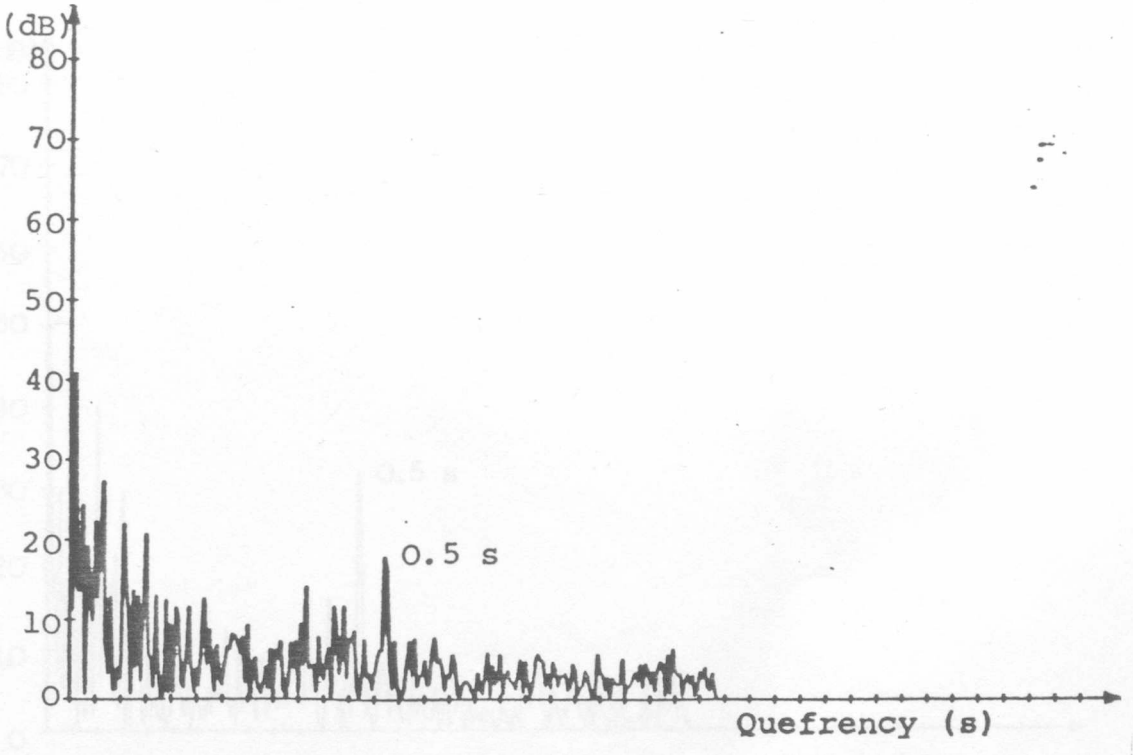

Figure 5.20 Cepstrum of Zoom Vibration - One Broken Bar

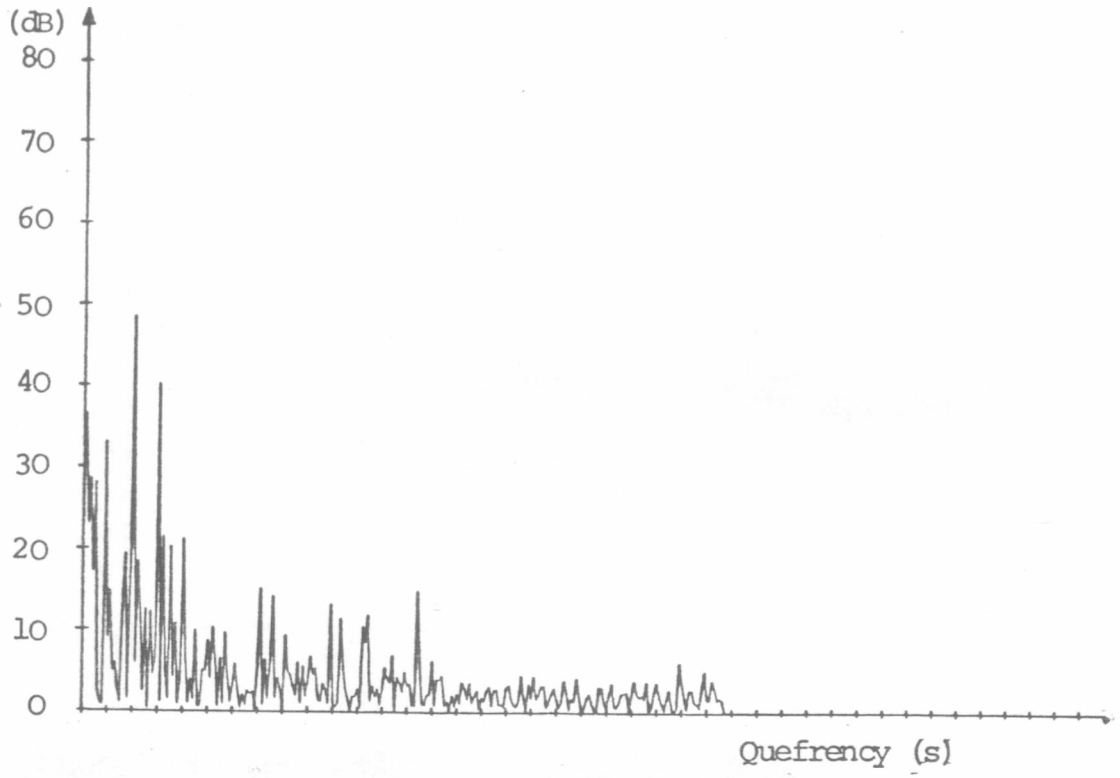

Figure 5.21 Cepstrum of Leakage Flux 0-200Hz – Normal Rotor

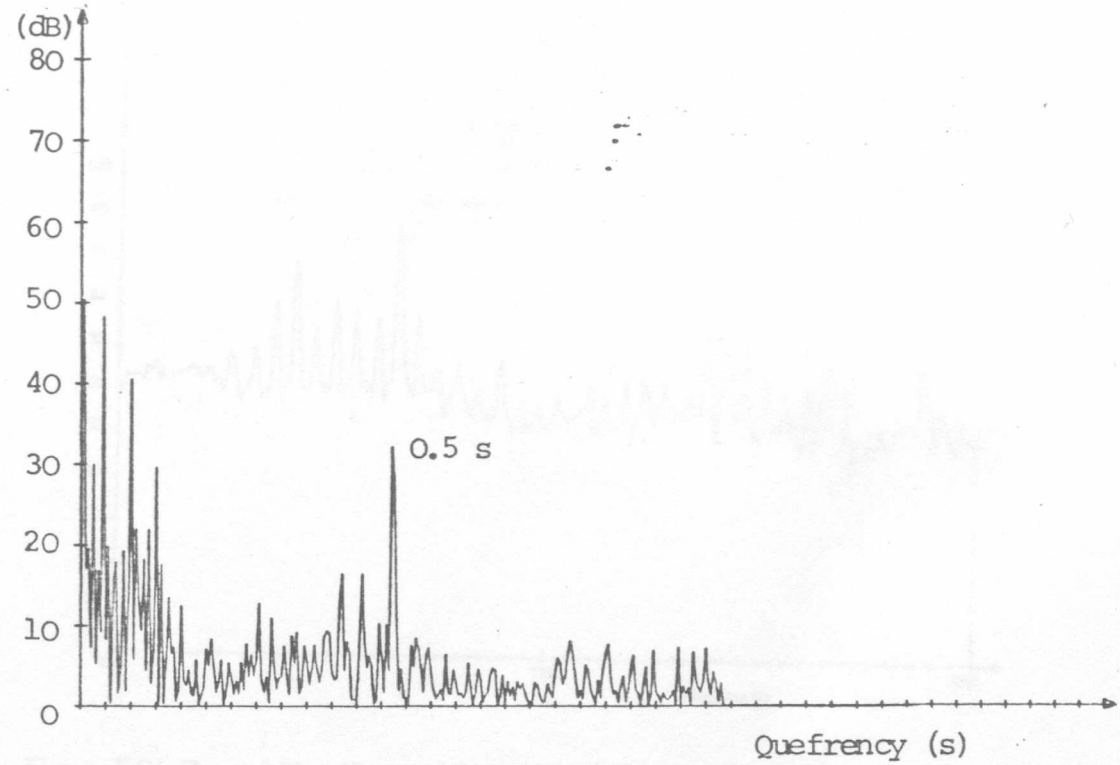

Figure 5.22 Cepstrum of Leakage Flux 0-200Hz – One Broken Bar

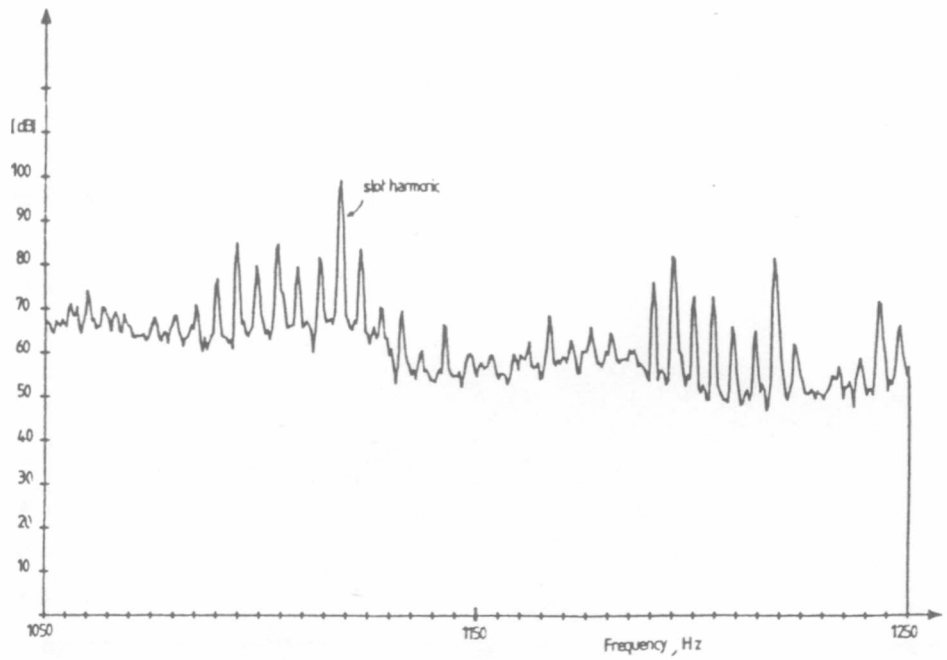

Figure 5.23 Zoom Vibration - 6 HighResistance Joints

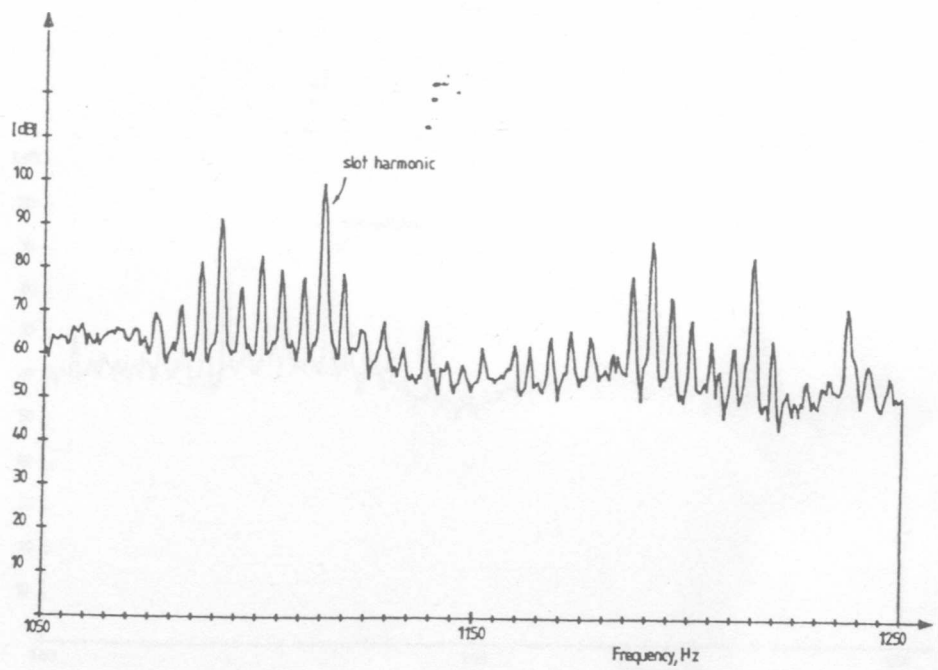

Figure 5.24 Zoom Vibration - 4 High Resistance Joints

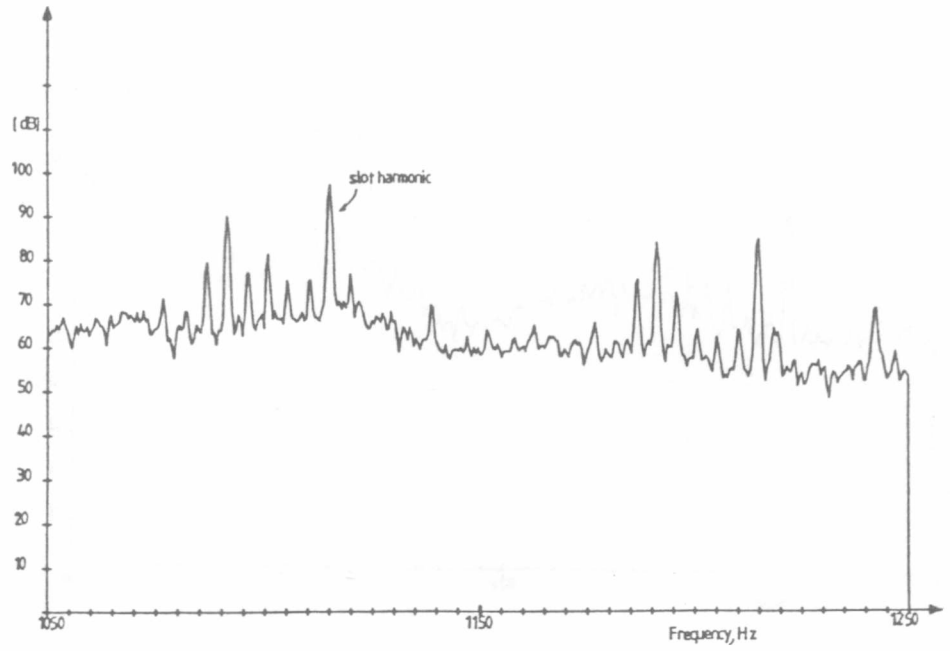

Figure 5.25 Zoom Vibration - 2 High Resistance Joints

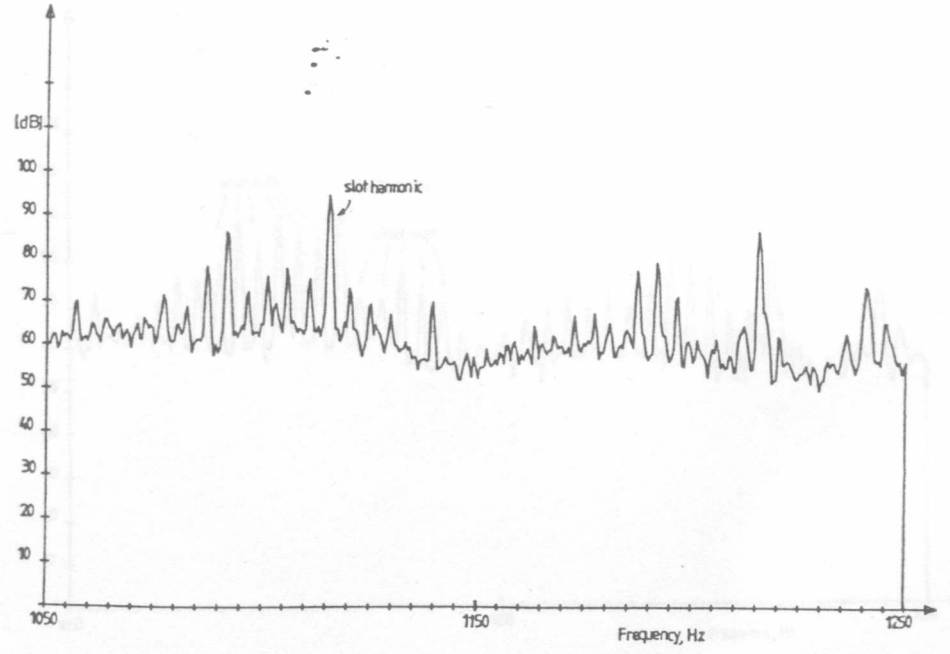

Figure 5.26 Zoom Vibration - 1 High Resistance Joint

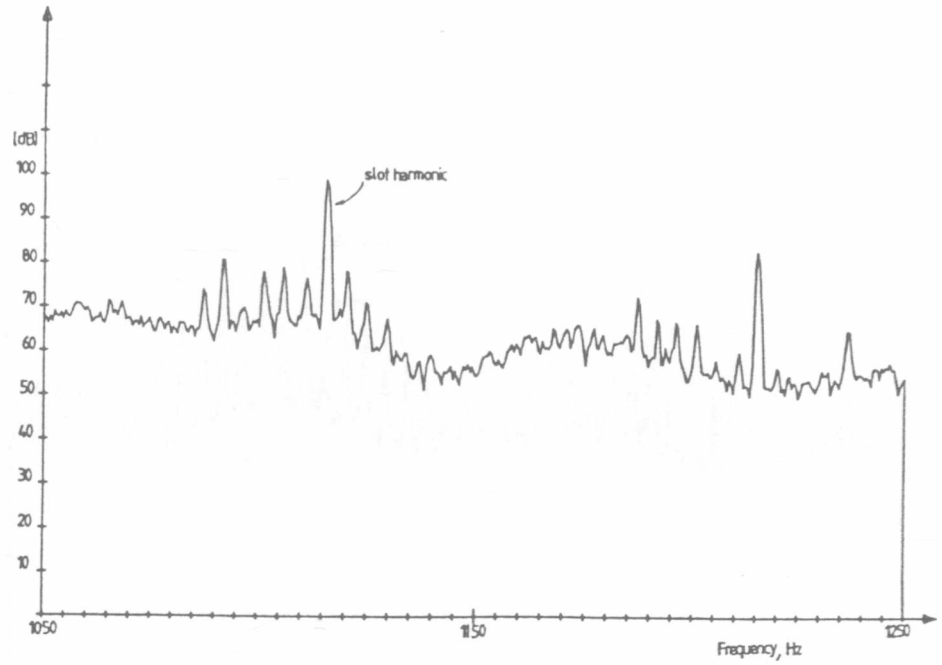

Figure 5.27 Zoom Vibration - No High Resistance Joints

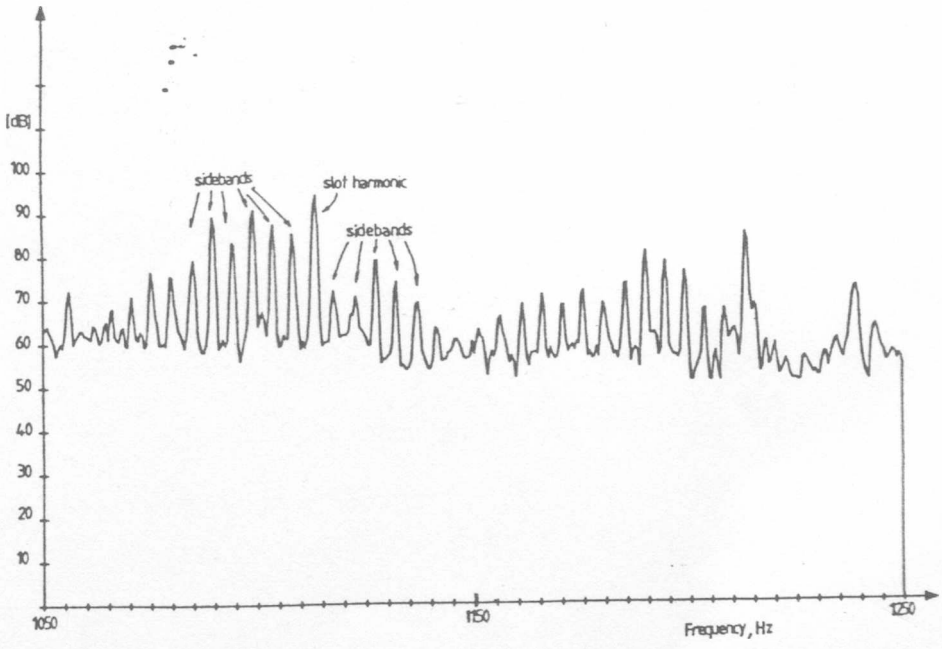

Figure 5.28 Zoom Vibration - One Broken Bar

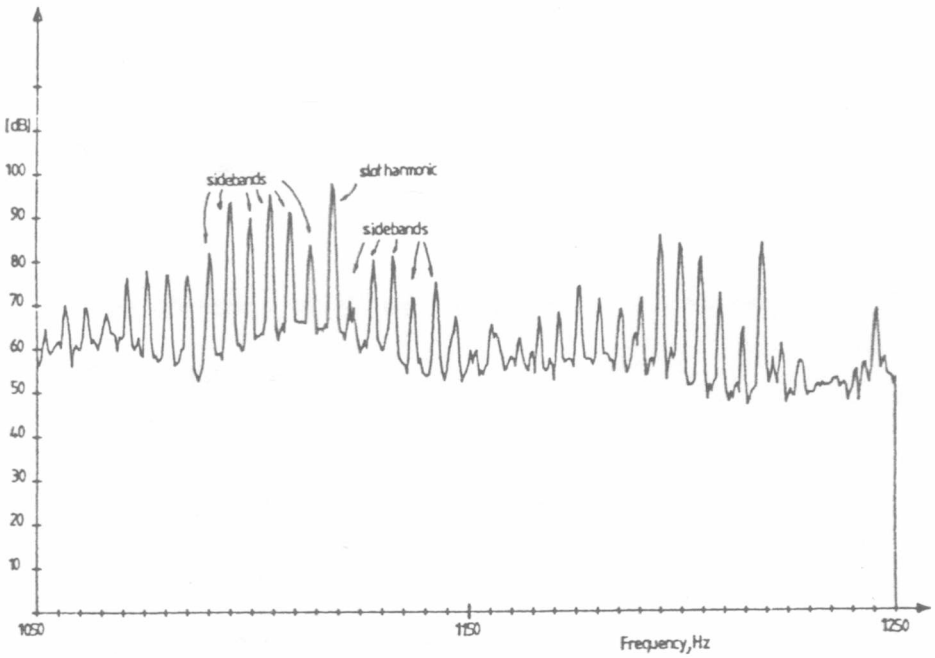

Figure 5.29 Zoom Vibration – Two Broken Bars

CHAPTER SIX

ECCENTRICITY & INTERTURN FAULTS

6.1 INTRODUCTION

Two further problem areas were investigated experimentally. These were:-

a) Rotor-Stator Static Eccentricity &

b) Interturn Winding Faults

Each of these areas will now be dealt with in turn.

6.2 ROTOR-STATOR STATIC ECCENTRICITY

Ellison and Yang's (32) work on SCIM noise indicated that machine acoustic noise increased with increasing static eccentricity. If the acoustic noise increases then it should be expected that the vibration increases as there is a direct correlation between the two. Therefore tests were undertaken to verify that there is an increase in vibration with increasing eccentricity.

6.2.1 EXPERIMENTAL

As described in Chapter Two the stator frame of the test SCIM could be moved with respect to the bearing pedestals and therefore the rotor. When the rotor and stator were nominally concentric there was a uniform airgap of 0.015 inches. Tests were done by moving the stator 0.001 in, 0.002 in, 0.004 in, 0.008 in and 0.012 in. This corresponded to eccentricities of 6.66%, 13.33%, 26.66%, 53.33% and 80% respectively.

Figures 6.1 to 6.4 show the vibration spectra for various levels of eccentricity at full load. During the course of the investigation it was realised that there were significant changes in the slot harmonic vibration with increasing eccentricity. Furthermore it was noted that the magnitude of the change in slot harmonic vibration was dependent on the vibration transducer position on the core. Figures 6.5 & 6.6 show how the slot harmonic vibration, at 885 HZ & 785 HZ respectively, vary with eccentricity and transducer position. The reason for the vast variation in magnitude of the vibration is the stator's structural response as described in Chapter Four. Examination of the other signals (line current, axial flux and end winding leakage flux) revealed very little change with increasing eccentricity.

6.3 INTERTURN WINDING FAULTS

When the insulation between conductors of the same coil breakdown the resulting fault is termed an "INTERTURN WINDING FAULT". The insulation breakdown may be caused by several factors including contamination, excessive coil vibration causing the insulation to fret and spark errosion due to discharges within the insulation and to the stator core. When an interturn fault occurs part of the coil is usually short circuited. The passing flux induces a voltage in the shorted turns/coil which in turn produces a current. Since the reactance of the shorted turn/coil is very low the circulating current can be large and produce excessive heat which will further degrade the insulation and lead to a complete winding failure.

6.3.1 EXPERIMENTAL

The test SCIM had a connection matrix where each end of each stator coil was terminated and then interconnected (see Figure 2.4).

To simulate an interturn winding fault a complete coil was disconnected from the stator winding and shorted through a resistor to limit the circulating current to approximately full load current ($\sim$ 20 Amps). This was to avoid heating effects and possible damage to the test machine.

The effect of shorting a stator coil on the rotating airgap field is similar to that of unbalanced supply as described in Chapter Four, i.e. a standing force wave is produced in the airgap thereby causing the twice supply frequency (100 HZ) vibration to change.

Figures 6.7 & 6.8 show the change in vibration with the shorted coil. (The vibration transducer being located at the position where maximum change occurs). The twice supply frequency (100 HZ) vibration increases from 71 dB for the normal winding to 86 dB when the coil is shorted - a significant change. It was further observed that the change in vibration was virtually independent of which coil was shorted.

Figures 6.9 & 6.10 show the axial flux spectra for the two conditions. As with the case of unbalanced supply (Chapter Four) it is the (2 - s)f component at approximately 100 HZ which increases significantly.

The end winding leakage flux spectra in Figures 6.11 & 6.12 show an increase in the third harmonic of the supply increasing with the shorted coil.

Figures 6.13 & 6.14, the line current spectra, show significant increases in the 150 HZ (third harmonic) and the 735 HZ slot harmonic components.

6.4 CONCLUSIONS

The experimental results presented in this chapter show again that the monitored signals are sensitive to faults. Further work is required to show theoretically why the observed changes occur particularly in the case of rotor-stator static eccentricity.

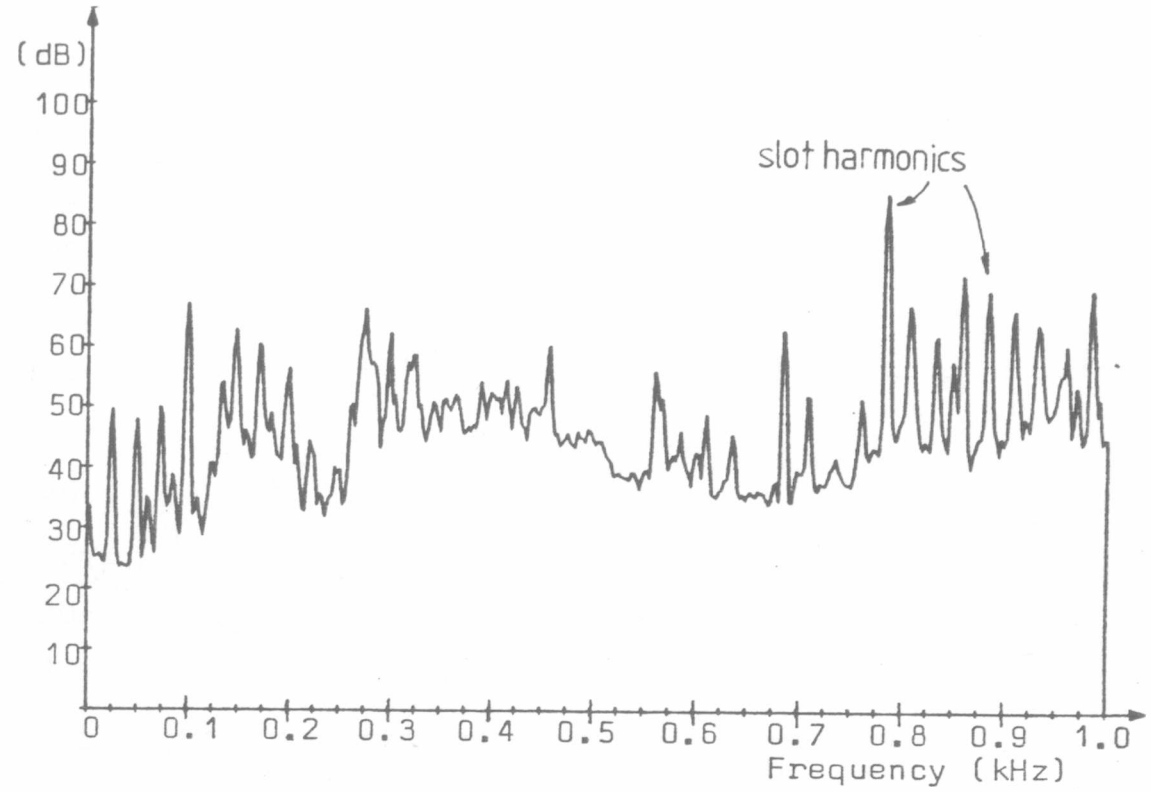

Figure 6.1 Vibration Spectrum - No Eccentricity

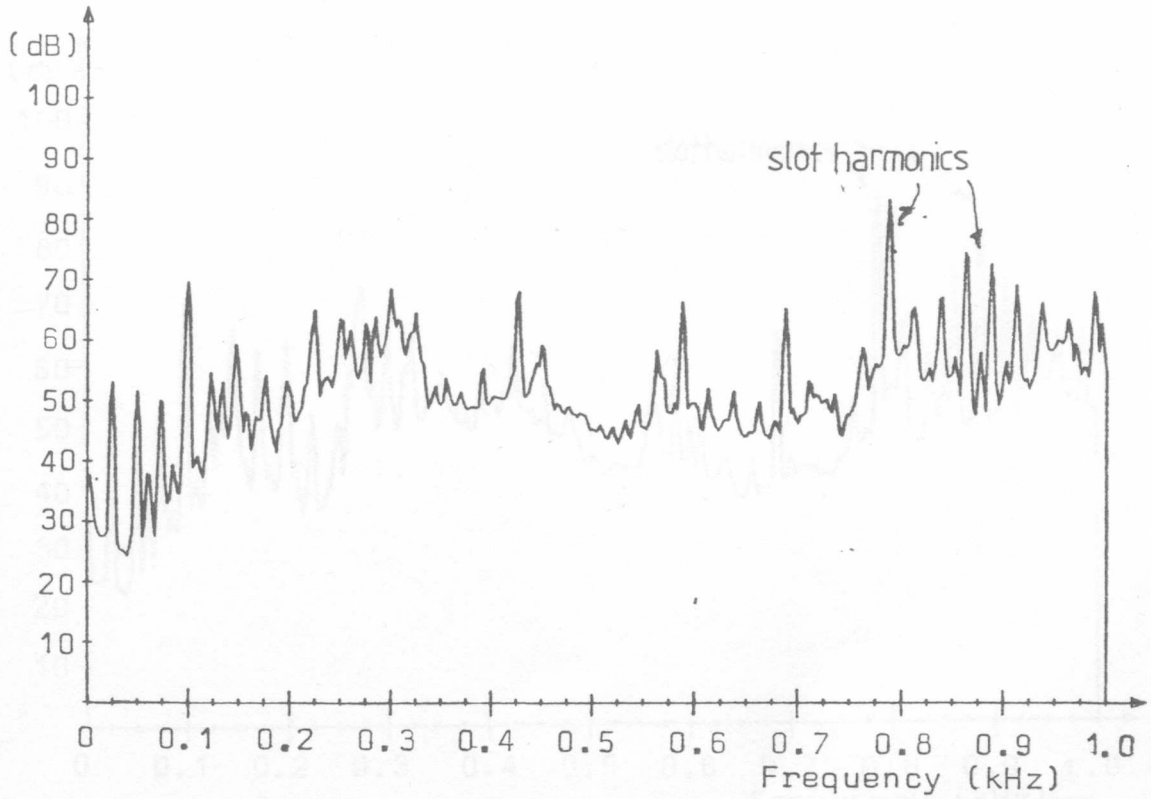

Figure 6.2 Vibration Spectrum - 6.66% Eccentricity

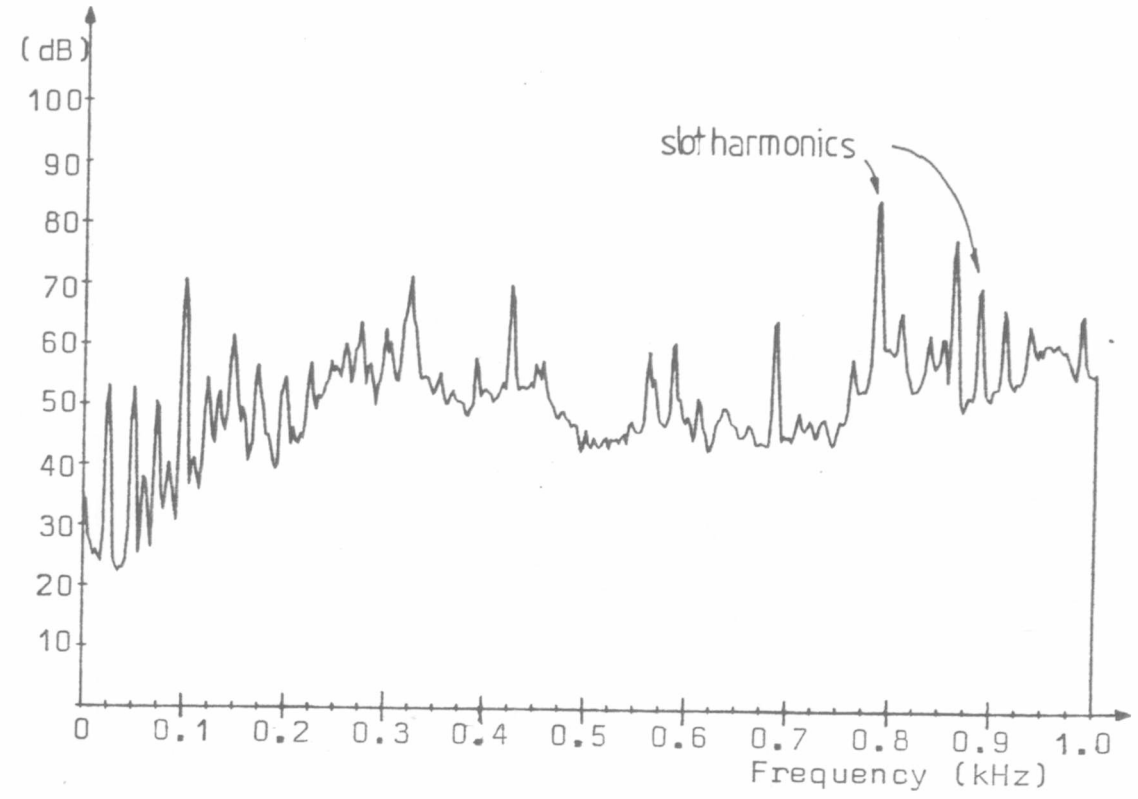

Figure 6.3 Vibration Spectrum -13.33% Eccentricity

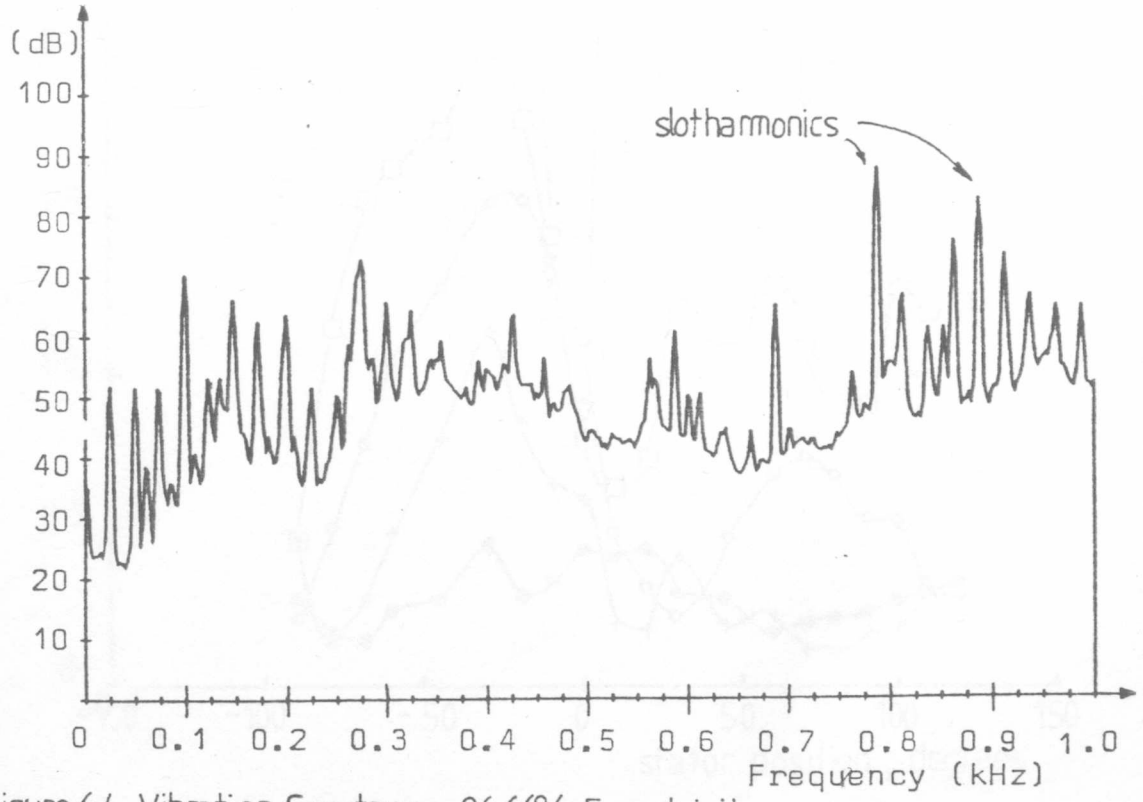

Figure 6.4 Vibration Spectrum -26.66% Eccentricity

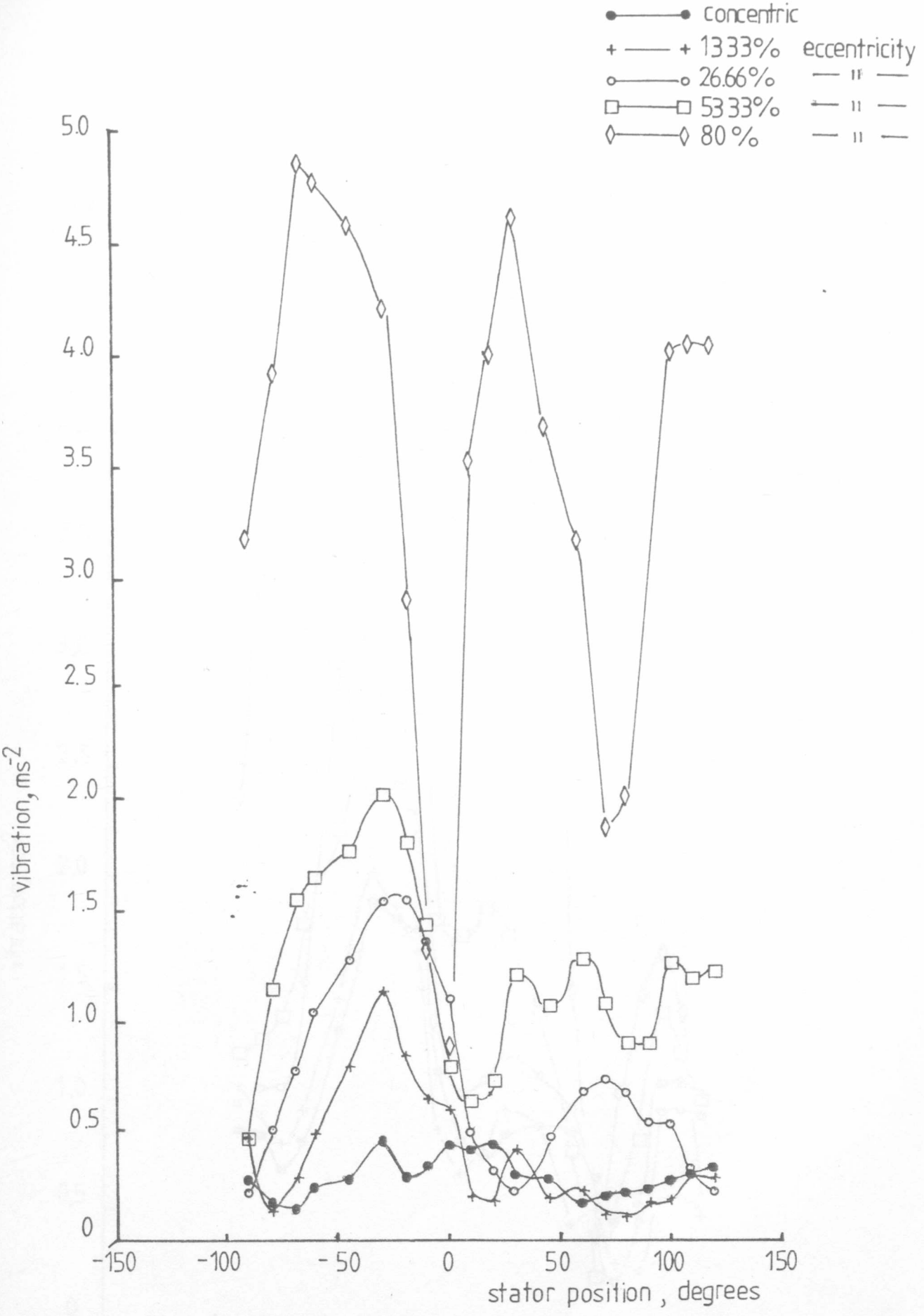

Figure 6.5 Effect of Eccentricity on 885 Hz Slot Harmonic

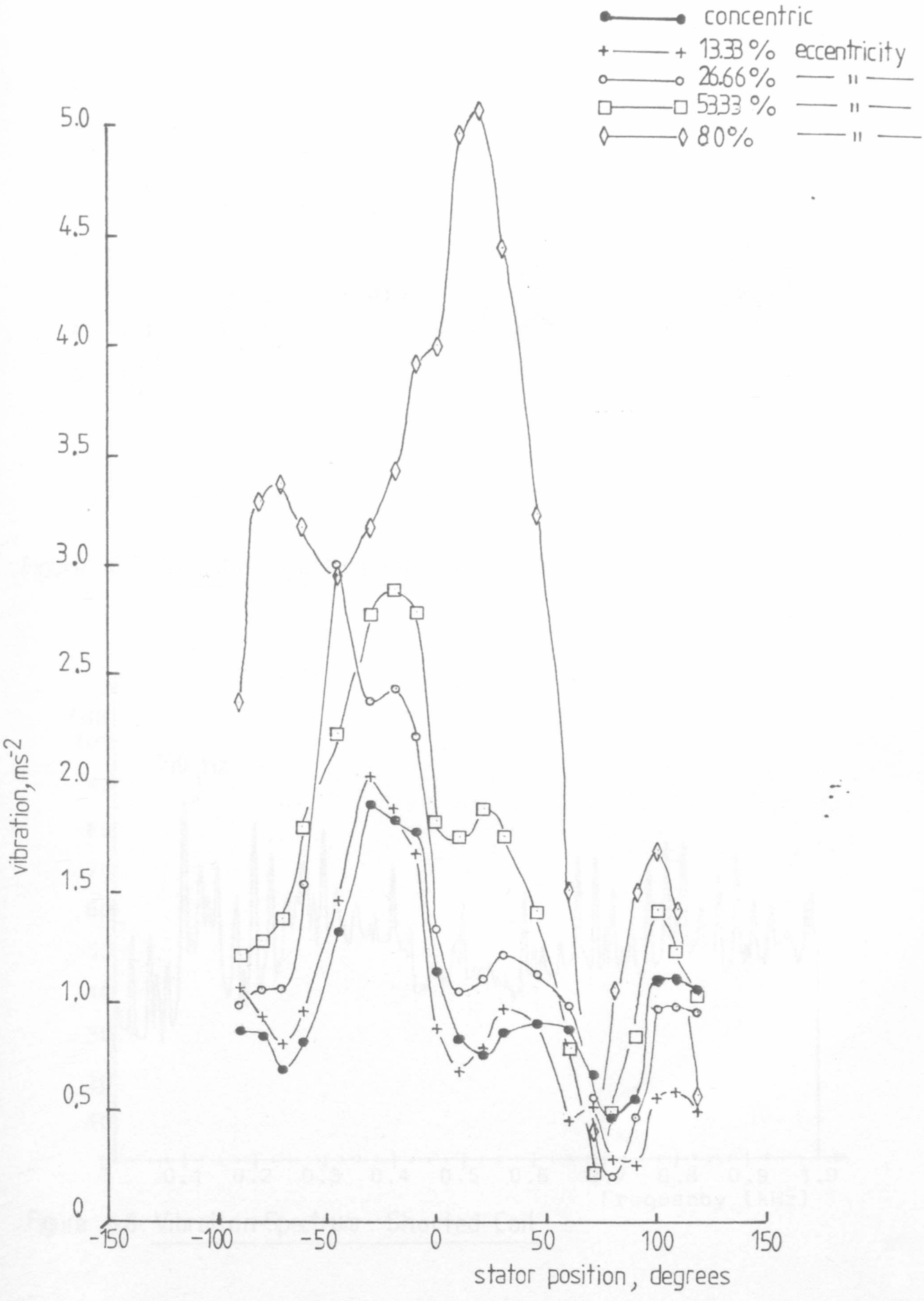

Figure 6.6 Effect of Eccentricity on 785 Hz Slot Harmonic

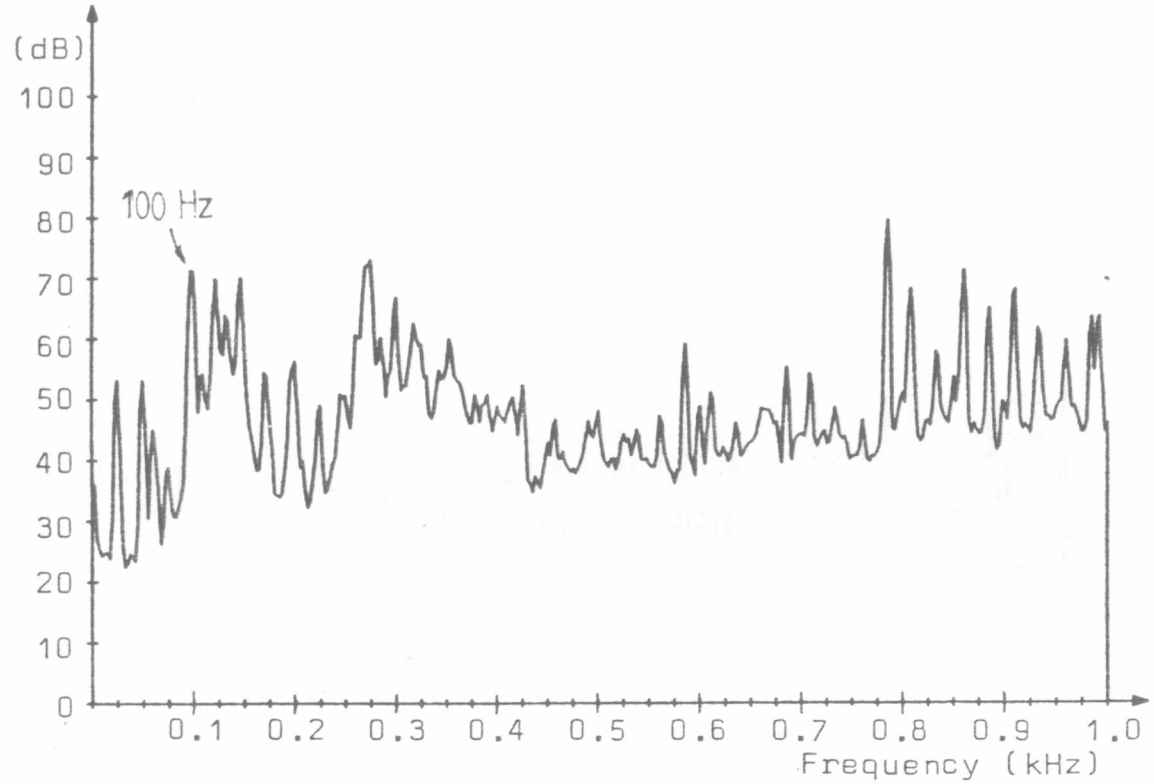

Figure 6.7 Vibration Spectrum – Normal Winding

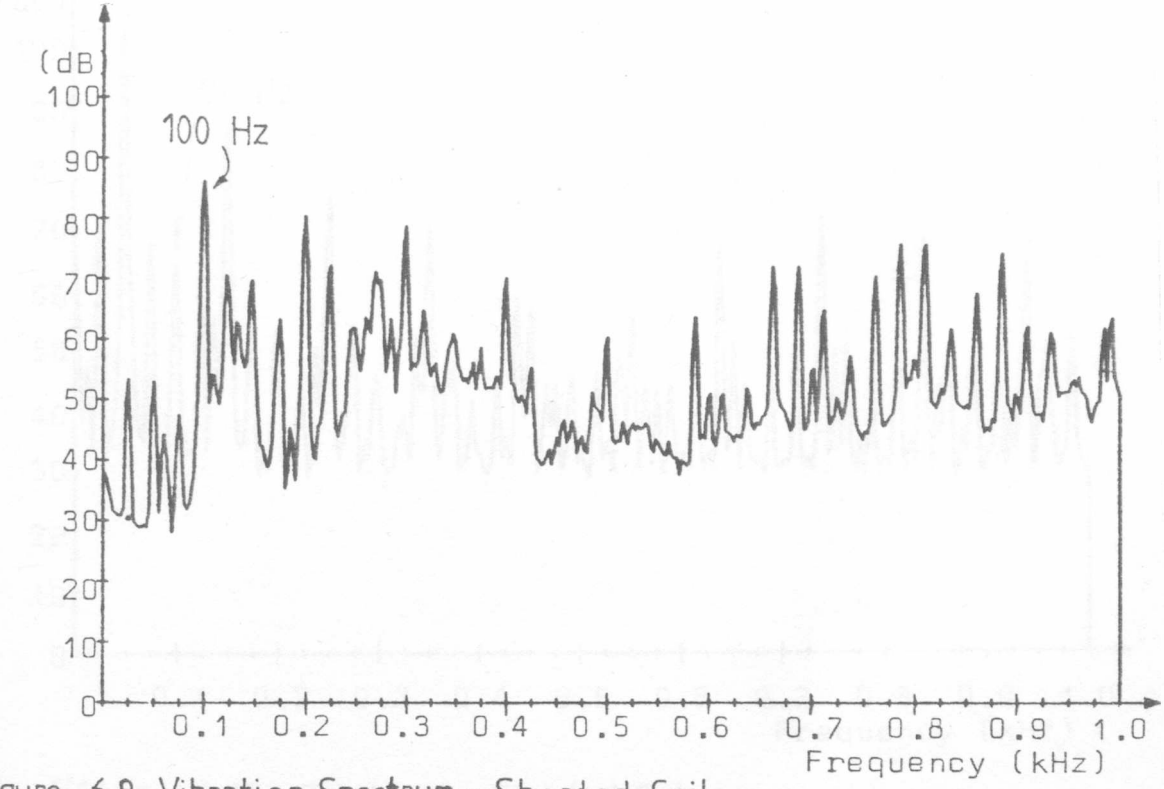

Figure 6.8 Vibration Spectrum – Shorted Coil

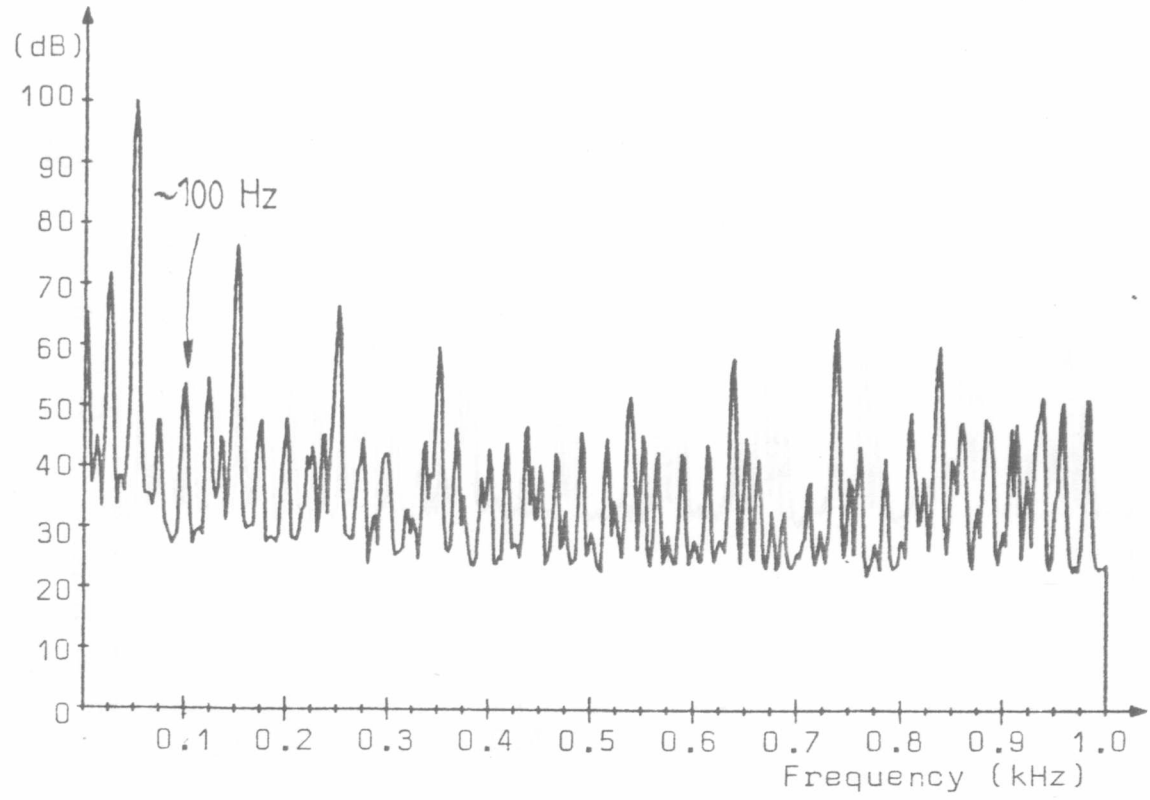

Figure 6.9 Axial Flux Spectrum – Normal Winding

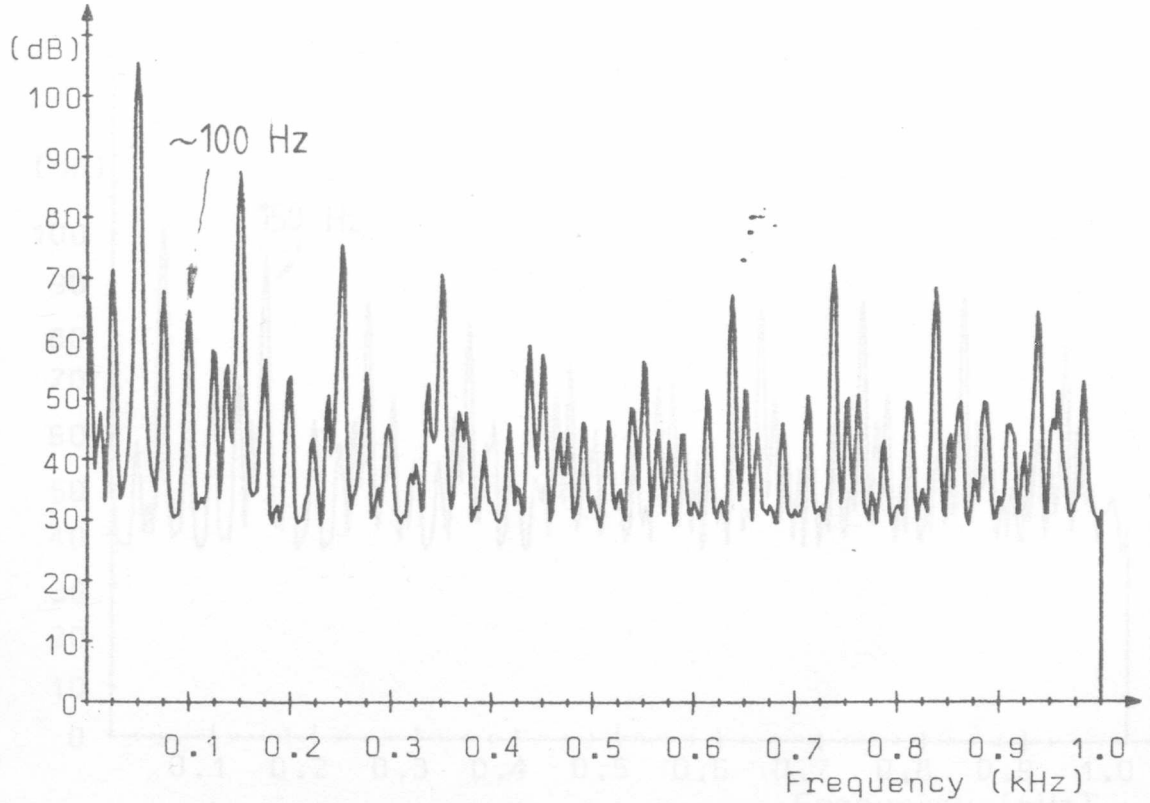

Figure 6.10 Axial Flux Spectrum – Shorted Coil

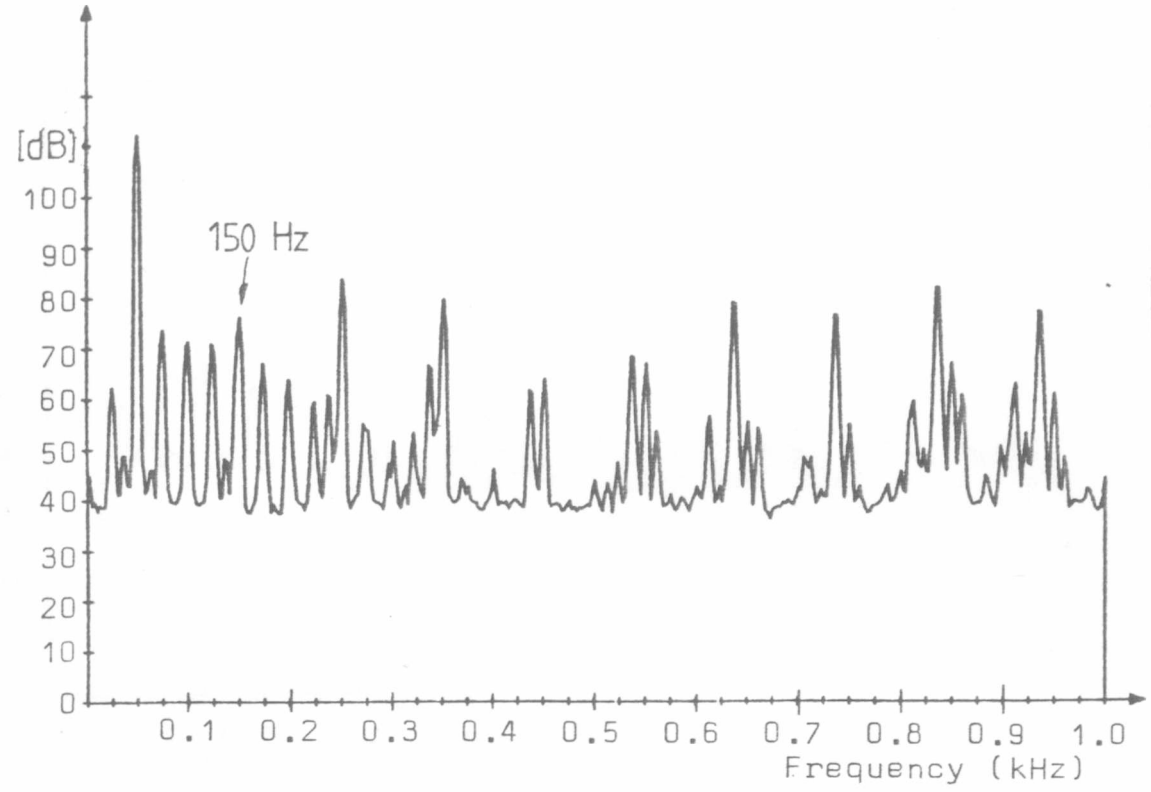

Figure 6.11 Endwinding Leakage Flux Spectrum - Normal Winding

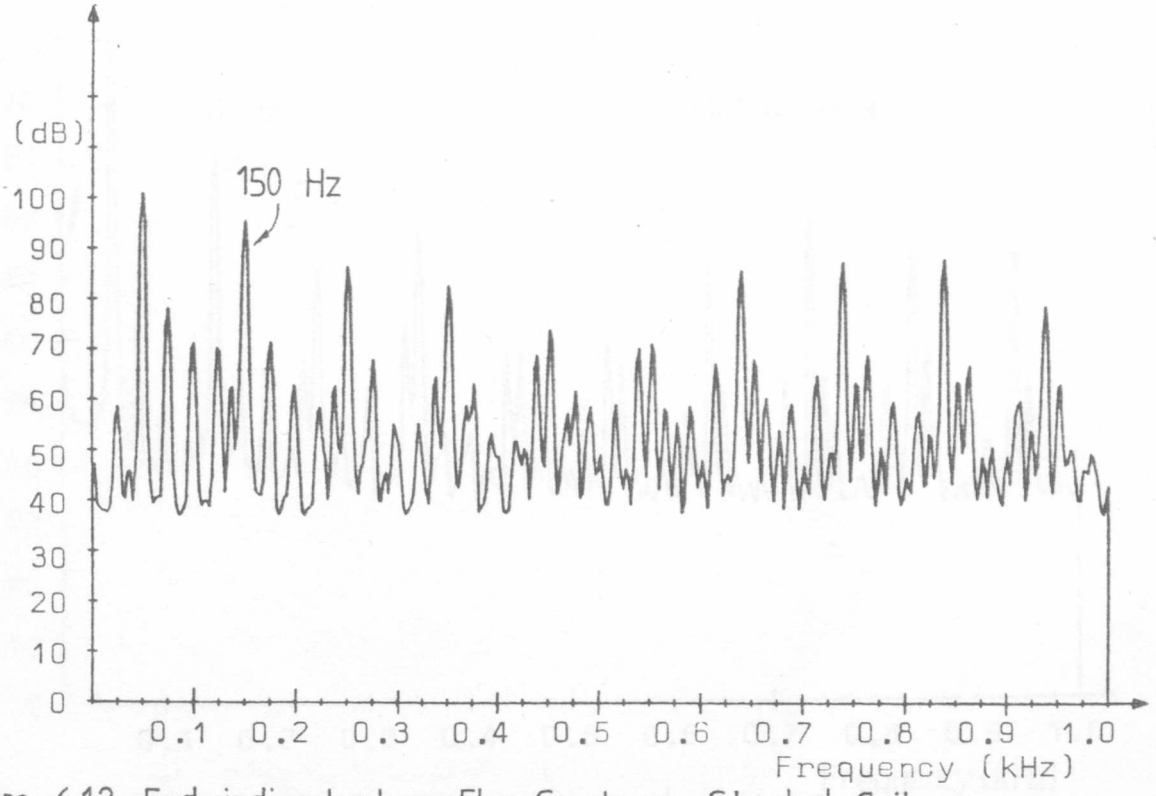

Figure 6.12 Endwinding Leakage Flux Spectrum - Shorted Coil

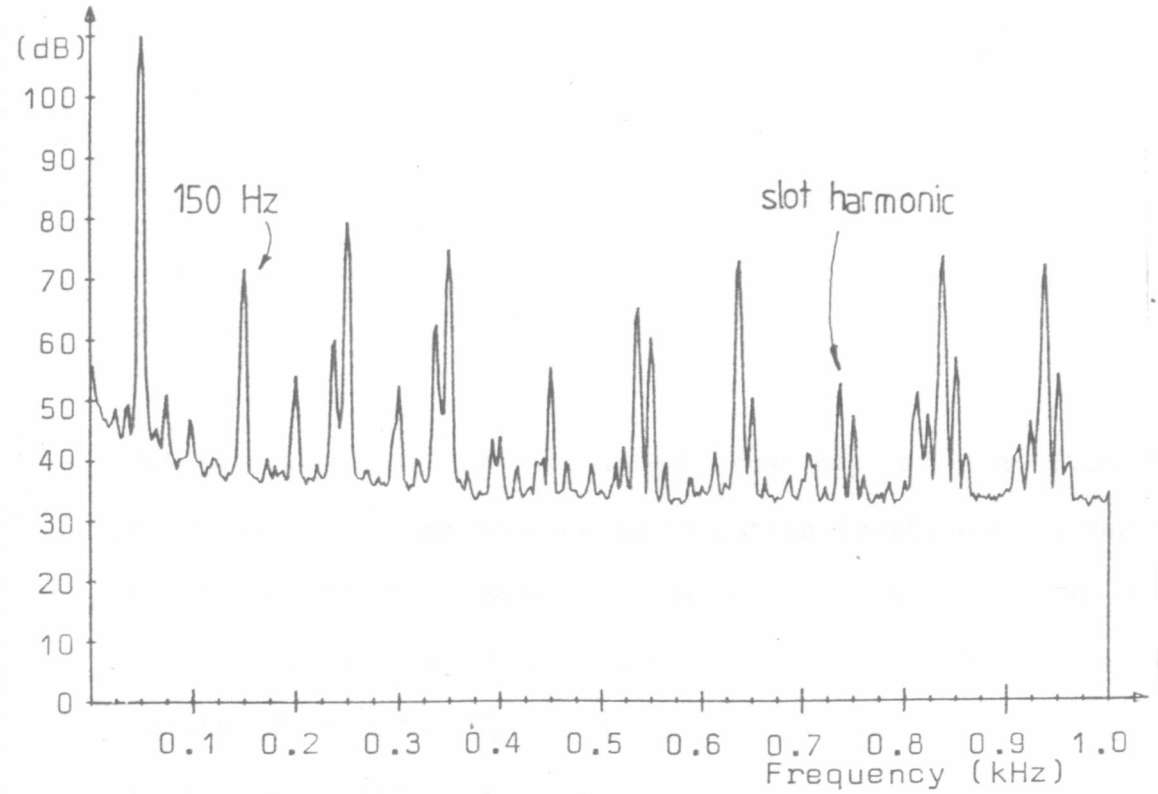

Figure 6.13 Current Spectrum – Normal Winding

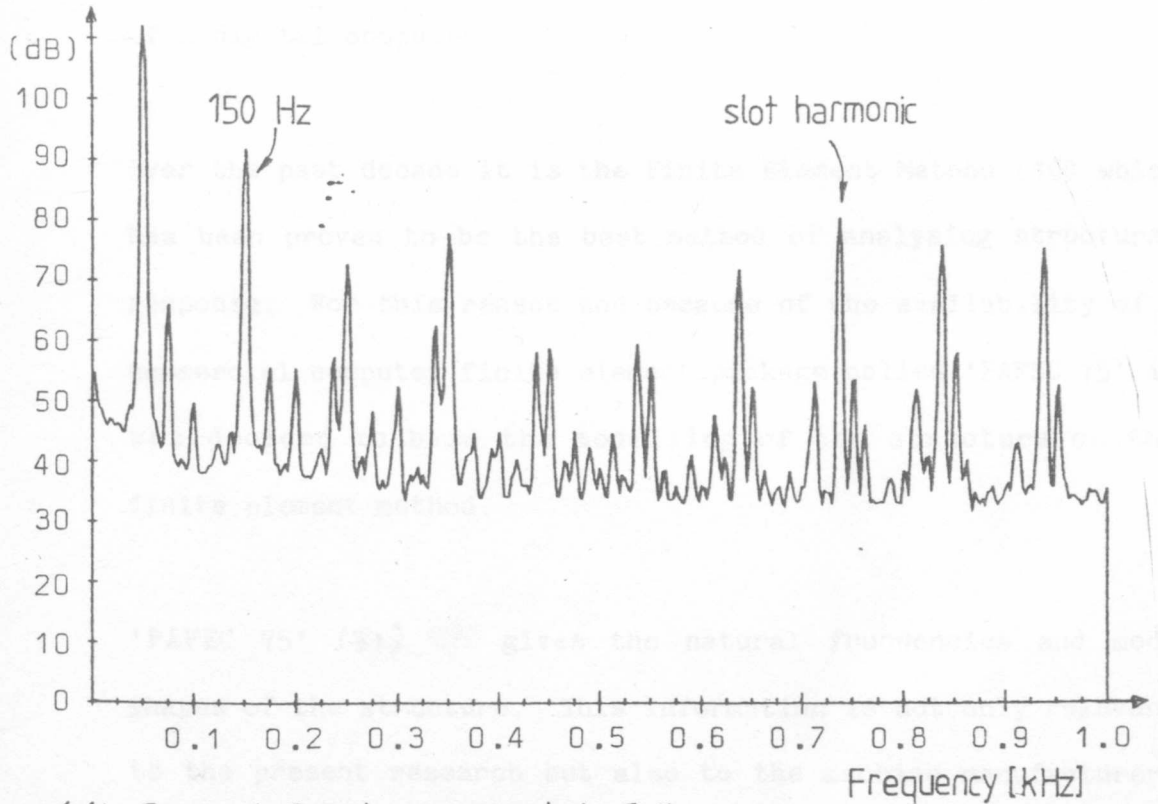

Figure 6.14 Current Spectrum – Shorted Coil

CHAPTER SEVEN

STRUCTURAL RESPONSE OF THE MACHINE

7.1 INTRODUCTION

Determination of the mechanical response of the SCIM is required before any changes in vibration levels due to faults can be quantified. Several analytical methods have been used already to determine the response. These methods include Finite Difference (26), applying Lagrange's Equation to three-dimensional elasticity theory (27, 28) and Finite Element (29) methods. Such methods invariably require the solution of large numbers of equations which can best be done with the use of a digital computer.

Over the past decade it is the Finite Element Method (30) which has been proven to be the best method of analysing structural response. For this reason and because of the availability of a commercial computer finite element package called 'PAFEC 75' it was decided to base the modelling of the structure on the finite element method.

'PAFEC 75' (31) gives the natural frequencies and mode shapes of the structure. This information is not only relevant to the present research but also to the machine manufacturers who are continually trying to improve the design by reducing machine vibration and noise. The designers main problem in reducing noise and vibration is to ensure that the natural

frequencies of the structure are kept well away from any frequencies produced from mechanical or electromagnetic sources.

7.2 THE FORMULATION OF THE FINITE ELEMENT MODEL

Using finite elements a model of the test machine's structure can be built up systematically. The proposed stages of development of the model were:-

(i) Stator Core (including teeth and slots)

(ii) Stator Core and Case

(iii) Stator Core, Case and feet

(iv) Stator Core, Case, feet and windings

(v) As (iii) and (iv) but with movement of feet restricted.

The natural frequencies and mode shapes can be obtained at each stage to compare the effects of structural additions.

7.3 MODEL DIMENSIONS AND ELEMENTS

The dimensions of the stator core are shown in Fig. 7.1. These dimensions correspond to a Brook Crompton Parkinson motor type D160M SCIM. Fig. 7.2 shows the division of a slot/tooth segment into its finite elements. Each slot/tooth segment contains 20 elements. With 36 slot/tooth segments the total number of elements in the core is 720.

7.4 THE DATA REQUIRED FOR 'PAFEC 75'

To run 'PAFEC 75' on data file, with the machines dimensions, elements and material is required. Fig. 7.3 shows the data file for the stator core of Fig. 7.1. To reduce the number of nodes and elements that have to be specified use has been made of the SIMILAR.NODES and GROUPS.OF.SIMILAR.ELEMENTS data modules. At the beginning of the data file is a control module which the user sets up to instruct 'PAFEC 75' on the type of solution that is required. The OUTDRAW module is used to stipulate which mode shapes are required.

7.5 RESULTS USING 'PAFEC 75'

'PAFEC 75' has been used to find the natural frequencies and mode shapes of the model core (Fig. 7.1). The laminations of the stator core are made of annealed steel. A controversy exists as to the effect of annealing on the Young's Modulus. Various values of Young's Modulus have been used to determine the effect of this factor on the natural frequencies and these

are tabulated in Fig. 7.4. Fig. 7.5 shows how the first natural frequency varies with Young's Modulus. Mode shapes for several natural frequencies are shown in Figs. 7.6 - 7.12.

Comparison with work done by Verma and Girgis (25) on a stator core of similar size shows that results for the finite element model are of the same order.

Other researchers have noted the existence of dual resonances. Dual resonances are caused by asymmetries, no matter how minor, in the stator's structure and are characterised by two resonances differing by a few cycles but belonging to the same mode of vibration. The plots of the mode shapes show this effect quite clearly. Figures 7.6 - 7.9 are of the n=2 mode. Fig. 7.6 and 7.7 have natural frequencies of 850.8 Hz and 862.3 Hz respectively (for Young's Modulus of 209 GN/m^2) and their mode shapes have a phase change between one another. Figures 7.8 and 7.9 again show dual resonance but this time there is axial variation in the mode shape.

The mode shapes show that each mode (i.e. n=2, 3, 4 etc.) has four resonant frequencies associated with it. The lower two frequencies of each mode are dual resonance of a radial variation and the higher two frequencies are dual resonance of the mode with axial variations.

COMPUTER USAGE

'PAFEC 75' is run on RGIT's DECSYSTEM 20 computer system. A typical run to obtain the natural frequencies of the stator core takes approximately one hour of C.P.U. time; a further hour is needed if six mode shapes are requested. 3,500 pages of disk space are required for the temporary working and back up files.

7.6 MORE COMPLICATED MODEL

A model of the stator core with the aluminium case was input into 'PAFEC 75'. This required so much storage space to run due to the increased number of elements that the computer storage space allocated to the author was continually exceeded. The author was at the time unable to overcome this problem.

Figure 7.10 shows that the model was in fact input to 'PAFEC 75'.

7.7 EXPERIMENTAL

The actual motor stator which was used for the computer model was tested experimentally for its resonant frequencies. Two methods of test were used, namely, swept sine and impulse shock tests.

The sine swept was conducted using standard B & K vibration test equipment i.e. a calibrated signal source, or power amplifier and an electromagnetic shaker. Feedback from the electromagnetic shaker was used to ensure that a constant amplitude force was applied to the stator core.

The experimental rig for these tests is shown in Figure 7.11. As seen the stator core was suspended from springs. Spectra showing the resonant frequencies for each test method are shown in Figures 7.12 and 7.13.

Figures 7.14 to 7.19 show plots of the mode shapes of several of the stator natural frequencies. The experimental results had to be interpreted to give the node points because only one accelerometer was used and it was therefore impossible to check the phase relationships of the vibrations on the various parts of the stator.

7.8 COMPARISON OF EXPERIMENTAL & THEORETICAL RESULTS

Although theoretical results from 'PAFEC 75' are for the core without the aluminium case the results for the first natural frequency (n=2) are of a similar order, 1093 Hz experimental compared to the computed value of between 850 Hz and 1504 Hz. It must be remembered that there are 4 for theoretical modes for n=2.

7.9 CONCLUSIONS

It is evident that it is possible to model a motor stator using finite elements. When trying to model a full machine core complete with its aluminium case the number of elements is high. This means that the number of resulting computations is high and the computer data storage requirements become excessive. This leads to the failure to compute the natural frequencies for the complete stator. However it is envisaged that by reducing the number of elements by, say, dispensing with the stator slots/teeth that this problem would be overcome and it is suggested that this be done in any work which follows up this thesis.

The experimental work was used to establish that the finite element program (PAFEC 75) did in fact give realistic answers.

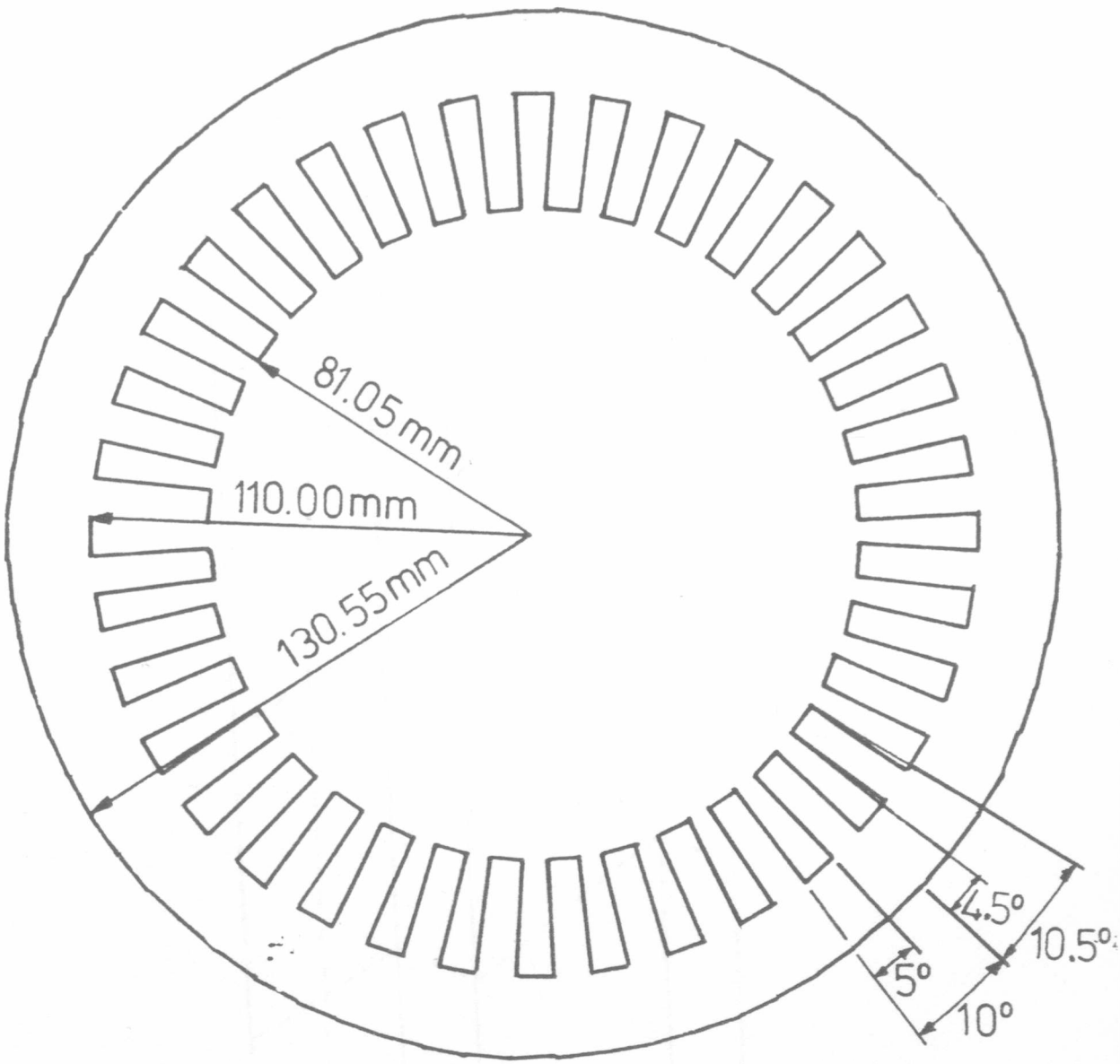

axial length =146.05mm

Figure 7.1 Dimensions of Stator Core

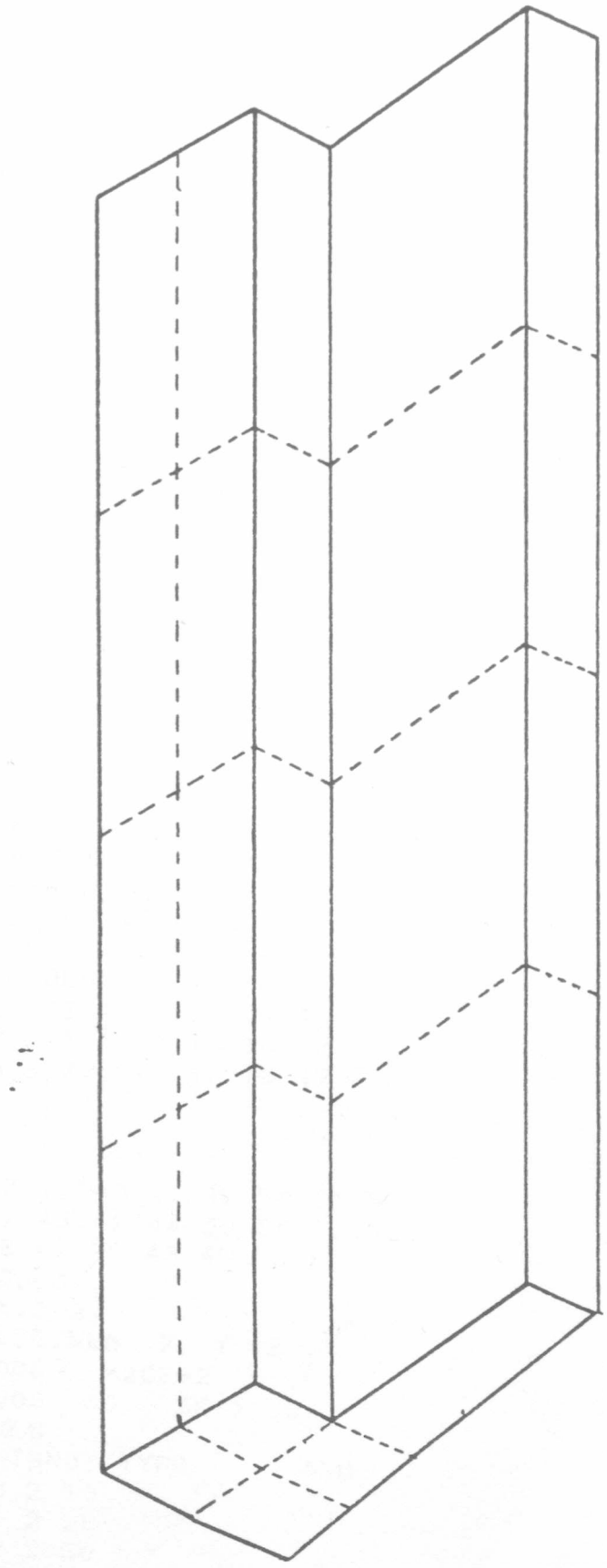

Figure 7.2 Division into Finite Elements

```
CONTROL
NAME.TTTT
SKIP.VALIDATION
SKIP.CHECK
SAVE.RESULTS
PHASE=1
BASE=30000
PHASE=4
BASE=90000
TIME=60
PHASE=6
BASE=90000
TIME=60
PHASE=7
BASE=90000
TIME=60
CONTROL.END
NODES
AXIS=2
X          Y          Z
0      8.105E-2     -10.5
0      11E-2        -10
0      8.105E-2     -4.5
0      11E-2        -5
0      12E-2        -10
    |
    |
    |
14.605E-2  13.055E-2  -5
14.605E-2  13.055E-2  0
ELEMENTS
ELEMENT.TYPE=37100
PROPERTIES=16
TOPOLOGY
1 2 3 4 12 13 14 15
2 5 4 6 13 16 15 17
4 6 7 8 15 17 18 19
    |
    |
    |
37 39 40 41 48 50 51 52
39 43 41 44 50 54 52 55
38 42 39 43 49 53 50 54
NODES
AXIS=2
NODE.NUM  X   Y   Z
4000    -20E-2  0   0
5000    0    5E-1   0
AXES
AXISNO  TYPE       ANG3
10 2 10
11 2 20
12 2 30
13 2 40
```

Figure 7.3 Data File for PAFEC 75

```
43 2 340
44 2 350
SIMILAR.NODES
ORIGINAL.NODE=1
NUMBER.OF.NODES=55
COPY.NODE     AXIS.OF.NEW.NODE
56    10
111   11
166   12
221   13
276   14
    |
    |
    |
    |
    |
1871  43
1926  44
GROUP.OF.SIMILAR.ELEMENTS
OLD=1
NUMBER=20
NEW    GROUP.NEW     TOPOLOGY.INCR
21     2     55
41     3     110
61     4     165
81     5     220
    |
    |
661   34    1815
681   35    1870
701   36    1925
MATERIAL
MATERIAL.NUM     E    NU   RO   ALPHA   MU    K   SH
16   195E9   0.3   7800    11E-6    25E-6   48     452
MODES.AND.FREQUENCIES
AUTOMATIC     MODES     START
   60     6          19
OUT.DRAW
PLOT.TYPE   NODE.NUM     CASE.NUM
1   4000      19
1   4000      20
1   4000      21
1   4000      22
1   4000      23
1   4000      24
END.OF.DATA
```

Figure 7.3 continued

No.	NATURAL FREQUENCIES, Hz			
	YOUNG'S MODULUS, GNm^{-2}			
	209	195	160	125
1	-1.1	2.6	-1.8	-3.0
2	1.3	3.5	3.0	2.6
3	3.2	4.5	3.4	3.6
4	8.7	7.7	6.2	6.4
5	9.2	9.2	8.7	7.5
6	11.1	11.0	8.9	8.6
→ 7	850.8	821.8	744.4	658.0
8	862.3	832.9	754.5	666.9
9	1486.1	1435.4	1300.3	1149.3
10	1504.6	1453.3	1316.4	1163.6
11	2465.7	2381.7	2157.4	1906.9
12	2519.4	2433.6	2204.4	1948.4
13	3686.9	3561.3	3225.9	2851.3
14	4150.4	4009.0	3631.4	3209.8
15	4852.6	4687.3	4245.8	3752.8
16	5073.6	4900.7	4439.1	3923.7
17	5989.0	5784.9	5240.1	4631.6
18	6891.3	6656.5	6029.6	5329.5
19	7219.6	6973.6	6316.8	5583.3
20	7377.0	7125.7	6454.6	5705.1

Note: Natural frequencies 1-6 are due to numerical errors in computation

Figure 7.4 Natural Frequencies of Stator Core

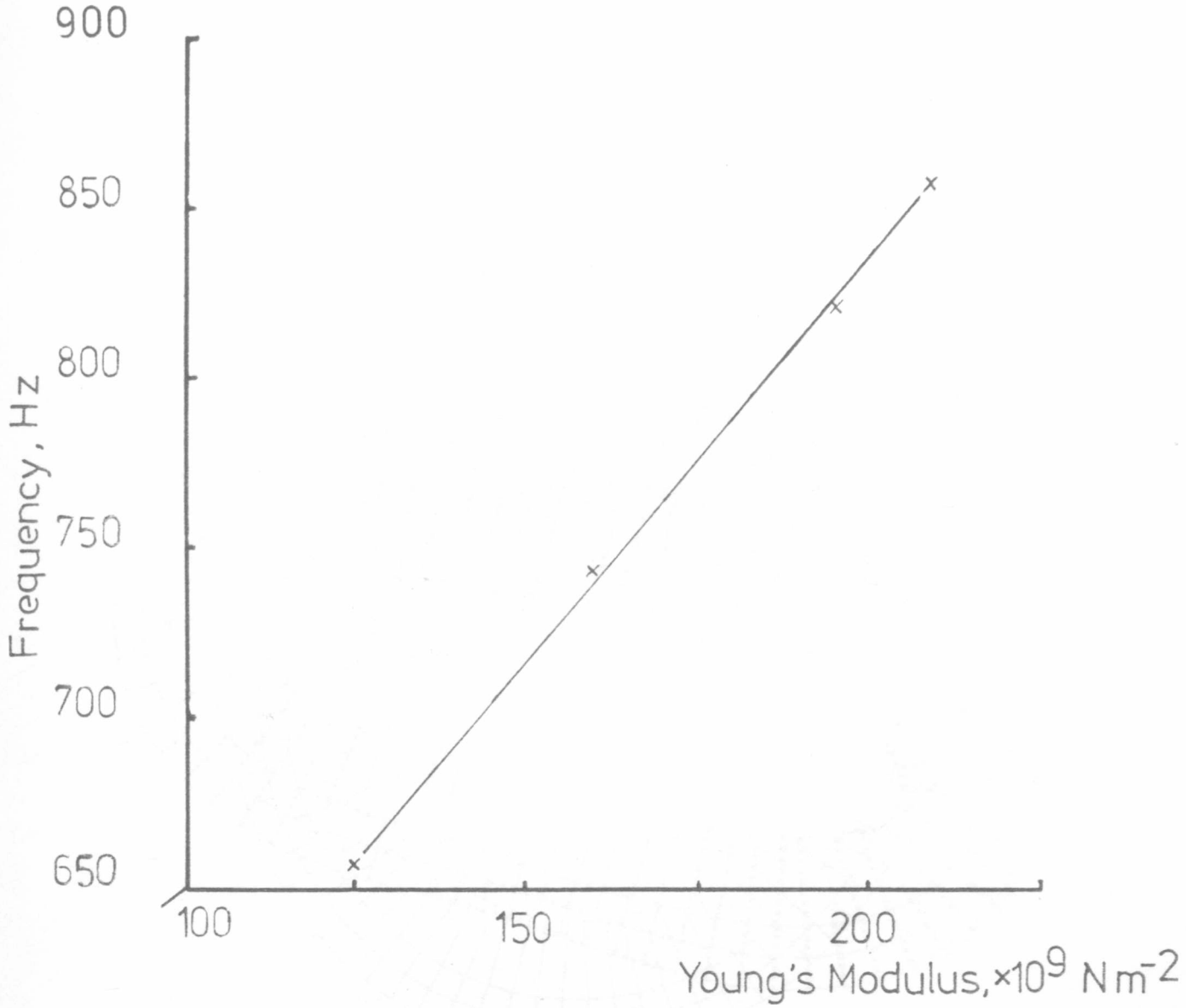

Figure 7.5 Variation of First Natural Frequency with Young's Modulus

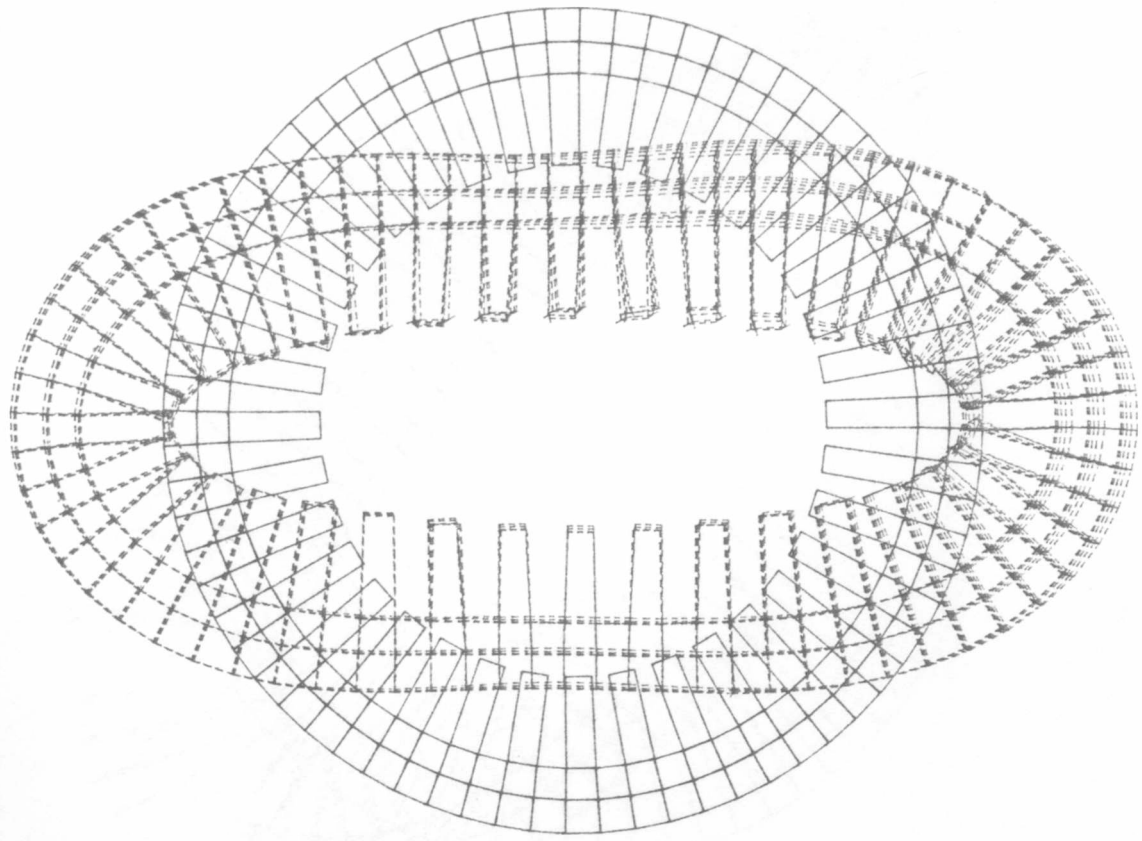

Figure 7.6 Mode Shape No.7

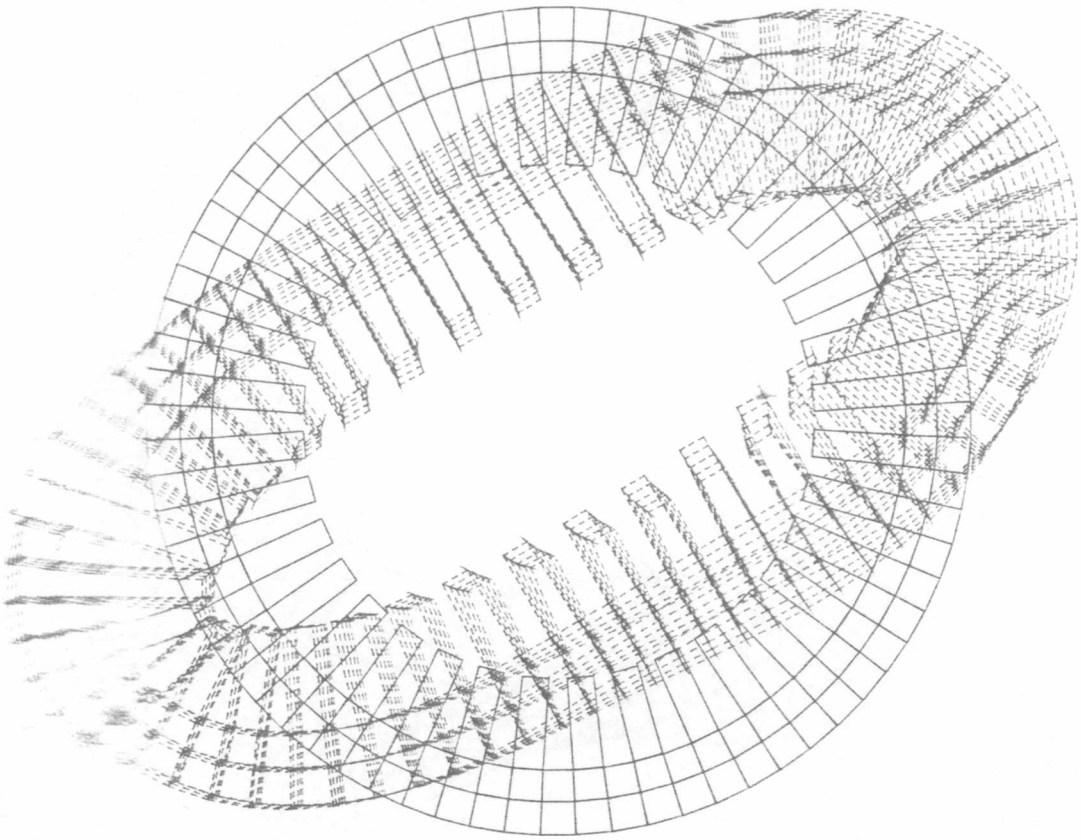

Figure 7.7 Mode Shape No. 8

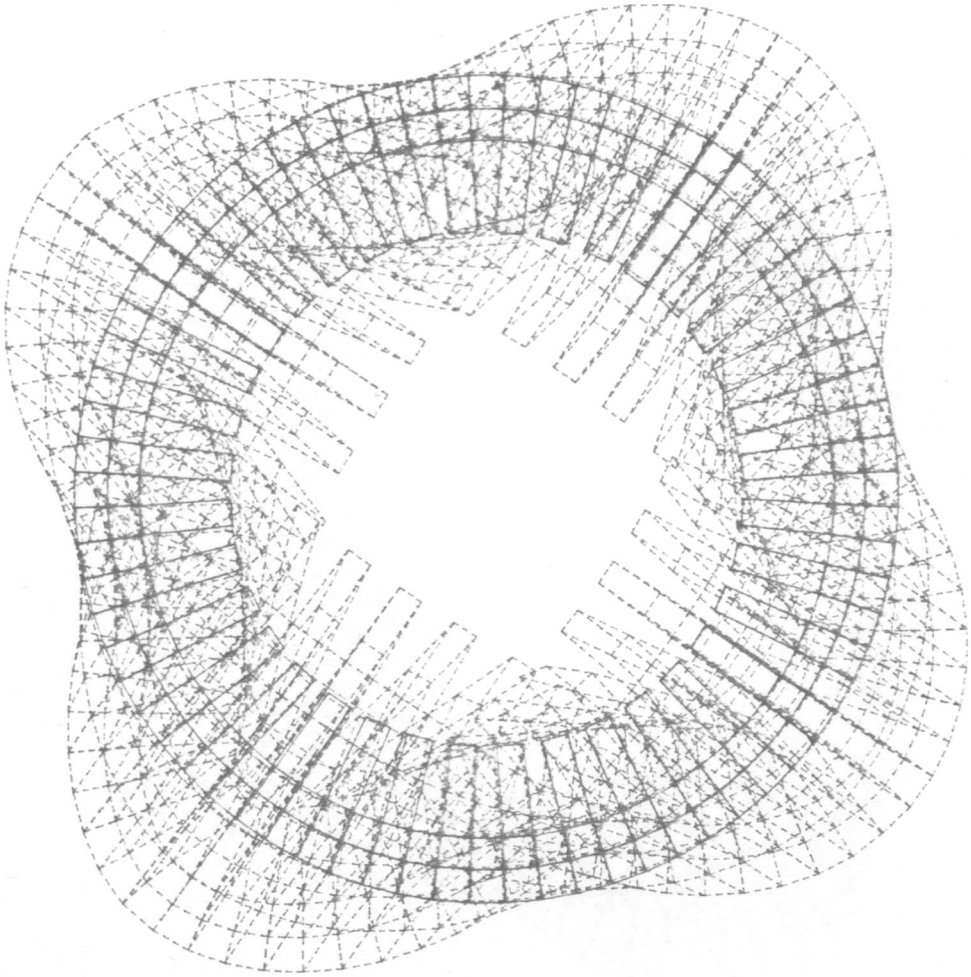

Figure 7.8 Mode Shape No.9

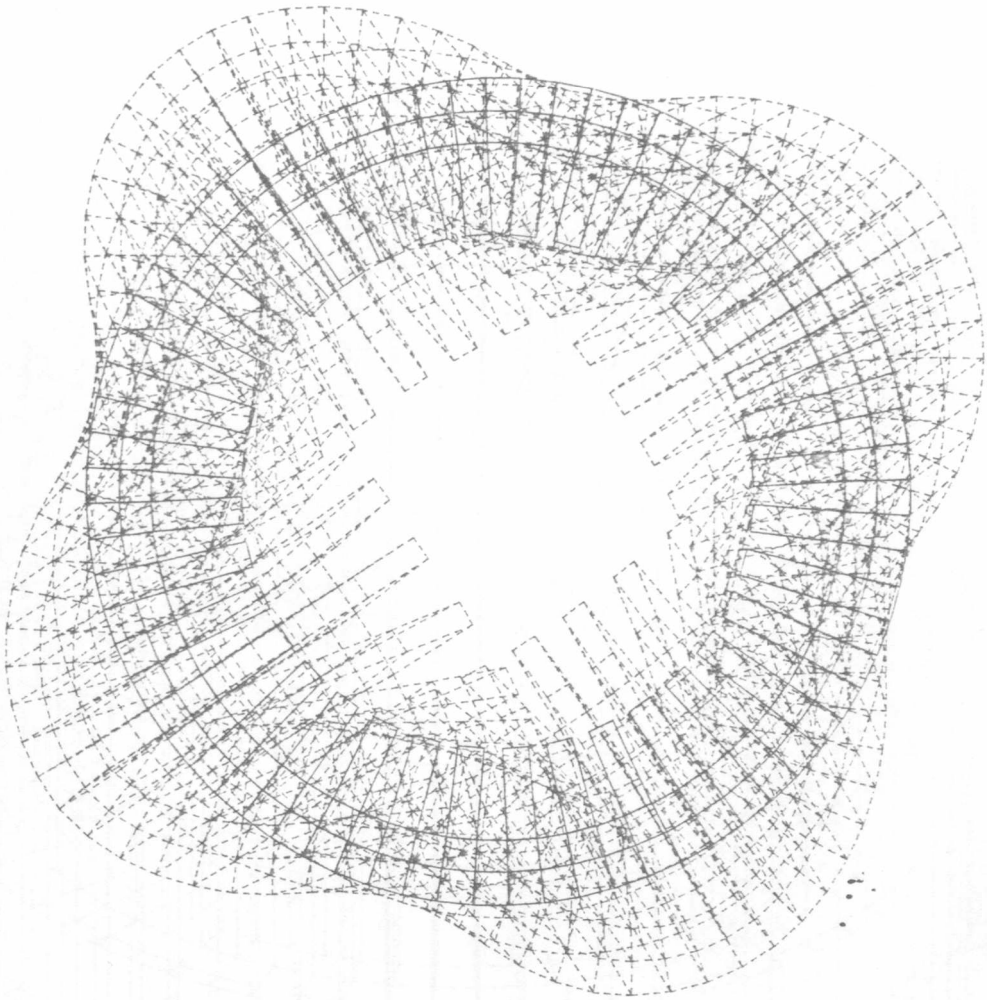

Figure 7.9 Mode Shape No. 10

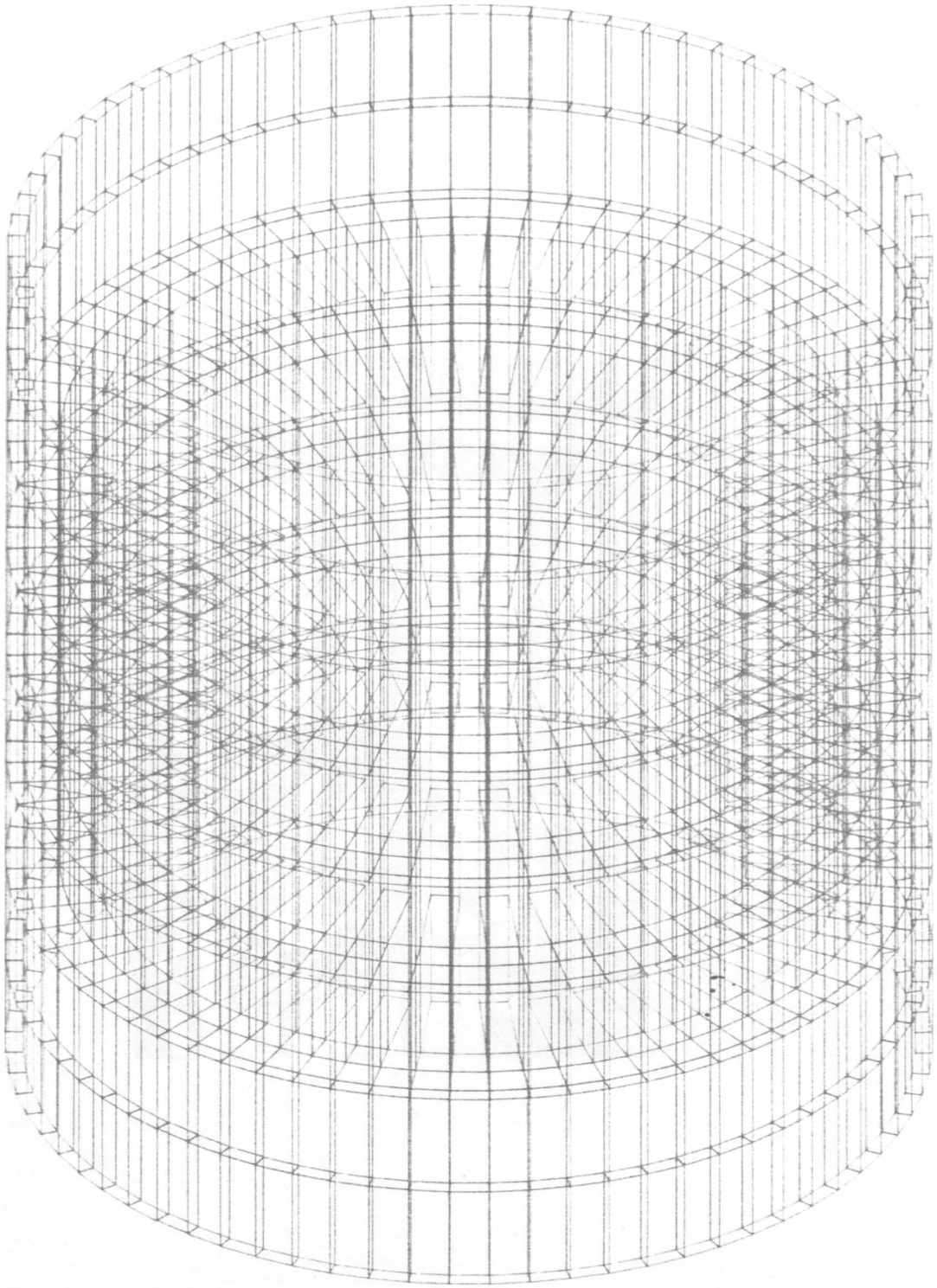

Figure 7.10 Stator Core with Case — Printout from PAFEC 75

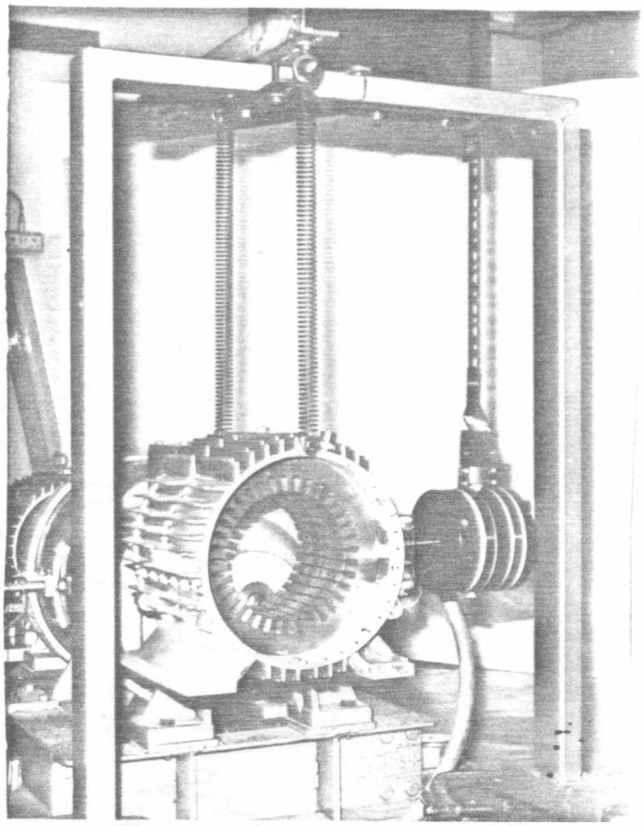

Figure 7,11 Experimental Rig

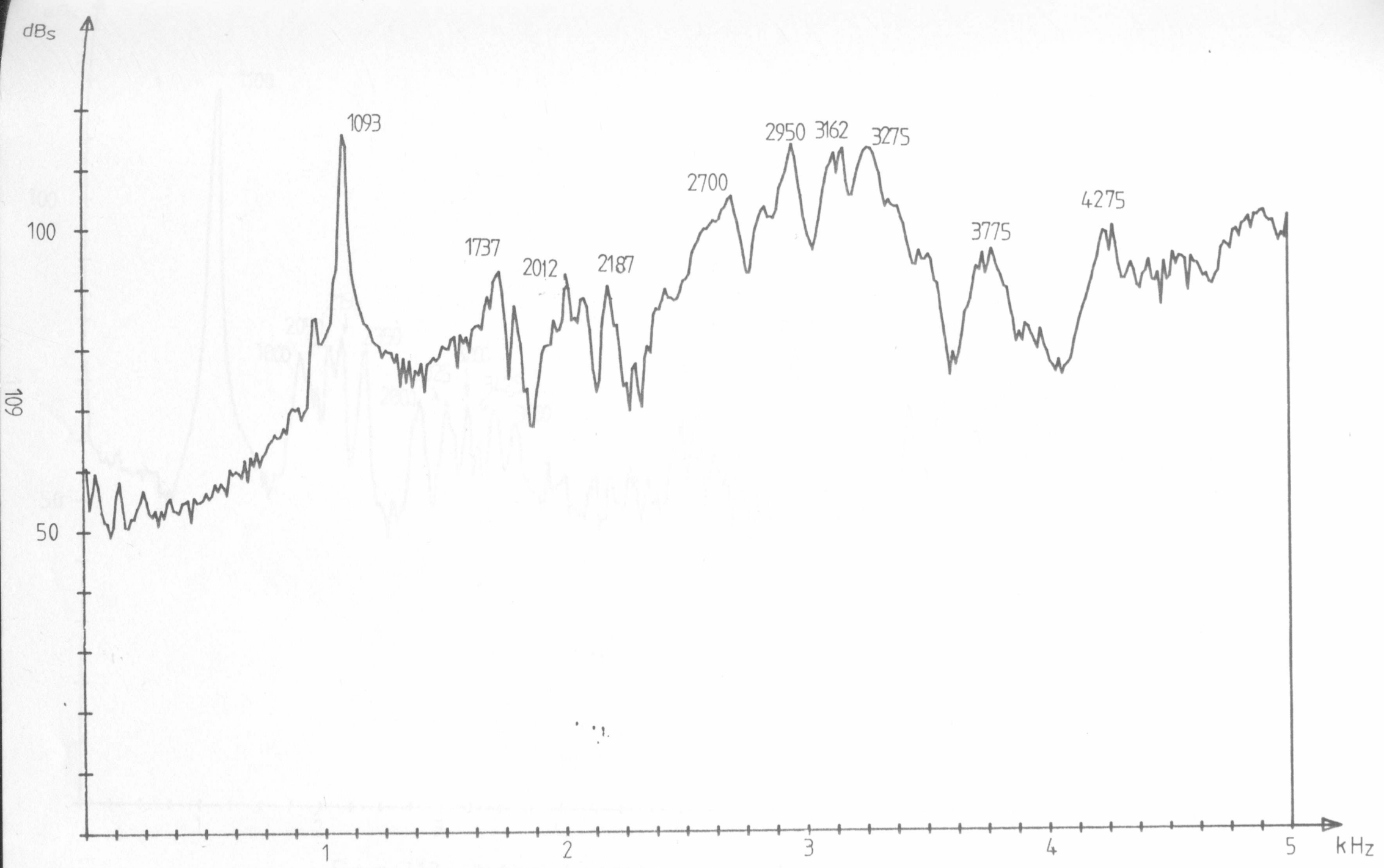

Figure 7.12 Natural Frequencies – Swept Sine Test

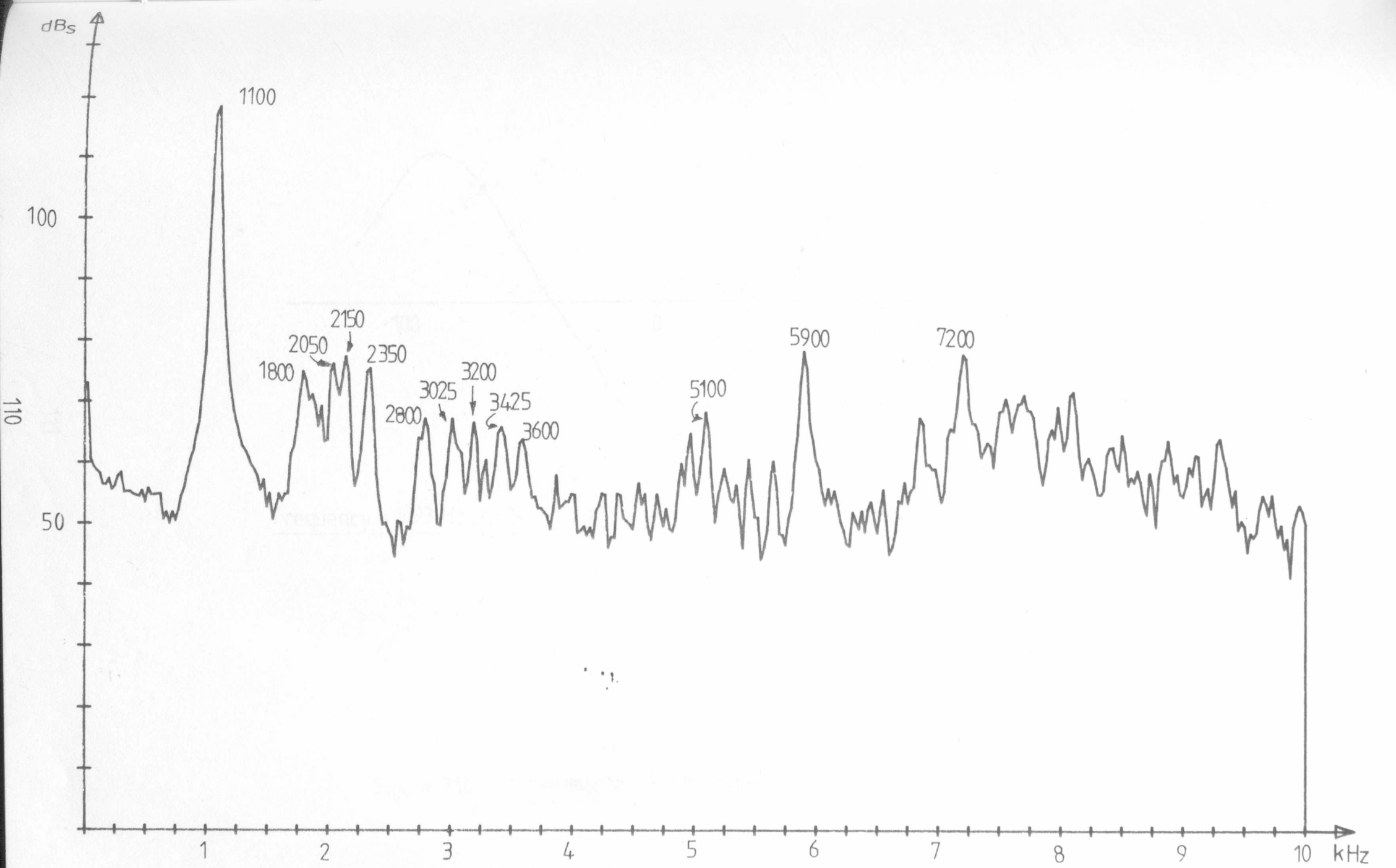

Figure 7.13 Natural Frequencies — Shock Test

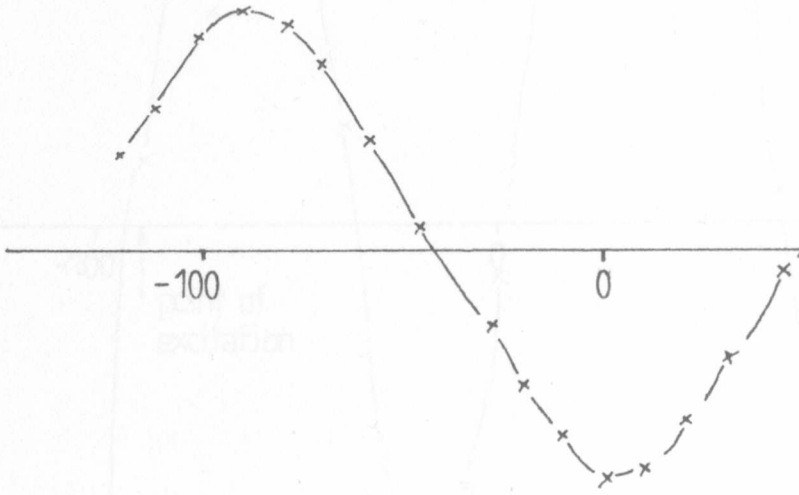

Frequency = 1093 Hz, n=2

Figure 7.14 Experimental Mode Shape

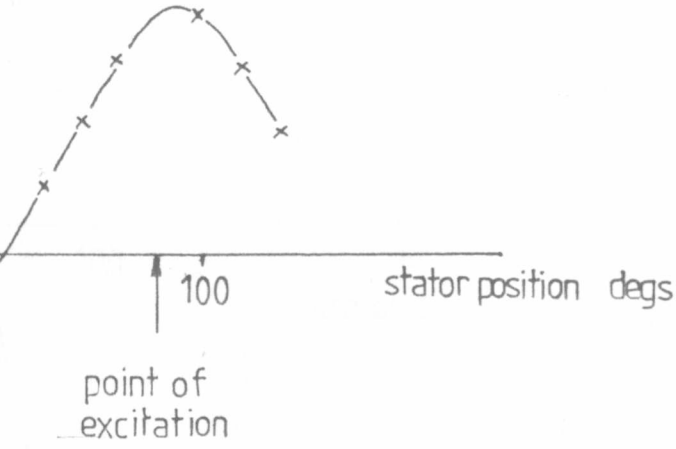

n=2

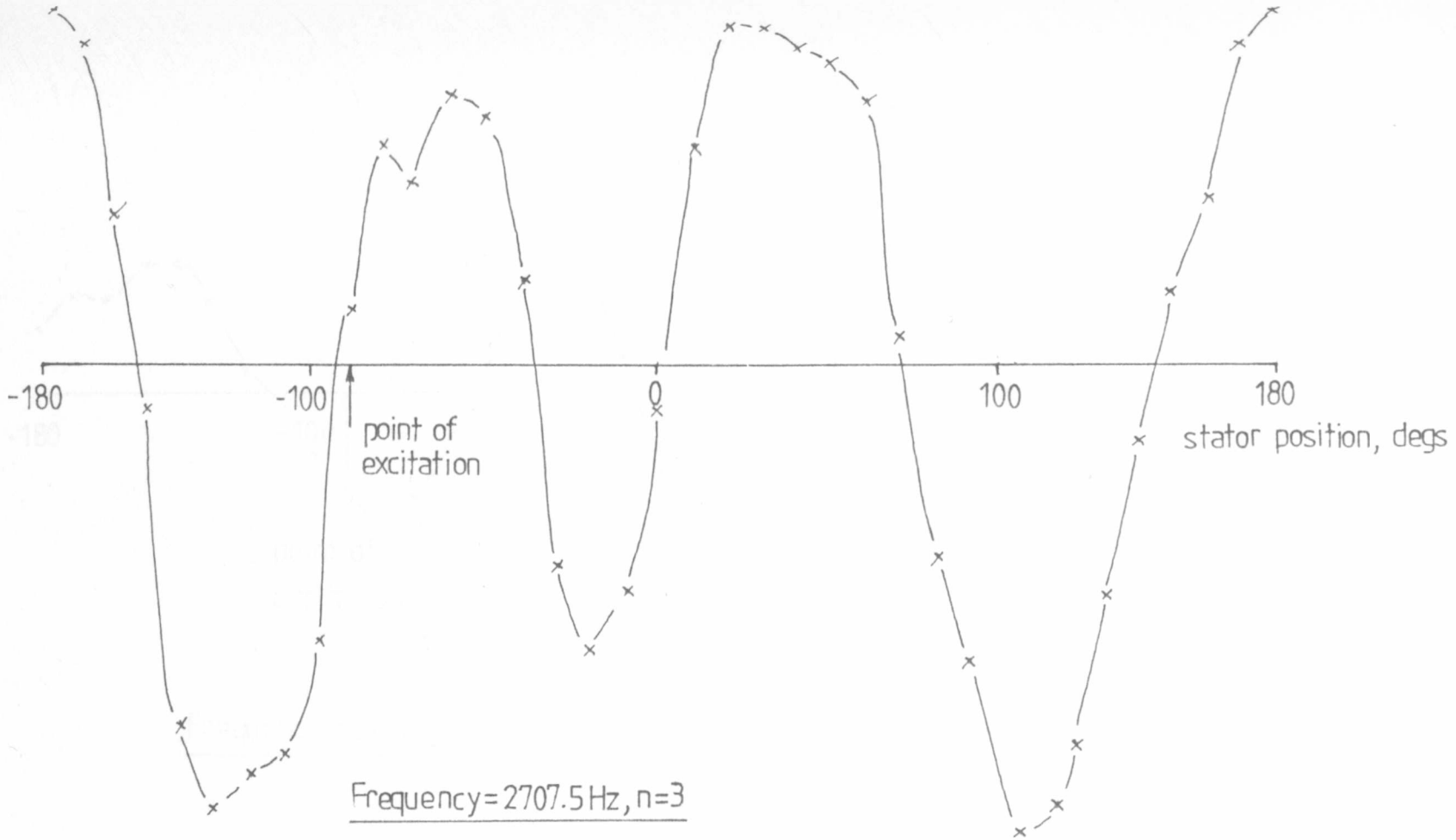

Figure 7.15 Experimental Mode Shape n=3

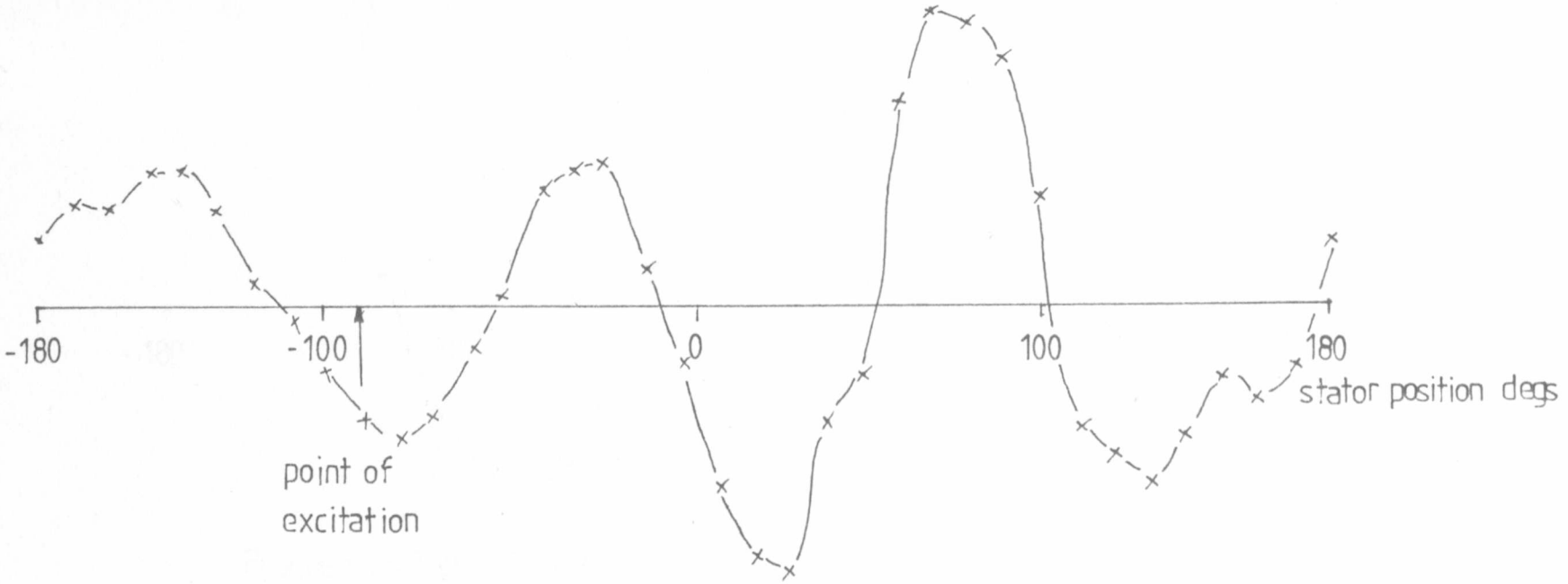

Frequency = 2812 Hz, n = 3

Figure 7.16 Experimental Mode Shape n=3

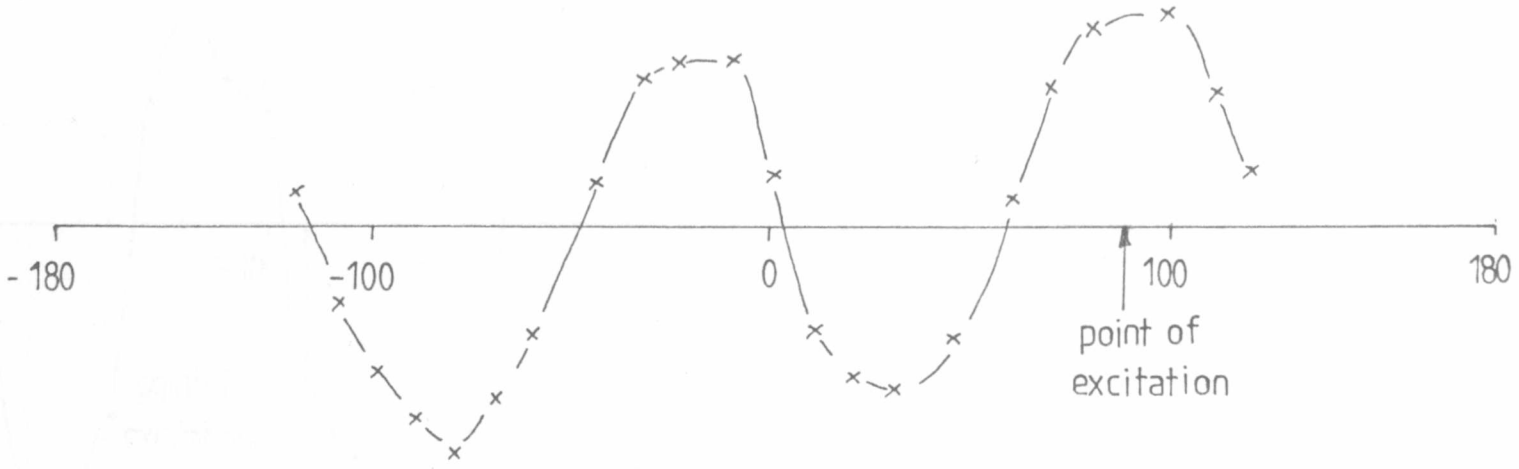

Frequency = 3126 Hz, n=3

Figure 7.17 Experimental Mode Shape n=3

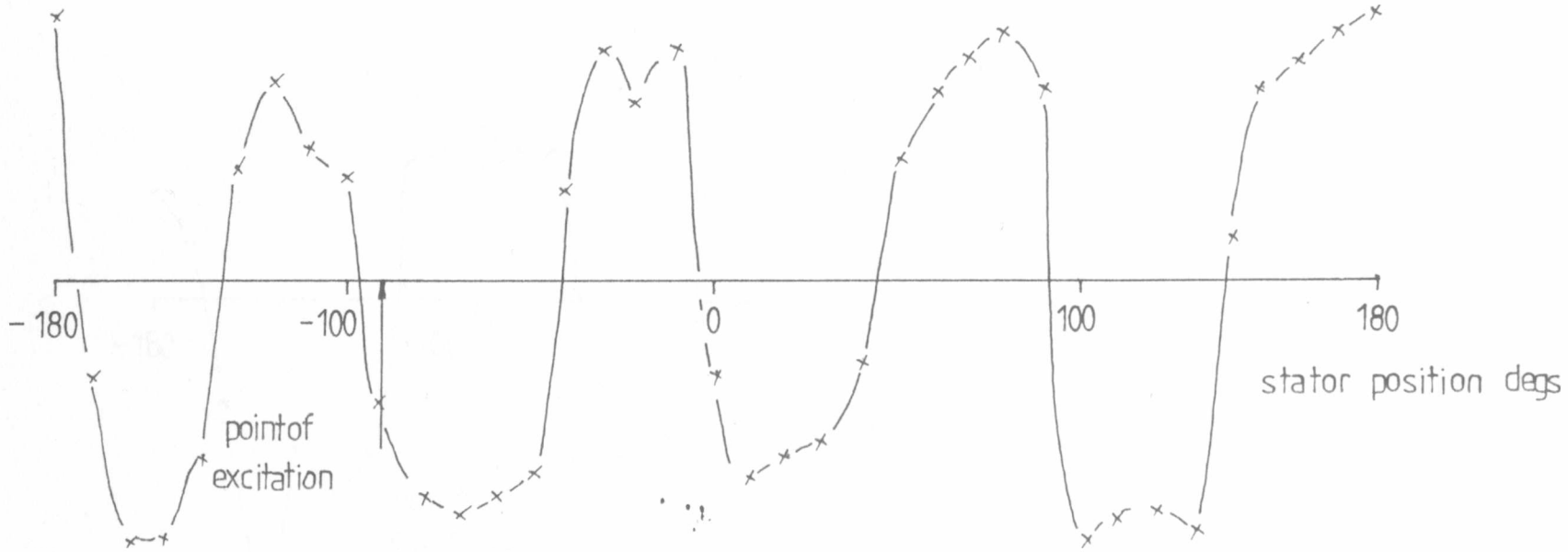

Frequency = 2950 Hz, n = 4

Figure 7.18 Experimental Mode Shape n = 4

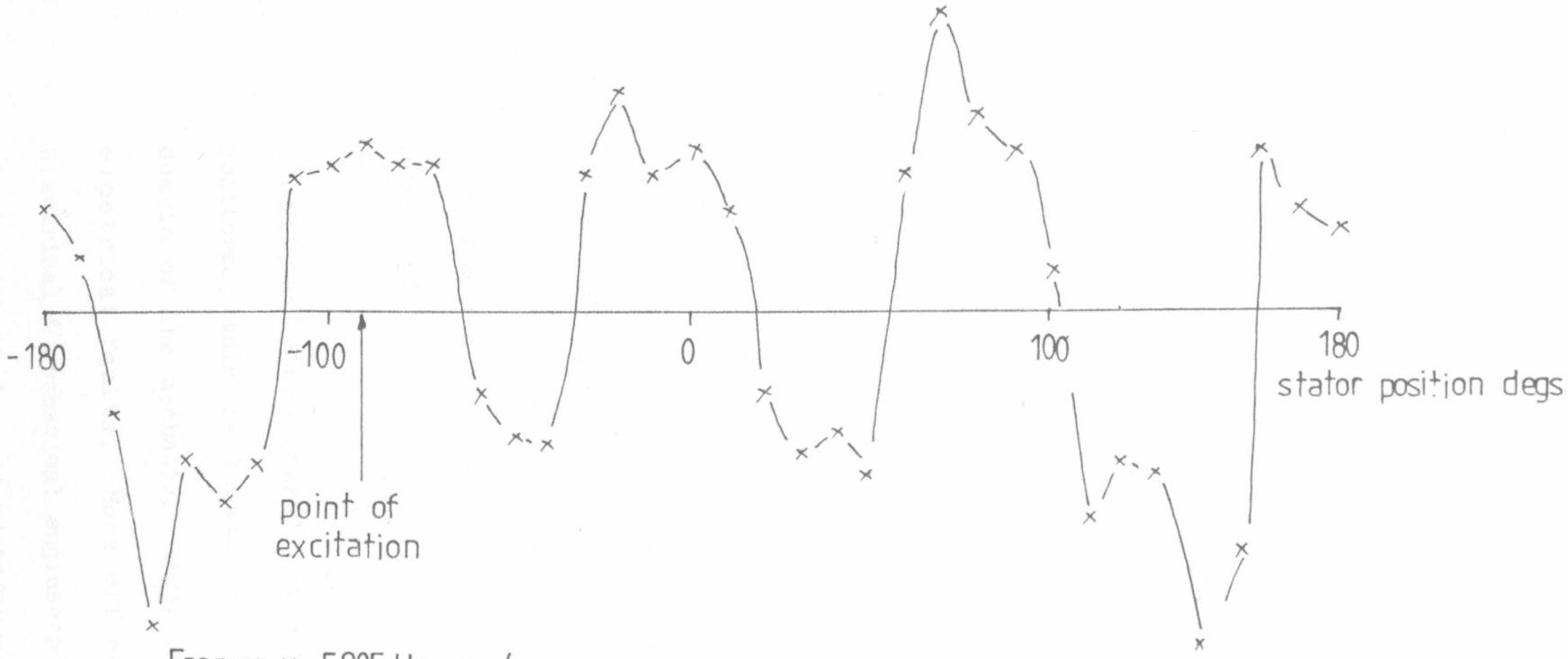

Figure 7.19 Experimental Mode Shape n=4

CHAPTER EIGHT

CONCLUSIONS & FUTURE WORK

8.1 DISCUSSION

The results of the work described in previous chapters shows that SCIM faults can be detected using vibration, line current and leakage flux signals. These signals are relatively easy to detect by means of readily available transducers. This thesis has shown how to interpret these signals by using a high resolution spectrum analyser and by applying fundamental machine knowledge.

It has been shown that stator core vibration is particularly sensitive to changes in electromagnetic forces caused by SCIM faults. Using basic SCIM design information such as supply frequency, running speed and the number of rotor slots the electromagnetic frequency components of vibration can be easily identified.

Usually only the overall vibration of a machine has been monitored, this is because this has traditionally been the domain of the mechanical engineer who is not concerned with electrical faults. More effort must be made to convince electrical & mechanical engineers that significant information can be gained from straightforward spectral analysis of the vibration signal.

8.2 FUTURE WORK

The work presented in this thesis has been based on SCIMs driving constant speed loads. Further work is therefore required to fully assess the effects of faults on SCIMs driving pulsating loads such as reciprocating compressors.

The results obtained during the course of this thesis could be used to develop a dedicated SCIM monitoring system. However if an operator has suitable transducers, a portable tape recorder and a Spectrum Analyser he could set up a Condition Monitoring programme based on periodic analysis of the various signals.

The practical difficulties of monitoring SCIMs, using techniques described in this thesis, which are sited in hazardous areas has not been covered by this thesis. This problem can be solved by close liaison with machine manufacturers and certifying authorities.

REFERENCES

1. Jackson, B., Pestle, J.B. and Wood, M.D.: 'Recent Advances in the Design of Circulator Motors for Advanced Gas Cooled Reactors', International Conference on Electrical Machines - Design and Applications, 1982, IEE Conf. Publ. No. 213, pp 18 - 12.

2. Smith, J.R., Stronach, A.F. and Tsao, T.: 'Digital Simulation of Marine Electromechanical Drive Systems', IEEE Transactions on Industry Applications, Vol. 1A - 18, No. 4, July/Aug 1982, pp 393 - 399.

3. 'Integrity Monitoring of Fixed Steel Platforms', Offshore Research Focus, Dept. of Energy, No. 34, Dec. 1982, ISSN: 0309 - 4189.

4. Kent, L.D. and Cross, R.J.: 'The Philosophy of Maintenance', 18IATA PPC - Sub Committee Meeting, Copenhagen, 19.10.73.

5. Neale, M. and Associates: 'A Guide to the Condition Monitoring of Machinery', HMSO, London, 1979, ISBN011 5121269.

6. Cornick, K.J. and Thompsin, T.R.: 'Steep-fronted Switching Transients and their Distribution in Motor Windings, Parts 1 & 2, IEE Proc., Vol. 129, Pt. B, No. 2, March 1982, pp 45 - 63.

7. Burns, R.L.: 'Rotor Bar Failures in Large A.C. Squirrel Cage Rotors' Electrical Engineering, 1977, 54 (10), pp 11-14.

8. Verma, S.P., Girgis, R.S. and Fleming, R.J.: 'The Problems Caused by Shaft Potentials and Bearing Currents in Turbogenerators; Methods of Prevention', CIGRE 1980 Session, 11 - 10, pp 13.

9. Penman, J., Hadwick, J.G. and Stronach, A.F.: 'Protection Strategy against the Occurrence of Faults in Electrical Machines', IEE Conf. Publ. 185, 1980, pp 54 - 58.

10. Erlicki, M.S., Porat, Y and Alexandrovitz, A.: 'Leakage Field Changes of an Induction Motor as Indication of Non-symmetric Supply', IEEE Transactions on Industry and General Applications, Vol. IGA - 7, No. 6, Nov/Dec. 1971, pp713 - 717.

11. Milne, A.J.: 'Computational Aspects of Machine Vibration Monitoring', Report No. EE822, RGIT, Aberdeen, 1982.

12. Alger, P.L.: 'The Nature of Induction Machines, Gordon & Breach, 1965.

13. Bonnett, A.H.: 'Analysis of Winding Failures in Three-Phase Squirrel-Cage Induction Motors', IEEE Transactions on Industry Applications, Vol. 1A - 14, No. 3, 1978.

14. Jones, C.V.: 'Unified theory of Electrical Machines', Butterworth, 1967.

15. Gleason, L.L. and Elmore, W.A.: 'Protection of 3 - Phase Motors against Single-Phase Operation', AIEE Trans., Part III, Vol. 77, 1958.

16. Lord, H. and Pearson, F.K.: 'Sensitive Protection for Induction Motor Supplies', Electrical Review, Vol. 207, No. 5, August 1980.

17. Vincent, C.E.: 'Maintenance of Large Industrial Drives', IEE Conference Publication, Colloquium on the Design and Applications of Large Industrial Drives, No. 170, 16 - 17, 1978.

18. British Standards, BS 4999: Part 31: 1971.

19. Gorges, H: 'On the Operation of Polyphase Induction Motors with Reduced Speed', Elektrotechnische Zeitschrift, Berlin, Germany, Vol. 17, 1896.

20. Vas, P.: 'Performance of Three Phase Squirrel-Cage Induction Motors with Rotor Asymmetrics', Periodical Polytechnica Electrical Engineering, Vol. 19, 1975.

21. Ito, M., Nobura, F., Okuda, H., Takahashi, N. and Watahiki, S.: 'Effect of Broken bars on Unbalanced Magnetic pull and Torque of Induction Motors', Electrical Engineering in Japan, Vol. 100, No. 1, 1980.

22. Williamson, S. and Smith, A.C.: 'Steady State Analysis of Three-Phase Cage Motors with Rotor Bar and End ring Faults', Proc. IEE, May 1982, Vol. 129, Pt. B.

23. Gaydon, B.G.: 'An Instrument to Detect Induction Motor Circuit Defects by Speed Fluctuation Measurements', IEE Conference on Electronic Test & Measuring Instrumentation, Testmex 79, 1979.

24. Hargis, C., Gaydon, B.G. and Kamash, K.: 'The Detection of Rotor Defects in Induction Machines', IEE International Conference on Electrical Machines - Design & Applications, 1982, No. 213, pp 216 - 220.

25. Pozanski, A.: 'Acoustic Measurement of three-phase asynchronous motors, with a broken bar in the cage rotor', ZesZ. Nauk. Politech. Lodz. Elecktr., 1977, 60 pp 121 - 131.

26. Thomson, W.T.: 'Vibration & Noise in Small-Power Electric Motors', M.Sc. Research Thesis, University of Strathclyde, Glasgow, 1977.

27. Girgis, R.S. and Verma, S.P.: 'Method for Accurate Determination of Resonant Frequencies and Vibration Behaviour of Stators of Electrical Machines', Proc. IEE, Vol. 128, Pt. B, No. 1, Jan. 1981.

28. Girgis, R.S. and Verma, S.P.: 'Experimental Verification of Resonant Frequencies and Vibration Behaviour of Stators of Electrical Machines, Parts I & II', Proc. IEE, Vol. 128, Pt. B, No. 1, Jan. 1981.

29. Shumilar, J.A.: 'Calculating Stator Vibrations in Electrical Machines', Proceedings of the International Conference on Electrical Machines, 1974.

30. Fenner, R.J.: 'Finite Element Methods for Engineers', Unwin Brothers Ltd., 1975.

31. 'Pafec 75 - Theory & Results', Pafec Development and Marketing, 1975.

32. Ellison, A.J. & Yang, S.J.: 'Effects of Rotor Eccentricity on Acoustic Noise from Induction Machines', Proc. IEE, Vol. 118 No. 1, Jan 1972.

APPENDIX I - SURVEY QUESTIONNAIRE

ROBERT GORDON'S INSTITUTE OF TECHNOLOGY, ABERDEEN
SCHOOL OF ELECTRONIC AND ELECTRICAL ENGINEERING

QUESTIONNAIRE ON CONDITION MONITORING OF MEDIUM/LARGE SQUIRREL-CAGE INDUCTION MOTORS

1 Do you use any of the following condition monitoring techniques on your squirrel-cage induction motors?

(a) Vibration Monitoring [YES | NO] If the answer is yes continue : proximity transducers on plain bearings [YES | NO] ; accelerometers [YES | NO] ; velocity transducers [YES | NO] ; vibration spectrum analysis [YES | NO] ; computer based vibration monitoring system [YES | NO]

(b) Winding temperature sensing [YES | NO]

(c) Stator core temperature sensing [YES | NO]

(d) Bearing temperature sensing [YES | NO]

(e) Meggar Insulation Testing [YES | NO]

(f) Tan (δ) Insulation Tests [YES | NO] ; DLA Tests [YES | NO]

(g) Measurement of shaft voltages across the rotor [YES | NO]

(h) Wear debris monitoring [YES | NO] if yes continue : Magnetic Plugs [YES | NO] ; oil sample testing/analysis [YES | NO]

(i) Apart from standard tests any other monitoring techniques you use ?

- -

- -

- -

- -

2 What is "On-Condition Maintenance?"

With on-condition maintenance, repairs are carried out only when the condition of the machine has deteriorated past a predetermined point. That is, repairs or part replacements take place at a point in time where it has definately been proved that a fault exists, and if left unrepaired would probably result in catastrophic breakdown, with possible damage to other machine parts and a disruption in production.

(a) /

(a) Do you apply only the standard planned maintenance schedules to your large squirrel cage induction motors? YES NO

(b) Do you apply on-condition maintenance programmes based on any of the measurement techniques stated in Question 1?

(c) Any comments about the concept of on-condition maintenance?

(d) Where possible, could you please complete the following tables (pages 3 and 4).

Motor Rating		Application of Motor	Starting DOL/Other	Total No. of Yrs. in Service	No. of Yrs. in Service prior to First Fault	Bearing Faults/Cause if Possible	Presence of Shaft Voltages
ltage and equency	Rating						

Bearing Damage Due to Bearing lectrical Currents	Do you Insulate the Bearing Pedestals ?	Stator Winding Insulation Failure	Cracked/Broken Rotor Bars	Cracked Shafts	Stator Core Faults	Any Other Faul Causing Failu

APPENDIX II

UNBALANCED SUPPLY BY SYMMETRICAL COMPONENTS

The symmetrical component analysis of an unbalanced three-phase system is based on the following equations (14):

$$V_+ = (V_r + a V_y + a^2 V_b)/\sqrt{3}$$
$$V_- = (V_r + a^2 V_y + a V_b)/\sqrt{3}$$
$$V_o = (V_r + V_y + V_b)/\sqrt{3}$$

where V_+, V_- and V_o are the positive, negative and zero sequence voltages respectively and V_r, V_y and V_b are the phase voltages a is the 120 operator.

In a balanced system

$$V_y = a^2 V_r$$
$$V_b = a V_r$$

Consider the case when one phase voltage, say V_r , is reduced in magnitude to xV_r , where $0 < x < 1$.

The symmetrical component voltages can now be written as:

$$V_+ = (xV_r + a V_y + a^2 V_b)/\sqrt{3}$$
$$V_- = (xV_r + a^2 V_y + a V_b)/\sqrt{3}$$
$$V_o = (xV_r + V_y + V_b)/\sqrt{3}$$

Simplifying gives:

$$V_+ = V_r(x + 2)/\sqrt{3}$$

$$V_- = V_r(x - 1)/\sqrt{3}$$

$$V_o = V_r(x - 1)/\sqrt{3}$$

Now unbalance is given as V_- / V_+ and V_o / V_+.

Therefore:

$$V_- / V_+ = (x - 1)/(x + 2)$$

$$V_o / V_+ = (x - 1)/(x + 2)$$

APPENDIX III

DERIVATION OF TORQUE AND SPEED FOR ROTOR WITH BROKEN BAR

To the rotor the revolving field of the stator is at the slip frequency (sf). The current in the rotor is due to induction and also varies at the slip frequency. So we have, for the rotor,

$$B = B_m \sin (2\pi\ s\ ft)$$

and

$$I_b = I_m \sin (2\pi\ s\ ft)$$

The torque produced by a single conductor can be written as:

$$T = F_b\ r$$

$$= B \ell\ I_b\ r$$

$$= \ell r\ I_m\ B_m \sin (2\pi\ s\ ft) \sin (2\pi s\ ft)$$

$$= K (1 - \cos 4\pi\ s\ \ ft)$$

where $K = \ell r\ B_m\ I_m$

So the torque produced by a single bar varies at twice the slip frequency and is always positive. In a well designed machine the torques from the individual conductors will sum to a constant

$$\text{ie } T_{TOT} = C$$

If however, a conductor cannot contribute its share of the torque the effective torque can be written as:

$$T_{BB} = C - K\,(1 - \cos 4\pi\, s\, ft)$$

$$= D - K \cos 4\pi\, s\, ft \quad , \text{ where } D = C - K$$

Thus a broken conductor will produce a component of torque which pulsates at twice the slip frequency.

The rotational speed of the rotor is related to the torque by the following equation

$$T_D = J\omega + F\omega + T_\ell$$

Where T_D is the drive torque, J is the inertia, F is the viscous damping and T_ℓ is the load torque. For small changes in speed the load torque, T_ℓ, can be written as:

$$T_\ell = T_0 - T_1\omega$$

For a broken rotor bar the torque and speed are related as follows:

$$D - K \cos 4\pi s\, ft = J\omega + F\omega + T_0 - T_1 \omega$$

rearranging the letting $4\pi sf = \rho$

$$J\omega + (F - T_1)\omega = (D - T_0) - K \cos \rho t$$

Taking Laplace transforms of each side gives

$$W(s)\,(sJ + (F - T_1)) = \frac{(D - T_0)}{s} - \frac{Ks}{s^2 + \rho^2}$$

$$W(s) = \frac{(D - T_0)}{s(sJ + (F - T_1))} - \frac{Ks}{(sJ + (F - T_1))\,(s^2 + \rho^2)}$$

Solving in the normal manner gives a steady state solution of the form

$$\omega_{BB} = \omega_0 - K_1 \cos 4\pi sft - K_2 \sin 4\pi sft$$

Therefore the effect of a broken rotor bar on the speed is to produce a fluctuation in speed at twice the slip frequency.

PUBLICATIONS

1. Thomson W.T., Deans N.D, Leonard R.A. and Milne A.J.

   'Condition Monitoring of Induction Motors for Availability Assessment in Offshore Installations'
   4th Euredata Conference, Venice, March 1983.

2. Thomson W.T., Deans N.D., Leonard R.A. and Milne A.J.

   'Monitoring Strategy for Discriminating between Different Types of Rotor Defects in Induction Motors'
   Universities Power Engineering Conference,
   University of Surrey, April 1983.

3. Thomson W.T., Leonard R.A. & Milne A.J.

   'Failure Identification of Offshore Induction Motor Systems using On-condition Monitoring'
   4th National Reliability Conference, Birmingham, July 1983.
   Later reprinted in Reliability Engineering 9, 1984 pp 49 - 64.

4. Leonard R.A. & Thomson W.T.

   'Vibration & Stray Flux Monitoring for Unbalanced Supply and Inter-turn Winding Fault Diagnosis in Induction Motors'.
   International Conference on Condition Monitoring, Swansea, April 1984.

4th EUREDATA CONFERENCE

CONDITION MONITORING OF INDUCTION MOTORS FOR AVAILABILITY ASSESSMENT IN OFFSHORE INSTALLATIONS

W.T. Thomson, N.D. Deans, R.A. Leonard, A.J. Milne

Robert Gordon's Institute of Technology,

Aberdeen, AB9 1FR, Scotland, U.K.

Introduction

In offshore oil and gas production platforms and in onshore refinery installations the three-phase squirrel-cage induction motor (SCIM) is used to drive gas compressors, sea water injection pumps and oil exporting pumps. Consequently, the assessment of the condition of the motor and its future availability are important, since failure caused by one of a number of fault conditions is costly and potentially dangerous. This is particularly evident when oil production and refinery installations are being considered. Here the handling costs associated with plant removal and loss of production makes down-time unacceptable unless absolutely necessary. It is essential therefore that the operator knows the condition of the motor while it is in service and if possible is able to predict when a motor might fail.

It has generally been believed by many engineers responsible for plant monitoring that damage and wear in rotating machines can be detected by analysing vibration signals and by monitoring shaft motion. It is true that the vibration signal contains information relating to damage and wear but the spectrum also contains information about the normal operation of the motor. The inherent difficulty is the separation of these two aspects of signal information. This is particularly difficult with a three-phase squirrel-cage induction motor since the resulting vibration spectrum is a by-product of electromagnetic forces and the normal mechanically transmitted forces.(1) Due to the motor being a complex electromechanical device, the fault mechanisms can be electrical, mechanical or electromechanical in nature. This means that the normal on-line protection devices for sensing overload and earth leakage currents and excessive bearing, winding and core temperatures are insufficient, and additional on-line monitoring techniques are required. One approach involves time consuming analysis of vibration data coupled with an in-depth appreciation of plant behaviour

assisted by historical records of performance.[2] This leads to a monitoring system based essentially on experience and can be particularly difficult to operate in an offshore installation due to such factors as the staff working shift cycles, 'hot' work permits being required and the generally hostile environment. A second approach and the one being considered as the main objective of the work referred to in this paper seeks to identify the fundamental causes of various electromechanical faults and to develop an on-line data processing system for detecting faults and predicting the availability of the motor.

The initial results of the research work are presented in the paper and are primarily concerned with providing a data base for identifying faulty SCIMs, with a view to developing fast and efficient processing techniques which are particularly applicable to SCIM fault recognition. The results of a survey carried out to determine the existing monitoring techniques and data collection methods currently being used for 3-phase induction motor fault recognition is presented, and the types of failure and their frequencies of occurrence are also reported. A brief discussion of the fault mechanisms and the development of a fault producing test rig is presented. The data acquisition and computer processing system is described, a data bank of the processed signals for 'healthy' and 'unhealthy' machines is presented and the results discussed.

Survey of Monitoring Techniques and Failure Mechanisms of 3-phase Squirrel-cage Induction Motors

A survey of a variety of major industrial organisations using large SCIMs in the offshore and onshore environment was conducted to gain information about the types of failure of SCIMs and the methods used for monitoring the condition of the machine. A questionnaire was sent to each of the operators and consisted of two sections. The first was concerned with identifying what types of condition monitoring techniques are currently being used and to also test the operators' reaction to the concept of on-line condition monitoring as part of an on-condition maintenance strategy. The second section consisted of specific questions on the types of failure to assess if there is a real need for developing on-line diagnostic techniques for SCIM fault recognition.

All of the industrial organisations completed Section 1 and six out of the eleven operators provided specific information about motor failures. The results are presented in Tables 1 and 2 respectively. A 100% response was not expected in Section 2 because the collection and compilation of the data

required a considerable effort in terms of man hours. Since the information gives details on the types of failure and frequencies of occurrence of eighty-two SCIMs in the range from 425 kW to 6.3 MW, the results are able to provide sufficient information for deciding whether or not a problem exists in SCIM fault recognition.

The main conclusions from the survey and personal discussions with the operators are :

(a) There can be considerable savings in maintenance procedures, outage time of plant and loss of revenue if reliable condition monitoring techniques are available as part of an On-condition maintenance strategy.

(b) Due to the number of failures reported by the operators, there is a need for fundamental studies of various types of fault mechanisms to be undertaken, and to also develop signal processing techniques to provide a data base for classification of 'healthy' and 'unhealthy' motors.

(c) The operators would welcome the development of a flexible microprocessor-based instrumentation system capable of performing an on-line analysis of different types of signal (e.g. vibration, current, stray flux) which could also identify the various types of fault mechanisms and assess the availability of the SCIM.

Fault Mechanisms

In response to the survey and additional discussions with other industrial users it was decided to investigate the following faults :

(a) Inter-Turn Winding Faults

The insulation between turns of a coil can breakdown due to contamination, thermal ageing or vibrational stresses. The breakdown process causes heating in the winding and a change in the current distribution which leads to a complete failure of the motor's insulation system.

(b) Broken Rotor Bars

This usually occurs when one of the conducting bars which forms part of the 'squirrel-cage' rotor winding breaks where it is joined to the conducting

end ring. The bars adjacent to the broken one carry extra current and overheat which in turn generally leads to additional broken bars. This results in torque pulsations, speed fluctuations and changes in the vibration spectrum and can lead to mechanical damage of the rotor, stator bore or bearing assembly.

(c) Static Rotor-Stator Eccentricity

In this situation, the axial centres of both rotor and stator are not coincident. This results in increased vibration levels and could lead to bearing failure.

(d) Single-Phasing

This is the term used when one of the supply lines or windings becomes open circuited. This is a severe fault condition and results in high current and vibration levels.

The results of the survey also indicate that bearing failure in SCIMs is a major problem. This is rather surprising since bearing fault detection has received considerable attention from researchers and industrial operators[3-7]. The difficulty of operating a vibration monitoring programme in a hostile environment has been mentioned and it is here that there is a need for the development of bearing monitoring techniques and instrumentation suitable for the offshore environment.

Previous investigators have tended to look at individual machine signals to determine the existence of a fault. Erlicki[8] has shown how axial flux could be used to indicate non-symmetric supply conditions. Penman[9,10] has clearly shown how inter-turn faults can be detected with axial flux but found the use of axial flux inconclusive for detecting broken rotor bars and dynamic rotor-stator eccentricity. Gaydon[11,12] has developed instrumentation techniques using shaft speed fluctuations as the signal source for the detection of broken rotor bars but has stated that "inherent asymmetries were found to give period fluctuations of the same magnitude as when one bar was deliberately open circuited." Hargis[12] has considered changes in the current and vibration spectra for detecting broken rotor bars but has only presented one set of results for a good rotor and one with three broken bars. Steele[13] has monitored current for the detection of electromechanical faults in small-power motors. His results clearly show the potential of the method but he states that "much further work is required to fully explain the current spectra and to produce a commercially viable system."

Hence the authors consider that further work is required under controlled experimental conditions for the following reasons :

(i) to evaluate the effectiveness of monitoring various types of signal

(ii) to explain fully the changes in the spectra

(iii) to develop signal processing techniques to highlight the fault conditions

(iv) to discriminate between the effects of high resistance joints, broken bars or end rings in squirrel-cage rotors

(v) to try and quantify the degree of severity of the different faults.

The philosophy proposed in this paper is to monitor various interrelated motor signals such as vibration, current, end winding leakage flux and axial flux during fault conditions and to present a data base of spectra. It is envisaged that an on-line monitoring system which utilizes three or four types of signals for identifying a particular fault will prove to be more useful than existing techniques which tend to look for changes in only one type of signal.

Test Rig and Signal Processing Equipment

Figure 1 shows the test motor and associated processing equipment. The test rig comprises an 11 kW SCIM loaded by a d.c. dynamometer and has been specifically designed for carrying out controlled experiments with the fault mechanisms described in the previous section. A number of transducers positioned on the test rig sense various parameters for determining the condition of the motor, viz :

T_I is an air-cored toroidal coil used to sense the electrical current in the main supply lead.

T_ϕ is a coil situated on the exterior casing of the motor to sense the extent of the end winding leakage flux.

T_{AX} is a coil wound on the main shaft of the induction motor to sense the degree of axial flux.

T_V is an accelerometer positioned to respond to mechanical vibration of the casing or bearing pedestals.

The electrical signals emanating from the transducers are pre-amplified, filtered and undergo frequency and time-domain analysis in a high-resolution spectrum analyser. The analyser exists as a peripheral device to a PDP11-03 minicomputer system, comprising an 11-03 processor, dual floppy-disc storage unit, keyboard, visual-display unit, printer and high-resolution plotter. The experimenter controls, via the interactive terminal, the operation of the analyser and the subsequent secondary processing of the analysed signals. A library of data processing programs is available to the experimenter to distil the data produced by the analyser in such a way as to highlight particular machine faults. Typical library programs are :

(i) control the analyser, write and read spectral values to and from the analyser and provide automatic scaling of all data values.

(ii) measure the energy content of the whole, or any part of the frequency spectrum of the signal emanating from any selected transducer.

(iii) determine the peak value of any frequency spectrum.

(iv) compute the autocorrelation coefficient of the frequency spectrum for any given offset.

(v) carry out a Fourier transform on a frequency spectrum, providing a Cepstrum of the original signal.

(vi) control the plotting facility so that single and multidimensional plots of the processed data can be produced.

(vii) control the allocation of storage areas on the disc storage units so that historical records of experiments carried out on the induction motor can be accessed at a later date for inspection and comparison.

Test Results

There are various frequency components in each signal which are expected from Induction machine theory.[14] For the current, end winding leakage flux and axial flux signals the expected frequencies are :

$$f_1 = F(Hz) \quad \ldots\ldots\ldots\ldots\ldots (1)$$

$$f_{SH} = F(R/P\ (1 - s) \pm n)(Hz) \ldots\ldots (2)$$

and for the vibration signal :

$$f_{1V} = 2F(Hz) \quad \ldots\ldots\ldots\ldots\ldots (3)$$

$$f_{SHV} = F(R/P\ (1 - s) \pm 2(n - 1))(Hz) \ldots (4)$$

where F = fundamental supply frequency (50 Hz)

R = number of rotor slots (28)

P = number of pole-pairs (2)

s = slip, 0.02 for full-load

n = 1, 2, 3 . . . .

SH = slot harmonic

An FFT analysis was initially applied to all the transducer signals. Where it was difficult to identify the difference between signature patterns for normal and abnormal conditions, a zoom analysis was applied around specific frequency components. The frequency at which the zoom analysis is applied depends on the type of fault and signal being analysed. Equations 1 to 4 can be used for this purpose. Figures 2 to 37 show spectra of the signals for normal and fault conditions.

Preliminary observations of the results indicate that the spectra for the broken rotor bar fault contains many sidebands. These sidebands can be explained by the application of rotor asymmetry theory.[15] A useful technique for determining the sideband content is cepstrum analysis.[16] The main observations from the data bank of spectra are as follows :

(i) Broken Rotor Bar

The tests were done under full-load operating conditions using two production type die-cast rotors. Both rotors have the same degree of dynamic balance but one has a broken bar. A spectrum analysis of the vibration signals is shown in Figures 2 and 3. The 0-2 kHz bandwidth spans the range of interest for detecting changes but it is difficult to observe any significant differences. However, using zoom analysis techniques, sidebands become apparent around the slot harmonic for the faulty rotor as indicated by comparing Figure 4 and 5. The same 'signature' patterns occur for the current, end winding leakage flux and axial flux signals, as shown in Figures 6 to 17. A cepstrum analysis was applied to highlight the increased sideband content, a sample of the results is

presented in Figures 39 to 46. The results clearly demonstrate that this fault can be identified from four signals. Based on the work so far the techniques will be used for discriminating between the effects caused by high resistance joints, number of broken bars or end rings.

(ii) Inter-turn Winding Faults

A comparison between Figures 18 and 19 show that the 100 Hz, 200 Hz and 300 Hz vibration components increase when a coil is short-circuited in the stator winding. In the axial flux spectrum the 50 Hz, 100 Hz and 150 Hz components increase, while in the current spectrum it is the 150 Hz and slot harmonic frequencies which increase significantly, as shown in Figures 20 and 21 and Figures 24 and 25 respectively. It was found that although there were changes in the end winding leakage flux spectrum the sense (increase or decrease) of the change was a function of transducer position as indicated in Figures 22 and 23.

(iii) Single-Phasing

Figures 23 to 33 indicate that the 100 Hz component has a pronounced increase in both the vibration and axial flux spectra. The 150 Hz component in the current spectrum is also increased. As in (ii) the change in the end winding leakage flux is a function of transducer position.

(iv) Static Rotor-Stator Eccentricity

The only significant changes occurred in the slot harmonics of the vibration spectrum as shown in Figures 34 to 37, and that the sense of the change was a function of transducer position around the motor's frame, as indicated in Figure 38. Further work is required on the signal processing side to try and detect changes in the other signals.

Conclusions

A study of the failure mechanisms of squirrel-cage induction motors has been carried out and reported. The fault mechanisms have been investigated under controlled experimental conditions and a computer-based instrumentation system has analysed signals representative of a motor's supply current, axial flux, end winding leakage flux and mechanical vibration. A comprehensive data bank of different types of spectra for SCIM fault recognition has been presented. The authors believe that this is the first time a data bank of spectra in this form has been put into print. The resulting data patterns reveal that different 'signatures' exist for 'healthy' and 'unhealthy' motors. In addition,

three or four different types of signal may show a particular pattern for one fault condition. The concept of looking for changes in four signals as opposed to only one, has the distinct advantage that an industrial user of SCIMs is more likely to believe the former as an indication of a fault. The tests have therefore been used to establish a data bank of machine signatures for use in predictive maintenance operations. Overall system reliability can then be improved.

Acknowledgements

The authors wish to acknowledge the support of the Science and Engineering Research Council Marine Directorate in this work and for the cooperation received from the industrial companies who participated in the survey. Thanks are also expressed to Mr A J Low for his advice and assistance in the design and development of the experimental test rig. Miss K Craighead and Mr B Davidson are also thanked for their assistance in the preparation of this paper.

References

1 Ellison, A. J., and Moore, C. J. : "Acoustic Noise and Vibration of Rotating Electric Machines", Proc I.E.E., Vol. 115, No. 11, Nov. 1968.

2 Neale, M., and Associates. : "Guide to the Condition Monitoring of Machinery", HMSO, London, England, 1979, ISBN011 5121269.

3 Ray, A. G. : "Monitoring Rolling Contact Bearings under Adverse Conditions", 2nd Int. Conf. on Vibrations in Rotating Machinery, I. Mech. E., Conference Publications, 1980.

4 Downham, E. : "Vibration in Rotating Machinery : Malfunction Diagnosis - Art and Science", Int. Conf. on Vibrations in Rotating Machinery, I. Mech. E., Conference Publications, 1976.

5 Hemmings, R. C., and Smith, J. D. : "Information from Bearing Vibration", ibid.

6 Stewart, R. M. : "Vibration Analysis as an Aid to the Detection and Diagnosis of Faults in Rotating Machinery" ibid.

7 Erskine, J. B., and Reeves, C. W. : "Vibration Problems on Rotating Machinery in the Chemical Industry", ibid.

8 Erlicki, M. S., Porat, Y., and Alexandrovitz, A. : "Leakage Field Changes of an Induction Motor as Indication of Nonsymmetric Supply", Trans. IEEE on Ind. and Gen. Appl., Vol. IGA-7, No. 6, Nov./Dec., 1971.

9 Penman, J., Hadwick, J. G., and Barker, B. : "Detection of Faults in Electrical Machines by Examination of the Axially Directed Fluxes", Third Int. Conf. on Electrical Machines, Brussels, 1978.

10 Penman, J., Hadwick, J. G., and Stronach, A. F. : "Protection Strategy Against the Occurrence of Faults in Electrical Machines", Int. Conf. on Developments in Power System Protection, IEE Publication, 1980.

11 Gaydon, B. G. : "An Instrument to Detect Induction Motor Rotor Defects by Speed Fluctuation Measurements", IEE Conf. on Electronic Test Measuring Instrumentation, Testmex 79, 1979.

12 Hargis, C., Gaydon, B. G., and Kamash, K. : "The Detection of Rotor Faults in Induction Motors", IEE Int. Conf. on Electrical Machines - Design and Applications, July, 1982.

13 Steele, M. E., Ashen, R. A., and Knight, L. G. : "An Electrical Method for Condition Monitoring of Motors", ibid.

14 Alger, P. L. : "The Nature of Induction Machines", Gordon and Breach Science Pub., 1965.

15 Jones, C. V. : "The Unified Theory of Electrical Machines", Butterworth Pub., 1967.

16 Bogert, B. P., Healy, M. J. R., and Tukey, J. W. : "Proceedings of the Symposium on Time Series Analysis", John Wiley and Sons, New York, 1963.

Monitoring Techniques & Types of Transducers	A	B	C	D	E	F	G	H	I	J	K	Percentage usage of Monitoring Techniques
Subjective look, feel and listen	Y	Y	Y	Y	Y	Y	Y	Y	Y	Y	Y	100%
Vibration monitoring as a general concept	Y	Y	Y	Y	Y	Y	Y	Y	Y	Y	Y	100%
Proximity transducers on plain bearings	Y	N	Y	Y	Y	N	Y	N	N	N	Y	54%
Accelerometers	N	N	Y	Y	Y	Y	N	Y	Y	Y	N	64%
Velocity transducers	N	Y	Y	N	Y	Y	N	Y	N	N	Y	54%
Vibration spectrum analysis	N	N	Y	Y	Y	Y	N	Y	Y	Y	Y	73%
Shock Pulse Monitoring for bearing defects	N	N	N	N	Y	N	N	Y	N	N	N	18%
Off-line computer processing of vibration signals	N	N	Y	N	Y	N	N	Y	N	N	N	27%
On-line computer based monitoring of vibration	N	N	N	N	N	N	N	N	N	N	N	0%
Winding temperature sensing	Y	N	Y	Y	Y	Y	Y	Y	N	Y	Y	82%
Stator core temperature sensing	Y	N	N	N	N	N	Y	N	N	N	N	18%
Bearing temperature sensing	Y	N	Y	Y	Y	Y	Y	Y	Y	Y	Y	91%
Meggar insulation tests	Y	Y	Y	Y	Y	Y	Y	Y	Y	Y	Y	100%
Tan (δ) insulation tests	Y	N	Y*	N	Y	N	Y	Y	Y	N	Y	64%
DLA tests	Y#	N	Y*	N	N	N	Y	Y*	N	N	N	36%
Measurement of shaft voltages	Y	N	Y*	Y	Y	B	Y+	N	N	N	Y	54%
Wear debris monitoring	N	Y	N	N	N	N	Y	N	N	N	N	18%
Magnetic plugs	N	N	N	N	N	N	N	N	N	N	N	0%
Oil sample analysis	N	Y	Y#	N	N	N	Y#	N	N	N	N	27%
Squirrel-cage rotor bar monitoring	Y	N	N	N	N	N	N	Y	Y	N	N	27%
Ultrasonic discharge detector	N	N	N	N	Y	N	Y	N	N	N	N	18%
Integrated discharge test	N	N	N	N	Y	N	N	N	N	N	N	9%
Stray flux monitoring	N	N	Y*	N	N	N	N	N	N	N	N	9%

A to K : Industrial operators Y : Yes N : No

* : occasionally # : if special problem arise

+ : only during installation

Table 1 : Survey of Monitoring Techniques used on 3-phase Squirrel-cage Induction Motors with ratings of 500 h.p. (0.373 MW) and above.

Fault	Occurrence
Bearings	44.68%
Windings	44.68%
Cracked/Broken Rotor Bars	4.25%
Miscellaneous	6.39%

Total number of machines = 82
Power supplies vary from 2.3 kV to 13.8 kV
Number of machines with no fault = 30
Total number of failures = 94
Percentage of machines started D.O.L. = 98%

Table 2 : Survey Results on Machine Failure

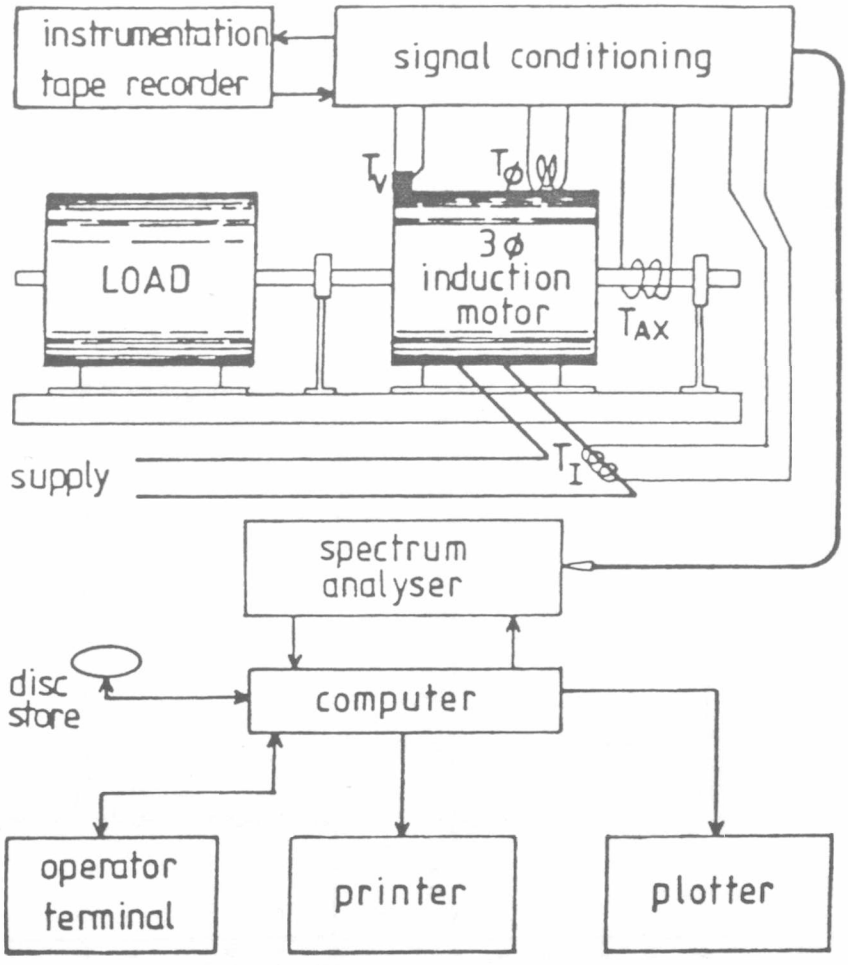

TEST RIG, DATA ACQUISITION AND PROCESSING EQUIPMENT

Figure 1

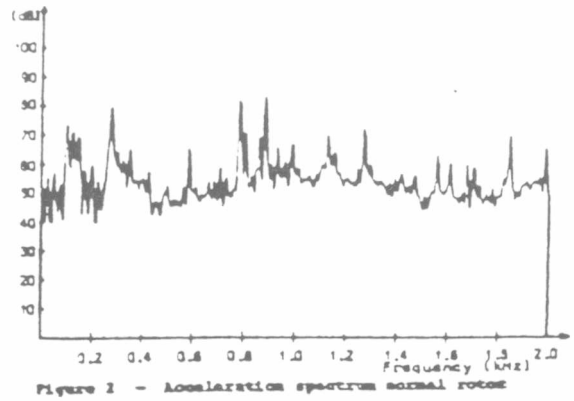

Figure 2 - Accelaration spectrum normal rotor

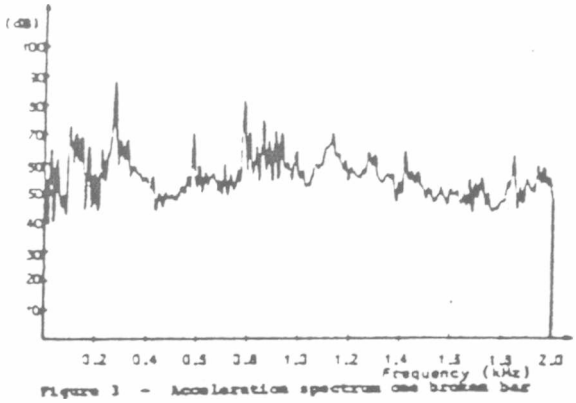

Figure 3 - Accelaration spectrum one broken bar

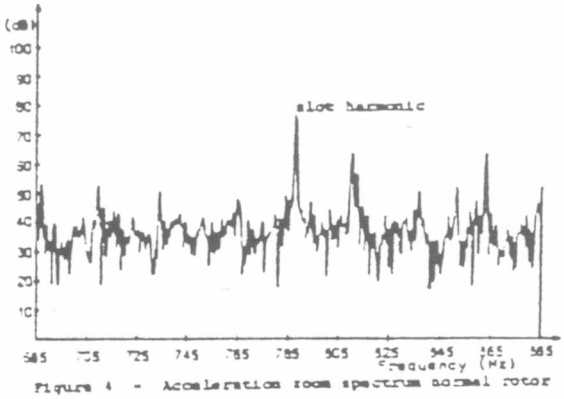

Figure 4 - Accelaration room spectrum normal rotor

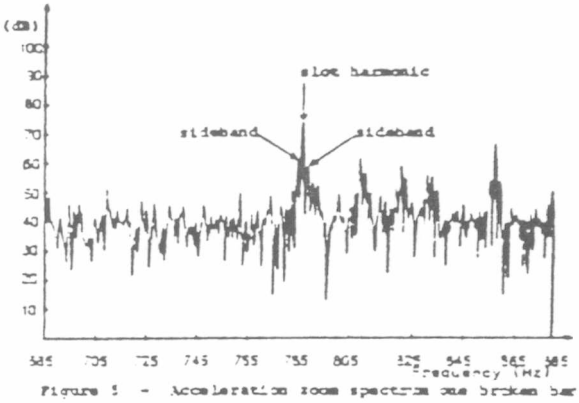

Figure 5 - Accelaration room spectrum one broken bar

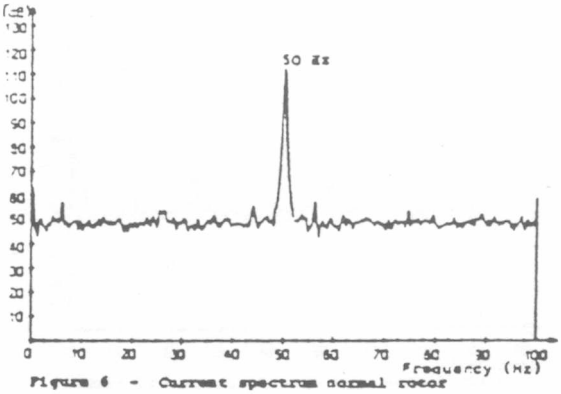

Figure 6 - Current spectrum normal rotor

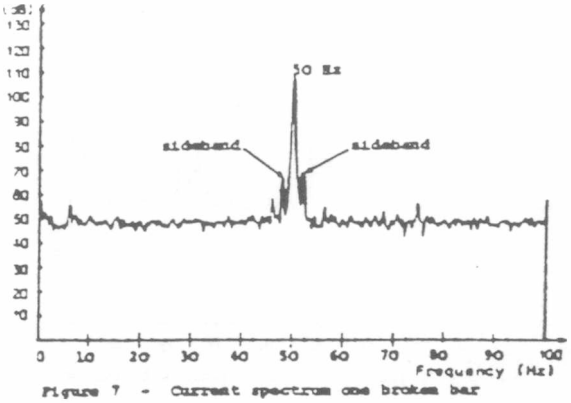

Figure 7 - Current spectrum one broken bar

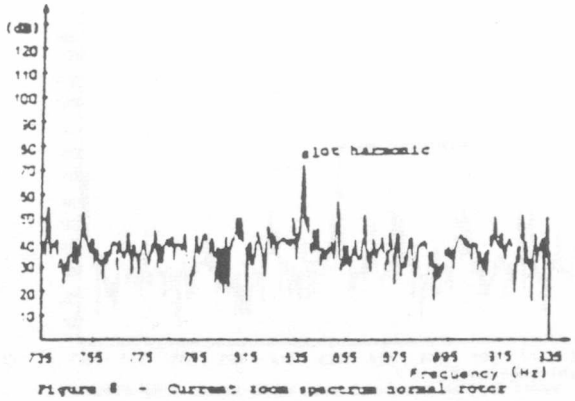

Figure 8 - Current room spectrum normal rotor

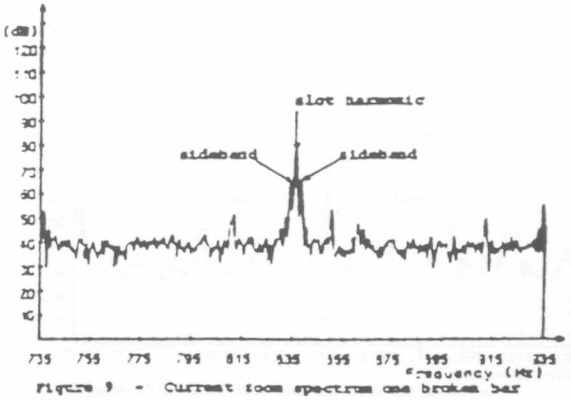

Figure 9 - Current room spectrum one broken bar

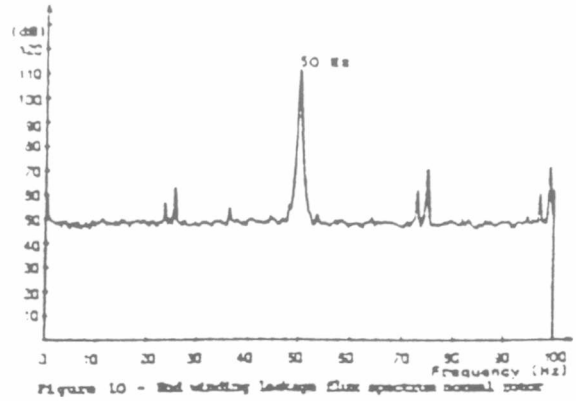

Figure 10 - End winding leakage flux spectrum normal rotor

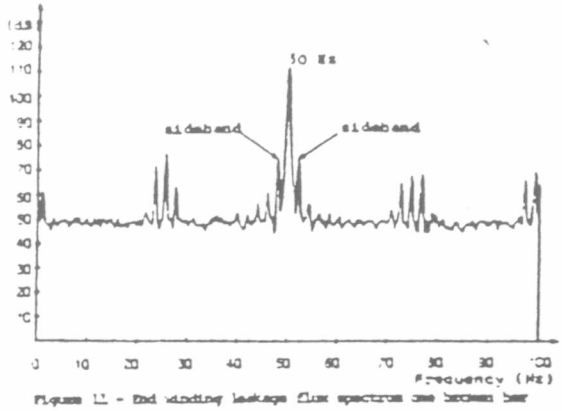

Figure 11 - End winding leakage flux spectrum one broken bar

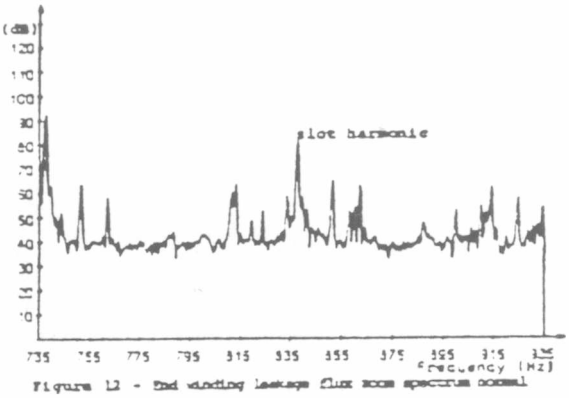

Figure 12 - End winding leakage flux zoom spectrum normal

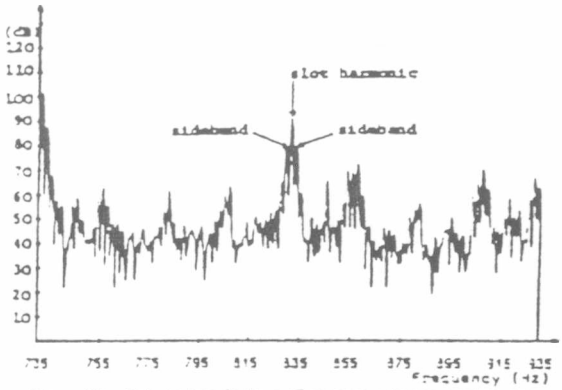

Figure 13 - End winding leakage flux zoom spectrum broken bar

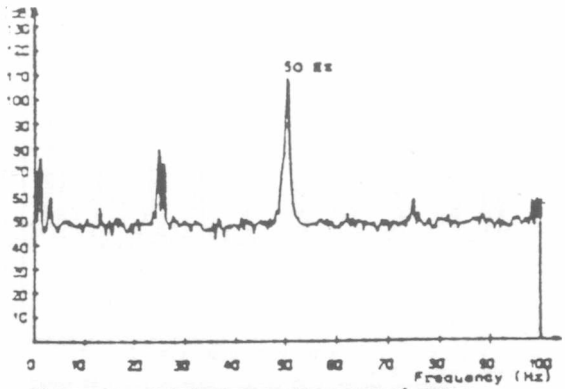

Figure 14 - Axial flux spectrum normal rotor

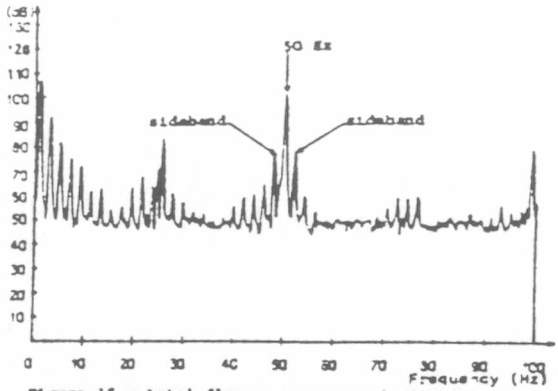

Figure 15 - Axial flux spectrum one broken bar

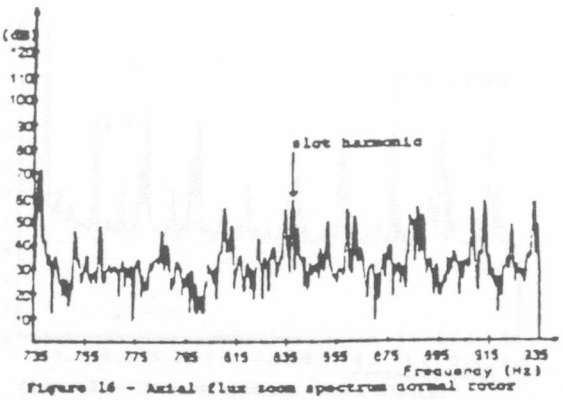

Figure 16 - Axial flux zoom spectrum normal rotor

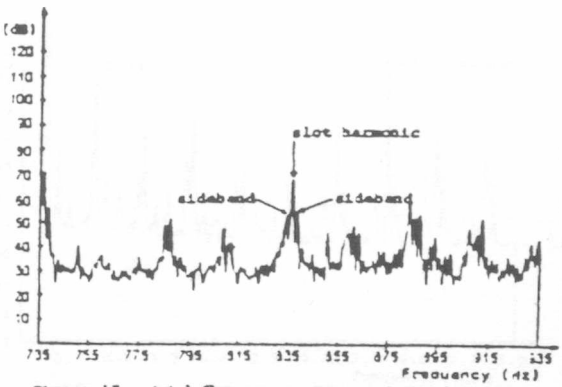

Figure 17 - Axial flux zoom spectrum one broken bar

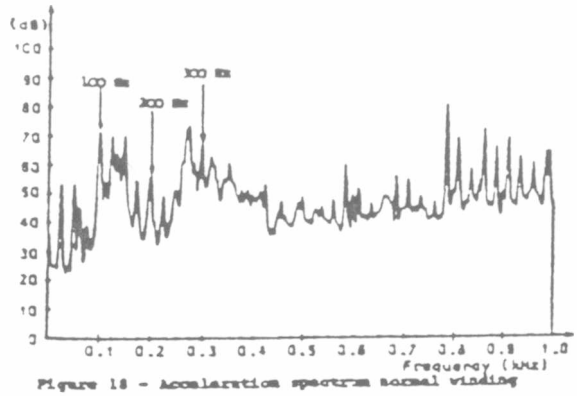

Figure 18 - Accelaration spectrum normal winding

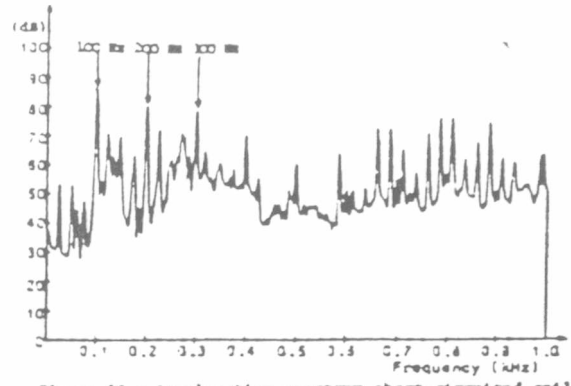

Figure 19 - Accelaration spectrum short-circuited coil

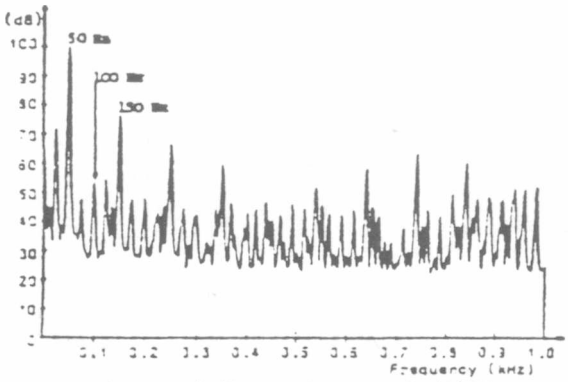

Figure 20 - Axial flux spectrum normal winding

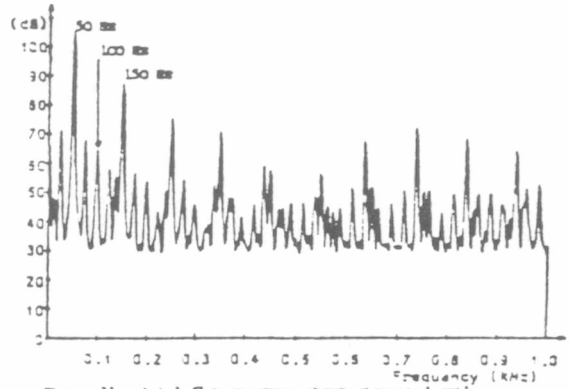

Figure 21 - Axial flux spectrum short-circuited coil

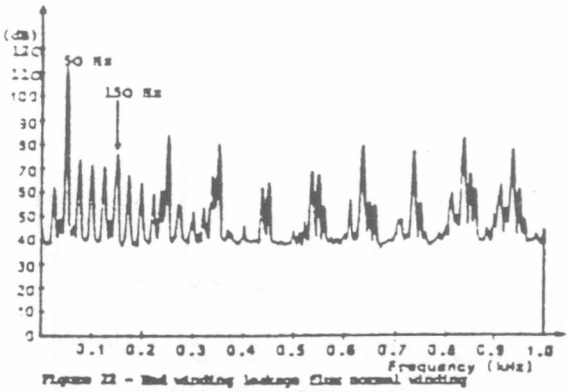

Figure 22 - End winding leakage flux normal winding

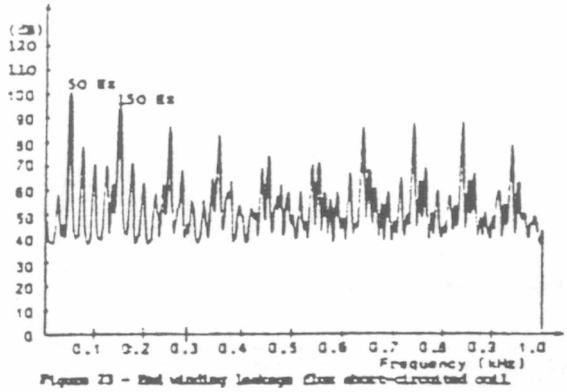

Figure 23 - End winding leakage flux short-circuited coil

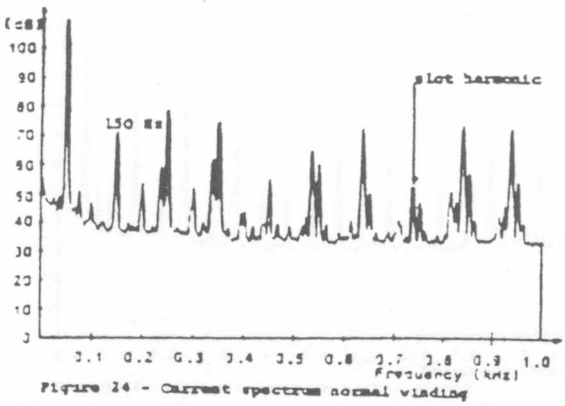

Figure 24 - Current spectrum normal winding

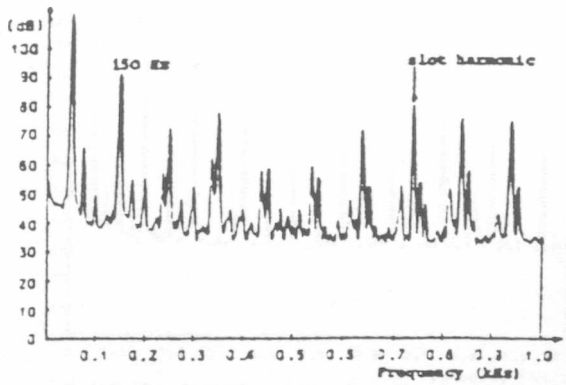

Figure 25 - Current spectrum short circuited coil

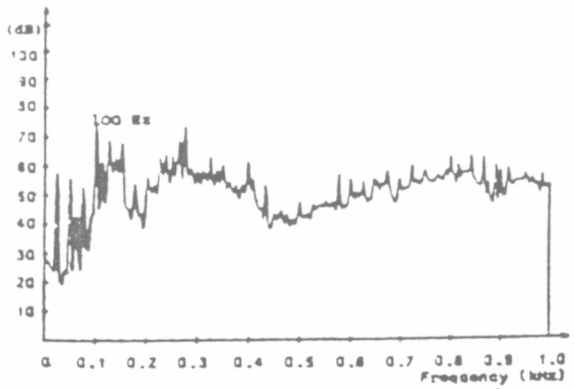

Figure 26 - Acceleration spectrum normal supply

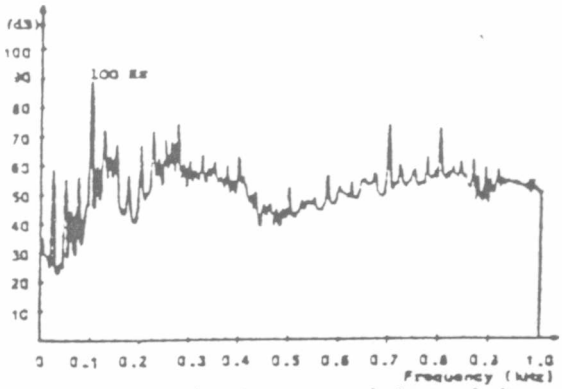

Figure 27 - Acceleration spectrum 1-phasing fault

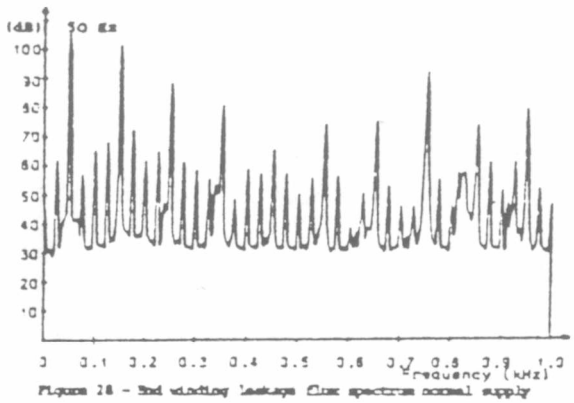

Figure 28 - End winding leakage flux spectrum normal supply

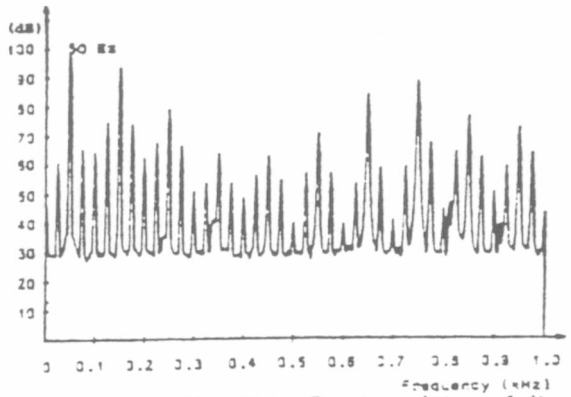

Figure 29 - End winding leakage flux spectrum 1-phasing fault

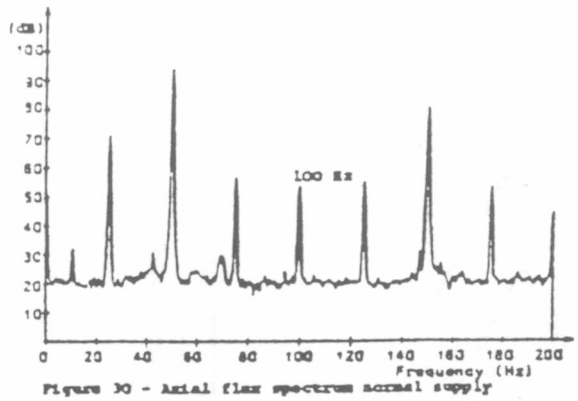

Figure 30 - Axial flux spectrum normal supply

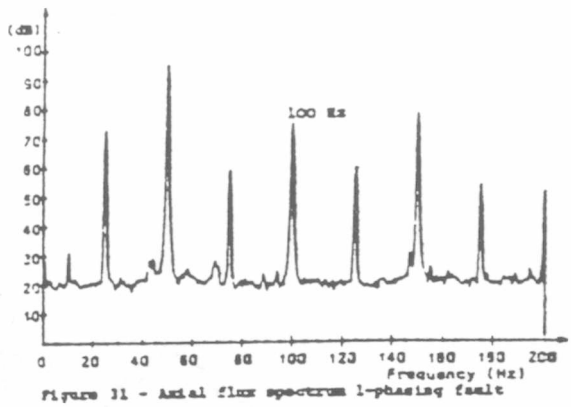

Figure 31 - Axial flux spectrum 1-phasing fault

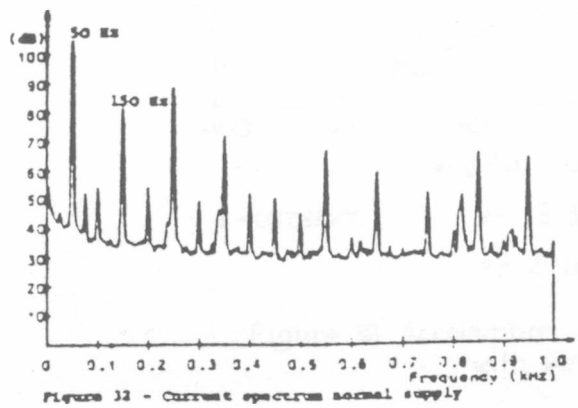

Figure 32 - Current spectrum normal supply

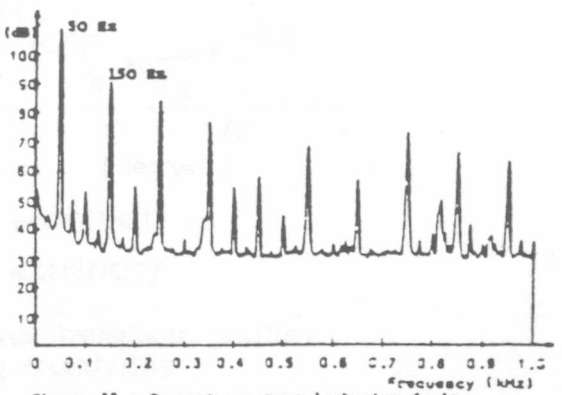

Figure 33 - Current spectrum 1-phasing fault

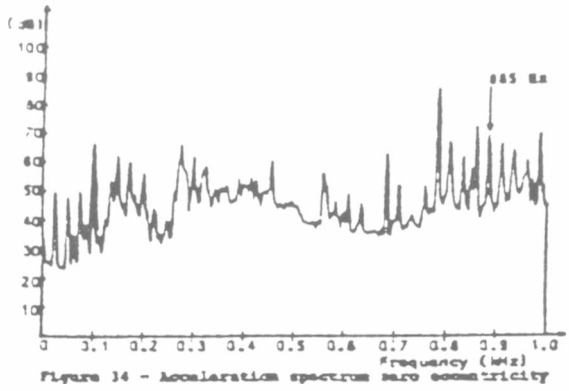

Figure 34 - Acceleration spectrum zero eccentricity

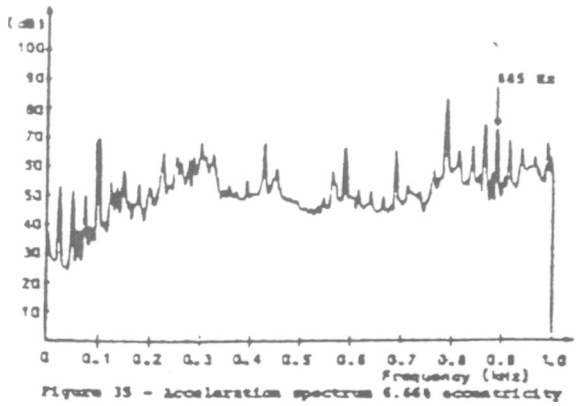

Figure 35 - Acceleration spectrum 6.66% eccentricity

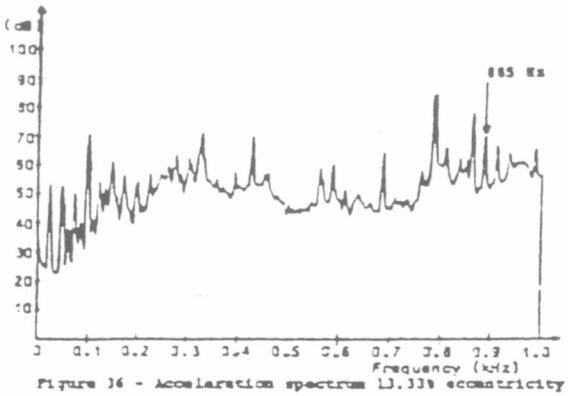

Figure 36 - Acceleration spectrum 13.33% eccentricity

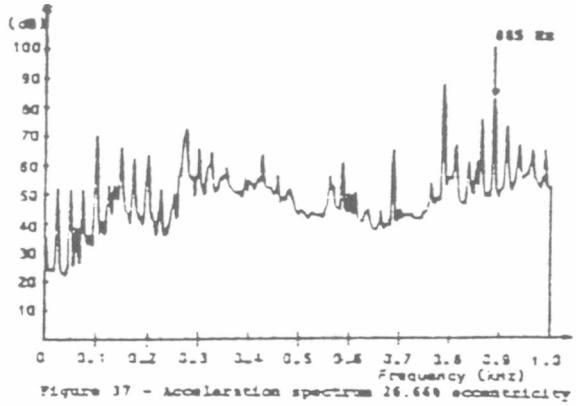

Figure 37 - Acceleration spectrum 26.66% eccentricity

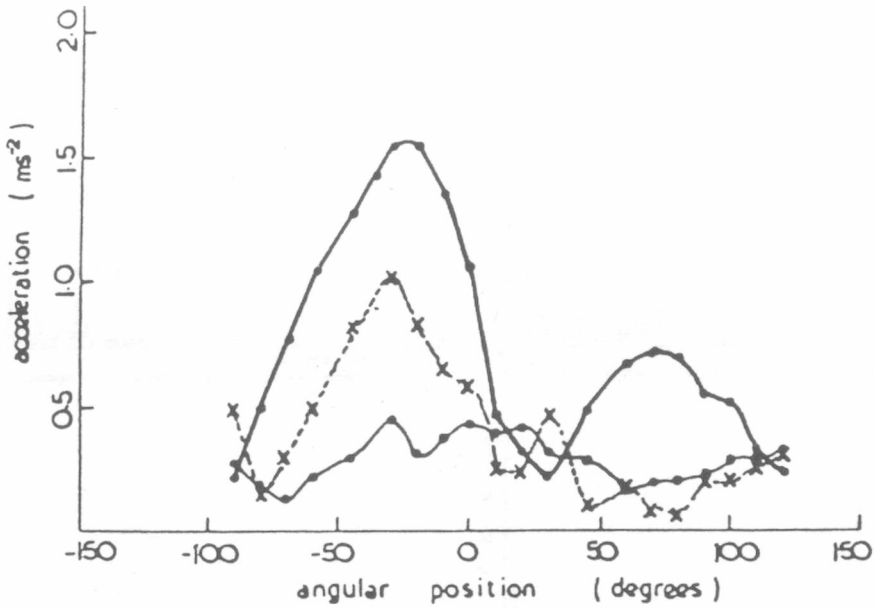

Figure 38 Acceleration versus transducer position with varying eccentricity

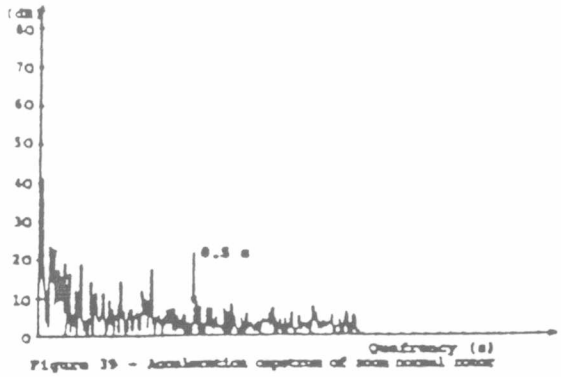

Figure 39 - Acceleration cepstrum of 200A normal rotor

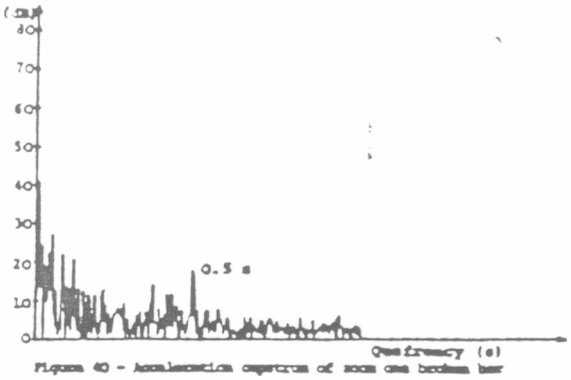

Figure 40 - Acceleration cepstrum of 200A one broken bar

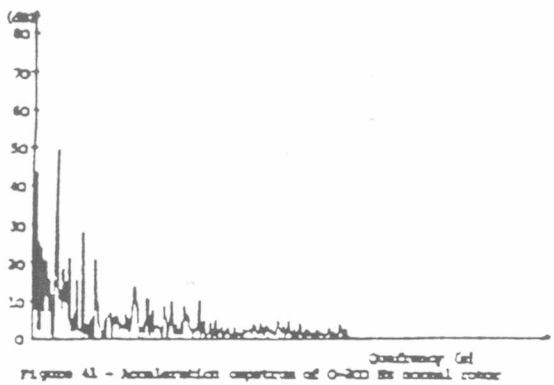

Figure 41 - Acceleration cepstrum of 0-200 Hz normal rotor

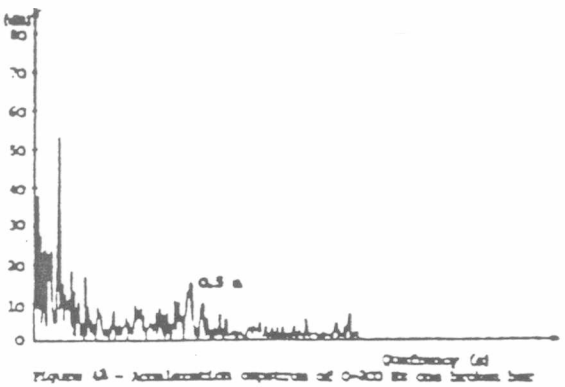

Figure 43 - Acceleration cepstrum of 0-200 Hz one broken bar

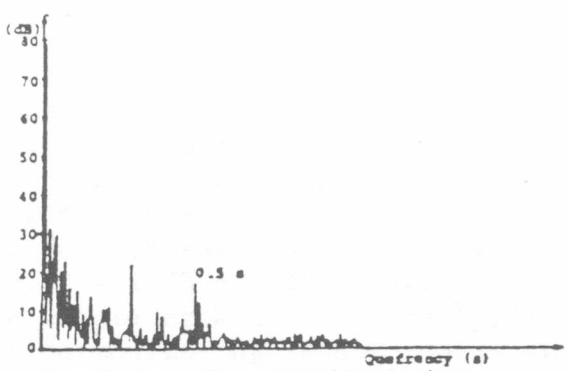

Figure 43 - Leakage flux cepstrum of 200A normal rotor

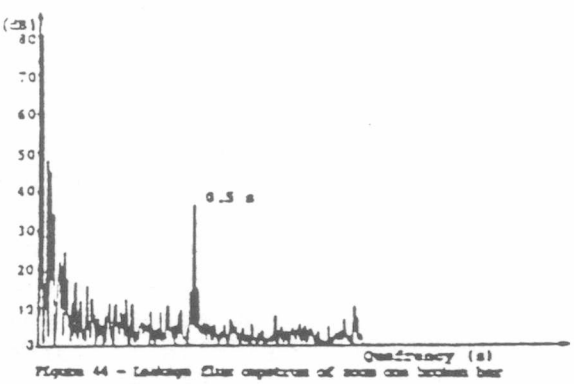

Figure 44 - Leakage flux cepstrum of 200A one broken bar

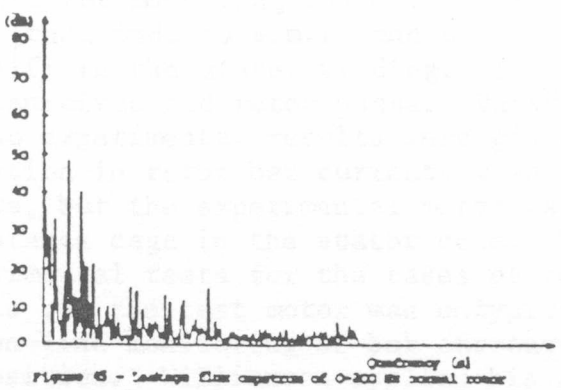

Figure 45 - Leakage flux cepstrum of 0-200 Hz normal rotor

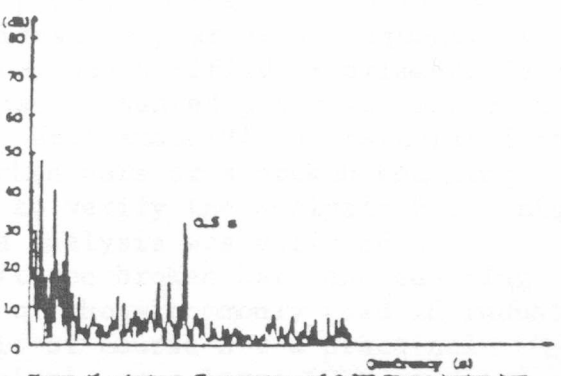

Figure 46 - Leakage flux cepstrum of 0-200 Hz one broken bar

MONITORING STRATEGY FOR DISCRIMINATING BETWEEN DIFFERENT TYPES OF ROTOR DEFECTS IN INDUCTION MOTORS

W T Thomson, N D Deans, R A Leonard, A J Milne
Robert Gordon's Institute of Technology, Aberdeen AB9 1FR

INTRODUCTION

A recent survey[1] of industrial companies using large 3-phase squirrel-cage induction motors (SCIM) in offshore and onshore installations indicated that rotor cage faults can lead to motor failures. Pulsating loads or the undesirable effects of direct-on-line starting can result in rotor bar fractures.[2,3] The fatigue mechanism causes a poor electrical/mechanical connection, arcing develops and this usually results in a broken bar. Torque pulsations, speed fluctuations and vibration changes occur and can cause rotor bearing failure[1] or stator core damage. There is a need for reliable on-line monitoring techniques for discriminating between high resistance bar to end ring joints, number of broken bars and end ring faults. It is proposed that a monitoring strategy which uses three or four interrelated types of signals for fault diagnosis is more credible than existing instruments monitoring only one signal.

REVIEW OF PREVIOUS WORK

Gaydon[4,5] has developed instrumentation techniques for rotor fault detection based on shaft speed fluctuations but has stated that "inherent rotor asymmetries can give period fluctuations of the same magnitude as when one bar was open circuited". Hargis[4] has presented a set of spectra of vibration and current for two nominally identical motors, one with a normal rotor, and one with three broken bars but the early detection of one broken bar is important so that further degradation can be avoided. Pozanski[6] has shown that acoustic noise measurements indicated a 1 dB - 3 dB change between a motor with a good rotor and one with a single broken bar. The application of noise measurements for condition monitoring is not really suitable for offshore installations or hostile onshore situations[1]. Jones[7] has developed an equivalent circuit for modelling the effect of an open-circuited rotor phase and shows that induced e.m.f. and current signals appear at a frequency of $|1-2s|f_1$ in the stator winding. The model was verified experimentally for an open-circuited rotor phase. Vas[8] has presented a similar approach but no experimental results were given. Williamson[9] has calculated the variation in rotor bar currents when broken bars or a broken end ring exists, but the experimental motor used to verify the analysis had a high resistance cage in the stator core. The analysis was verified by experimental tests for the cases of two/three broken bars and end ring faults but the test motor was untypical of those commonly used in industry. The on-line monitoring of bar currents is of course not a practical proposition. Williamson applied his analysis to a large SCIM and predicted that it may be difficult to detect a single bar fault in terms of the $|1-2s|f_1$ component of current or the $2sf_1$ component of pulsating torque. Williamson's prediction has still to be verified by experimental tests. Penman[10] has reported that the use of axial flux monitoring was inconclusive for detecting a rotor bar fault. Steele[11] has monitored current for the detection of one broken bar in a small-power motor but did not present results for the cases of two or three broken bars. Controlled experimentation is required if rotor cage faults are to be quantified in terms of the magnitudes of specific frequency components or by using

Cepstrum analysis[11] to identify the sideband content of spectra.

PRINCIPLES

Alger[12] has shown that the air-gap flux density in a SCIM consists of five principal rotating fields. If time harmonic fluxes of the fundamental are included then a general expression for the slot harmonic frequency components is : $f_1 (\frac{R}{P} (1 - s) \pm n)$. If Jones'[7] analysis is applied to the fundamental and third harmonic time components of the stator flux then upper and lower sidebands occur at $|1 \pm 2s| f_1$ around the fundamental. The slot harmonic frequencies for a rotor with asymmetry become : $f_1(n \pm R(1 - s)/P) \pm 2s\ f_1$, where f_1 = fundamental frequency; s = slip; R = No. of rotor slots; P = pole pairs; n = 1, 2, 3...

These effects can be detected in the current, end winding and leakage flux spectra[1] using simple external pick up coils and spectrum analysis. Since magnetic forces are proportional to flux density squared, then sidebands occur around the principal slot harmonic vibration components. These sidebands appear in four interrelated[1] spectra and can be used as a basis for identifying various types of rotor fault.

EXPERIMENTAL EQUIPMENT AND TEST RESULTS

A test rig has been developed to investigate the effects of faults on the current, flux and vibration spectra of a machine. A 3-phase, 50 Hz, 11 kW, 4-pole SCIM, loaded by a d.c. dynamometer, has transducers attached to sense current, leakage and axial flux, and vibration. The sensed signals are amplified and filtered and subjected to spectral analysis in a high-resolution spectrum analyser acting as a peripheral device to a mini-computer. A suite of programs in the minicomputer control the analyser and present the processed data to the experimenter in graphical or numerical form. Figure 1 shows the test rig and associated processing equipment.

Tests were initially done using two 28-slot production type die-cast rotors, one as the normal reference and the other for introducing controlled rotor cage faults. For the experiments with the 28-slot rotors, the motor developed its nominal full-load torque at 1470 r.p.m. An FFT analysis was applied to the vibration, current, end winding and axial flux signals. Upper and lower sidebands appeared around various frequency components when the rotor with one broken bar was tested. An FFT zoom analysis of the vibration and end winding flux signals is presented in Figures 2-5. The spectra for the faulty rotor have a pronounced sideband content around the principal slot harmonics. A Cepstrum analysis was used to obtain a value for the sideband content. Figures 6 and 7 show that this technique can detect a single rotor bar failure. Several bars were broken adjacent to the single broken bar and the resulting Cepstra are shown in Figures 8 and 9. A similar pattern occurred for the other signals and a sample of Cepstra for the end winding flux signals is given in Figures 10 and 11.

A standard type 51-slot rotor was redesigned to investigate the effects of high resistance bar to end ring joints. A number of the bars could be broken and reconnected in situ via special bolted connections. The remaining 43 copper bars were soft soldered into the end rings. A high-resolution micro-ohmmeter was used to measure the resistances of a number of similar soft soldered joints and bolted connections on a separate rotor cage, and it was found that they were of the order of 5 to 6 μΩ and 21 to 22 μΩ respectively. The 51 slot rotor developed the motor's nominal full-load torque at a speed of 1430 r.p.m. and is typical of a standard

production model. The transducer signals were analysed when the rotor had no broken bars and sidebands appeared in the vibration, current and flux signals. This suggests that high resistance joints can be interpreted as broken bars. Figure 12 shows the pronounced sideband content. With a bar disconnected from the end ring, the changes in the current and flux signals were inconclusive. However, the sideband content in the vibration signal increased as shown in Figure 13. A further increase occurred with two broken bars.

CONCLUSIONS

A study of different rotor cage faults has been carried out under controlled experimental conditions and a set of spectra and cepstra presented. The results show that cage faults can be identified in four interrelated signals and that Cepstrum analysis can provide a single value for the relevant sideband content. Sidebands also appear in the spectra when the rotor cage has high resistance bar to end ring joints and it was observed that only the vibration signal showed a significant change when bars were subsequently broken. The concept of looking for changes in four different signals as opposed to one or two, has the distinct advantage that an industrial user of SCIMs is more likely to believe the former as an indication of a fault. This is particularly relevant in the offshore oil industry where loss of production is extremely costly. Further work is required to study the effects of decreasing/increasing the number of high resistance joints compared to broken bars, and end ring faults compared to broken bars.

ACKNOWLEDGEMENTS

The authors wish to acknowledge the support of the Science and Engineering Research Council Marine Directorate in this work. Thanks are also expressed to Mr A J Low for his advice and assistance in the design and development of the experimental test rig. Mr B Davidson and Miss K Craighead are also thanked for their assistance in the preparation of this paper.

REFERENCES

1. THOMSON, W. T., DEANS, N. D., LEONARD, R. A., and MILNE, A. J.: Condition monitoring of induction motors for availability assessment in offshore installations, 4th Euredata conference, Venice, Italy, March, 1983.

2. BURNS, R. L.: Rotor bar failures in large a.c. squirrel cage rotors, Electr. Eng., 1977, 54, (10), pp 11-14.

3. GAYDON, B. G., and HOPGOOD, D. J.: Faltering pulse can reveal an ailing motor, Electrical Review, Vol. 205, No. 14, Oct. 1979, pp 37-38.

4. HARGIS, C., GAYDON, B. G., and KAMASH, K.: The detection of rotor defects in induction motors, IEE International conference on Electrical Machines - Design and Applications, 1982, No. 213, pp 216-220.

5. GAYDON, B. G.: An instrument to detect induction motor rotor circuit defects by speed fluctuation measurements, electric test and measuring instrumentation - Testemex 79 conference papers, 1979, pp 5-8.

6. POZANSKI, A.: Acoustic measurement of three-phase asynchronous motors with a broken bar in the cage rotor, Zesz. Nauk. Politech. Lodz. Elektr., 1977, 60, pp 121-131.

7. JONES, C. V.: Unified theory of electrical machines, Butterworth, 1967.

8. VAS, P.: Performance of three-phase squirrel-cage induction motors with rotor asymmetries, Period. Polytech. Electr. Eng. 1975, 19, pp 309-315.

9. WILLIAMSON, S., and SMITH, A. C.: Steady-state analysis of 3-phase cage motors with rotor-bar and end-ring faults, Proc IEE, Vol. 129, PT. B, No. 3, May, 1982, pp 93-100.

10. PENMAN, J., HADWICK, J. G., and STRONACH, A. F.: Protection strategy against the occurrence of faults in electrical machines, IEE Conf. Publ. 185, 1980, pp 54-58.

11. STEELE, M. E., ASHEN, R. A., and KNIGHT, L. G.: An electrical method for condition monitoring of motors, IEE international conference on Electrical Machines - Design and Applications, 1982, No. 213, pp 231-235.

12. ALGER, P. L.: The nature of induction machines, Gordon and Breach Science Publications, 1965.

AUTHORS

W T Thomson, a graduate of the University of Strathclyde (B Sc HONS 1973, M Sc 1977) is currently a Lecturer in the School of Electronic and Electrical Engineering, RGIT, Aberdeen, U.K. His research interests are vibration and noise from electrical machines and condition monitoring of rotating machines.

N D Deans, a graduate of the Universities of Aberdeen and Heriot-Watt (B Sc ENG HONS 1966, Ph D 1973) is currently Deputy Head of the Department of Electronic and Electrical Engineering, RGIT. His research interest is special purpose digital systems design.

R A Leonard, a graduate of RGIT (B Sc HONS, 1981) is currently a Research Assistant at RGIT. His research interests are condition monitoring of rotating machines and instrumentation development.

A J Milne, a graduate of the University of Aberdeen (B Sc ENG HONS 1980) is currently a Research Student at RGIT. His research interest is microcomputer instrumentation.

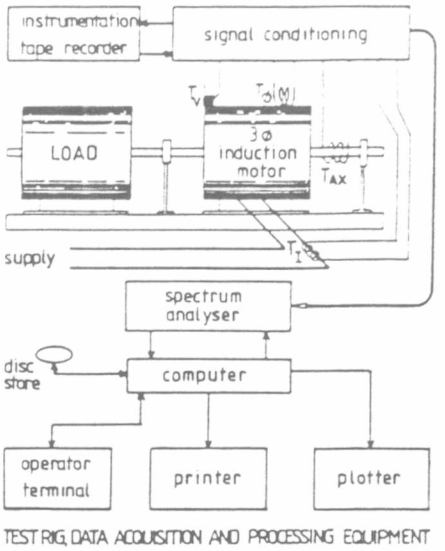

Figure 1

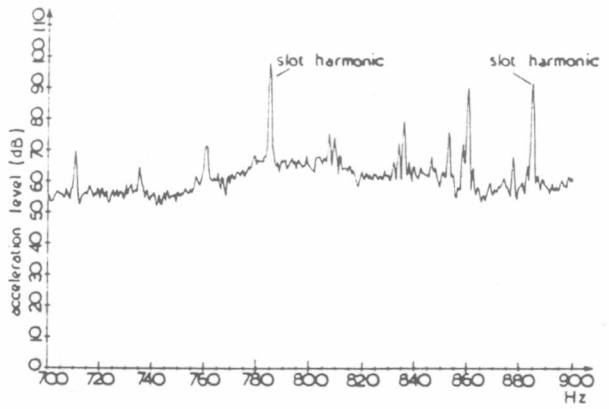

Figure 2

acceleration zoom spectrum, normal rotor

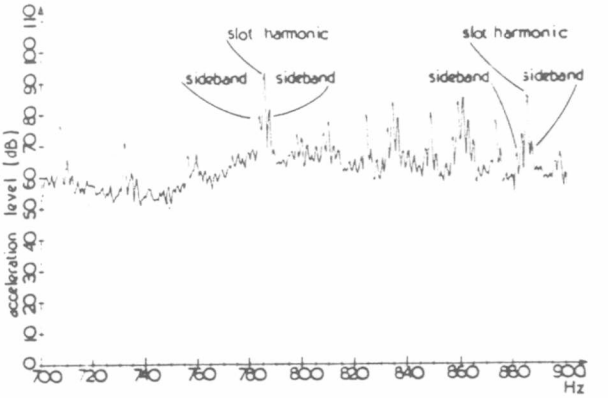

Figure 3

acceleration zoom spectrum, one broken bar

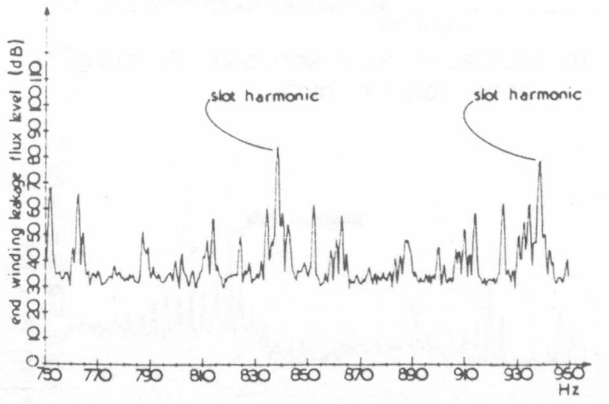

Figure 4

end winding leakage flux zoom spectrum normal rotor

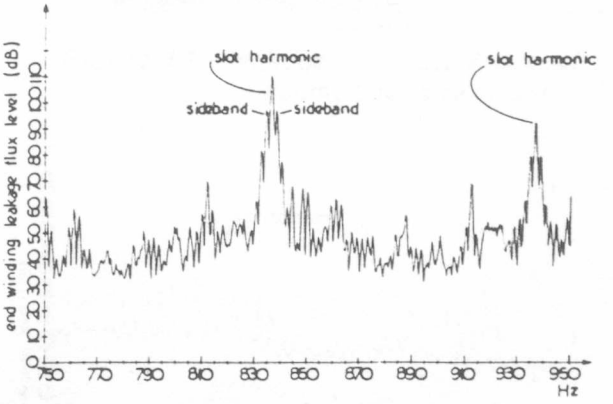

Figure 5

end winding leakage flux zoom spectrum one broken bar

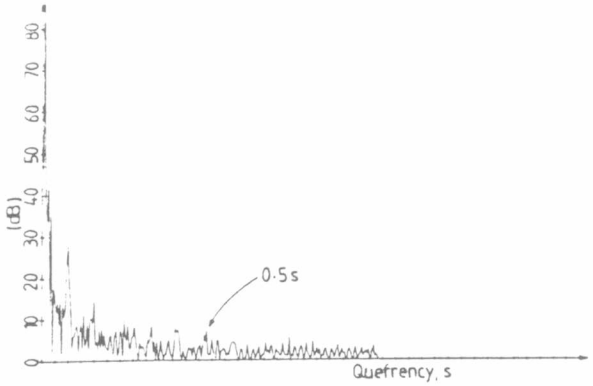

Figure 6 acceleration cepstrum of zoom, normal rotor

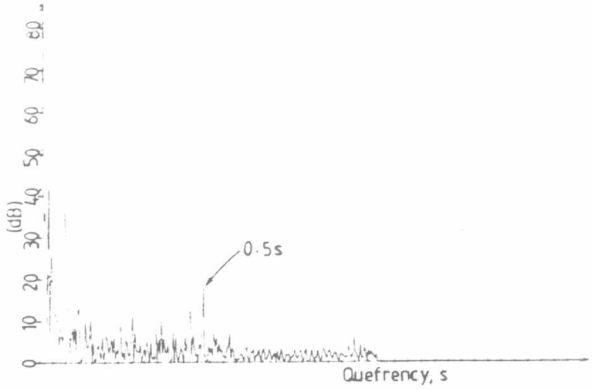

Figure 7 acceleration cepstrum of zoom, one broken bar

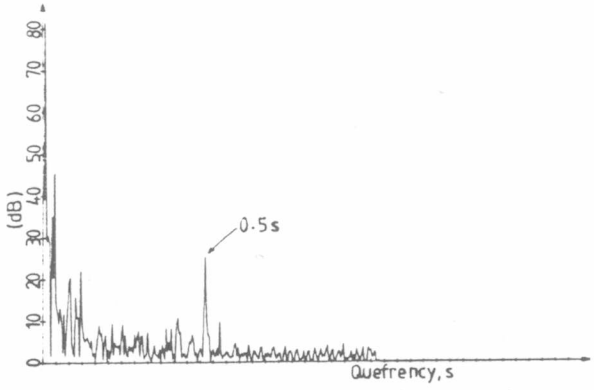

Figure 8 acceleration cepstrum of zoom, two broken bars

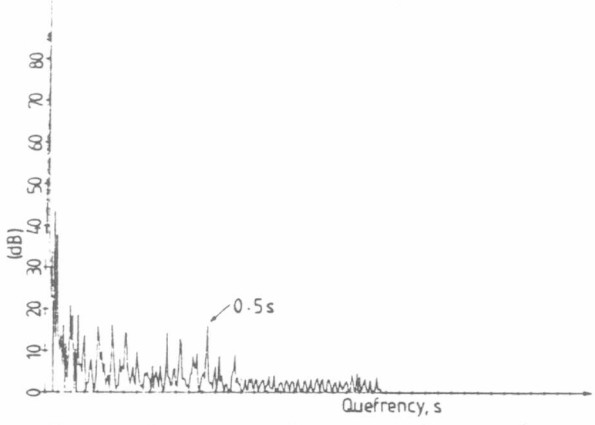

Figure 9 acceleration cepstrum of zoom, three broken bars

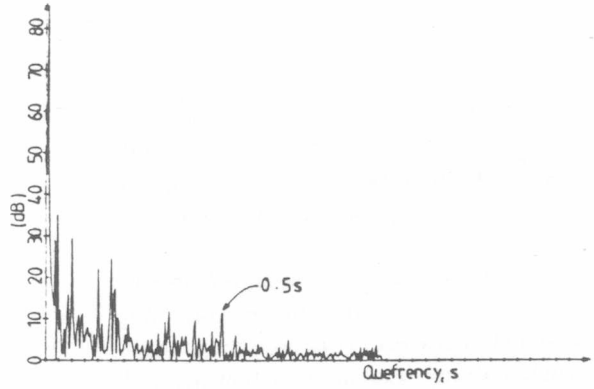

Figure 10 leakage flux cepstrum of zoom, normal rotor

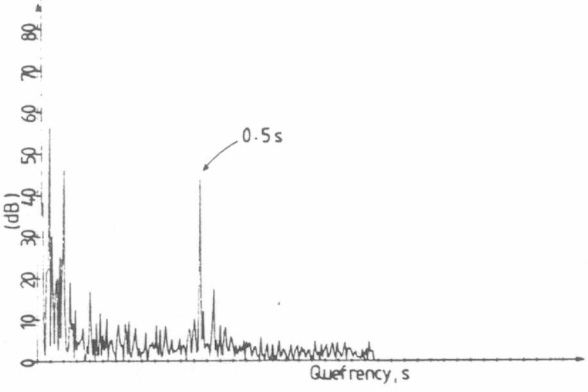

Figure 11 leakage flux cepstrum of zoom, one broken bar

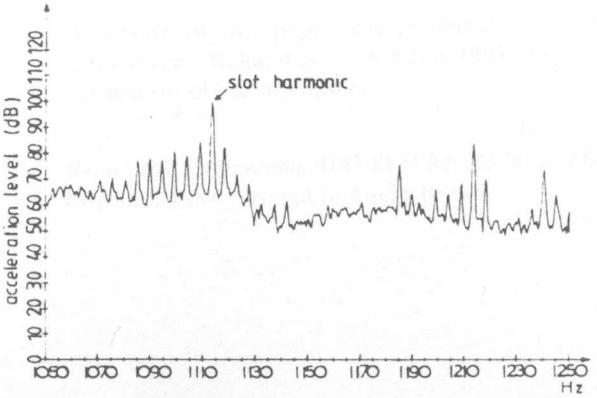

Figure 12 acceleration spectrum for 51 slot rotor, high resistance joints

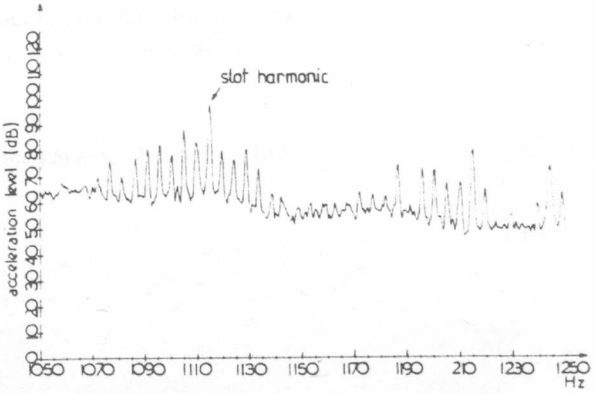

Figure 13 acceleration spectrum for 51 slot rotor, one broken bar

Reliability Engineering 9 (1984) 49–64

Failure Identification of Offshore Induction Motor Systems Using On-condition Monitoring

W. T. Thomson, R. A. Leonard and A. J. Milne

Robert Gordon's Institute of Technology,
Schoolhill, Aberdeen AB9 1FR, Great Britain

and

J. Penman

Marischal College, University of Aberdeen,
Aberdeen AB9 1AS, Great Britain

(Received: 3 November 1983)

ABSTRACT

This paper reports a study carried out into the identification of faults in three-phase squirrel cage induction motors. The reasons for monitoring vibration, current and stray flux signals in a unified approach are presented and a fault producing test rig and computer-based signal processing system are described. The changes which occur in the signals during single-phasing, broken rotor bar, rotor-stator eccentricity and inter-turn winding fault conditions are discussed and a sample of the signature patterns is presented. The results show that a malfunction can be identified from various signals and in certain instances the reliability of fault diagnosis could be improved by the monitoring strategy proposed in this paper.

A version of this paper was presented at the 4th National Reliability Engineering Conference—Reliability '83, 6–8 July 1983, Birmingham, UK, and is reproduced by kind permission of the organisers.

Reliability Engineering 0143-8174/84/$03·00 © Elsevier Applied Science Publishers Ltd, England, 1984. Printed in Great Britain

NOTATION

B Flux density (Tesla)
f_1 Supply frequency (Hz)
f_{sh1} Slot harmonics of the flux (Hz)
f_{1v} Fundamental vibration component due to magnetic forces (Hz)
f_{shv} Vibration slot harmonics (Hz)
f_{sh2} Slot harmonics of the flux with an asymmetric rotor cage (Hz)
n Integer—0, 1, 2, ...
p Pole pairs
R Rotor slots
s Per unit slip of the induction motor

1. INTRODUCTION

In offshore oil and gas production platforms the three-phase squirrel cage induction motor (SCIM) is used to drive gas compressors, sea water injection pumps and oil exporting pumps. The assessment of the condition of the motor and its future availability and reliability are important since failure caused by one of a number of faults is costly and potentially dangerous, Thomson *et al.*[1] It is desirable that fault mechanisms can be detected at an early stage so that planned outages can take place to prevent catastrophic failure. In offshore power installations the majority of SCIMs are started direct-on-line, resulting in large starting currents and torques which can contribute to end winding, rotor cage or bearing failures.[1] Voltage unbalance in the supply system may occur and cause premature failure of the windings. Sea water contamination of the stator windings has been reported as being one of the causes of insulation failure.[1] A recent survey has shown that the methods used for on-line fault diagnosis tend to look at sources of information in isolation.[1] Vibration monitoring is traditionally done by mechanical engineers and insulation monitoring by electrical engineers. However, the SCIM is a complex electromechanical device and the fault mechanisms can be identified from various types of signals, Thomson *et al.*[2] The motor may fail because of a faulty bearing but the fundamental fault mechanism could be electrical, for example, bearings can fail due to electrical bearing currents, Verma *et al.*[3] From the results of the survey and discussions with the operators of SCIMs it was clear that the present

techniques used for fault diagnosis in electrical machines are not always successful.[1,2] It is proposed that an on-line monitoring strategy which utilises vibration, current and stray flux signals in a unified approach will prove to be more successful than existing techniques. This paper reports an experimental investigation into various fault mechanisms and the development of data acquisition and signal processing techniques for fault identification from non-invasive measurements of interrelated signals.

2. FAULT MECHANISMS

The fault conditions being considered in this paper are as follows:

Unbalanced voltage supply

In offshore installations where the power supply system is relatively small, the three-phase voltage supply could become unbalanced due to such factors as single-phasing of primary/secondary circuits or unbalanced single-phase loads, Howell and Hogwood.[4] When a SCIM is fed from an unbalanced supply the motor currents are unbalanced and at full load the current unbalance is usually six to ten times the voltage unbalance.[4] This leads to excessive heating of the windings, thermal ageing occurs and can result in insulation failure. Brighton and Ranade[5] have reported that the normal protection circuits which operate when the temperature or current increases above a pre-set level are not always reliable for protecting against failure due to unbalanced voltage supply. From a sample of 380 breakdowns of standard a.c. drives up to 25 kV, Vincent[6] has reported that 12% of the total failures were due to the worst unbalanced supply condition—known as single-phasing—which occurs when one of the supply lines is open-circuited.

Broken rotor bars

This occurs when one of the conducting bars of the squirrel cage rotor winding breaks where it is joined to the conducting end ring, Burns.[7] Adjacent bars carry a higher than normal current and overheat which usually leads to additional broken bars.[2] Rotor cage faults can cause torque pulsations, speed fluctuations and changes in the vibration signal.

Gaydon and Hopgood[8] have reported that these factors can cause mechanical damage to the rotor or stator winding.

Rotor–stator eccentricity

Static eccentricity exists when the axial centre of the rotor and stator are not coincident, this causes unbalanced magnetic pull (Binns and Dye[9]) and may lead to bearing damage.

Inter-turn winding faults

If the insulation between adjacent turns of a coil breaks down due to contamination or other causes, then shorting can occur and a hazardous situation results. This is because the shorted coil now lies in the main air-gap field due to the rest of the machine circuits and consequently has a voltage induced in it. The induced voltage drives current around the coil, and its magnitude is limited only by the resistance and inductance of the local circuit. The resulting currents can be very high, leading to insulation gassing with the possibility of explosion if and when sparking occurs.

The unbalance that occurs in the stator electrical circuits results in changes in the harmonic content of the air-gap flux, and this can be related to changes in the current time harmonics. One of the authors has investigated this and predicted the harmonic changes to be expected under current conditions, Penman *et al.*[10,11] They have also shown that although such changes could be observed in the line currents of the machine, this would require the sensing of terminal quantities and the measurement of small changes with respect to the fundamental. The alternative proposed[10,11] is to monitor the axially transmitted fluxes, for such a signal effectively magnifies the effects of small unbalance in the magnetic or electric circuit of the machine, and can also provide information concerning other fault conditions such as eccentric running and phase unbalance.

3. TEST RIG AND PROCESSING EQUIPMENT

The fault producing test motor and associated processing equipment are shown in Fig. 1. The test motor is a standard 11 kW SCIM which has been redesigned to carry out controlled experiments with the fault mechanisms described in the previous section. A number of transducers positioned on

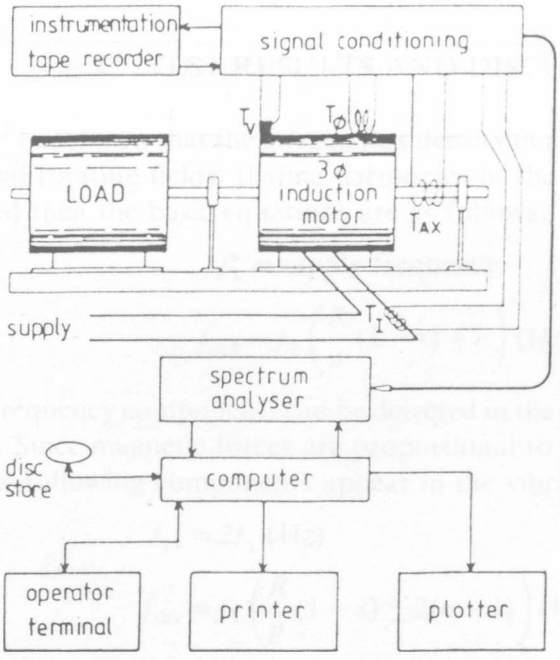

Fig. 1. Test rig, data acquisition and processing equipment.

the test rig sense various signals for on-line analysis and fault diagnosis, namely:

- T_i an air-cored toroidal coil used to sense electrical current in any of the main supply lines
- $T_{c\phi}$ a coil situated on the exterior casing of the motor in an appropriate position to sense the end winding leakage flux
- $T_{a\phi}$ a coil wound on the main shaft of the motor to sense the axial flux
- T_v an accelerometer positioned to sense the vibration on the casing or bearing pedestals

The transducer signals are pre-amplified and then subjected to spectral analysis in a high resolution spectrum analyser acting as a peripheral device to a minicomputer. A suite of programs in the minicomputer controls the analyser and presents the processed data to the experimenter in graphical or numerical form. The system can control the allocation of storage areas on the disc storage units so that historical records of experiments carried out on the induction motor can be accessed at a later date for inspection and comparison.

4. TEST RESULTS AND DISCUSSION

Alger[1,2] has shown that the air-gap flux density in a SCIM consists of five principal rotating fields. If time harmonics of the fundamental flux are included then the basic equations are as follows:

$$f_1 = \text{supply frequency} \tag{1}$$

$$f_{sh1} = f_1\left(\frac{R}{p}(1-s) \pm n\right)\text{(Hz)} \tag{2}$$

These frequency components can be detected in the current and stray flux signals. Since magnetic forces are proportional to flux density squared, then the following components appear in the vibration spectrum:

$$f_{1v} = 2f_1\ \text{(Hz)} \tag{3}$$

$$f_{shv} = f_1\left(\frac{R}{p}(1-s) \pm 2(n-1)\right)\text{(Hz)} \tag{4}$$

If the rotor cage winding is asymmetrical, then sidebands appear around the fundamental current component and the slot harmonics of the current, end winding and axial flux, and vibration signals.[1,2] An FFT analysis was initially applied to the transducer signals and a study made of the signature patterns. Where it was difficult to identify the difference between signature patterns for normal and abnormal operation, a zoom analysis was applied around specific frequency components. The frequency at which the zoom analysis is applied depends on the type of fault and signal being analysed. Equations (1)–(4) should be used for this purpose. Cepstrum analysis can be used to determine the sideband content of spectra.[2]

Test conditions. The spectra shown in Figs. 9–12 were obtained using a specially designed 51-slot rotor[2] and the other experiments were conducted using a 28-slot rotor. The results shown in Figs. 2–15 were recorded when the motor was delivering full-load output at the rated speed; the motor specification is as follows:

3-phase, 11 kW, 415 V, 50 Hz, 4-pole, squirrel cage induction motor
28-slot rotor; full-load rated speed 1470 rpm
51-slot rotor; full-load rated speed 1430 rpm
36-slot stator
air-gap length = 0·381 mm (0·015 in)

In addition, a 4 kW SCIM was also used to investigate inter-turn winding faults.

Single-phasing/unbalanced voltage supply fault detection

A comparison of Figs. 2 and 3 indicates that the 100 Hz component of vibration increases when one of the supply lines to the motor is open-circuited. The 100 Hz component of vibration also changes when a stator coil is short-circuited. In addition, the $(2-s)f_1$ component (approximately 100 Hz) of the axial flux increases with single-phasing or a short-circuited stator coil.[1] Hence the reliability of diagnosing a particular fault

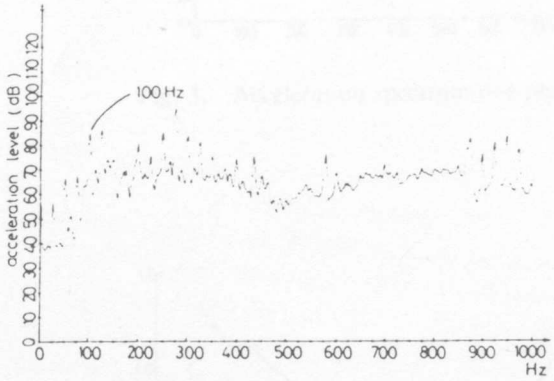

Fig. 2. Acceleration spectrum normal supply.

mechanism is suspect. Conversely, if the 100 Hz component changes in various interrelated signals then it can be used as a reliable indicator that a malfunction exists in the machine. If fundamental electrical machine concepts are considered then the condition of single-phasing will produce a standing wave flux pattern which should be reflected into the 100 Hz component of vibration. Further tests were conducted and Fig. 4 shows the variation of the 100 Hz component between normal three-phase operation and with one phase open-circuited. The curves indicate that during the fault condition, the level of the 100 Hz component varies dramatically with transducer position—a standing wave pattern occurs around the periphery of the motor. The other phases were open-circuited in turn and the resulting curves were nearly coincident with the one shown in Fig. 4. If this fundamental knowledge is used in a condition monitoring

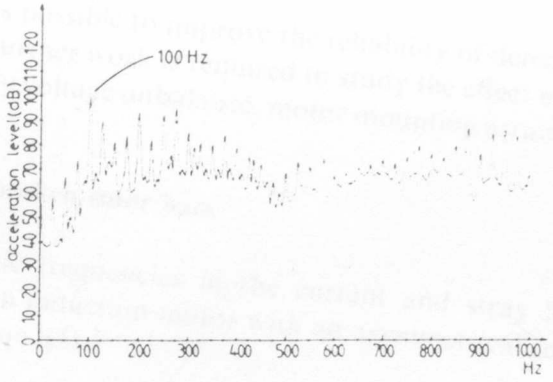

Fig. 3. Acceleration spectrum one-phase open circuit.

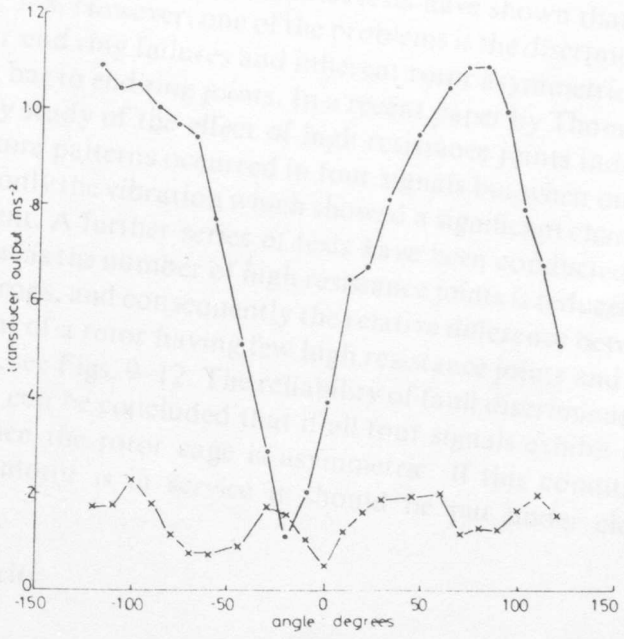

Fig. 4. 100 Hz vibration component as a function of positive and operating condition. (×) Normal three-phase operation; (○) one-phase open-circuit.

system, then it is possible to improve the reliability of detecting a single-phasing fault. Further work is required to study the effect of varying the amount of supply voltage unbalance, motor mounting arrangements and pole numbers.

Identification of broken rotor bars

The slot harmonic frequencies in the current and stray flux signals emanating from an induction motor with an asymmetrical rotor can be calculated using eqn. (5).[2]

$$f_{sh2} = f_1(R(1-s)/p \pm n) \pm 2sf_1 \tag{5}$$

Sidebands at twice the 'slip' frequency also appear around the principal slot harmonic vibration components. This means similar signature patterns occur in four interrelated signals and can be used as a basis for identifying a rotor cage fault. Experimental tests have shown that this is the case, see Figs. 5–8. However, one of the problems is the discrimination between rotor bar/end ring failures and inherent rotor asymmetries such as high resistance bar to end ring joints. In a recent paper by Thomson *et al.*,[2] a preliminary study of the effect of high resistance joints indicated that similar signature patterns occurred in four signals but when one bar was broken it was only the vibration which showed a significant change in the sideband content. A further series of tests have been conducted and the results show that as the number of high resistance joints is reduced the sideband content drops, and consequently the relative difference between the sideband content of a rotor having few high resistance joints and one broken bar is larger, see Figs. 9–12. The reliability of fault discrimination is still suspect but it can be concluded that if all four signals exhibit this signature pattern then the rotor cage is asymmetric. If this condition develops while the motor is in service it should be put under close surveillance.

Rotor–stator eccentricity

In contrast to the previous fault mechanisms, the only significant change occurred at one of the slot harmonic components (885 Hz) of the vibration spectrum. The sense of the change was a function of transducer position around the periphery of the motor frame as shown in Fig. 13. The results show that at least one of the four interrelated signals is

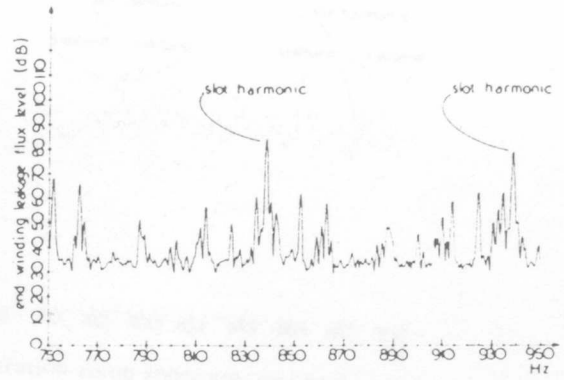

Fig. 5. End winding leakage flux zoom spectrum, normal rotor.

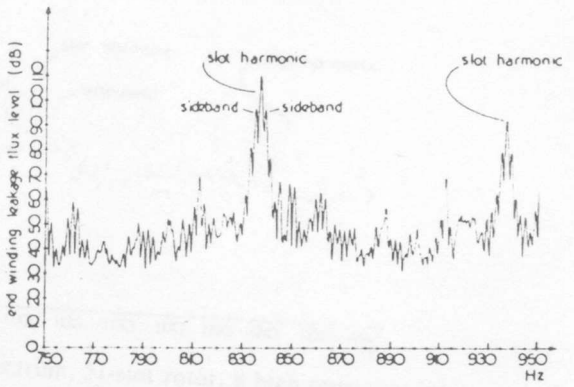

Fig. 6. End winding leakage flux zoom spectrum, one broken bar.

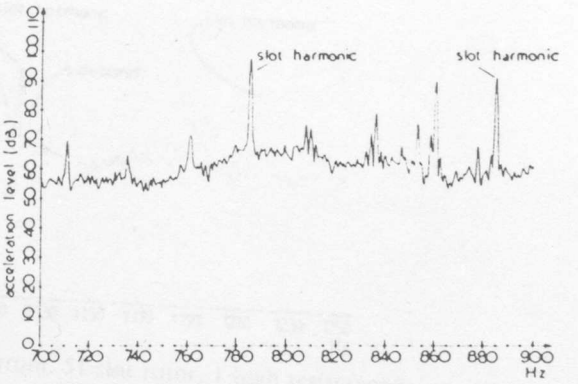

Fig. 7. Acceleration zoom spectrum, normal rotor.

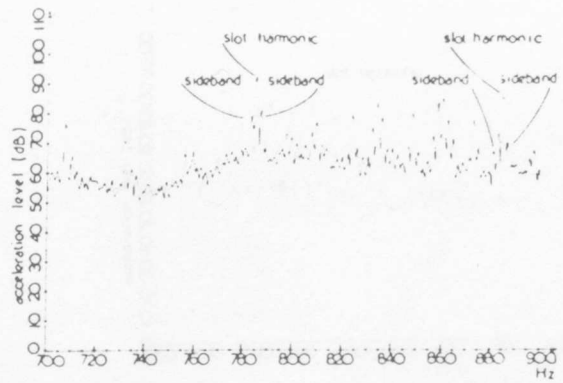

Fig. 8. Acceleration zoom spectrum, one broken bar.

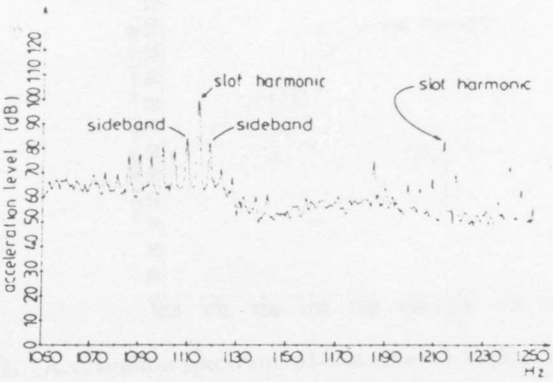

Fig. 9. Acceleration spectrum, 51-slot rotor, 8 high resistance joints.

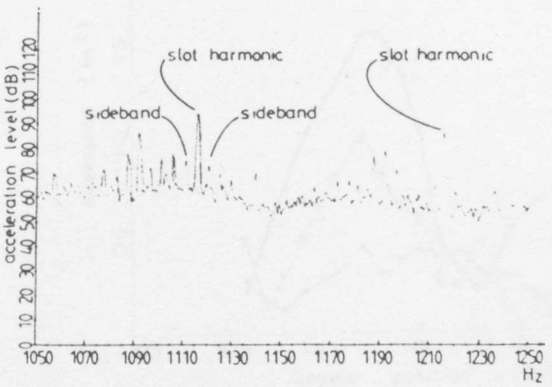

Fig. 10. Acceleration spectrum, 51-slot rotor, 1 high resistance joint.

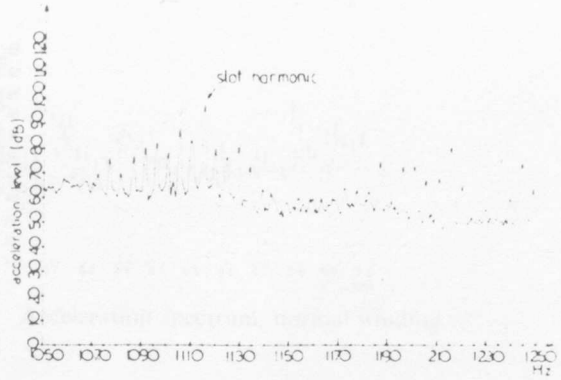

Fig. 11. Acceleration spectrum, 51-slot rotor, 1 broken bar, 7 high resistance joints.

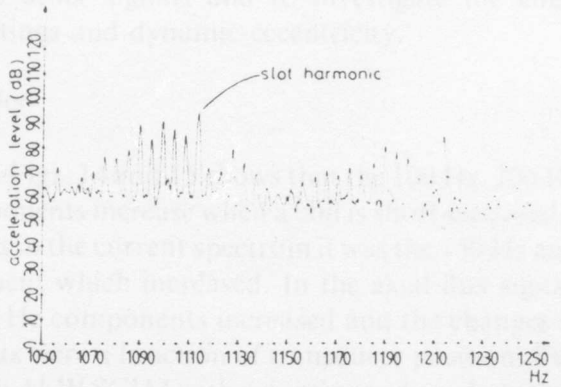

Fig. 12. Acceleration spectrum, 51-slot rotor, 1 broken bar, no high resistance joints.

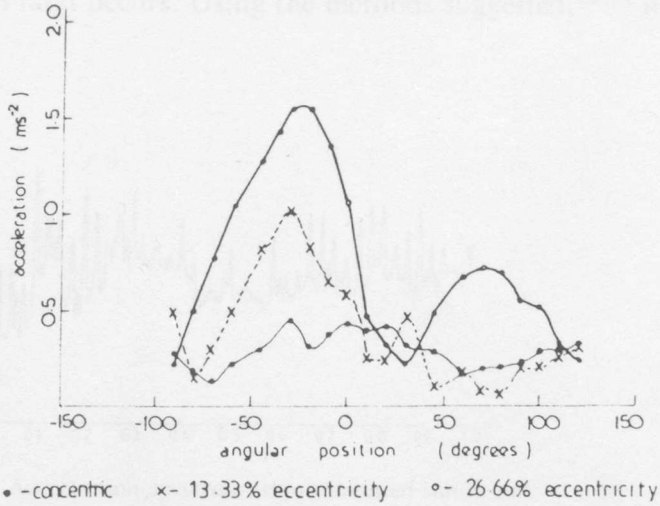

Fig. 13. Acceleration level of 885 Hz component versus transducer position with varying eccentricity.

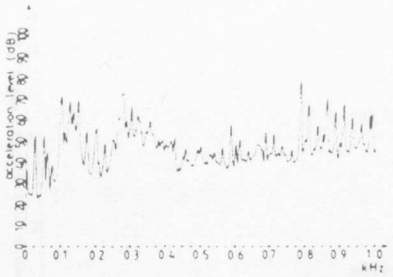

Fig. 14. Acceleration spectrum, normal winding.

sensitive to rotor stator eccentricity. Further work is required to try and detect changes in the other signals and to investigate the effects of different motor mountings and dynamic eccentricity.

Inter-turn winding faults

A comparison between Figs. 14 and 15 shows that the 100 Hz, 200 Hz and 300 Hz vibration components increase when a coil is short-circuited in the stator winding, whereas in the current spectrum it was the 150 Hz and one slot harmonic component which increased. In the axial flux signal, the 50 Hz, 100 Hz and 150 Hz components increased and the changes in the end winding leakage flux were a function of transducer position. Further test results taken from a 4 kW SCIM with a 4-pole winding show that it is possible to identify specific harmonic components in the axial flux signal when an inter-turn fault occurs. Using the methods suggested,[10,11] it is

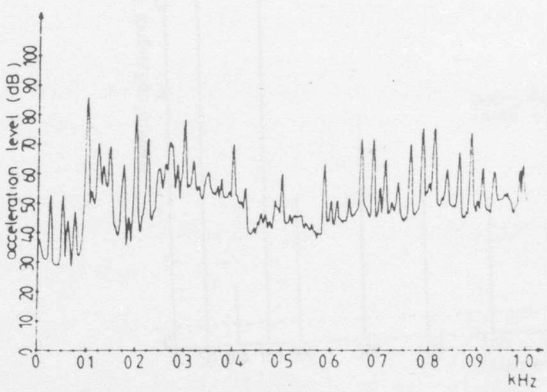

Fig. 15. Acceleration spectrum, short-circuited stator coil.

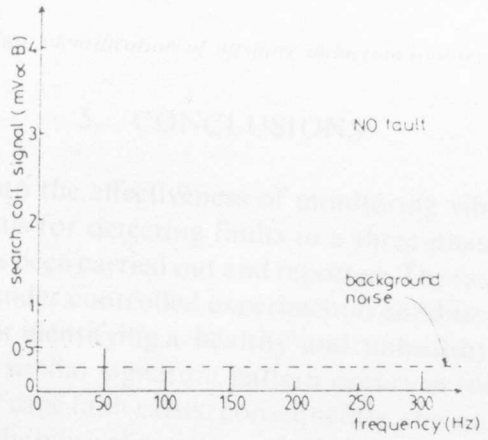

Fig. 16. Axial flux signal versus frequency with normal winding.

predicted that time harmonics of order 1, plus all even orders, should appear in addition to the usual $6n \pm 1$ orders. Figures 16 and 17 show that this is the case, particularly with reference to the fundamental and even harmonics. There is also growth in the third harmonic, most likely caused by local saturation effects in the vicinity of the shorted turns.

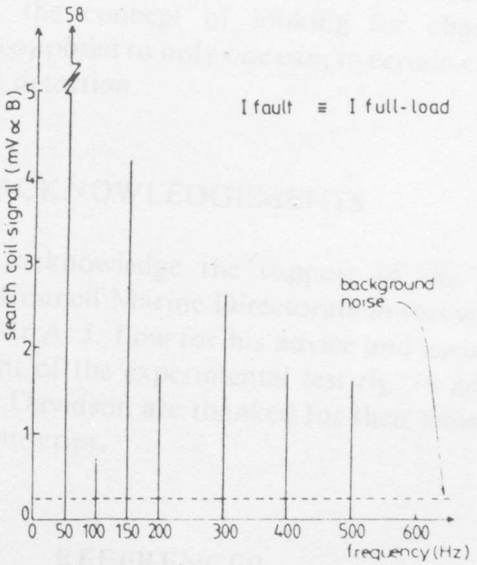

Fig. 17. Axial flux signal versus frequency with an inter-turn fault.

5. CONCLUSIONS

An investigation into the effectiveness of monitoring vibration, current and stray flux signals for detecting faults in a three-phase squirrel cage induction motor has been carried out and reported. The fault mechanisms have been studied under controlled experimental conditions and a set of spectra presented for identifying a 'healthy' and 'unhealthy' motor. It has been verified that a similar signature pattern occurs in four interrelated spectra when a rotor cage fault exists; consequently, this unified approach could improve the reliability of rotor cage fault detection. The results also show that the 100 Hz component of the vibration signal changes instantaneously when a single-phasing or inter-turn winding fault occurs. If the transducer is correctly positioned it is possible to discriminate between the two fault mechanisms. It has been verified by experiment that the predicted harmonic components[10,11] do appear in the axial spectrum when an inter-turn fault exists. In addition, the slot harmonic components in the vibration spectrum can be used to detect static rotor stator eccentricity. Further work is required to try and detect changes in the other signals and apply the techniques for detecting dynamic eccentricity. Finally, the concept of looking for changes in four interrelated spectra as opposed to only one can, in certain cases, improve the reliability of fault detection.

ACKNOWLEDGEMENTS

The authors wish to acknowledge the support of the Science and Engineering Research Council Marine Directorate in this work. Thanks are also expressed to Mr A. J. Low for his advice and assistance in the design and development of the experimental test rig. In addition, Mrs M. Gordon and Mr B. Davidson are thanked for their assistance in the preparation of the manuscript.

REFERENCES

1. Thomson, W. T., Deans, N. D., Leonard, R. A. and Milne, A. J. Condition monitoring of induction motors for availability assessment in offshore installations, *Fourth Euredata Conf. Proc.*, Venice, March 1983.

2. Thomson, W. T., Deans, N. D., Leonard, R. A. and Milne, A. J. Monitoring strategy for discriminating between different types of rotor defects in induction motors, *18th Universities Power Eng. Conf. Proc.*, University of Surrey, England, April 1983.
3. Verma, S. P., Girgis, R. S. and Fleming, R. J. The problems and failures caused by shaft potentials and bearing currents in turbogenerators; methods of prevention, *CIGRE Int. Conf. Proc. on Large High Voltage Electric Systems*, 1980, 11-10.
4. Howell, J. K. and Hogwood, E. E. *Electrified Oil Production*, Penwell Publishing Company, 1981.
5. Brighton, R. J. and Ranade, P. N. Why overload relays do not always protect motors, *IEEE Trans. on Industry Applications*, **IA 18** (1982), p. 691.
6. Vincent, C. E. Maintenance of large industrial drives, *Colloquium on The Design and Applications of Large Industrial Drives, IEE Conf. Publ. No. 170*, 1978, p. 16.
7. Burns, R. L. Rotor bar failures in large a.c. squirrel cage rotors, *Electr. Eng.*, **54**(19) (1977), p. 11.
8. Gaydon, B. G. and Hopgood, D. J. Faltering pulse can reveal an ailing motor, *Electrical Review*, **205**(14) (1979), p. 37.
9. Binns, K. J. and Dye, M. Identification of principal factors causing unbalanced magnetic pull in cage induction motors, *Proc. IEE*, **120**(3) (1973), p. 349.
10. Penman, J., Hadwick, J. G. and Stronach, A. F. *Protection Strategy against the Occurrence of Faults in Electrical Machines*, Int. Conf. on Developments in Power System Protection, IEE Publ. No. 185, 1980, p. 54.
11. Penman, J., Dey, M. and Hadwick, J. G. A microcomputer based machine protection system, *Proc. 17th Universities Power Eng. Conf.*, Manchester, 1980.
12. Alger, P. L. *The Nature of Induction Machines*, Gordon and Breach Science Publications, London, 1965.

VIBRATION AND STRAY FLUX MONITORING FOR UNBALANCED SUPPLY AND INTER-TURN WINDING FAULT DIAGNOSIS IN INDUCTION MOTORS

R A Leonard, B Sc(Hons)[i] W T Thomson, B Sc(Hons), M Sc, MIEE, C Eng[ii]

This paper discusses the philosophy of on-line fault diagnosis using vibration, current and stray flux signals in a unified monitoring strategy as opposed to the traditional monitoring techniques used for electrical machine fault detection. Fault mechanisms in induction motors are discussed in general and a theoretical analysis is presented to show how the vibration pattern on the frame of the motor changes due to unbalanced supplies and inter-turn winding faults. The experimental test rig and signal processing system are described and a set of experimental results are presented and discussed. An assessment of the effectiveness of vibration and stray flux monitoring for detecting electrical malfunctions is presented in the conclusions.

1 INTRODUCTION

In British industry the 3-phase squirrel-cage induction motor (SCIM) is widely used for reasons of economy, robust construction and reliability. In the offshore oil industry, which is currently the United Kingdom's major financial asset, they are used to drive gas compressors, sea-water injection pumps and oil exporting pumps. Due to the harsh environmental operating conditions the motor's reliability is being tested to the limit. To prevent catastrophic failure which can be very

(i) Electrical Engineer
Brown & Root (UK) Ltd
ABERDEEN

(ii) Senior Lecturer in
Electrical Engineering
Robert Gordon's Institute of
Technology,
ABERDEEN

costly and potentially dangerous it is essential that fault mechanisms are detected at any early stage so that repairs can occur at a convenient time. In offshore installations the SCIM is usually started direct-on-line which causes large starting currents and torques and can contribute to end winding, rotor-cage and bearing failures. In addition, sea-water contamination of the windings and winding vibration problems have caused insulation failure. The traditional approach for detecting faults in electrical machines is that vibration monitoring is used to detect mechanical faults such as drive misalignment, shaft whirl and bearing wear [1] - normally done by mechanical engineers. Similarly, electrical engineers have concentrated on the detection of high voltage winding insulation deterioration, rotor winding problems and shaft voltages/bearing currents. However, an electrical machine is a complex electro-magnetic and electromechanical device which means the failure mechanisms are often not simply mechanical or electrical in origin.[2] For example, insulation failure can be a by-product of excessive core and end winding vibration[3] and bearings can fail due to the flow of electrical currents in the bearing assembly.[4] The final failure may appear to be electrical or mechanical but the fundamental cause can be quite different. A recent survey to determine the condition monitoring techniques used by the operators and the frequency of occurrence of different types of failure has shown that the present techniques used for fault diagnosis are not always successful. [2] Sources of information tend to be studied in isolation by the particular vibration or insulation expert and the general opinion is that correlation studies between different signals should improve the reliability of fault diagnosis. The authors have responded to this need for a new look at SCIM fault diagnosis and have shown that an on-line monitoring strategy which utilises vibration, current and stray flux signals in a unified approach should prove to be more successful than existing techniques [2,3,5]: the philosophy being that if 4 or 5 interrelated signals all indicate a particular fault then the operator is likely to believe the information and repair the motor. This paper presents further experimental results for assessing the effectiveness of vibration and stray flux monitoring for diagnosing electrical malfunctions.

2 VIBRATION MONITORING FOR DIAGNOSING ELECTRICAL MALFUNCTIONS

In offshore installations where the supply system is relatively small then the 3-phase voltage supply could become unbalanced due to single-phasing of primary/ secondary circuits or unbalanced single-phase loads. [6]

This causes overheating of the windings, thermal ageing occurs and can result in insulation failure. For example, insulation life can be halved for every 10^{o} C rise over the rated temperature. [7] Numerous protection schemes are available for preventing motor failure due to unbalanced supply and are usually based on sensing over-current, voltage or current asymmetry or stator winding temperature. [8] However, they are not always successful and unfortunately motors still fail due to the effects of unbalanced supplies. [9] Vincent [10] has reported that from a sample of 380 failures of standard a.c. drives up to 25 kV, 12% of the total breakdowns were due to the most severe unbalanced supply condition known as single-phasing. This condition occurs when one of the supply lines is disconnected or one of the phase windings develops an open-circuit. With the conventional protection techniques it is very difficult to protect the motor against the effects of single-phasing over the complete operating range from no-load to full-load. Lord and Pearson [11] have developed a sensitive protection scheme which will detect a single-phasing fault provided the motor is running with a load greater than one-third full-load. The device will also trip with a minimum current in a fault between lines of one quarter full-load current for a fully loaded motor, and one half full-load current for an unloaded motor. This is a significant improvement on the conventional techniques but the protection strategy does not cater for all load conditions. What is still required is the development of a monitoring scheme/protection device which will protect the motor against unbalanced supplies for all load conditions.

During normal operation of a 3-phase induction motor it is reasonable to assume that the magnitude of the fundamental air-gap flux remains constant between no-load and full-load operation. This is true since the basic e.m.f. equation for a 3-phase motor is given by [12]

$$E = 4.44 \Phi N f_1 k_w \quad \ldots\ldots\ldots\ldots\ldots\ldots (1)$$

Where N, f_1, k_w are constants for a given motor design and for practical operating considerations the difference between the normal applied voltage and the induced e.m.f. E due to load variations is negligible. It is also known that the magnetic forces which act on the stator core of the motor can be determined from :

$$P = \frac{B^2}{2\mu_o} \quad \ldots\ldots\ldots\ldots\ldots\ldots\ldots\ldots\ldots (2)$$

The resulting force components act directly on the core and the resulting vibration pattern is a function of the electromagnetic force waves and the mechanical response of the core and frame.[13] Since this force is directly

proportional to the air-gap flux squared then any change in the flux distribution will be observed as an instantaneous change in the vibration spectrum. The following analysis will show how the vibration pattern changes due to unbalanced supply or inter-turn winding faults. Consider the delta connected winding shown in Figure 1.

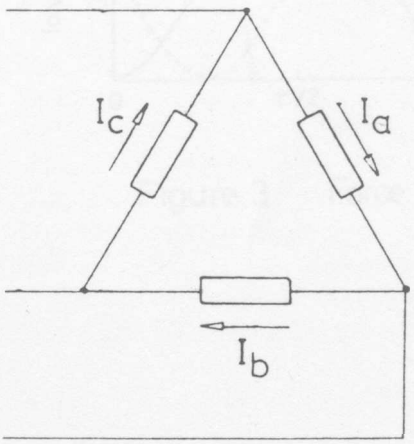

Figure 1

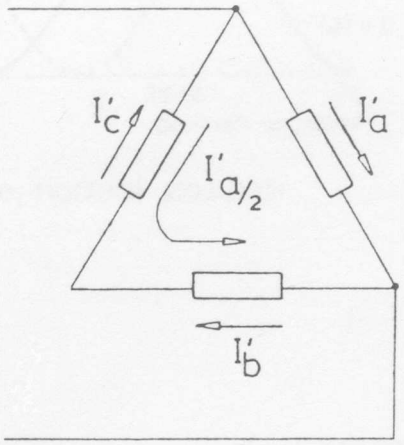

Figure 2

If the system is symmetrical then the resultant magneto-motive force (m.m.f.) is given by [12] :

$$F_{m3} = 1.5\ F_m \sin\left(\omega t - \frac{\pi x}{\tau}\right) \quad \ldots\ldots\ldots\ldots\ldots\ldots \quad (3)$$

For simplicity let the permeance be a constant and since B = m.m.f.x permeance then by combining equations (2) and (3) the force on the stator core will be of the form :

$$F_3 = K_1 \left[1 - \cos\left(2\omega t - \frac{2\pi x}{\tau}\right)\right] \quad \ldots\ldots\ldots\ldots\ldots \quad (4)$$

If one of the supply lines is disconnected as shown in Figure 2, then the m.m.f. will contain a pattern of the form :

$$F_{m1} = M_1 \sin \omega t \cos \frac{\pi x}{\tau} \quad \ldots\ldots\ldots\ldots\ldots\ldots \quad (5)$$

and the force acting on the core will be of the form :

$$F_1 = K_2 \left[1 + \cos \frac{(2\pi x)}{\tau}\right] . \left[1 - \cos (2\omega t)\right] \ldots\ldots \quad (6)$$

Plots of equations (4) and (5) are shown in Figures 3 and 4 respectively.

From the curves and equations it is observed that the frequency of vibration is 100 Hz and the force wave for normal 3-phase operation (no-load to full-load) is a

travelling wave but due to single-phasing a pulsating component appears. The analysis shows that during the fault there will be optimum positions for sensing the change in the 100 Hz component of the vibration spectrum.

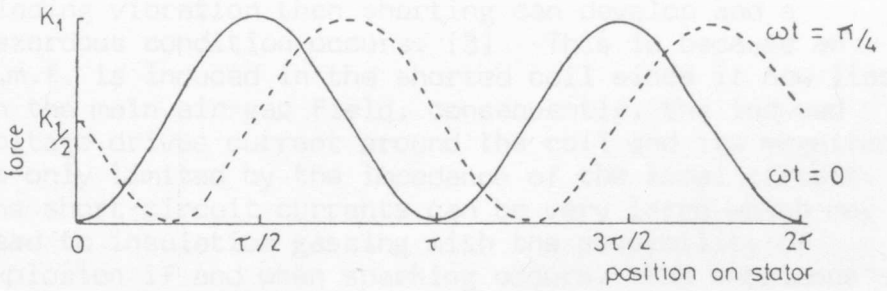

Figure 3 Force wave, normal position

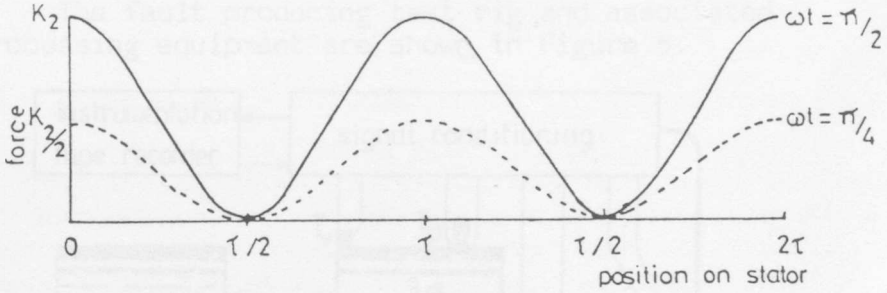

Figure 4 Force wave, single-phasing fault

For other unbalanced supply conditions and inter-turn winding faults a similar pattern will occur around the core. It has of course been known for some time that the 100 Hz vibration component changes [14] but this information has only been used as an indication that an electrical malfunction exists. [1] This is because vibration monitoring is generally used to detect mechanical malfunctions [15, 16, 17] and the transducers are normally placed on the bearings. In most cases vibration monitoring of the core has been neglected by condition monitoring engineers. The results presented in previous publications by the authors [2, 3, 5] and the contents of this paper clearly show that vibration monitoring of the core should be one of the parameters

used for on-line induction motor fault diagnosis.

3 STRAY FLUX MONITORING FOR SENSING UNBALANCED SUPPLIES/WINDING FAULTS

If the insulation between adjacent turns of a coil breaks down due to contamination or because of excessive winding vibration then shorting can develop and a hazardous condition occurs. [3] This is because an e.m.f. is induced in the shorted coil since it now lies in the main air-gap field, consequently, the induced voltage drives current around the coil and its magnitude is only limited by the impedance of the local circuit. The short-circuit currents can be very large which may lead to insulation gassing with the possibility of explosion if and when sparking occurs. The unbalance which occurs in the stator winding causes changes in the air-gap flux and Penman [18, 19] has shown that the fault can be detected in the axial flux signal. Thomson [3] (et al) has also shown that this is the case and in addition a change can also be observed in the end-winding leakage flux signal.

4 TEST RIG AND PROCESSING EQUIPMENT

The fault producing test rig and associated processing equipment are shown in Figure 5.

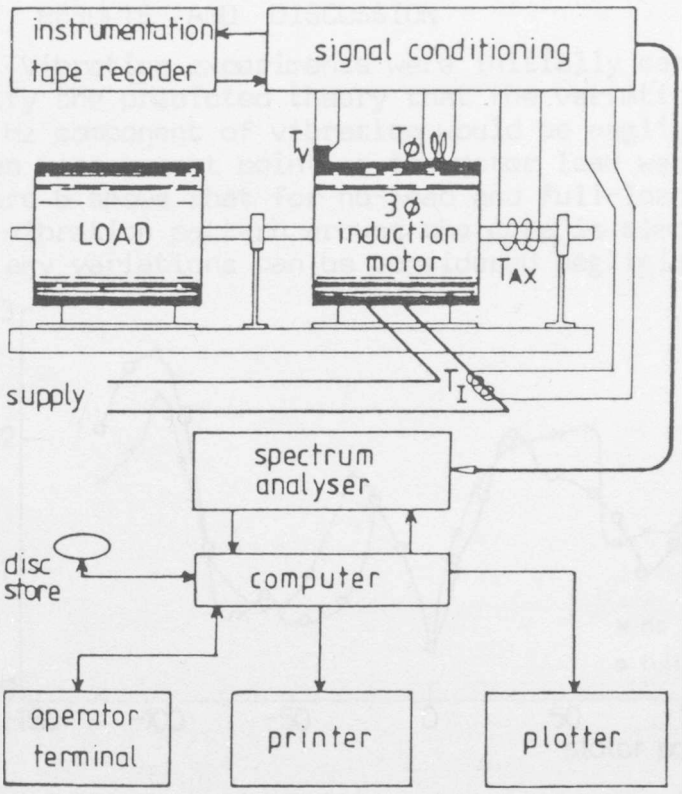

Figure 5

The test motor is a standard 3-phase, 50-Hz, 11-kW, 415-V, 4-pole, SCIM, which has been redesigned to conduct controlled experiments with the fault mechanisms discussed previously. A number of transducers positioned on the test rig sense various signals for on-line analysis and fault diagnosis, namely :

T_i - is an air-cored toroidal coil used to sense electrical current

$T_{e\phi}$ - is a coil situated on the exterior casing to sense the end-winding leakage flux

$T_{a\phi}$ - is a coil wound on the main shaft of the motor to sense the axial flux

T_a - is an accelerometer positioned to sense the vibration at any position around the frame/bearing pedestals

The transducer signals are preamplified and then analysed in a high resolution spectrum analyser. A suite of programmes in the minicomputer can control the analyser and perform further signal analysis and present the processed data in graphical or numerical form.

5 TEST RESULTS AND DISCUSSION

Vibration experiments were initially carried out to verify the predicted theory that the variations in the 100 Hz component of vibration would be negligible for a given measurement point as the motor load was changed. Figure 6 shows that for no-load and full-load operation the vibration pattern around the core is almost identical and any variations can be considered negligible.

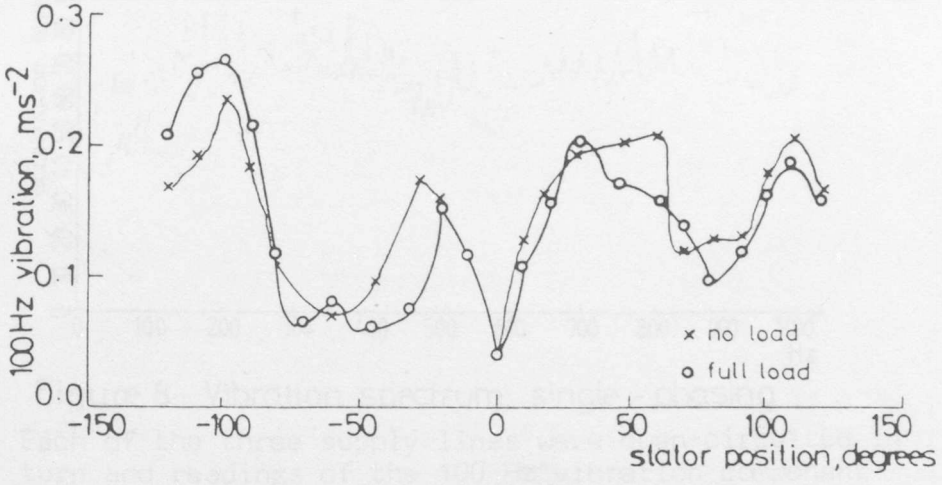

Figure 6 Variation of 100Hz component with load

Due to inherent magnetic/winding asymmetries and the effect of nodes occurring at the foot mountings then there is a variation around the frame for each load condition. Having established the normal vibration patterns, one of the supply lines was open-circuited with the motor running on no-load. For one particular transducer position the resulting vibration spectra are shown in Figures 7 and 8 and it was noted that the 100 Hz component increased by 15 dB during the fault. However, it was not known whether a standing wave vibration pattern did occur.

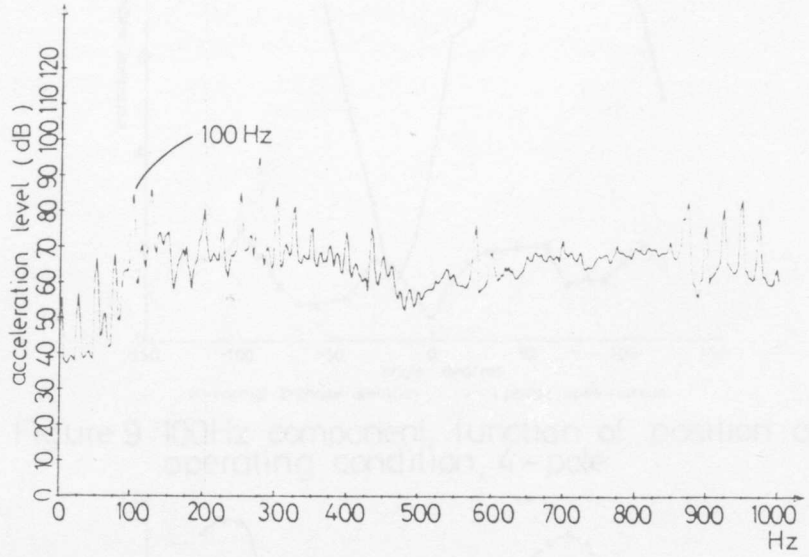

Figure 7 Vibration spectrum, normal supply

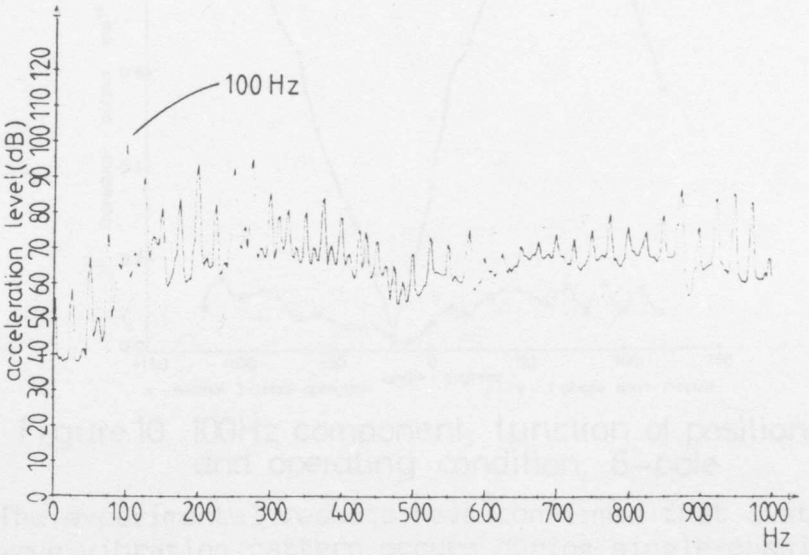

Figure 8 Vibration spectrum, single - phasing

Each of the three supply lines were open-circuited in turn and readings of the 100 Hz vibration component around the periphery of the motor's frame were recorded for no-load operation. The same vibration pattern occurred in each case and Figure 9 shows that at the

± 100 degrees measurement point the vibration increased by a factor of approximately five. Further tests were carried out with different winding connections, and Figure 10 shows the result for the 6-pole configuration.

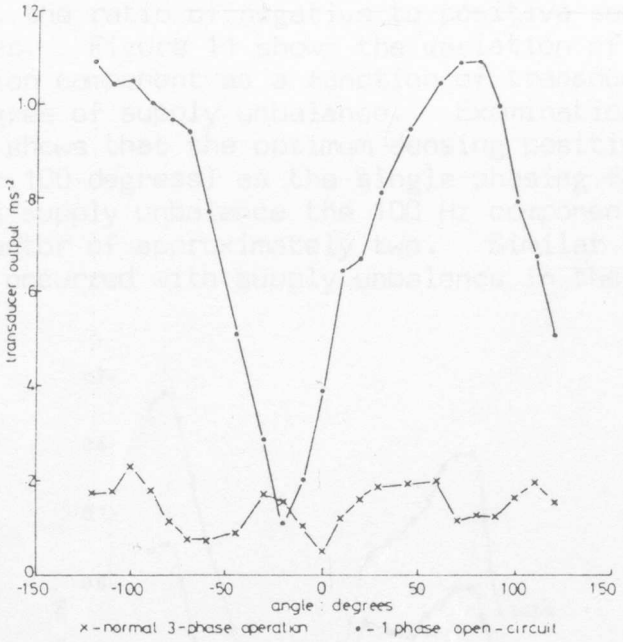

Figure 9 100Hz component, function of position and operating condition, 4-pole

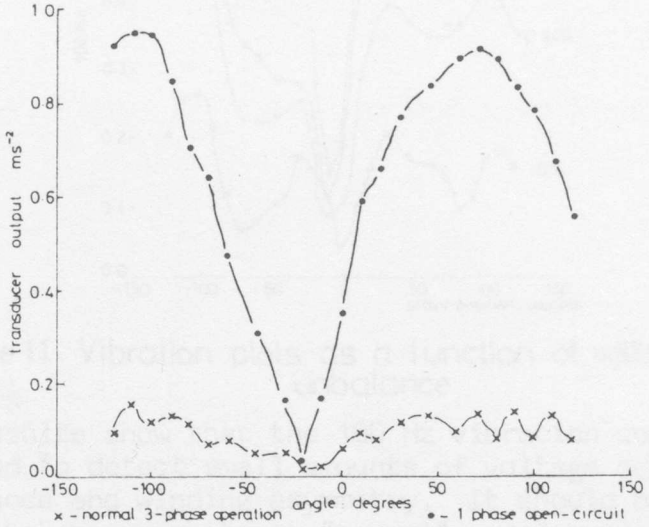

Figure 10 100Hz component, function of position and operating condition, 6-pole

The experimental results have confirmed that a standing wave vibration pattern occurs during single-phasing and is independent of the speed and pole number. If the transducer is correctly positioned then the 100 Hz component can be used to sense a single-phasing fault during all load conditions.

Another set of experiments were conducted to

determine if the 100 Hz vibration component could detect small amounts of voltage supply unbalance. The tests were carried out during full-load operation and the standard definition of unbalanced supply was used, [20] namely, the ratio of negative to positive sequence voltages. Figure 11 shows the variation of the 100 Hz vibration component as a function of transducer position and degree of supply unbalance. Examination of the curves shows that the optimum sensing positions are the same (± 100 degrees) as the single-phasing fault. For a 0.84% supply unbalance the 100 Hz component increased by a factor of approximately two. Similar families of curves occurred with supply unbalance in the other two phases.

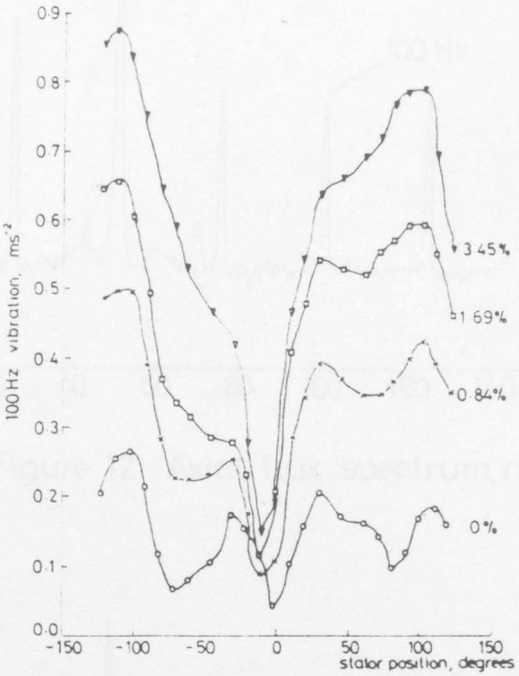

Figure 11 Vibration plots as a function of voltage unbalance

The results show that the 100 Hz vibration component can be used to detect small amounts of voltage supply unbalance and winding asymmetry. It should be mentioned that the changes between "normal" and "abnormal" operation will be different for each particular motor and its mounting arrangement, but the standing wave vibration pattern will still occur and the change will be significant. The axial flux signal was also monitored during single phasing and Figures 12 and 13 show the change between normal and fault conditions.

The results show that the $(2 - s)f_1$ component (approximately 100 Hz) increases by approximately 20 dB. In addition, inter-turn winding faults were studied and

Figures 14 and 15 show that the vibration spectrum changed, in particular, the 100, 200 and 300 Hz components all increased. The axial flux spectrum also changed, [2] consequently, the results clearly demonstrate the potential of vibration and stray flux monitoring for detecting short-circuited coils in the stator winding. Further tests are required to determine the changes in the vibration as a function of transducer position with short-circuited coils.

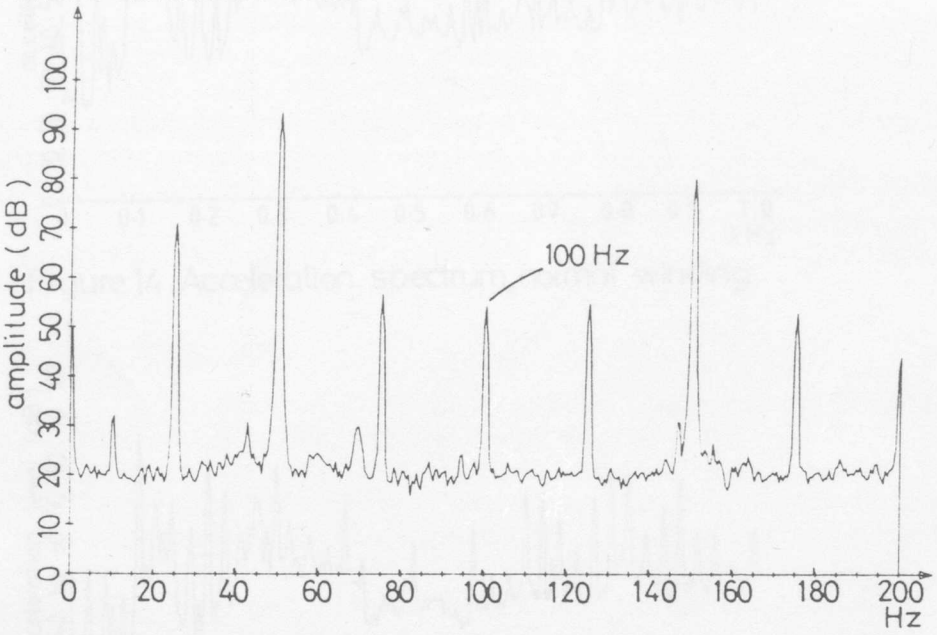

Figure 12 Axial flux spectrum, normal

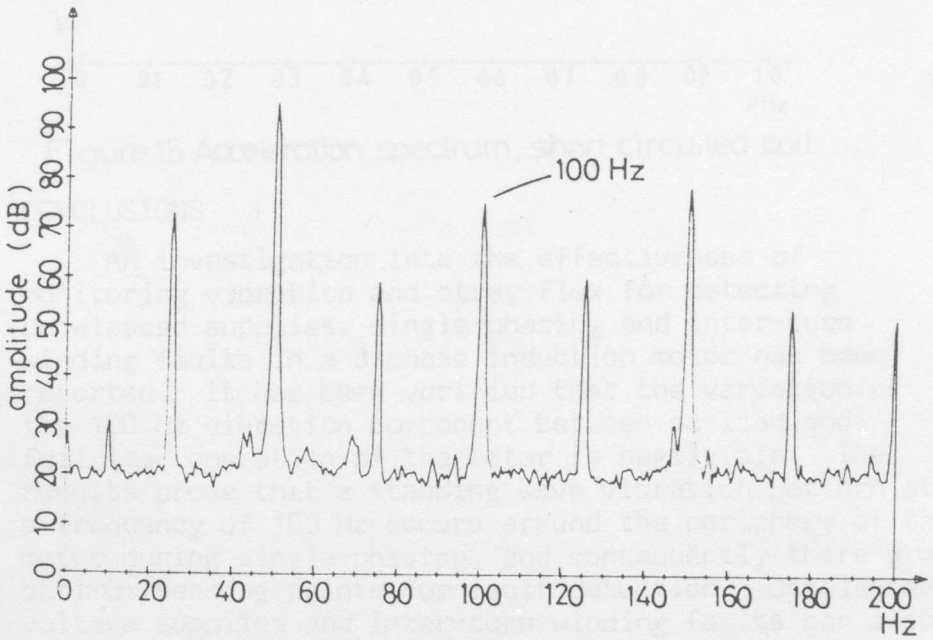

Figure 13 Axial flux spectrum, single-phasing

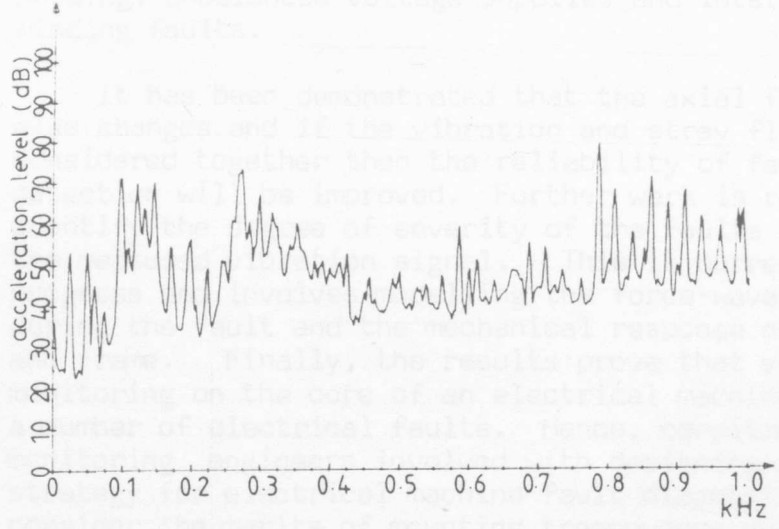

Figure 14 Acceleration spectrum, normal winding

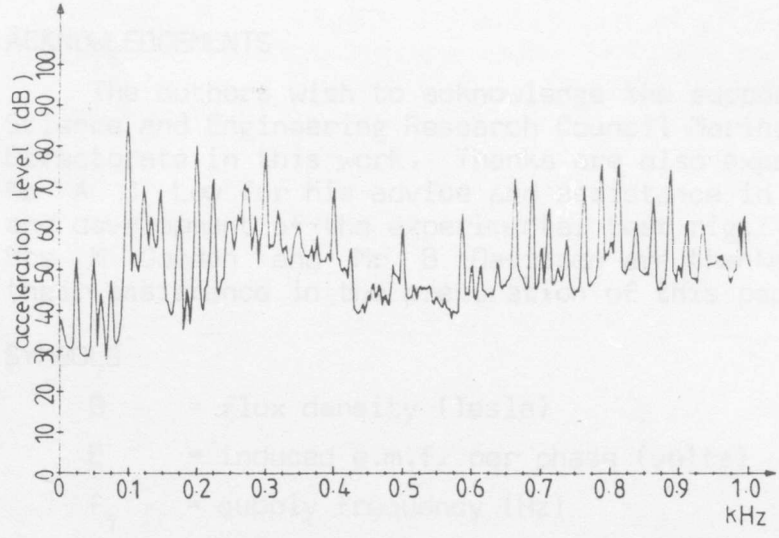

Figure 15 Acceleration spectrum, short circuited coil

6 CONCLUSIONS

An investigation into the effectiveness of monitoring vibration and stray flux for detecting unbalanced supplies, single-phasing and inter-turn winding faults in a 3-phase induction motor has been reported. It has been verified that the variation of the 100 Hz vibration component between no-load and full-load operation of the motor is negligible. The results prove that a standing wave vibration pattern at a frequency of 100 Hz occurs around the periphery of the motor during single-phasing, and consequently there are optimum sensing points for fault detection. Unbalanced voltage supplies and inter-turn winding faults can also be detected using the 100 Hz vibration component. This means the vibration signal could be used in a protection strategy for preventing winding failure due to single-

phasing, unbalanced voltage supplies and inter-turn winding faults.

It has been demonstrated that the axial flux spectrum also changes and if the vibration and stray flux are considered together then the reliability of fault detection will be improved. Further work is required to quantify the degree of severity of the faults in terms of the measured vibration signal. This is currently in progress and involves modelling the force-wave functions during the fault and the mechanical response of the core and frame. Finally, the results prove that vibration monitoring on the core of an electrical machine can detect a number of electrical faults. Hence, condition monitoring engineers involved with designing a monitoring strategy for electrical machine fault diagnosis should consider the merits of mounting transducers on the core as well as on the bearing assemblies.

7 ACKNOWLEDGEMENTS

The authors wish to acknowledge the support of the Science and Engineering Research Council Marine Directorate in this work. Thanks are also expressed to Mr A J Low for his advice and assistance in the design and development of the experimental test rig. In addition, Mrs M Gordon and Mr B Davidson are thanked for their assistance in the preparation of this paper.

8 SYMBOLS

B = flux density (Tesla)

E = induced e.m.f. per phase (volts)

f_1 = supply frequency (Hz)

F_{m3} = magnetomotive force, normal supply (ampere-turns)

F_{m1} = magnetomotive force, single-phasing supply (At)

F_3 = force wave, normal

F_1 = force-wave, single-phasing

I = current (amps)

k_w = winding constant

N = number of turns/phase

P = magnetic pull (Nm^{-2})

s = slip

t = time (s)

τ = distance between pole centres

x = distance from centre of phase A pole

μ_o = permeability, $4\pi \times 10^{-7}$)

ω = angular speed (rad s^{-1})

Φ = flux per pole (webers)

9 REFERENCES

1 NEALE, M and ASSOCIATES - Guide to the Condition Monitoring of Machinery, HMSO, London, 1979

2 THOMSON, W T, DEANS, N D, LEONARD, R A, and MILNE, A J - Condition Monitoring of Induction Motors for Availability Assessment in Offshore Installations. Fourth Euredata Conference Proceedings, 25 March 1983, Venice, Italy

3 THOMSON, W T, LEONARD, R A, PENMAN, J, and MILNE, A J. - Failure Identification of Offshore Induction Motor Systems using On-Condition Monitoring. 4th National Reliability Conference, July 1983, Birmingham, England

4 VERMA, S P, GIRGES, R S, and FLEMING, R J, - The Problems and Failures caused by Shaft Potentials and Bearing Currents in Turbogenerators; Methods of Presentation. CIGRE International Conference Proceedings on Large High Voltage Electric Systems, 1980, 11-10

5 THOMSON, W T, DEANS, N D, LEONARD, R A, and MILNE, A J. - Monitoring Strategy for Discriminating between different types of Rotor Defects in Induction Motors. 18th Universities Power Engineering Conference Proc., 12th April 1983, University of Surrey, England

6 HOWELL, J K, and HOGWOOD, E E. - Electrified Oil Production, 1981, Penwell Publishing Company

7 BRIGHTON, R J, and RANADE, P N. - Why Overload Relays do NOT always Protect Motors. IEEE Trans on Industry Applications, Vol 1A-18, No 6, Nov/Dec 1982

8 GLEASON, L L and ELMORE, W A. - Protection of 3-Phase Motors against Single-Phase Operation. AIEE Trans, Part III, Vol 77, 1958

9 BONNETT, A H. - Analysis of Winding Failures in Three-Phase Squirrel-Cage Induction Motors. IEEE Trans on Industry Applications, Vol 1A-14, No 3, 1978

10 VINCENT, C E. - Maintenance of Large Industrial Drives. IEE Conference Publication. Colloquium on the Design and Applications of Large Industrial Drives, No 170, 16-17, 1978

11 LORD, H, and PEARSON, F K. - Sensitive Protection for Induction Motor Supplies. Electrical Review Vol 207, No 5, August 1980

12 ALGER, P L. - The Nature of Induction Machines, Gordon and Breach Science Publications, 1965

13 ELLISON, A J, and MOORE, C J. - Acoustic Noise and Vibration of Rotating Electric Machines, Proc IEE Vol 115, No 11, November 1968

14 ALGER, P L. - Magnetic Noise in Polyphase - Induction Motors. Trans Amer Inst Electrical Engineering, 1954, 73, Pt IIIA, pp 118-125

15 STEWART, R M. - Vibration Analysis as an Aid to the Detection and Diagnosis of Faults in Rotating Machinery. 1st Int Conf on Vibrations in Rotating Machinery, I Mech E, Conference Publications, 1976

16 DOWNHAM, E. - Vibration in Rotating Machinery : Malfunction Diagnosis - Art and Science. ibid

17 HEMMINGS, R C, and SMITH, J D. - Information from Bearing Vibration, ibid

18 PENMAN, J, HADWICK, J G, and BARKER, B. - Detection of Faults in Electrical Machines by Examinations of the Axially Directed Fluxes. 3rd Int. Conf. on Electrical Machines, Brussels, 1978

19 PENMAN, J, HADWICK, J G, and STRONACH, A F. - Protection Strategy against the Occurrence of Faults in Electrical Machines. Int. Conf. on Developments in Power System Protection, IEE Publication, 1980

20 British Standards, BS 4999 : Part 31 : 1971